THE UNIVERSITY
of EDINBURGH

RNA pull-down-confocal nanoscanning (RP-CONA), a novel method for studying RNA/protein interactions in cell extracts that detected potential drugs for Parkinson's disease targeting RNA/HuR complexes

Siran Zhu

THE UNIVERSITY *of* EDINBURGH

Thesis presented for the degree of Doctor of Philosophy

2021

Declaration

I declare that this thesis was composed by myself, that the work contained herein is my own except where explicitly stated otherwise in the text, and that this work has not been submitted for any other degree or processional qualification except as specified.

The work presented in Chapter 1 & 5 of introduction has been published in International Journal of Molecular Biosciences, Volume 21, Issue 8, Page 2996, 23 April 2020, under the title "RNA-Targeted Therapies and High-Throughput Screening Methods" by authors Siran Zhu, Saul Rooney and Gracjan Michlewski.

The work presented in the results has been published in Nucleic Acid Research, Volume 49, Issue 11, 21 June 2021, Pages 6456–6473, under the title "RNA pull-down confocal nanoscanning (RP-CONA) detects quercetin as pri-miR-7/HuR interaction inhibitor that decreases α-synuclein levels" by authors Siran Zhu, Nila Roy Choudhury, Saul Rooney, Nhan T Pham, Joanna Koszela, David Kelly, Christos Spanos, Juri Rappsilber, Manfred Auer, and Gracjan Michlewski.

Siran Zhu

August 2021

Contents

Acknowledgements

Three years ago, I quit my job and said goodbye to my family in China, coming here in Edinburgh to fulfil my dream of working for a PhD degree and becoming an excellent scientist. I have made wonderful memories here and I would like to thank many people. Without them I would not have accomplished this challenging task.

My first and foremost gratitude goes to my supervisor Prof. Gracjan Michlewski. Thanks for having me as your student and offering me timely help whenever I had problems for my research. Gracjan came up with great ideas and set up this amazing project. Thanks for trusting me and acknowledging my progress. Gracjan will always be a model to teach me how to become a superb scientist.

I thank all my funding bodies, including Edinburgh Global Research Scholarship, the Deanery of Biomedical Sciences, and the Dioscuri Centre for RNA-Protein Interactions in Human Health and Disease in the International Institute of Molecular and Cell Biology in Warsaw, Poland.

I would like to thank everyone in the Michlewski's lab, especially Dr. Nila Roy Choudhury, Dr. Angela Downie, Dr. Gregory Heikel, Laura Croenen and Saul Rooney. Nila became my assistant supervisor for my last year. Thanks for supervising me every experiment, supporting and taking care of the whole lab, and selflessly sharing valuable experience. Nila also helped me to revise my publications and thesis and carry out experiments during paper revision. I cannot imagine how my project would have gone without her. Thank you Nila! Angie and Greg also helped me when I was new in the lab. I supervised Saul for his undergraduate project. His hard work paid off and got published. His work is an important part of my project and I do appreciate all his efforts. I had incredible time with everyone both in the lab, as well as when we hung out for fun. We always help each other and share our life experiences. Thanks everyone!

I want to thank everyone in my thesis committee, Prof. Till Bachmann, Prof. Maïwenn Kersaudy-Kerhoas and Dr. Tilo Kunath for giving me valuable suggestions, pointing out my shortcomings and encouraging me throughout the PhD project. I sent my sincere gratitude to all the members of our collaborative labs, especially Prof.

Manfred Auer, Dr. Nhan Pham, and Dr. David Kelly. Their profound knowledge helped me to broaden my understanding beyond my original scope and improve my research so much.

I also thank every student and staff in Infection Medicine. We were like a big family and shared so many happy moments. I have obtained priceless friendship with fellow students, especially Elizabeth Southam, Sarah Yusoff and Nelly Mak. We supported each other no matter who were sad or frustrated. We had unforgettable experiences exploring Edinburgh and other parts of UK. I must emphasise my acknowledgement to Lizzie. She took care of me during the tough time of lockdown when I felt panic about the pandemic. I also thank all my Chinese friends and previous flatmates, for helping me through difficulties in my daily life. Hope our friendship will continue even though we will live in different countries in the future.

Finally, and the most importantly, I thank my dear family, especially my parents and my husband. Thanks for your supports and understanding. I love you very much. This degree is not only mine, but also yours.

Abstract

MicroRNAs (miRNAs, miRs) are a class of small non-coding RNAs that regulate gene expression through specific base-pair targeting. The functional mature miRNAs usually undergo a two-step cleavage from primary miRNAs (pri-miRs), then precursor miRNAs (pre-miRs). The biogenesis of miRNAs is tightly controlled by different RNA-binding proteins (RBPs). The dysregulation of miRNAs is closely related to a plethora of diseases. Targeting miRNA biogenesis is becoming a promising therapeutic strategy.

HuR and MSI2 are both RBPs. MiR-7 is post-transcriptionally inhibited by the HuR/MSI2 complex, through a direct interaction between HuR and the conserved terminal loop (CTL) of pri-miR-7-1. Small molecules dissociating pri-miR-7/HuR interaction may induce miR-7 production. Importantly, the miR-7 levels are negatively correlated with Parkinson's disease (PD).

PD is a common, incurable neurodegenerative disease causing serious motor deficits. A hallmark of PD is the presence of Lewy bodies in the human brain, which are inclusion bodies mainly composed of an aberrantly aggregated protein named α-synuclein (α-syn). Decreasing α-syn levels or preventing α-syn aggregation are under investigation as PD treatments. Notably, α-syn is negatively regulated by several miRNAs, including miR-7, miR-153, miR-133b and others. One hypothesis is that elevating these miRNA levels can inhibit α-syn expression and ameliorate PD pathologies.

In this project, we identified miR-7 as the most effective α-syn inhibitor, among the miRNAs that are downregulated in PD, and with α-syn targeting potentials. We also observed potential post-transcriptional inhibition on miR-153 biogenesis in neuroblastoma, which may help to uncover novel therapeutic targets towards PD.

To identify miR-7 inducers that benefit PD treatment by repressing α-syn expression, we developed a novel technique RNA Pull-down Confocal Nanoscaning (RP-CONA) to monitor the binding events between pri-miR-7 and HuR. By attaching FITC-pri-miR-7-1-CTL-biotin to streptavidin-coated agarose beads and incubating them in human cultured cell lysates containing overexpressed mCherry-HuR, the bound RNA

and protein can be visualised as quantifiable fluorescent rings in corresponding channels in a confocal high-content image system. A pri-miR-7/HuR inhibitor can decrease the relative mCherry/FITC intensity ratio in RP-CONA. With this technique, we performed several small-scale screenings and identified that a bioflavonoid, quercetin can largely dissociate the pri-miR-7/HuR interaction. Further studies proved that quercetin was an effective miR-7 inducer as well as α-syn inhibitor in HeLa cells.

To understand the mechanism of quercetin mediated α-syn inhibition, we tested the effects of quercetin treatment with miR-7-1 and HuR knockout HeLa cells. We found that HuR was essential in this pathway, while miR-7 hardly contributed to the α-syn inhibition. HuR can directly bind an AU-rich element (ARE) at the 3' untranslated region (3'-UTR) of α-syn mRNA and promote translation. We believe quercetin mainly disrupts the ARE/HuR interaction and disables the HuR-induced α-syn expression.

In conclusion, we developed and optimised RP-CONA, an on-bead, lysate-based technique detecting RNA/protein interactions, as well as identifying RNA/protein modulators. With RP-CONA, we found quercetin inducing miR-7 biogenesis, and inhibiting α-syn expression. With these beneficial effects, quercetin has great potential to be applied in the clinic of PD treatment. Finally, RP-CONA can be used in many other RNA/protein interactions studies.

Lay summary

DNA is the basic information unit carried in the human body that make everyone unique. DNA codes instructions which our bodies follow to make RNA. There are two types of RNA. One called 'coding RNA' that guides the production of proteins, which are essential for building up all living organisms. While the other type is known as 'non-coding RNAs' that are not converted into proteins. MicroRNAs (miRNAs, miRs) are one of the subtypes of non-coding RNAs. MiRNAs can bind to specific coding RNAs and prevent them producing proteins. Abnormal miRNA levels can affect the functions of corresponding proteins, so are often linked to human diseases.

Parkinson's disease (PD) is a common disease affecting people's movement, especially in the elderly. The cause of PD is still not fully understood and there is no cure for it. Scientists have found that PD may be related to the deposits of a protein called α-synuclein (α-syn) in human brain. Eliminating these deposits and lowering α-syn levels may prevent progression of this disease.

MiR-7 is a miRNA that effectively reduces α-syn level. In PD patients, miR-7 level is often lower than it is in healthy people. The production of miR-7 can be slowed by a protein named HuR through direct binding. Therefore, drugs that stop HuR from interacting with miR-7 may help with miR-7 production, and decrease the level of α-syn, which will finally benefit PD patients.

Here we developed a new tool named RP-CONA. In RP-CONA, the miR-7 RNA will appear as green rings, while the HuR protein as red rings. If a drug stops HuR from interacting miR-7, the red rings will appear fainter but there will be no effect on the green rings. Using RP-CONA we found that a drug called quercetin can largely reduce the brightness of red rings. Additionally, we proved that quercetin could increase miR-7 levels while decreasing α-syn levels. By controlling the levels of RNA and protein, quercetin may become a drug used to treat PD in the future. Furthermore, as RP-CONA can be used to monitor the binding events of different RNA and proteins, it will be a very useful tool for the discovery of novel drugs for other human diseases.

Abbreviations

2DCS	two-dimensional combinatorial screening
6-OHDA	6-hydroxydopamine
AAV	adeno-associated virus
AD	Alzheimer's disease
AGO	Argonaute
ALP	autophagy-lysosomal pathway
APP	amyloid precursor protein
ARE	AU-rich element
ASO	antisense oligonucleotide
Aβ	amyloid-β
BBB	blood brain barrier
CMA	chaperone-mediated autophagy
CNS	central nervous system
CPC	cetylpyridinium chloride
CRISPR	clustered regularly interspaced short palindromic repeats
CSD	cold-shock domain
CSF	cerebrospinal fluid
CTL	conserved terminal loop
CV	coefficient of variation
DA	dopaminergic
DHTS	15,16-dihydrotanshinone-I
DMSO	dimethyl sulfoxide
DTT	dithiothreitol
EDTA	ethylenediaminetetraacetic acid
EMT	epithelial-mesenchymal transition
ER	endoplasmic reticulum
FDA	Food and Drug Administration
FITC	Fluorescein isothiocyanate
FP	fluorescence polarization
FRET	fluorescence resonance energy transfer

GFP	green fluorescent protein
HCS	high content screening
HCV	hepatitis C virus
HD	Huntington's disease
HDL	high density lipoprotein
HTS	high-throughput screening
HuR	Hu protein R
IC_{50}	half maximal inhibitory concentration
iPSC	induced pluripotent stem cells
Kd	dissociation constant
KO	knockout
L-DOPA	levodopa
LNA	locked nucleic acid
lncRNA	long non-coding RNA
mDA neuron	midbrain DA neuron
miRNA/miR	microRNA
MPP+	1-methyl-4-phenyl-pyridinium
MPTP	1-methyl-4-phenyl-1, 2, 3, 6-tetrahydrodropyridine
mRNA	messenger RNA
MS	mass spectrometry
MSI1/2	Musashi RNA binding protein 1/2
NAC	nonamyloid component
NGS	next-generation sequencing
NSCLC	non-small cell lung cancer
OA	oleic acid
PCR	polymerase chain reaction
PD	Parkinson's disease
PMSF	phenylmethylsulfonyl fluorid
pre-miRNA/pre-miR	precursor miRNA
pri-miRNA/pri-miR	primary miRNA
qRT-PCR	quantitative real-time PCR
RBP	RNA-binding protein

RIP	RNA immunoprecipitation
RISC	RNA-induced silencing complex
RNA	ribonucleic acid
RNAi	RNA interference
Ro	Ro 08-2750
ROS	reactive oxygen species
RP-CONA	RNA pull-down-confocal nanoscanning
RP-SMS	RNA pull-down-SILAC mass spectrometry
RRM	RNA recognition motif
SD	standard deviation
SDS-PAGE	sodium dodecyl sulphate–polyacrylamide gel electrophoresis
SEM	standard error mean
shRNA	small hairpin RNA
SMA	spinal muscular atrophy
snoRNA	small nucleolar RNA
SNP	single nucleotide polymorphism
SNpc	substantia nigra pars compacta
TH	tyrosine hydroxylase
TNF-α	tumour necrosis factor-α
TRBP	TAR RNA-binding protein
tRNA	transfer RNA
UPS	ubiquitin-proteasome system
UTR	untranslated region
α-syn	α-synuclein

Introduction

1. The biogenesis and functions of microRNAs

MicroRNAs (miRNAs, miRs) are a class of short non-coding RNAs that act as post-transcriptional regulators of gene expression. In 1993 the first miRNA, lin-4, was uncovered as a negative regulator of lin-14 gene expression during *Caenorhabditis elegans* development[1]. However, not until the discovery of the widely conserved let-7 in 2000[2] were these two small RNAs characterised as members of a large miRNA family which spans across most complex organisms[3]. According to the miRNA database miRbase v22, 2,654 mature human miRNAs have been annotated so far[4]. A recent estimation of the total number of bona fide miRNAs in *Homo sapiens* is 2,300[5].

1.1 The canonical pathway of miRNA biogenesis

Most miRNAs are derived from hairpin-like structures as a part of longer transcripts, named primary miRNAs (pri-miRNAs, pri-miR), which are mainly transcribed by RNA polymerase II (Pol II)[6]. In animals, pri-miRNAs undergo canonical biogenesis to produce mature, functional miRNAs (**Figure 1**). In the nucleus, pri-miRNA is cleaved by the Microprocessor. The Microprocessor complex consists of one molecule of the RNase III enzyme Drosha and two molecules of the DGCR8 protein (known as Pasha in flies and nematodes)[7, 8]. Drosha recognises the basal junctions (single strand-double strand junction) of pri-miRNAs and cuts at a specific distance, while DGCR8s bind to the apical junctions (double strand-terminal loop junction) and ensure accuracy of the cleavage activity[8, 9]. The product of the Microprocessor cleavage is a 60-80-nt stem-loop intermediate, termed precursor miRNA (pre-miRNA, pre-miR)[10]. The pre-miRNA is subsequently exported from the nucleus to the cytoplasm by the protein Exportin-5, in a RanGTP-dependent manner[11]. In the cytoplasm, another RNase III enzyme Dicer excises the apical loop of the pre-miRNA, leaving a ~22-nt miRNA duplex, with a ~2-nt 3' overhang on each strand[12]. Dicer associates with TAR RNA-binding protein (TRBP) and PACT, both of which are double strand RNA-binding cofactors involved in Dicer cleavage[13]. The duplex is loaded into Argonaute (AGO) proteins with the help of the Hsc70/Hsp90 chaperone,

to assemble the RNA-induced silencing complex (RISC). The strand with less 5' stability is usually retained and becomes the functional mature miRNA, while the passenger strand is ejected from the AGO proteins [28]. The mature miRNA derived from the 5' arm or 3' arm is annotated as 5p or 3p respectively.

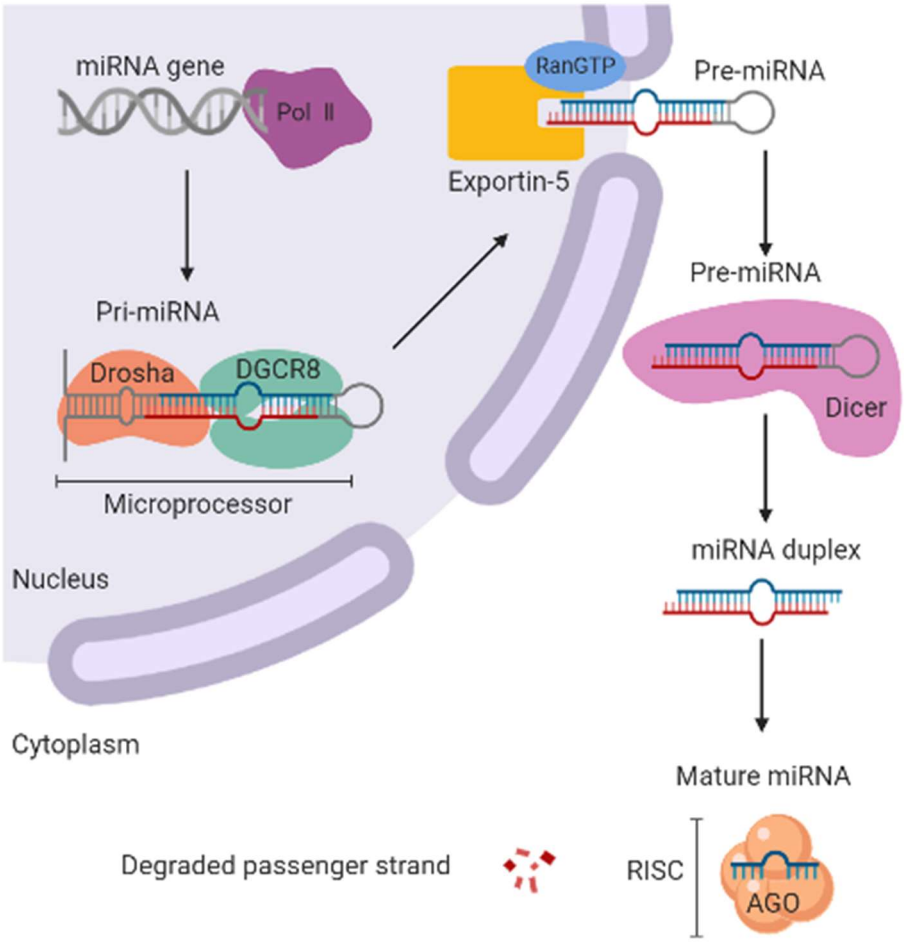

Figure 1 Canonical pathway of miRNA biogenesis. The pri-miRNA is transcribed from the miRNA gene by RNA polymerase II. The transcript harbours one (or more) hairpin-like structure which is recognised and cleaved by the Microprocessor to produce a stem-loop pre-miRNA. The pre-miRNA is exported to the cytoplasm by the aid of Exportin-5 and RanGTP. In the cytoplasm the pre-miRNA is further processed by Dicer, resulting in a miRNA duplex. The duplex is then loaded into AGO proteins where only one strand is selected as the mature miRNA and the passenger strand is ejected and degraded. The mature miRNA is incorporated into AGO proteins to form the RISC assembly. Figure was drawn in BioRender.

1.2 Non-canonical pathways of miRNA biogenesis

Non-canonical miRNAs are produced through Drosha or Dicer independent pathways. One class of miRNAs arise from intronic precursors, characterised as

mirtrons. Mirtrons rely on splicing factors and a lariat debranching enzyme, bypassing Drosha cleavage to generate pre-miRNA-like hairpins[14, 15]. The pathway then merges with the canonical biogenesis pathway for Exportin-5 mediated nuclear export and Dicer processing[15].

Another class of miRNAs that evade Microprocessor cleavage are endogenous small hairpin RNAs (shRNAs). In this pathway a m^7G capped pre-miRNA is yielded directly by Pol II transcription[16, 17]. The hairpin transcript is preferentially exported by Exportin-1 and proceed to Dicer cleavage in the cytoplasm. However, only the 3p-miRNA is favoured during AGO-mediated RISC assembly[17].

There are a few miRNAs derived from other types of small non-codling RNAs, such as tRNAs and small nucleolar RNAs (snoRNAs). These allow the generation of hairpin-like Dicer substrates from Drosha-independent processing mechanisms[18]. For example, murine γ-herpesvirus 68 (MHV68) pri-miRNAs are transcribed by Pol III harbouring tRNA moieties. tRNA processing enzyme tRNase Z is responsible for the initial cleavage, before the miRNAs entering the remaining maturation steps[19]. snoRNA ACA45 is identified as a miRNA precursor, which requires Dicer and an unknown nuclease during processing, but not the Microprocessor[20]. In *Giardia lamblia*, where Drosha is absent, miR-2 is originated from the GlsR17 snoRNA through Dicer digestion[21].

Mammalian miRNA-451 is a paradigm of a miRNA liberated through an alternative Microprocessor-dependent, but Dicer-independent pathway of biogenesis. Pri-miR-451 is first processed by Drosha and DGCR8. The resultant pre-miRNA, however, is too short to become a Dicer substrate, instead, the 3' arm of pre-miR-451 is directly cleaved by AGO2[22]. The 3' end is then further trimmed by the poly(A)-specific ribonuclease, to make the mature RISC[23].

1.3 Mechanism of miRNA-mediated gene silencing

Metazoan miRNAs function by base-pairing with the target mRNAs, usually at the 3' untranslated regions (UTRs). This leads to interference with the translational machinery and repression of the encoded proteins[24]. Target recognition is largely determined by complementarity between the seed region (2^{nd} to 8^{th} miRNA

nucleotides from its 5') and the target site, whereas the first nucleotide of the miRNA is bound by AGO[25, 26]. Additional base-pairs beyond the seed, especially nucleotides 13-16, also contribute to the target recognition[26].

MiRNA mediates gene silencing through translational inhibition or mRNA decay. These two modes are interconnected, with a dominant percentage of silencing activities caused by mRNA degradation[26].

In humans, only AGO2 possesses silencing activities among the AGO1-4 proteins[27]. Additional factors are recruited by AGO proteins to mediate gene silencing. GW182 proteins play a vital role in this, by interacting with AGO proteins and linking the downstream factors including the cytoplasmic poly(A)-binding protein (PABPC) and cytoplasmic deadenylase complexes PAN2–PAN3 and CCR4–NOT[28]. The mRNA decay process is initiated with deadenylation by PAN2-PAN3 and CCR4–NOT. The deadenylated mRNAs are then decapped by decapping protein 2 (DCP2), with the aid of a few decapping cofactors. After that, the mRNAs are degraded by 5′-to-3′ exoribonuclease 1 (XRN1)[29]. Meanwhile, translation repression is achieved by interfering with the translation initiation through the eukaryotic initiation factor 4F (eIF4F) complex (**Figure 2**). Unfortunately, the precise mechanism remains debated[28].

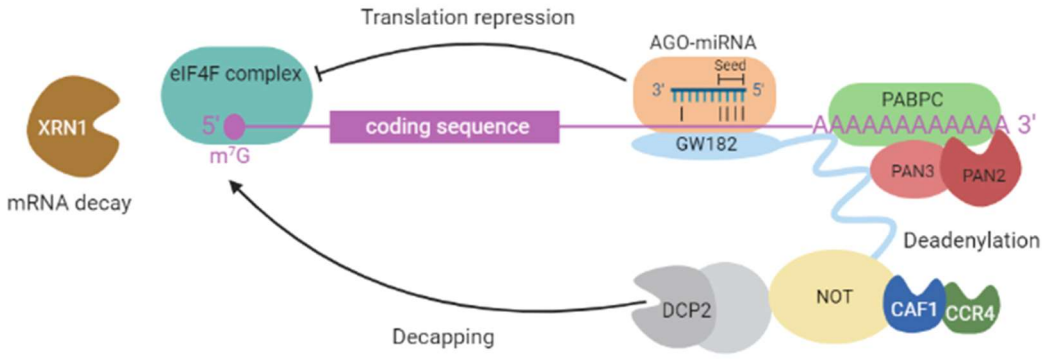

Figure 2 Mechanism of miRNA-mediated gene silencing in metazoan. The miRNA recognises the target mRNA (purple) at the 3'-UTR. The base-pairing occurs at seed region, with additional base-pairs formed at 3' of miRNA. The miRNA is incorporated with AGO to form the RISC complex, which interacts with GW182 at the N-terminus. GW182 in turn binds the PolyA-bound PABPC, as well as the

deadenylase complexes PAN2-PAN3 and CCR4-NOT. The mRNA deadenylation is catalysed by the PAN2-PAN3 and CCR4-NOT complexes. It is followed by decapping by DCP2 and its co-enzymes. Finally, the deadenylated and decapped mRNA is rapidly degraded by XRN1. Besides mRNA decay, miRNA also mediates gene silencing through the repression of translation initiation. This is achieved by interfering with the activity or assembly of the eIF4F complex. Figure was drawn in BioRender.

1.4 MiRNA functions implicated in diseases

MiRNAs are grouped into families, according to similarities in their seed regions[26]. One miRNA can target multiple genes. For example, human miR-155 has been identified to target 173 genes according to miRTarBase 2020[30]. Conversely, one mRNA can be regulated by more than one miRNA. Experimental evidence has shown that the human tumour suppressor gene PTEN (phosphatase and tensin homologue) is co-regulated by up to 83 miRNAs[30]. Strikingly, more than 18,000 miRNA-mRNA interactomes have been identified using the CLASH technique[31]. All these suggest that miRNAs assemble a complicated interactive network in the human genome that contributes to cellular function and homeostasis.

It has been well established that miRNAs play pivotal roles in controlling development and maintaining homeostasis in different organisms[32]. Despite that most of the endogenous miRNAs exhibit modest repression on individual targets *in vivo*, loss of a single miRNA can lead to serious phenotypical consequences[33]. This is partially due to some miRNAs targeting a wide spectrum of genes, which are key regulators of functional bioprocesses or signalling pathways. miR-155 knockout (KO) mice developed immunodeficiency, as miR-155 controls a range of genes involved in immune responses[34]. Since miR-128 targets are major components of the ERK2 network, miR-128 deletion activated ERK2 phosphorylation indirectly, resulting in an increased motor activity and fatal epilepsy in mice[35]. Furthermore, some miRNA-mediated phenotype changes can be observed in a stress-dependent manner. For example, the miR-208 KO mice only displayed impaired cardiac remodelling in different cardiac stress models, but not under normal physiological conditions[36]. This evidence implies that miRNAs are fine tuners of gene expression, which buffers expression networks against environmental or genetic stress[33].

However, miRNAs can present abnormal activities, as a result of genetic alteration,

epigenetic modification, as well as dysregulated biogenesis[37]. Aberrant levels of numerous miRNAs are tightly related to a variety of human diseases[38].

1.4.1 Cancer

MiRNA signatures have been identified in cancerous specimens with the help of next-generation sequencing (NGS) techniques, covering a wide range of solid tumours and hematologic malignancies[39]. Some miRNAs are known as tumour suppressors, by constantly silencing oncogenes, while some miRNAs are defined as oncomiRs, which drive oncogenic events[40]. However, the underlying mechanism could be much more intricate.

Epithelial-mesenchymal transition (EMT) is a common feature during tumorigenesis, contributing to invasive and metastatic activities of cancer cells[41]. Members of the miR-200 family are considered as EMT mediators through epigenetic regulation[42]. Briefly, CpG island hypermethylation drives miR-200 silencing, which upregulates the target proteins ZEB1 and ZEB2, and in turn, downregulates the downstream epithelial marker E-cadherin. These changes are responsible for EMT in a plethora of cancers, including colon cancer and lung cancer[42]. Additionally, emerging evidence has shown miR-200 modulating cancer cell apoptosis and cancer stem cell differentiation, emphasising its role as a tumour suppressor[43].

The c-Myc transcription factor coordinates a complex network in human malignancies with a diversity of miRNAs. Myc directly activates the transcription of the miR-17-92 cluster[44]. MiRNAs derived from this cluster are frequently overexpressed in tumours, such as lymphoma and colon cancer[40]. Myc also induces the expression of other miRNAs that are involved in cancer cell apoptosis, angiogenesis and metastasis, such as miR-9 and miR-214[45]. On the contrary, several miRNAs are negatively regulated by Myc, including the well-recognised tumour suppressor let-7[46]. This is related to post-transcriptional interruption of let-7 maturation, which will be described in detail in Chapter 4[47]. The expression of Myc is controlled by miRNAs directly or indirectly, presenting interesting feedback loops within the Myc/miRNA network[45].

1.4.2 Neurodegenerative disease

Some miRNAs are particularly enriched in the human adult brain and are fundamental to brain development[48]. Dysregulation of these miRNAs are frequently found in disorders of the central nervous system (CNS), especially in neurodegenerative diseases like Parkinson's disease (PD), Alzheimer's disease (AD) and Huntington's disease (HD)[49]. The pathology of PD and the related miRNAs will be systematically reviewed in the following two chapters.

In sporadic AD, the depleted levels of miR-29a/b are correlated with an elevated level of its target, BACE1[50]. BACE1 is a β-secretase that cleaves the amyloid precursor protein (APP), contributing to amyloid-β (Aβ) accumulation in AD[51]. The knockdown of miR-29a/b in mice resulted in neuronal apoptosis and ataxia phenotypes. However, the level changes of BACE1 were not observed *in vivo* and miR-29 knockdown-induced cell death seem to be correlated with the upregulation of the VDAC1 (voltage-dependent anion-selective channel 1) protein, a miR-29a target that was not predicted before[52].

The abnormal aggregation of the microtubule associated protein tau forms neurofibrillary tangles. This is another pathologic feature of AD, known as tauopathy, which is regulated by a plethora of miRNAs through various mechanisms[53]. The brain-specific miR-132 has shown neuroprotective effects in mice, and its levels in different brain regions are positively correlated with cognitive decline in AD patients[54]. MiR-132 regulates the alternative splicing of the tau mRNA by targeting the splicing factors PTPB2 and Rbfox1[55, 56]. It also targets the expression of kinases such as GSK3β and ITPKB, acetyltransferase EP300 as well as tau itself, thereby inhibiting hyperphosphorylation, acetylation and expression of tau[53, 54, 56, 57].

Interestingly, miR-29a and miR-132 are also dysregulated in HD patient cortices. This is accompanied by a mislocalised transcriptional repressor REST[58]. Moreover, the brain-enriched miR-9 is an important player in HD, as it targets the 3'-UTR of the REST mRNA while also being targeted by REST[59].

The case of PD will be described in detail in the Chapter 3.

1.4.3 Cardiovascular disease

The cardiac specific miR-208 regulates the balance between the isoforms of primary contractile protein MHC in response to cardiac stress and is essential for stress-induced heart hypertrophy and fibrosis in mice[36]. The inhibition of miR-208 reduces the cardiac remodelling and improves the cardiac function during heart failure in hypertension rat models[60]. Abnormal accumulation of miR-21 in cardiac fibroblasts contributes to cardiac dysfunction. MiR-21 activates ERK-MAP kinase signalling by inhibiting the expression of SPRY1 (sprouty homologue 1) protein in cardiac failure mouse models and induces metalloprotease-2 through repressing PTEN expression in ischaemia–reperfusion heart[61]. However, unlike miR-208, the miR-21 KO mice can still develop cardiac remodelling upon different stress, suggesting the existence of possible compensating pathways[62]. On the contrary, miR-1 and miR-133 play protective roles against cardiac hypertrophy[63]. Mice lacking miR-133a developed dilated cardiomyopathy with ventricular wall thinning and severe cardiac fibrosis, however, without evidence of cardiac hypertrophy[64]. Nevertheless, miR-1 exacerbates arrhythmogenesis in myocardial infraction rats[65].

In acute myocardial infraction patients, plasma miR-1, miR-133, miR-208 and miR-499 are extensively elevated[66]. More circulating miRNAs have been implied as indicators in different cardiovascular diseases, including coronary artery disease, atrial fibrillation, heart failure and hypertrophic cardiomyopathy. Although some miRNAs have shown inconsistencies in different studies, these miRNAs are still promising biomarkers for risk stratification, diagnosis, or prognosis for cardiac injuries[66, 67].

1.4.4 Metabolic disorders

MiR-122 is the most abundant miRNA in the human adult liver, accounting for more than 70% of the total hepatic miRNA expression. It regulates a myriad of genes that are involved in lipid metabolism and is critical for the survival of hepatitis C virus (HCV)[68, 69]. Antisense inhibition of miR-122 in mice lowers plasma cholesterol level, accelerates hepatic fatty acid oxidation, and slows down hepatic lipid synthesis. This is concurrent with a reduction of key lipogenic enzymes including stearoyl-CoA desaturase 1 (SCD1) and acetyl-CoA carboxylase (ACC2), despite that these

enzymes seem not direct targets of miR-122[70]. Circulating miR-122 is positively correlated with risks in obesity, type 2 diabetes, and non-alcoholic fatty liver disease (NAFLD)[68, 71].

MiR-143 is recognised as an inducer of adipocyte differentiation[72]. Consistent with this, the miRNA is overexpressed in mesenteric adipose in obesity mice, and the level is positively correlated with adipocyte differentiation markers, including leptin[73]. However, the changes of adipocyte morphology and the plasma leptin level were not seen *in vivo* when miR-143 was absent. Despite this, liver miR-143 is upregulated in both obesity and diabetes mouse models and it has shown an impairment on glucose metabolism through obesity-induced insulin resistance[74].

Adipose-enriched miR-222 is elevated in diabetes and negatively regulates insulin sensitivity. It is significantly upregulated in the plasma of diabetic patients, as well as in the high-density lipoproteins (HDL) from patients with familial hyperchosterolemia[75]. In particular, circulating miR-222 level is sensitive to insulin administration[76]. With this evidence, miR-222 is annotated as the most promising biomarker for metabolic diseases[77].

1.4.5 Immune disorders

MiRNAs are extensively involved in the regulation of immune homeostasis, controlling the development and function of immune cells in both innate and adaptive responses. Diseases associated with immune disorders, exemplified by autoimmune diseases and haematological cancers, are strongly related to miRNA dysregulation[78].

MiR-155 is a key player in the immune system by mediating the expression of numerous genes in natural killer (NK) cells, macrophages, T cells and B cells[79]. Suppressor of cytokine signalling 1 (SOCS1) and SH2-domain-containing inositol-5-phosphatase 1 (SHIP1) are negative regulators of the toll-like receptor pathway and are both repressed by miR-155 in immune cells. MiR-155-mediated SOCS1 inhibition is important in maintaining regulatory T (T_{reg}) cell homeostasis, NK cell response to viral infection, as well as antiviral T cell response during chronic infection[80]. The repression of SHIP1 activates Akt signalling and influences B cell

differentiation, which may contribute to leukaemia and lymphoma[81]. MiR-155 also targets the myeloid transcription factor PU.1 and activation-induced cytidine deaminase (AID), regulating immunoglobulin class switching[82].

MiR-155 is highly expressed in lymphoblastic leukaemia (ALL), chronic myeloid leukaemia (CML), Hodgkin's, Burkitt's and diffuse large B cell lymphoma (DLBCL)[78, 83]. The miRNA is also upregulated in autoimmune disorders, for instance, rheumatoid arthritis and multiple sclerosis[83, 84]. Due to its interactions with the cytokine network, miR-155 is implicated in inflammatory disorders like allergic inflammation and atopic eczema[84, 85]. Aside from miR-155, miR-146 is another miRNA that is frequently dysregulated in immune-related diseases, displaying critical roles in the regulation of immune system[78, 84].

1.4.6 Therapies targeting miRNAs

Owing to the pivotal roles of miRNAs in the onset and progression of diverse diseases, emerging miRNA-targeted therapeutics are being studied. Several of the therapies have entered clinical trials (**Table 1**). MiRNA antagonism and miRNA replacement are the two major approaches.

Table 1 Therapies targeting miRNA entering clinical trials

Drug	Disease	Target miRNA	Therapy type	Phase	Trial Number
AZD4076/ RG-125	NASH with type II diabetes/ pre-diabetes	miR-103/107	ASO(s)	I/II	NCT02612662 NCT02826525
TargomiRs	malignant pleural mesothelioma/ NSCLC	miR-16	miRNA mimic	I	NCT02369198
MRG-106/ Cobomarsen	cutaneous T-cell lymphoma/ mycosis fungoides	miR-155	ASO	I/II	NCT02580552 NCT03713320 NCT03837457
MRG-110/ S95010	wounds	miR-92a	ASO	I	NCT03603431
MRG-201/ MiR-29/ Remlarsen	keloid	miR-29b	miRNA mimic	II	NCT02603224 NCT03601052
MRX34	cancer	miR-34	miRNA mimic	I/II	NCT01829971 NCT02862145
RG-012/ SAR339375/ Lademirsen	Alport syndrome	miR-21	ASO	II	NCT03373786 NCT02136862 NCT02855268
RG-101	chronic hepatitis C	miR-122	ASO	I/II	2013-002978-49 2016-002069-77 2015-001535-21 2015-004702-42
SPC3649/ Miravirsen	chronic hepatitis C	miR-122	ASO	II	NCT02508090 NCT02452814 NCT01200420
CDR132L	heart failure	miR-132	ASO	I	NCT04045405

Mir-33 mediates cholesterol trafficking by targeting the cholesterol transporter ABCA1[86]. Antagonism of miR-33 induces plasma HDL in mice and monkeys, suggesting therapeutic potentials towards atherosclerosis, dyslipidaemia, and other metabolic diseases[86, 87]. Nevertheless, long-term therapeutic repression of miR-33 in high-fat diet mice may trigger adverse events such as hepatic steatosis and hypertriglyceridemia.

Miravirsen is the most advanced miRNA therapy to date. The drug candidate is a locked nucleic acid (LNA) modified antisense oligonucleotide (ASO), which sequesters miR-122 through sequence-specific hybridisation[88]. MiR-122 is essential for HCV survival. Upon binding with the 5'-UTR of HCV RNA, miR-122 protects the virus from viral RNA decay, activates viral protein translation, and supports virus

replication[69, 89]. Miravirsen treatment has shown prolonged suppression of HCV RNA levels in patients with chronic HCV infection, without observed viral resistance in a completed Phase II clinical trial[90]. RG-101 is another miR-122 targeted HCV therapy. The ASO is conjugated with N-acetylgalactosamine (GalNAc) to obtain an enhanced hepatocyte uptake[91]. Unfortunately, the trial of this drug was halted due to serious adverse events[92].

Cobomarsen (MRG-106) is an LNA-ASO inhibiting miR-155, a key regulator of the human immune system[93]. This drug targets mycosis fungoides, the most common form of cutaneous T-cell lymphoma. Cobomarsen has shown good potency in preclinical and Phase I studies and is being investigated in Phase II trials named SOLAR and PRISM[93, 94]. Lademirsen is a miR-21 antisense drug and has entered a Phase II trial for Alport syndrome (NCT02855268). The drug exerts kidney protective effects by activating PPARα pathway and ameliorating mitochondrial function[95]. CDR132L, an ASO targeting miR-132 exhibited promising safety profiles and functional cardiac improvements in patients with chronic ischaemic heart failure in a completed Phase 1b trial[96] (NCT04045405).

The first-in-class attempt of miRNA replacement therapy was MRX34, a liposomal mimic of the tumour suppressor miR-34a, that entered a clinical Phase I trial to treat multiple solid tumours[97]. However, the trial was terminated as 5 immune-related severe adverse events were reported. Another MRX34 Phase I trial targeting melanoma was also withdrawn (NCT02862145). TargomiRs is a miR-16 supplement therapy, where a double-stranded miR-16 mimic is packaged in EDV nanocells and equipped with an EGFR antibody targeting EGFR-expressing cancer cells[98]. In a Phase I trial named MesomiR-1, for the treatment of malignant pleural mesothelioma (MPM) and non-small cell lung cancer (NSCLC) (NCT02369198), TargomiRs showed good tolerance and safety in patients, with one patient giving significant objective response[98, 99]. Recently, the miR-29 mimic Remlarsen has completed a Phase I study including safety evaluation (NCT02603224) and has initiated its Phase II trial in keloid formation (NCT03601052). Moreover, several pre-clinical studies of miRNA replacement therapies for NSCLC have shown great clinical potential, including miR-200c, miR-29b and a miR-34/let-7 combinatory therapy[100].

Since none of these miRNA-targeted drugs have been approved so far, it is unclear whether miRNA antagonism or replacement would be appropriate therapeutic strategies, considering the complexity of regulatory networks and the fine-tuning characteristics of most miRNAs. Despite this, it is encouraging that a large number of studies focus on this field, especially for cancer therapies[101].

2. Parkinson's disease

2.1 Parkinson's disease (PD): epidemiology, aetiology, and pathology

PD is the second most common progressive neurodegenerative disease after AD. Clinical symptoms of PD are dominated by motor symptoms termed as parkinsonism, including resting tremor, muscular rigidity, bradykinesia, and postural instability[102, 103]. Some non-motor symptoms are also frequently observed in PD patients, such as sleep behaviour disorder, pain, restless legs syndrome and depression[104].

Generally, PD incidence rises with age, and a higher incidence has been found in males[105]. According to a meta-analysis including epidemiological studies before 2010, the worldwide prevalence of PD is 41 per 100,000 in the 40-49 age group, compared to 1,903 per 100,000 in individuals more than 80 years old[106]. There is an increasing trend of total incidence, and it has been estimated that PD will affect about 9 million people by the year 2030[107].

Unfortunately, the cause of PD is unclear, but it has been gradually accepted that PD is contributed by a combination of environmental and genetic risk factors. Pesticide exposure has been correlated with late-onset of PD, while smoking, caffeine intake and some metabolic factors are often conversely correlated with PD[108]. Genome-wide association studies have identified single nucleotide polymorphisms (SNPs) associated with an increased risk of PD in several loci, including SNCA, MAPT, LRRK2 and BST1[109]. Further, some specific mutations in SNCA, LRRK2, Parkin, DJ-1, PINK1 and VPS35 are monogenic risk factors for PD[110].

A characteristic feature of PD is a loss of pigmented dopaminergic (DA) neurons in the substantia nigra pars compacta (SNpc) of the midbrain. The resultant dopamine deficiency is considered as the major cause of the motor symptoms of PD. The loss of DA neurons can occur in the early stages of PD before the onset of motor symptoms and become widespread into other brain regions[111, 112]. Another hallmark of PD is the presence of Lewy bodies, which are intraneuronal, round inclusions largely composed by aggregated α-synuclein (α-syn) proteins[111-113]. Lewy pathology is not restricted to PD, but also found in other neurodegenerative disorders like AD and dementia with Lewy bodies (DLB) but is only a pathological biomarker for

PD[112, 114].

2.2 Molecular pathways of PD pathogenesis

PD pathogenesis is related to impaired protein homeostasis or proteostasis; aberrant synaptic structure and function; as well as mitochondria dysfunction[111]. In this section, I will focus on the α-syn aggregation, as the most prominent aspect of PD pathogenesis.

2.2.1 α-syn aggregation

α-syn is a small intracellular protein encoded by the SNCA gene. The first missense mutation identified in SNCA was p.A53T, from several independent families with PD[110, 115]. Another 5 point mutations (A30P, E46K, H50Q, G51D and A53E), and triplication of SNCA are also found in familial PD[110, 116]. Interestingly, SNCA duplication has been reported from both familial and sporadic PD[110, 117].

The N-terminus (residues 1 to 60) of α-syn is made up by a repeated 11-mer sequence harbouring a consensus KTKEGV and adopts an α-helical structure upon lipid binding. The middle nonamyloid component (NAC) domain (residues 61 to 95) is highly hydrophobic and prone to aggregate, while the C-terminal tail (residues 96 to 140) is flexible and unstructured. Interestingly, all the 6 aforementioned PD-related SNCA mutations are located in the N-terminus[112, 118]. All mutations except A30P are within the core of α-syn fibrils as presented in a Cryo-EM structure of recombinant α-syn (residues 1-121) fibrils[119]. Additionally, phosphorylation of specific residues, including S129 and S87, is also closely associated with α-syn aggregation[118].

Soluble, membrane-bound monomeric α-syn undergoes physiological multimerisation at presynaptic terminals, where it is believed to regulate synaptic transmission[118, 120]. However, α-syn assembles neurotoxic β-sheet stranded oligomers (protofibrils) under pathological conditions, which develop into amyloid fibrils and deposit into Lewy bodies[120].

The accumulation of aggregated α-syn seems a result of impaired proteostasis, mainly intracellular clearance mechanisms including autophagy-lysosomal pathway (ALP) and ubiquitin-proteasome system (UPS)[112, 121]. Moreover, there is a prion-like

hypothesis proposing that the α-syn aggregations can transmit from cell to cell, and region to region, leading to progressive propagation of pathology over the CNS. This hypothesis has been supported by accumulated evidence over the past decade[122].

The physiological function of α-syn is still under debate. Since α-syn is enriched in the presynaptic terminals of neurons, it has been strongly implicated in synaptic processes, including modulating synaptic vesicle trafficking, chaperoning SNARE-complex assembly, and regulating dopamine transporter (DAT)[123, 124]. α-syn is also implicated in regulation of mitochondrial function and Ca^{2+} homeostasis, as well as dopamine biosynthesis[125]. With respect to interaction with DNA and histones, α-syn localised in the nucleus may relate to transcription regulation and histone function, but this is still contentious[118, 123].

Due to the lack of knowledge of the physiological function of α-syn, how the dysregulated α-syn contributes to the pathogenesis of PD is poorly understood. The mechanism may involve a loss-of-function of α-syn in physiological forms, and a gain-of-toxicity from α-syn oligomers or fibrils[126]. The neurotoxicity of α-syn has been revealed in the interference of cellular structural components, endoplasmic reticulum (ER) and mitochondrial function, as well as protein degradation through ALP and UPS[118, 127].

2.2.2 Mitochondrial dysfunction

PD pathogenesis is closely associated with mitochondrial dysfunction and oxidative stress. Toxins inhibiting complex I, a critical component of the electron transport chain, can induce dopaminergic neurodegeneration in animals and humans. These toxins include 1-methyl-4-phenyl-1, 2, 3, 6-tetrahydrodropyridine (MPTP), rotenone, pyridaben and so forth[128]. Together with respiratory chain dysfunction, alteration of mitochondrial DNA and imbalanced mitochondrial homeostasis are major factors contributing to mitochondria-related pathogenesis in PD. The indispensable function of PINK1/Parkin in mitophagy, mitochondrial fusion and fission, as well as vesicular trafficking are key to the maintenance of mitochondrial homeostasis[129]. The protein deglycase DJ-1 is involved in mitochondrial respiration and reactive oxygen species (ROS) metabolism and plays a role in mitophagy independent from the PINK1/Parkin pathway[130, 131]. Mutations and dysfunction of these proteins in human

PD suggests the significance of mitochondrial activities during PD pathogenesis[131, 132]. Particularly, there is a reciprocal regulation between mitochondrial dysfunction and α-syn aggregation in PD, where oxidative stress and apoptosis are thought to be crucial in this relationship[131, 133].

2.2.3 Other pathways

Neurodegenerative diseases are often accompanied by neuroinflammation, which has shown great contribution towards PD progression, although the neuroprotective potential of cytokines like tumour necrosis factor-α (TNF-α) cannot be simply excluded[134]. Interestingly, pathogenic α-syn can provoke neuroinflammatory activities, while neuroinflammation stimulates α-syn pathology in mice midbrain[135]. Furthermore, motor cortex circuitry activities are altered as a result of dopamine deficiency, which can partially explain the movement disorders of PD[112]. That said, other pathways and more complex networks need to be elucidated to fully understand the cause of parkinsonism.

2.3 Treatment for PD

Currently, there is no cure for PD, but treatments that help to relieve symptoms are available. The main approach of medication is to rescue the decreased dopamine level, exemplified by levodopa (L-DOPA), dopamine agonists, monoamine oxidase type B (MAO-B) inhibitors and catechol-O-methyltransferase (COMT) inhibitors. Some non-dopaminergic drugs are under clinical investigation to treat specific symptoms. For example, amantadine, an N-methyl-d-aspartate receptor antagonist, has already been used in the clinic to relieve L-DOPA-induced dyskinesia. Moreover, a range of drugs are applied to treat the non-motor symptoms[103, 111, 112]. Beyond drug interventions, surgical interventions exemplified by deep brain stimulation (DBS) is available[103]. Transplantation of dopamine-producing cells is being tested in clinical trials[136].

2.4 Potential therapies for PD

There are a large number of therapeutic studies targeting different pathogenic pathways of PD, covering small molecules, RNA interference (RNAi), gene therapies as well as immunotherapies[137]. Most of the studies are focused on α-syn

pathologies, while a few on other targets such as DJ-1 and mitochondrial proteins.

2.4.1 Therapies targeting α-syn

It has been reviewed previously that there are 5 major strategies of potential treatments for synucleinopathies including PD, DLB and multiple system atrophy (MSA)[138]. Here strong candidate therapies and pioneering studies belonging to these 5 sections are introduced, and those that have entered clinical trials are summarised in **Table 2**.

Table 2 Therapies targeting α-syn pathologies in clinical trials for PD treatment

Name	Format	Pathway	Sponsor	Phase
NPT200-11	Peptidomimetic compound	Anti-α-syn aggregation	Neuropore therapies	I
Anle138b	Small molecule		MODAG GmbH	I
Lithium	Small molecule	Intracellular α-syn degradation	University at Buffalo	I
GZ/SAR402671	Small molecule		Genzyme/Sanofi	II
Ambroxol	Small molecule		UCL& Lawson	II
Nilotinib	Small molecule		Georgetown University	II
ABBV-0805	Antibody	Extracellular α-syn neutralisation	AbbVie	I
MEDI1341	Antibody		AstraZeneca	I
AFFITOPE® PD01A	Vaccine		AFFiRiS	I
AFFITOPE® PD03A	Vaccine		AFFiRiS	I
PRX002	Antibody		Roche	II
BIIB054	Antibody		Biogen	II

1) Repression of α-syn production.

   Delivery of adeno-associated virus (AAV)-shRNA provided a 35% knockdown of endogenous α-syn in the substantial nigra of rat brain. The RNAi therapeutic showed protective effects towards motor function, striatal DA terminals and nigral DA neurons in a rotenone induced PD model, without notable toxicity[139]. However, similar strategies led to nigrostriatal degeneration in the SNpc of rats when the α-syn was extensively reduced (more than 90%)[140]. This is confirmed in non-human primates, where PD-like patterns were developed by midbrain DA neurons upon α-syn knockdown[126]. The two contradictory cases are consistent with previous evidence that α-syn

is critical to neuron survival, and thereby supports the α-syn loss-of-function hypothesis for PD. Since α-syn pathology could be a combination of both gain-of-toxicity and loss-of-function, the knockdown efficiency of α-syn needs to be tightly controlled within a rational level, in terms of safety and efficacy of potential RNAi drugs[126, 138]. Indeed, another siRNA therapy reducing SNpc α-syn less than 50% didn't exhibit neurodegenerative side effects in normal squirrel monkeys[141]. Furthermore, an α-syn-silencing shRNA imbedded in a miR-30 backbone showed less toxicity *in vitro* but is still not applicable *in vivo*[142]. A diversity of novel vectors carrying RNAi oligonucleotides targeting α-syn are being explored and seem to be effective in preliminary studies[143].

The injection of AAV-ribozyme reduced α-syn expression in the SNpc of rat brain and protected DA neuron apoptosis from neurotoxin[144]. From a high-throughput screen, β2-adrenoreceptor (β2AR) agonists (eg. metaproterenol, clenbuterol and salbutamol) were identified to transcriptionally inhibit α-syn production. Salbutamol intake is associated with a lower risk of PD in Norwegians. Clenbuterol can cross the blood brain barrier (BBB) and rescue neurotoxicity in PD models *in vitro* and *in vivo*[145]. Synucleozid is a highly selective compound designed to bind a structured iron-responsive element (IRE) in the 5'-UTR of α-syn mRNA. The molecule inhibits loading of functional ribosomes and protects neurons against toxicity conferred by preformed α-syn fibrils[146].

2) Prevention of α-syn aggregation

NPT200-11 is an inhibitor of α-syn oligomerisation. It is developed based on a cyclic peptidomimetic compound designed to target the C-terminus of α-syn protein[147, 148]. Administration of the drug candidate has shown ameliorated α-syn pathology, reduced neuroinflammation and improved motor function in transgenic PD mouse models overexpressing human wildtype α-syn[147]. Neuropore therapies has completed a Phase I clinical trial of orally administrated NPT200-11, in collaboration with UCB Pharma (NCT02606682). The compound anle138b was identified from high-

throughput screenings which can prevent the formation of α-syn oligomers. It is supposed to bind intrinsically disordered proteins, α-syn aggregates in this case, but not monomeric proteins. In A30P human α-syn transgenic mice, intervention of anle138b lowered the level of brain α-syn oligomers, promoted motor performance, and extended disease-free survival[149]. A phase I study has been initiated recently to monitor the oral administration of anle138b in healthy subjects (NCT04208152).

Immunoglobulin based therapies are being extensively studied for PD solutions. Antibody fragments expressed intracellularly are termed intrabodies, such as single-chain variable fragments (scFVs; linked VH and VL) and nanobodies (single domain antibody; VH or VL only). Several intrabodies specifically inhibiting α-syn aggregation have been identified[150]. Among these, NbSyn87 and VH14 (NAC14) are anti-α-syn nanobodies. NbSyn87 interacts both monomeric and fibril forms of α-syn at C-terminus while VH14 binds the NAC domain of α-syn monomer[151]. Both nanobodies gain increased solubility and enhanced α-syn clearance by fusing with a proteasome-targeted PEST motif[152]. In α-syn-overexpressed PD model rats, PEST-fused NbSyn87 and VH14 treatment can attenuate pathological α-syn aggregation, restore striatal dopamine and induce functional motor recovery, to various extent[153].

Other therapeutic approaches focusing on intracellular α-syn aggregation activities includes bacteriophage capsid protein and small heat shock proteins (HSPs) [138].

3) Degradation of intracellular α-syn aggregates

Enzymes involved in ALP are attractive targets for enhancing α-syn degradation. Mutations in the glucocerebrosidase gene (GBA) occurs in 7 to 10% of PD cases, conferring a high risk for PD development[154]. A decreased activity of the lysosomal enzyme glucocerebrosidase (GCase) results in α-syn pathology and other PD-related symptoms, which can be rescued by exogenous GCase[155]. Two compounds focusing on GCaseA-related activities are now advanced in the development of PD therapy. GZ/SAR402671, a

brain penetrating small molecule, can reduce α-syn deposit, but not the soluble α-syn in an A53T-SNCA synucleinopathy mouse model, by inhibiting the synthesis of a GCase substrate[156]. Genzyme/Sanofi has launched a MOVES-PD Phase II trial of this oral available drug for PD patients carrying a GBA mutation (NCT02906020). Ambroxol, an FDA approved drug, is a GCase chaperone that restores GCase activity, reduces α-syn pathologies and ameliorates motor impairment in different PD rodent models[157]. In addition, oral administration of ambroxol in non-human primates can induce brain GCase activity[158]. In a recently completed Phase II clinical trial (NCT02941822), ambroxol was safe and well tolerated. Surprisingly, the drug decreased GCase activity and elevated α-syn levels in the cerebrospinal fluid (CSF) of PD patients both with and without GBA mutations. The outcomes, however, are interpreted positively as an improved GCase activity in brain and a facilitated extracellular export of α-syn from the brain parenchyma[159]. In the meantime, another independent placebo-controlled Phase II study of ambroxol treating PD dementia (NCT02914366) is currently ongoing, which will make the future of the drug clearer[160]. Moreover, another GCase chaperone, isofagomine, has shown promising therapeutic potential for PD in pre-clinical studies[161].

An alternative approach is to stimulate macroautophagy through mTOR dependent or independent pathways, exemplified by rapamycin and lithium respectively. Both molecules exhibit beneficial effects on relieving PD-related pathologies including α-syn aggregation and mitochondrial dysfunction, but with relatively poor selectivity[162]. A Phase I trial of lithium has initiated recruitment very recently to test if the drug can engage blood-based therapeutic targets implicated in PD (NCT04273932). By inhibiting a tyrosine kinase c-Abl, nilotinib treatment induced autophagic clearance and lysosomal deposition of α-syn in mice with synucleinopathies[163]. Nilotinib also reversed DA loss and motor deficits that were induced by overexpressed α-syn or neurotoxins[163, 164]. The drug has been approved in the clinical treatment of leukaemia, and it is now being repurposed for PD under Phase II trials (NCT02954978, NCT03205488). Long-term treatment of nilotinib is

safe and tolerated in PD patients and has exerted alterations on exploratory CSF biomarkers including oligomeric α-syn levels[165]. More agents are being explored by targeting ALP elements, for instance, transcription factor EB, chaperone-mediated autophagy (CMA) regulators as well as lysosomes directly[162].

4) Neutralisation of extracellular α-syn

While anti-α-syn intrabodies are expected to work intracellularly, full-length antibodies are utilised to sequester, neutralise, or clear extracellular α-syn, by means of either active or passive immunotherapies. Active immunotherapies utilise vaccines that can induce immune responses, especially antibodies targeting α-syn. So far, synthetic peptide or protein vaccines, DNA vaccines and dendric cell-based vaccines specifically designed for α-syn pathologies have been tested in preclinical PD models[166]. A biotechnology company AFFiRiS has translated their two vaccine candidates into clinics with a novel AFFITOPE® technique. These vaccines contain synthetic small peptides that mimic a C-terminal region of α-syn (residues 110-130). During preclinical development, active immunisation with these candidates reduced the accumulation of oligomeric α-syn and alleviated neurodegenerative pathology as well as motor deficits in different transgenic mouse models with synucleinopathies. The mechanism could be relevant with activated microglial α-syn clearance and boosted anti-inflammatory cytokines[167]. The lead vaccines AFFITOPE® PD01A and PD03A are well-tolerated and have triggered good immune responses in most PD patients during Phase I studies (NCT01568099, NCT02267434) and extended trials followed up[168].

Passive immunotherapies are normally achieved by the delivery of therapeutic antibodies that act on α-syn pathology with high affinity and specificity. A few α-syn-targeted antibodies have entered early phases of clinical trials, namely PRX002 (Roche), BIIB054 (Biogen), ABBV-0805 (AbbVie) and MEDI1341 (AstraZeneca)[138, 169]. PRX002 (prasinezumab) is a humanised monoclonal IgG1 antibody that targets α-syn aggregates by recognising the C-terminal epitopes. PRX002 is derived from a murine

antibody 9E4, which can effectively penetrate in the CNS, clear neuronal α-syn aggregates via autophagy, and ameliorate behavioural deficits in α-syn transgenic mice[170]. The antibody is thought to block the extracellular C-terminal truncation of α-syn, therefore preventing α-syn accumulation and propagation[171]. According to two Phase I studies launched by Roche and Prothena Biosciences (NCT02095171, NCT02157714), single or multiple intravenous infusion of PRX002 demonstrated favourable safety, tolerability, and pharmacokinetic profiles, along with a prolonged, dose-dependent reduction of free serum α-syn in both healthy volunteers and PD patients. The therapeutic antibody did not present immunogenicity, with no anti-drug antibody detected[172]. The outcomes support the design of an ongoing Phase II PASADENA trial (NCT03100149). Another human-derived IgG BIIB054 is highly selective towards pathological forms of α-syn, through interactions at the N-terminal residues. Passive immunisation of this antibody prevented the spreading of α-syn pathology while mitigating other PD-like symptoms in mouse models inoculated with preformed α-syn fibrils[173]. BIIB054 performed well in a Phase I clinical study (NCT02459886) and is being tested in a Phase II trial for treatment and prevention of PD (NCT03318523)[174].

5) Blockage of extracellular α-syn uptake

Until now, the knowledge about how α-syn is transmitted between neurons is very limited. It has been identified that a transmembrane protein lymphocyte-activation-gene3 (LAG3) is required for the endocytosis of α-syn fibrils. LAG3 antibodies attenuated α-syn transmission and pathology *in vitro*. Deletion of LAG3 gene substantially delayed α-syn fibril-induced DA neuron loss and behavioural deficits *in vivo*[175]. Since LAG3 is a well-identified immune checkpoint, cancer immunotherapies targeting this receptor are under extensive investigation both pre-clinically and clinically[176]. Thus, it is promising to anticipate LAG3 antibodies to be purposed in PD treatment. Another study has shown that α-syn internalisation is also mediated by heparan sulfate proteoglycans (HSPGs). Importantly, the uptake of α-syn fibrils can be blocked by heparin and chlorate in murine neural precursor cells, because of an interfered HSPG function[177]. Therefore, specific HSPG

inhibitors would be interesting agents that prevent the propagation of pathological α-syn.

Here in each category, only the most promising or best developed disease-modifying strategies are described. A comprehensive summary of all the α-syn-targeted therapeutic attempts for PD treatment can be found in a recent review[143].

2.4.2 Other targeted therapies

Glycerol phenylbutyrate is being evaluated in a repurposed Phase I study for PD (NCT02046434). Prior research has demonstrated that phenylbutyrate can induce expression of DJ-1, which works to relieve PD pathologies through multiple mechanisms *in vitro* and *in vivo*[178]. By targeting the mitochondrial pyruvate carrier (MPC), a compound MSDC-0160 exhibits strong therapeutic potentials in different animal models of PD. The modulation of MPC poses an immediate effect on mitochondrial metabolism and mTOR signalling, rescuing autophagy and attenuating neuroinflammation[179]. Before the initiation of the first-in-human study of PD, MSDC-0160 has shown good safety profiles in patients with diabetes or AD[180]. Several gene therapies delivering glutamic acid decarboxylase (GAD), glial cell line-derived neurotrophic factor (GDNF) or neurturin gene have once entered clinical stage, but the trials were terminated due to financial reasons or failures to meet the end points[181]. Aiming for replacing dopamine loss in PD brains, gene therapies (VY-AADC01 and ProSavin) encoding dopamine biosynthetic enzymes, have seen positive clinical outcomes in individuals with PD[182]. Agonists of glucagon-like peptide-1 (GLP-1), including exenatide, lixisenatide and liraglutide, are medications prescribed for Type 2 diabetes. Having shown neuroprotective effects relevant with reduced insulin resistance, these drugs are under investigation in ongoing clinical trials[183].

3. MiRNAs and Parkinson's disease

The miRNA regulatory network is crucial to the homeostasis of the CNS. Dysfunction of proteins responsible for miRNA biogenesis is strongly associated with PD. Adults carrying 22q11.2 deletions, where DGCR8 is located, have a higher occurrence of early-onset PD[184]. Notably, deletion of this chromosome segment in mice resulted in coordination deficits, along with elevated α-syn expression in the SNpc[185]. Dicer depletion is detrimental to neuron phenotypes, especially midbrain DA neurons[186]. Dicer-ablated mice developed progressive locomotor abnormalities, due to a loss of DA neurons in the SNpc[187]. Differentially expressed miRNAs are identified in brain and blood specimens from patients with idiopathic PD[188]. The expression of key proteins involved in PD pathogenesis are regulated by a plethora of miRNAs (**Figure 3**). The following sections provide a systematic review of those PD-related miRNAs and their implicated targets, especially α-syn.

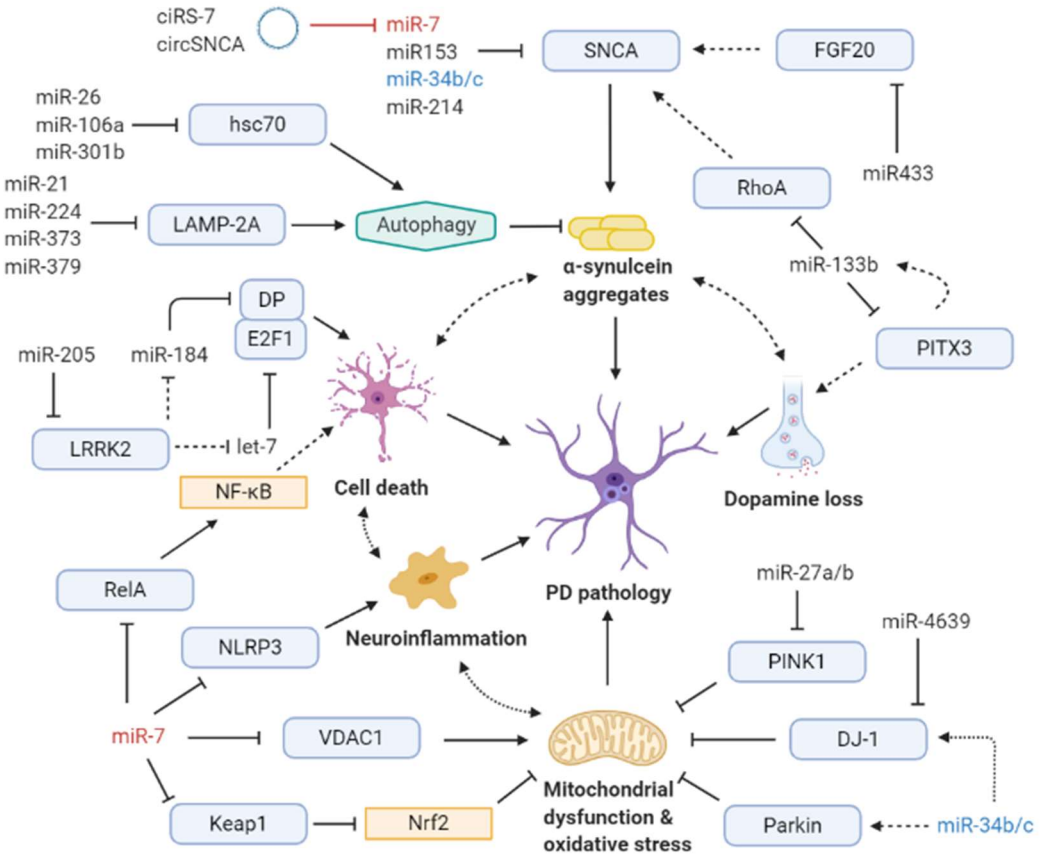

Figure 3 MiRNA-mediated network in PD pathology. MiRNAs regulate expression of target genes that are involved in the PD pathology including α-syn

aggregation, neuronal cell death, neuroinflammation, loss of dopamine, mitochondrial dysfunction and oxidative stress. These pathological activities are highly connected in PD. MiRNAs showing up more than once are highlighted with the same colour. Regulations known to be indirect are linked with dashed lines. Circular RNAs functioning as miR-7 sponges are presented. Figure was drawn in BioRender.

3.1 MiR-7

MiR-7 is the most established miRNA that regulates α-syn. miR-7 effectively prevents endogenous α-syn expression in HEK293T cells, through a conserved site embedded in the 3'-UTR of the α-syn mRNA[189]. The interaction site was validated using a luciferase reporter, where the α-syn 3'-UTR was encoded downstream of the luciferase gene. Overexpressed miR-7 can significantly reduce the luciferase levels, which can be rescued by minor mutations within the seed region on α-syn 3'-UTR. MiR-7 inhibitors can elevate the endogenous level of α-syn in human DA neuroblastoma SH-SY5Y cells and promote the expression of luciferase bearing wildtype α-syn 3'-UTR, but not mutated α-syn 3'-UTR[189]. Notably, miR-7 mediated α-syn silencing protects mouse neuroblastoma cells from oxidative stress[189].

The DA neurotoxin MPP+ (1-methyl-4-phenyl-pyridinium) is metabolised from MPTP. Both toxins are widely applied to induce PD models in cells or in animals. A significant decrease of miR-7 level was observed in MPP+ treated SH-SY5Y cells, as well as in the midbrain of MPTP administrated mice, possibly contributing to the corresponding α-syn upregulation[189].

MiR-7 is significantly downregulated in the SNpc of PD patients, accompanied by evident accumulation of α-syn aggregates[190]. MiR-7 knockdown induced both monomeric and oligomeric α-syn levels in mice SNpc. A loss of tyrosine hydroxylase (TH)-positive neurons in SNpc and reduced striatal DA were also observed. Although locomotor deficits were not seen upon miR-7 loss, a slight trend towards weakened motor activities was noticed in mice[190].

MiR-7 activity can be suppressed by ciRS-7, a circular RNA identified as a miR-7 sponge, resulting in elevated levels of miR-7 targets, including α-syn[191]. Of note, the expression of ciRS-7 and miR-7 is largely overlapped in the mouse brain[191]. Circular SNCA RNA (circSNCA) serves as another miR-7 sponge, which is upregulated in

MPP+ induced neurons and downregulated upon treatment of a dopamine agonist drug pramipexole. Decreased sponge RNA levels contributes to restored miR-7 levels and a re-suppressed α-syn expression, consequently attenuating cell apoptosis while enhancing autophagy in a PD cell model[192].

Dysregulated miR-7 and α-syn can be reversed by an antioxidant, Astaxanthin, in an MPP+ induced PD model *in vitro*. A knockdown of miR-7 in an MPTP-induced mouse model leads to a deteriorated neuron injury, including athletic performance, that can be rescued by Astaxanthin[193]. Atrazine (ATR) is a herbicide that has been previously found to pose DA toxicity in rats[194]. Rats exposed to ATR manifested miR-7 downregulation along with α-syn upregulation in SNpc[195]. Manganese (Mn) exposure is also neurotoxic and implied an association with parkinsonism[196]. Reduced miR-7 level has been detected in Mn exposed SH-SY5Y cells, which partially contributes to the raised α-syn mRNA level[197].

Remarkably, injection of miR-7 mimics into the striatum of MPTP-induced PD mice ameliorated PD pathogenesis, including less DA neuronal degeneration and microglial activation. This highlights a key role of miR-7, which directly inhibits α-syn in neurons while prevents NLRP3 inflammasome activation in microglia[198]. Beyond PD, miR-7 delivery showed neuroprotective effects against cerebral ischemia *in vivo*, in an α-syn dependent manner[199].

On the other hand, miR-7 facilitates the clearance of α-syn and its aggregates by inducing autophagy in neuron-like cells differentiated from human neural progenitor cells. Particularly, this is independent of the 3'-UTR of α-syn mRNA[200].

Furthermore, miR-7 also relieves PD pathogenesis through other direct targets via the 3'-UTR of their mRNAs. By targeting the expression of RelA, a subunit of the nuclear factor-κB (NF-κB) transcription factor complex, miR-7 protects neurons from MPP+ induced cell death through the relief of NF-κB depression[201]. Strikingly, this signalling does not rely on the miR-7/α-syn axis[201]. The same research group declared that miR-7 decreased mitochondrial permeability transition pore (PTP) through VDAC1 inhibition and accordingly protected neurons treated by MPP+[202]. As α-syn is associated with VDAC1 in brains expressing A53T α-syn mutants, which is also relevant to the opening of mitochondrial PTP, miR-7 may work through the

repression of both VDAC1 and α-syn synergistically[202]. The Junn group also identified that miR-7 activated the Nrf2 pathway via inhibiting Keap1, thereby reducing oxidative stress in the similar PD cell model[203]. Another study showed that the neuron protective role of miR-7 against MPP+ induced apoptosis was achieved through Bax and Sirt2[204]. Additionally, the long non-coding RNA (lncRNA) SNHG1 negatively regulates miR-7 as a competing endogenous RNA (ceRNA). MiR-7 was upregulated as a consequence of SNHG1 knockdown, which in turn repressed NLRP3 inflammasome and attenuated neuroinflammation in the SNpc of MPTP-induced PD mice[205].

In summary, all this evidence points to a paramount importance of miR-7 in the aetiology of PD.

3.2 MiR-153

MiR-153 has shown inconsistent expression profiles in different types of PD body fluid. Reduced miR-153 levels were detected in saliva from PD patients, compared to non-neurological controls, though the levels didn't alter along with disease progression or duration[206]. However, a correlation between the levels of miR-153 and α-syn in PD saliva was not observed[206]. In contrast, exosomal miR-153 was overexpressed in PD CSF[207]. Moreover, plasma miR-153 levels didn't show significant changes in PD patients[208].

MiR-153 is also firmly confirmed as an effective regulator of α-syn, with a conserved binding site in α-syn 3'-UTR across vertebrates[209]. In a transgenic parkinsonian mouse model, neural and circulating miR-153 were both downregulated, mirrored by a corresponding α-syn accumulation[210]. The negative regulation of miR-153 on endogenous α-syn mRNA and protein was confirmed in human M17 neuroblastoma cells[210].

Similar to miR-7, the expression pattern of miR-153 is negatively correlated with α-syn mRNA in different tissues and neuronal developmental stages[209]. Transfection of miR-153 significantly decreased both mRNA and protein levels of overexpressed α-syn in HEK293 cells. Importantly, co-transfection of miR-7 and miR-153 exerted additive effects on α-syn[209]. The combination of miR-7 and miR-153 also mediated a

significant reduction on endogenous α-syn expression in primary neurons[209]. MiR-153 alone, or together with miR-7, can protect neurons against MPP+ induced toxicity by activating mTOR signalling[211]. Interestingly, co-expression of miR-7 and miR-153 rescued the AKT activity, whereas neither of them showed this effect when working alone. In contrast, miR-153, but not miR-7, can repress the MPP+ activated P38, but the repression is compensated by the addition of miR-7. Although both miRNAs activated SAPK/JNK phosphorylation significantly, there was no detectable accumulative effect[211]. In another study, HEK293 cells stably overexpressing both miR-7 and miR-153 displayed a significantly lower luciferase level compared to wildtype cells, as a response to transient transfection of a luciferase reporter bearing α-syn 3'-UTR. The repression could be relieved by MPP+ mediated mitochondrial ROS[212]. Collectively, the coordination between miR-7 and miR-153 remains to be elucidated and is likely to be target-dependent.

One C to A mutation on α-syn 3'-UTR within the seed region of miR-153 has been identified in one sporadic PD case, but not in familial PD cases[213]. The single nucleotide variance attenuates the suppressive role of miR-153 through α-syn 3'-UTR, as shown in a luciferase reporter assay[213]. It is obvious that more cases are required to support the correlation between this mutation and PD pathogenesis.

A conflicting study reported that miR-153 was upregulated upon MPP+ treatment in DA neuroblastoma and it promoted oxidative stress by targeting the Nrf2/HO-1 pathway[214]. Also, serum miR-153 levels were elevated in a limited number of PD patients[214]. Similarly, miR-153 was elevated in a 6-hydroxydopamine (6-OHDA) induced neurodegenerative cell model, which can be repressed by a neuroprotective compound Tanshinone IIA through the miR-153/Nrf2 axis[215].

3.3 MiR-133b

MiR-133b is specifically enriched in healthy midbrain, but deficient in the same region of PD patients[186]. The miRNA forms a negative feedback regulatory machinery with the transcription factor Pitx3 and mediates the maturation and function of midbrain DA neurons[186]. However, PD-associated miR-133b reduction was only identified at the tissue level of whole SN, but not in individual DA neurons[216]. Furthermore, miR-133b KO mice showed neither altered midbrain DA

neuron morphology, nor impaired motor function[217]. The level of circulating miR-133b was significantly downregulated in PD patients, but it did not show a correlation with age, disease severity or motor phenotypes[208, 218].

It remains controversial whether and how miR-133b coordinates with α-syn. In MPP+ induced PD model cells, miR-133b can ameliorate PD-like phenotypes and decrease α-syn mRNA level. It was attributed to an RhoA inhibition mediated by miR-133b[219]. RhoA is a negative regulator of neurite extension and it controls α-syn level indirectly[220]. Yet more evidence is required to prove this miR-133b/RhoA/α-syn pathway. It has been reported that miR-133b inhibits α-syn expression through a direct interaction on the 3'-UTR of α-syn mRNA, using a luciferase reporter assay[221]. However, the targeting site is not canonical, since the first 2-nt of the seed don't bind. Moreover, all the 10-nt of the binding site were completely mutated during site validation, which may cause unexpected changes that affect luciferase expression, in addition to the abolishment of miR-133b binding[221]. So, the conclusion of a direct regulatory mechanism is not convincing. In addition, the correlation of miR-133b with α-syn level in DA neurons was not detected[216].

3.4 MiR-34b and miR-34c

The clustered miR-34b and miR-34c are downregulated in a wide range of PD brains as shown in a global miRNA profiling[222]. Depletion of miR-34b/c exerts indirect inhibition on the expression of Parkin and DJ-1, and triggers mitochondrial dysfunction and oxidative stress[222]. Another study confirmed the reduction of striatal miR-34b in early PD[223]. Moreover, miR-34b regulates the striatal adenosine A_{2A} receptor, suggesting a novel regulatory pathway during PD progression[223]. Interestingly, neither miRNA display level changes in CSF of PD patients and only miR-34c is significantly reduced in CSF from MSA patients[224].

Both miR-34b and miR-34c repress α-syn expression in human DA SH-SY5Y cells. The inhibition of both miRNAs induced α-syn expression and aggregation[225]. TargetScan predicted three binding sites on α-syn 3'-UTR for each miRNA, with two miR-34b sites and one miR-34c site proven by luciferase reporter assays[225]. MiR-34b/c were downregulated upon extremely low-frequency magnetic fields (ELF-MF) exposure in DA SH-SY5Y cells, as a consequence of promoter CpG island

hypermethylation[226]. This stimulates degenerative phenotypes via miR-34b/c mediated α-syn regulation. However, similar effects were observed in mouse neurons, even though mouse α-syn lacks miR-34b/c binding sites[226]. Therefore, it is possible that more factors are involved in the MF-induced neuron pathogenesis. Nevertheless, miR-34b can induce rather than inhibit the expression of a luciferase carrying α-syn 3'-UTR and this can be abolished by SNPs that block miR-34b targeting[227]. This rare phenomenon may involve other proteins or lncRNAs that compete at this region.

3.5 MiR-214，miR-199a and miR-3120

MiR-214 is regulated during neuronal differentiation, and it modulates neurite outgrowth *in vitro*[228]. A significant reduction of serum miR-214 has been found in PD patients, along with a remarkable decrease of miR-141 and miR-193a-3p[229]. Bioinformatic predictions imply these three miRNAs share a common target, DGKQ, an enzyme being associated with susceptibility and risk contribution towards PD[229].

The level of miR-214 is attenuated in the midbrain of MPTP induced PD mouse models, as well as in MPP+ induced SH-SY5Y cells, with a concomitant increase of α-syn expression level. Notably, these changes could be reversed by a neuroprotective natural compound Resveratrol[230]. MiR-214 regulates α-syn expression both *in vitro* and *in vivo* through the α-syn 3'-UTR, as shown in a luciferase reporter study[230]. However, the binding site has not been validated yet.

Pri-miR-199a-2 is transcribed in a cluster with pri-miR-214 on chromosome 1, while pri-miR-199a-1 is encoded on chromosome 19. Partial miR-199a shares an E-box promoter with miR-214, which allows them to be co-regulated transcriptionally[231]. MiR-199a showed a significantly downregulated expression pattern in the peripheral blood mononuclear cells (PBMC) of PD patients, as well as in induced pluripotent stem cells (iPSC) derived DA neurons from PD patients[232].

MiR-214 has a mirror miRNA named miR-3120, produced by the opposite strand from the same locus. MiR-3120 harbours a distinct seed sequence from miR-214, thereby they are assumed to target different mRNAs[233]. Intriguingly, α-syn 3'-UTR bears two predicted sites for miR-3120, and one site for miR-214 at a different position[234]. The relationship of miR-3120 and PD has not been reported so far.

3.6 MiR-433

Significant reductions of miR-433 level have been identified in both plasma and CSF from human diagnosed with PD[208, 235]. A PD-associated SNP located in the 3'-UTR of fibroblast growth factor 20 (FGF20) could disrupt the binding of miR-433. The miRNA is likely to indirectly downregulate α-syn expression by silencing FGF20[197, 236]. However, another study claimed that this SNP and miR-433 variations were not identified in their cohorts of PD patients[237].

3.7 MiR-132

MiR-132 is significantly downregulated in the brain of A30P α-syn transgenic mice and PD individuals[188, 238]. The interaction between brain miR-132 and 3'-UTR of α-syn was identified by HITS-CLIP (high-throughput sequencing of RNA isolated by crosslinking immunoprecipitation), which is not predicted by TargetScan[239]. Evidence supporting the regulatory role of miR-132 on α-syn is not available.

3.8 MiRNAs targeting CMA proteins

The downregulation of CMA proteins lysosomal-associated membrane protein 2A (LAMP-2A) and heat shock cognate protein 70 (hsc70) is in parallel with an upregulation of 7 miRNAs in PD brain, of which miR-21, miR-224, miR-373 and miR-379 negatively regulate LAMP-2A via its 3'-UTR, while miR-26, miR-106a and miR-301b target hsc70[186, 240]. Overexpression of these miRNAs mediates a depression of LAMP-2A or the hsc70 protein, resulting in neuronal accumulation of α-syn *in vitro*[240]. This suggests that the impairment of α-syn degradation could be contributed by miRNAs through inhibition of CMA proteins. The miR-21/LAMP-2A/α-syn axis was confirmed in PD model cells and mice[241]. MiR-21 also directly targets the anti-apoptotic protein Bcl-2. The depression of miR-21 enhanced cell survival in MPP+ treated DA neuronal cells, by inhibiting apoptosis, as well as ROS and neuroinflammation[242].

3.9 MiRNAs targeting other PD-related proteins

Upregulated plasma miR-4639 is considered as a biomarker in early PD diagnosis. By targeting DJ-1, overexpressed miR-4639 caused oxidative stress and neuronal death *in vitro*[243]. MiR-27a/b negatively regulate PINK1-mediated mitophagy,

whereas chronic mitophagic flux dramatically stimulates the level of miR-27a/b, suggesting a negative feedback circuit upon mitochondrial damage[244]. MiR-5701 attenuates the expression of proteins crucial to mitochondrial and lysosomal functions. In line with this, the miRNA contributes to the dysfunction of mitochondria and ALP, and further sensitises 6-OHDA-stimulated neuronal cell death[245].

Pathogenic LRRK2 interferes the inhibitory effect of let-7 and miR-184 on their targets, impairing the maintenance and function of DA neurons in flies[246]. LRRK2 expression is significantly elevated in PD brains, with an inversely correlated miR-205 level. As an inhibitive factor of LRRK2, miR-205 can rescue impaired neurite outgrowth caused by pathogenic LRRK2[247]. Moreover, the lncRNA MALAT1 can hybridise to miR-205 and exacerbate the MPP+ induced DA neuron death via the miR-205/LRRK2 axis[248]. Interestingly, MALAT1 can positively control the neuronal α-syn levels[249]. Thus, there might be a potential pathway that miR-205 indirectly downregulates α-syn by antagonising MALAT1.

A lower level of miR-124 has been found in the plasma of PD patients, as well as the SNpc of PD model mice[250, 251]. Acting on multiple signalling pathways, miR-124 shows neuroprotective effects against neurotoxins *in vitro* and *in vivo*[251, 252]. Moreover, this miRNA is also inhibited by the lncRNA MALAT1[253]. Strikingly, the intracerebral administration of therapeutic miR-124 nanoparticles induced neurogenesis and neuron migration, which further enhanced brain repairment and mitigated motor deficits in 6-OHDA lesioned mice[254].

Collectively, miRNAs are playing vital roles in PD pathogenesis. Some miRNAs are potential PD biomarkers, despite discrepancies of miRNA profiling among different studies. MiRNA supplement or antagonism render an alternative for novel PD therapies, especially through inhibiting the synthesis of α-syn.

4. Regulation of miRNA biogenesis

The biogenesis of miRNAs is tightly controlled at both transcriptional and post-transcriptional levels, giving rise to tissue-specific and development-specific expression patterns of different miRNAs[255, 256]. A summary of examples is presented in **Figure 4**. Regulatory factors affecting miRNA biogenesis are divided by different processing stages, including transcription, Microprocessor-mediated processing, Dicer cleavage, as well as turnover of mature miRNA.

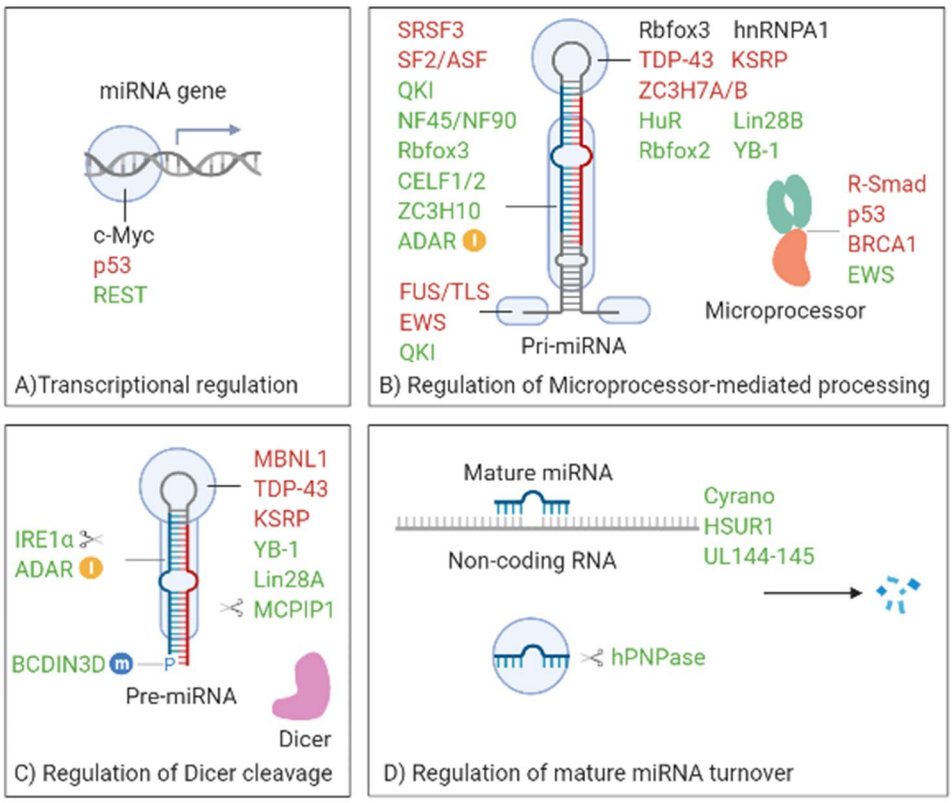

Figure 4 Regulation of miRNA biogenesis. (A) Transcriptional regulation mediated by transcription factors on the miRNA genes. (B) Regulation of Microprocessor-mediated processing occurs at the terminal loop, stem region or flanking single strand of pri-miRNAs. Alternatively, some proteins modulate the function of the Microprocessor complex directly. (C) Regulation of Dicer cleavage on the terminal loop, stem region or 5' phosphate of pre-miRNAs. (D) Regulation of mature miRNA turnover by RNase or non-coding RNAs. Proteins or non-coding RNAs that positively regulate miRNA biogenesis are present in red, while negative factors are displayed in green. Those that play dual roles are in black and the targeting sites are specified. Ribonucleases are labelled as scissors. Enzymes performing A to I editing are notified by a yellow "I" symbol, and the methyltransferase is shown with a blue "m" symbol.

4.1 Transcriptional regulation

The transcriptional regulation of miRNAs is similar to that of protein-coding RNAs, with their promoters controlled by a selection of transcription factors[255]. As mentioned in the Chapter 1, c-Myc alters the expression of the selected miRNAs that are associated with cancer progression. Moreover, p53 promotes transcription of the miR-34 family, whereas the production of miR-124 is transcriptionally inhibited by REST-mediated activities[257].

4.2 Post-transcriptional regulation

The conserved terminal loops (CTLs) of miRNA precursors are important features of post-transcriptional regulation. CTLs are recognised and bound by specific RNA-binding proteins (RBPs), resulting in an upregulation or downregulation of mature miRNA levels[258].

The following sections will begin with the post-transcriptional regulation of let-7 by Lin28 proteins, as their interactions are the best characterised examples. Then I will focus on the main research object - miR-7 and its regulatory RBPs, and end up with a brief review of other RBP/miRNA pairs.

4.2.1 Let-7 family and Lin28 proteins

Let-7 was first discovered as a regulator of stem cell differentiation in *C.elegans*. There are 9 mature let-7 miRNAs in the human let-7 family, encoded by 12 different genomic loci[259]. The biogenesis of let-7 is blocked by Lin28 proteins through the interactions with the let-7 CTL[260, 261]. Let-7a-3 is an exception that evades Lin28a regulation[262]. Lin28 is abundantly expressed in undifferentiated cells and its expression declines during differentiation, which is reciprocal to mature let-7 levels[263]. Lin28a and Lin28b are two paralogs in human cells, sharing a conserved cold-shock domain (CSD) and two tandem Cys-Cys-His-Cys (CCHC) zinc finger domains. The CSD domain and CCHC motifs bind the terminal loop of let-7 precursors at the GNGAY and GGAG motifs respectively[264]. Lin28a recruits TUT4 (terminal uridylyltransferase 4) together with the E3 ligase Trim25 to induce a 3'-uridylation of pre-let-7, thereby, preventing Dicer processing[265]. Subsequently, the uridylated pre-let-7 is degraded by the exoribonuclease DIS3L2[266]. Alternatively,

Lin28b retains pri-let-7 in the nucleoli where the Microprocessor is not available[267].

4.2.2 MiR-7, and HuR/MSI2

There are three miR-7 loci in the human genome. The predominant expressed pri-miR-7-1 resides in intron 15 of the hnRNP K gene on chromosome 9, while pri-miR-7-2 and pri-miR-7-3 are transcribed from chromosome 15 and 19 respectively. The levels of pri-miR-7-2 and pri-miR-7-3 are about 100-fold lower than pri-miR-7-1 level in human tissues[268]. A qRT-PCR test in glial cells also confirmed that pri-miR-7-1 was abundantly expressed while pri-miR-7-2 and pri-miR-7-3 were almost undetectable[269]. Mature miR-7 is highly enriched in brain and endocrine pancreas[270]. As described in the previous chapter, miR-7 is a negative regulator of α-syn and the overexpression of miR-7 has shown therapeutic benefits to reverse PD pathologies. In addition, miR-7 binds to EGFR mRNA via two of the three predicted binding sites in its 3'-UTR, inhibiting EGFR expression in human glioblastoma cells post-transcriptionally[271].

Previously, our group has identified that the biogenesis of miR-7 is regulated by two RBPs, namely HuR (Hu protein R, ELAVL1) and MSI2 (Musashi RNA binding protein 2), using RNA pull-down–SILAC mass spectrometry (RP–SMS)[268, 272]. The CTL of pri-miR-7-1 is specifically recognised and bound by HuR. HuR recruits MSI2 and the two RBPs work synergistically to increase the rigidity of the pri-miR-7 stem-loop, thereby preventing the cleavage step by Microprocessor. This also explains the brain enrichment of miR-7 where MSI2 is weakly expressed[268].

4.2.3 Other miRNA regulations through terminal loop interactions

As many as 74 pri-miRNAs have been identified with their terminal loops conserved across vertebrates[273]. Generally, regulatory RBPs initiate conformational changes of miRNA precursors via their terminal loops and affect the recruitment of key enzymes during miRNA biogenesis.

HnRNP A1 (heterogeneous nuclear ribonucleoprotein A1) functions by binding to the CTLs but show dual roles towards different target miRNAs. The tandem RNA recognition motifs (RRMs) of hnRNP A1 recognise two UAG motifs of pri-miR-18a CTL and allosterically relax the stem-loop structure of the miRNA precursor,

facilitating the Drosha-mediated processing[274]. In contrast, hnRNP A1 negatively regulates the biogenesis of let-7a by competing with the positive factor KSRP (KH-type splicing regulatory protein)[275]. Aside from let-7, KSRP also promotes the maturation of a few miRNAs via CTL interaction, including miR-26b, miR-20, miR-106a, miR-21, and miR-16[276].

Lin28a inhibits the biogenesis of miR-9 through a uridylation-independent mechanism, which is distinct from the let-7 regulation[277]. MBNL1 competes with Lin28 for a UGC motif within the CTL of pre-miR-1. When MBNL1 is sequestered by abnormal expansions of CUG or CCUG repeats in myotonic dystrophy, Lin28 enhances TUT4-mediated uridylation on pre-miR-1 and inhibits Dicer processing[278]. The MCPIP1 ribonuclease directly cleaves the terminal loop of target pre-miRNAs and inhibits miRNA biogenesis by antagonising with Dicer, including miR-146a, miR-16, let-7g, miR-135b, and miR-143[279].

ZC3H7A and ZC3H7B both recognise the CTL of pri-miR-7-1, and positively regulate miR-7 levels[280]. YB-1 interacts the CTL of the miR-29b-2 precursors and antagonises both Drosha and Dicer during miRNA maturation. Downregulation of miR-29b by overexpressed YB-1 is responsible for the cell proliferation in glioblastoma[281]. Rbfox3 can positively or negatively regulate the processing of selected miRNAs by binding to the terminal loop or stem region respectively. In the cases of pri-miR-15a and pri-miR-485, the inducive or reductive effects of Rbfox3 is independent of its consensus UGCAUG recognition motif[282]. However, a later study elucidated that the conserved RRM of Rbfox2 recognised the GCAUG motif located at the terminal loop of pri-miR-20b and pri-miR-107, and prevented their nuclear processing[283]. An hnRNP protein TDP-43 facilitates the processing of some pre-miRNAs, such as pre-miR-143 and pre-miR-574, in the cytoplasm by binding to their terminal loops and the Dicer complex. The nuclear TDP-43 protein associates with the Microprocessor as well as the pri-miRNAs to promote the Drosha cleavage, such as pri-miR-132 and pri-miR-558[284].

4.2.4 MiRNAs regulated through other mechanisms

Beyond CTL, post-transcriptional regulation also occurs at other regions of the selected miRNA precursors, or acts on relevant enzymes and cofactors, where RNA

modification, editing and turnover are involved[285].

The biogenesis of neuronal miR-9, miR-125b and miR-132 is enhanced by FUS/TLS. FUS/TLS is recruited to the chromatin encoding these miRNA transcripts, where it aids Drosha loading[286]. With the same mechanism, a subset of miRNAs is positively regulated by EWS, including miR-34a, miR-122 and miR-222[287]. Meanwhile, EWS downregulates the expression of Drosha and plays an opposite role to inhibit miRNA processing, as in the cases of miR-29b and miR-18b[288].

SF2/ASF is an SR protein splicing factor encoded by the SRSF1 gene. The RBP promotes the maturation of miR-7, miR-29b, miR-221 and miR-222. Moreover, SF2/ASF interacts with a putative motif on the stem of pri-miR-7 and induces the conversion to pre-miR-7[289]. The processing of miR-7 is also negatively controlled by the NF45-NF90 complex, which binds pri-miR-7 at an unspecified region and contributes to EGFR signalling and tumourigenesis of hepatocellular carcinoma[290]. Similarly, QKI isoforms attenuate the efficiency of miR-7 production by sequestering pri-miR-7 via QKI response elements. This affects the proliferation of glia cells driven by the EGFR pathway[269]. ZC3H10 binds the basal segment of pri-miR-143 and inhibits Drosha processing[280]. CELF1 and CELF2 block the biogenesis of pri-miR-140 under a similar process[280]. SRSF3 specifically recognises a conserved CNNC motif at the basal junction of pri-miRNAs and enhances the Microprocessor-mediated processing[291]. In particular, a G to A mutation on the CTL of pri-miR-30c-1 rearranges the secondary structure of the stem-loop and improves the accessibility of SRSF3 to CNNC binding, resulting in an increased level of miR-30c processing[292]. Of note, SRSF3 not only promotes the efficiency of miRNA processing, but also regulates a widespread unproductive (nick) or alternative (inverse) processing[293].

Modulating proteins belonging to the Microprocessor complex can also trigger post-transcriptional regulation. TGF-β and BMP stimulate the processing of pri-miR-21 and pri-miR-199a. The transducers of TGF-β and BMP signals, R-Smads, associate with a consensus region at the stem of miRNA transcripts, as well as the RNA helicase p68 (or DDX5) within the Microprocessor, allowing the post-transcriptional regulation through this pathway[294]. The tumour suppressor p53 also promotes miRNA maturation by recruiting p68 in response to DNA damage, including miR-16,

miR-143 and miR-145[295]. Another tumour suppressor BRCA1 interacts with the Microprocessor components Drosha and p68, and enhances the biogenesis of let-7a, miR-16, miR-145 and miR-34a by recognising the branched site on the secondary structure of their precursors. BRCA1 also recruits p53, Smad3 and an RBP DHX9 during this process[296].

RNA modification and editing can affect the loading of miRNA biogenesis enzymes. An RNA methyltransferase BCDIN3D modifies the 5'monophosphate of pre-miR-145, and blocks the Dicer cleavage[297]. ADAR1 and ADAR2 mediate adenosine (A) to inosine (I) editing on pri-miR-142 and destabilise the stem-loop structure. Consequently, Drosha processing is inhibited and mature miR-142 undergoes degradation by a RISC component Tudor-SN[298]. ADAR1 edits pri-miR-151 at two specific positions, leading to accumulation of an edited pre-miR-151 that is not further processed by Dicer[299]. ADAR2 also edits the precursors of oncogenic miR-221, miR-222 and miR-21, and reduces the level of mature miRNAs, which prevents proliferation and migration of glioblastoma[300]. Interestingly, the biogenesis of miR-376a is negatively modulated by ADAR2, but independently of its catalytic RNA editing activity[301].

The stability of miRNAs can be affected by ribonuclease or non-coding RNAs. An ER transmembrane kinase-endoribonuclease IRE1α is activated upon ER stress, terminating the miRNA process by direct cleavage of the selected pre-miRNAs (pre-miR-17, pre-miR-34a, pre-miR-96 and pre-miR-125b)[302]. A 3'-5' exoribonuclease hPNPase is responsible for the degradation of specific mature miRNAs in human melanoma cells, including miR-221, miR-222 and miR-106b[303]. A lncRNA Cyrano specifically promote miR-7 degradation through base-pair hybridisation, resulting in a universal reinstation of miR-7 targeted mRNAs[304]. Viral non-coding RNA HSUR 1 from *Herpesvirus saimiri* can cause mature miR-27a decay during T cell infection, in a sequence-specific and binding-dependent manner[305]. UL144-145 RNA is produced by human cytomegalovirus. The RNA induces turnover of mature miR-17 and miR-20a through interactions at the intergenic non-coding region, which is essential to viral replication during lytic infection[306].

5. Therapeutic strategies targeting protein/miRNA interactions

As has been described before, the development of miRNA-based therapies is still in very preliminary stages. Thus, it will be even more challenging to seek a cure for PD with this category of drugs. The knowledge of miRNA post-transcriptional regulation opens a new field of therapeutic strategies targeting miRNAs, which is, finetuning miRNA levels by intervening with their biogenesis. This chapter describes the known miRNA modulators and their therapeutic implications, with particular focus on those targeting HuR/MSI2 and miR-7. Current high-throughput screenings (HTS) methods identifying protein/RNA disruptors are also discussed.

5.1 Targeting let-7/Lin28

Let-7 inhibits the expression of many oncogenes such as HMGA2, KRAS and MYC, marking its function as a general tumour suppressor for carcinomas, exemplified by its role in lung cancer and multiple myeloma[259, 307, 308]. Interestingly, the let-7 family also targets the 3'-UTR of Lin28a and Lin28b mRNAs, downregulating the expression of Lin28 proteins in embryonic neural stem (NS) cells[261]. This suggests a negative feedback mechanism of the let-7/Lin28 pathway. Lin28a/b overexpression is found in a plethora of advanced carcinomas, where let-7 levels are frequently repressed[309]. Lin28 mediated let-7 inhibition leads to the let-7 targets being reinstated. This contributes to accelerated tumorigenesis, increased metastasis, as well as resistance to radiation and chemotherapies[310]. Based on this evidence, the interruption of let-7/Lin28 is considered an attractive therapeutic approach[307]. A group of small-molecule let-7/Lin28 disruptors have been identified using different HTS strategies[311]. Most of the compounds block the CSD domain of Lin28 proteins. These lead compounds can induce the level of let-7 family members by up to 6-fold; reduce the expression of oncogenic let-7 targets; and exert anti-cancer effects in human malignant cell lines[311].

5.2 Targeting HuR/MSI2/miR-7

5.2.1 RRMs of HuR and Musashi proteins

HuR is expressed ubiquitously across human tissues. The protein often stabilises mRNAs bearing AU-rich elements (AREs) in their 3'-UTRs. Most of the targeted

ARE-RNAs encode oncogenic proteins, highlighting a crucial role of HuR in regulating the development and progression of multiple human cancers[312]. Inhibition of this RBP can sensitise tumour cells to cancer therapies[313, 314]. HuR contains three RRMs. The N-terminal tandem RRMs (RRM1 and RRM2) are responsible for ARE binding. The C-terminal RRM (RRM3) can bind ARE and poly-A, with suggested roles in protein-protein interaction, dimerisation, post-transcriptional modifications and stabilisation[315, 316]. However, the roles of RRM3 in the context of full-length HuR remain controversial[315-317].

Human Musashi proteins have two paralogues MSI1 and MSI2, sharing approximately 80% amino acid similarity. Both proteins have two highly conserved N-terminal RRMs. MSI1 mainly binds (G/A)$U_{1–3}$AGU sequences, whereas MSI2 prefers ACCUUUUUAGAA and UAG motifs[318, 319]. The C-terminal region of Musashi proteins harbours protein interaction sites and modulates the translation of Musashi targets[320]. Musashi proteins are normally expressed in stem and progenitor cells and regulate cell differentiation and organ development[321]. Aberrantly high expression of Musashi proteins is associated with aggressive tumours, consistent with their roles as translational modulators of some well-recognised oncogenic signalling pathways, including Numb/Notch and PTEN/mTOR[321]. Overexpressed Musashi proteins are found in gliomas, colorectal adenocarcinomas, pancreatic adenocarcinomas, breast cancer, lung cancer and hematopoietic malignancies[319, 321, 322]. Interestingly, the 3'-UTR of MSI1 mRNA, but not MSI2, bears ARE targeted by HuR and MSI1 expression is positively regulated by HuR in glioblasomas[323]. Notably, transcripts targeted by MSI2 are significantly enriched in neurodegenerative diseases, including PD, implying a potential role of MSI2 in the development of this disease[319].

5.2.2 Oleic acid facilitates miR-7 production through remodelling of HuR/MSI2

Oleic acid (OA) is an 18-carbon ω-9 monounsaturated fatty acid. OA binds the RRM1 of MSI1 and MSI2 and induces an allosteric conformational change that abrogates their RNA binding activities[324]. Based on this, our group identified OA as a disruptor that dissociated the interaction between pri-miR-7 and HuR/MSI2. Interacting with both RBPs, OA remodels the miRNA/RBP complex and rescues

miR-7 biogenesis in HeLa extracts and cells (**Figure 5**)[325].

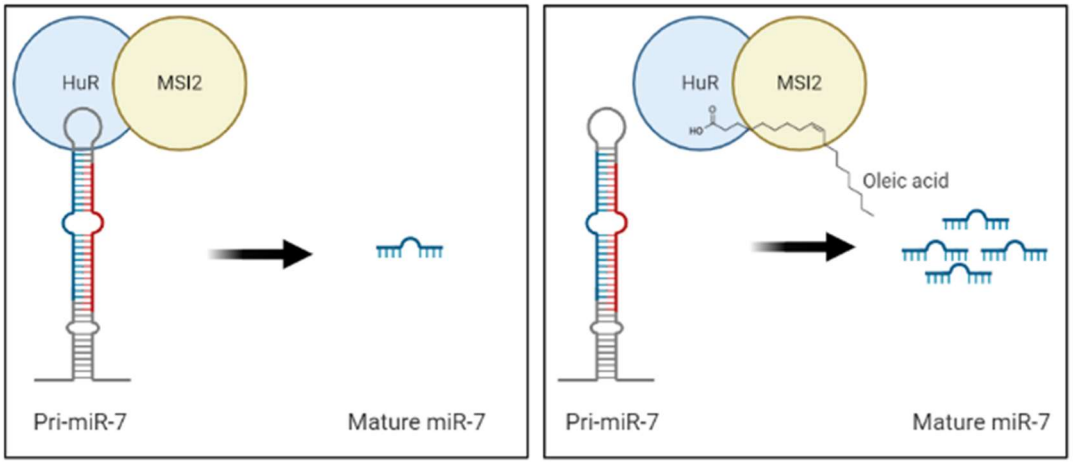

Figure 5 OA facilitates miR-7 production through remodelling of HuR/MSI2. Left: HuR binds the terminal loop of pri-miR-7 and recruits MSI2 to inhibit the processing activities. Right: OA interacts with both HuR and MSI2 and disrupts the association between HuR and pri-miR-7, facilitating the generation of mature miR-7. Figure was drawn in BioRender.

5.2.3 Small-molecule disruptors of HuR and MSI2 identified from HTS

There are several ligands blocking the target mRNA from binding HuR or MSI2. Whether they can affect the association of pri-miR-7 like OA requires further investigation. Novartis' MS-444 is the best-known HuR inhibitor that effectively interferes with the interaction of ARE-RNAs, decreases the RNA stabilities and reduces ARE cytokine (e.g. interlukin-6) expression in primary human monocytes[314, 326, 327]. The molecule acts at the RRM1-RRM2 interface of HuR and prevents protein homodimerisation[326]. Notably, anti-cancer effects of MS-444 through HuR inhibition were observed in malignant pancreatic [314, 328], colorectal [329], melanoma[330] and glioma cells[331] *in vitro* or in xenograft mouse models. With a similar mechanism, DHTS (15,16-dihydrotanshinone-I), a bioactive component from a traditional Chinese medicine practice, prevents the mRNA of TNF-α from interacting with HuR[332]. The natural compound, along with its derivative tanshinone mimics, also exhibits anti-tumour properties in an HuR-dependent manner in human breast cancer, pancreatic cancer, colon cancer and glioma cells[332, 333]. Other potent ARE/HuR disruptors have been reviewed in our recent publication, including CMLD-2, cetylpyridinium chloride (CPC), mitoxantrone, azaphilone-9, quercetin, suramin and etc (**Figure 6**)[311].

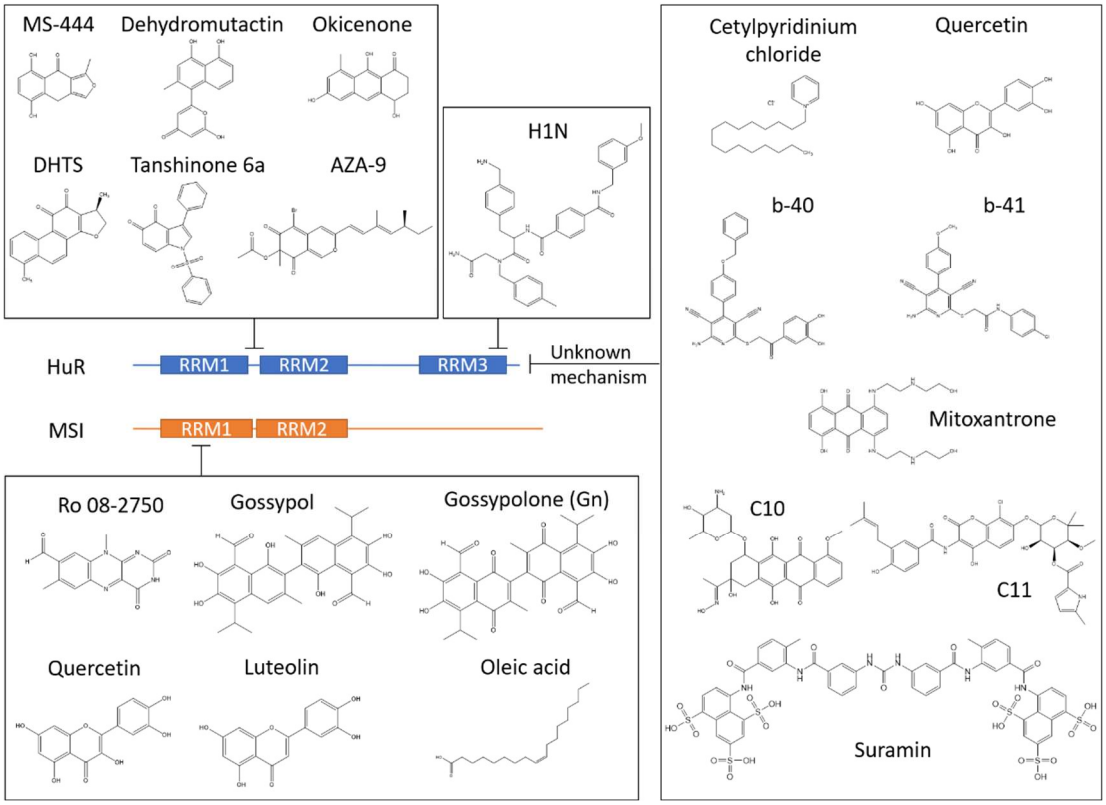

Figure 6 Small molecules inhibiting HuR or MSI1/MSI2 from binding to the target mRNAs. RNA recognition motifs (RRMs) of HuR are shown in blue, and RRMs of MSI are shown in orange. Small molecules interrupting RNA binding activities of HuR or MSI are displayed. The known targeting RRMs are indicated. HuR inhibitors with unknown mechanisms are shown. Compounds are drawn in ChemDraw.

Ro 08-2750 (Ro) is a highly selective MSI2 inhibitor that represses the expression of MSI2-targeted mRNAs, such as TGFBR1 and c-MYC[334, 335]. Notably, Ro treatment can prevent leukemogenesis in myeloid leukaemia model mice, with a possible mechanism of downregulating intracellular c-MYC levels[335]. (-)-gossypol is extracted from cottonseed, with its major metabolite named gossyopolone (Gn). Both (-)-gossypol and Gn are inhibitors of Musashi proteins and can impede tumorigenesis of colon cancer *in vitro* and *in vivo* by regulating the Numb/Notch signalling[336]. Luteolin is an analogue of quercetin, a disruptor of HuR/TNF-α mRNA[337]. Surprisingly, both luteolin and quercetin function as MSI1 inhibitors and display similar anti-proliferation effects in glioblastomas[338]. This suggests that quercetin and its structural analogues are promising candidates as dual inhibitors of HuR and MSI2, and further as potential miR-7 enhancers.

So far, structural knowledge of HuR and MSI2 is very limited, as no full-length protein structures have been solved. Most of the ARE/HuR disruptors target the RRM1-2, while the sole RRM3 ligand has shown weak interference with the full-length ARE/HuR complex[315]. How RRM3 coordinates with the N-terminal RRMs is yet to be completely understood. For Musashi proteins, all the above inhibitors interact with RRM1 (**Figure 3**)[311]. The binding modes of the molecules with full-length Musashi proteins are unknown. Based on a model structure of RNA-bound MSI1-RRM1-2, it has been deduced that the tandem RRMs will adopt certain orientations upon RNA binding[339]. Moreover, unlike let-7 and Lin28 proteins, the interaction between pri-miR-7, HuR and MSI2 has not been studied yet, and the binding motif is completely unknown. Collectively, to identify potent miR-7 enhancers by disrupting HuR/MSI2 is challenging. Although utilising the already identified inhibitors of HuR or Musashi proteins can extensively narrow down the scale of assay and increase the rate of success, reliable screening and validation platforms are extremely necessary.

5.3 Targeting biogenesis of other miRNAs

The discovery of small-molecule miRNA regulators has been previously reviewed, summarising three major strategies including HTS from large libraries; focused screening using known RNA binders, such as aminoglycosides; as well as drug design targeting RNA secondary structures or relevant RBPs[340].

Streptomycin is an aminoglycoside antibiotic, as well as a miR-21 inhibitor[341]. Streptomycin blocks Dicer cleavage through direct binding to pre-miR-21, rescuing the level of miR-21 targeted proteins, such as PDCD4 (Programmed Cell Death 4). This could translate into potential for cancer therapy[341]. Further studies identified small molecules and peptides with anti-cancer potentials by binding miR-21 precursor and blocking its processing[342].

Disney *et al.* developed a novel focused screen technique known as dubbed two-dimensional combinatorial screening (2DCS), which identifies interacting pairs of compound/steric RNA structures utilising a hybridisation of a small molecule microarray and an RNA element library[343]. With the help of a 2DCS against compounds consisting of two aminoglycosides derivatives, G Neo B was recognised

as a binder of the internal loop of pri-miR-10, which prevents Drosha processing during miR-10 biogenesis[344]. A new computational approach termed Inforna was developed, by integrating the output of 2DC2 with RNA structure data and StARTS, a statistical approach that predicts the affinity and selectivity of RNA binders. With the help of Inforna, a highly selective lead compound Targaprimir-96 was identified to target miR-96 precursor and inhibit its maturation[345]. Similarly, a miR-544 inhibitor was identified using Inforna by targeting the UU internal loops present at the Drosha and Dicer cleavage sites of the miR-544 precursor. The inhibitor induced hypoxic apoptosis response and sensitised tumour cells to chemotherapies[346]. Targapremir-210 binds to the miR-210 precursor at the Dicer cleavage site and selectively inhibits the biogenesis of this miRNA. Treatment of Targapremir-201 prevents tumorigenesis of hypoxic triple negative breast cancer in a mouse xenograft model[347]. Recently, the Disney group developed a novel ligand from Inforna, which was designed to target the Dicer site as well as an adjacent bulge of pre-miR-17, pre-miR-18a and pre-miR-20a. Of note, conjugating with a bleomycin A5 cleaving module, the ligand drives cleavage of the entire pri-miR-17-92 cluster and inhibits all 6 miRNAs, further rescuing cancerous phenotypes in breast and prostate cancer cells[348].

5.4 Approaches to identifying RNA or RBP ligands

Fluorescence resonance energy transfer (FRET) and fluorescence polarization (FP) are the most common assays applied in the HTS of disruptors between two-component RNA/protein interaction, according to our recent review[311]. These fluorescence-based assays require the purification of functional target RBPs and appropriate labelling of RNAs or proteins. Novel techniques provide fluorescence-free alternatives for the screen assays. For instance, cat-ELCCA (catalytic enzyme-linked click chemistry assay) has been developed to identify let-7/Lin28 disruptors by integrating click chemistry with enzyme-linked chemiluminescence assays[349].

An on-bead HTS platform termed CONA (confocal nanoscanning) was previously established. In CONA, micro beads are coupled with fluorescently-tagged proteins, which can be visualised as fluorescent rings, where the amount of bound proteins is proportional to the ring intensities. The only known ligand targeting the RRM3 of

HuR was identified by CONA from one-bead-one-compound libraries[315]. Notably, using the RRM3 binder and CONA, an ATP-binding pocket was discovered in RRM3, which was not detected using conventional binding assays[315, 316]. CONA is very flexible in the applications of biomolecule interactions and it can be modified to monitor complex biological processes in real time, such as ubiquitination-related enzymatic activities and aggregation of α-syn[350, 351]. It will be interesting to explore the usage of CONA in RNA/protein interplays.

Phenotypic assays are very useful tools to study the effects of ligands on relevant phenotypes at the cellular level. Compared to previously described assays targeting specific pairs of RNA/protein interactions, phenotypic assays are suitable to identify small-molecule correctors of abnormal RNA activities. The discovery of the first spinal muscular atrophy (SMA) drug, Spinraza, was based on a phenotypic *in vitro* splicing assay. The drug showed the best potency to correct the aberrant splicing activities of the target pre-mRNA[352]. Two small molecules, risdiplam and branaplam were both found using luciferase reporter assays, where the alternative splicing could be monitored by luminescence signals[353, 354]. Mechanistically, Spinraza is an ASO drug that base-pairs an intronic splicing silencer within the RNA and blocks the splicing suppressors hnRNPs[352]. Whist the two small-molecule drugs stabilise the interaction between the splicing site and spliceosome[354, 355]. Reporter assays have been applied to look for molecules that disrupt miRNA-mediated silencing, by encoding a miRNA targeting site downstream of a reporter gene[356].

The focused screen and in silico drug design have been described above. The use of focused screening leads to a higher success rate than HTS, however, the resultant RNA ligands are likely to lack selectivity. As for the drug design, it relies on previously validated, functional RNA modulators, and comprehensive understanding of the steric structures of target RNA[340].

Aims

α-syn plays a significant role in PD pathology. The expression of α-syn is co-regulated by a subset of miRNAs both directly and indirectly. Moreover, abnormal miRNA levels are frequently found in the brain or body fluid of PD patients or animal models. However, how these miRNAs orchestrate and contribute to PD is not fully understood. Since miRNA levels are tightly controlled post-transcriptionally by specific RBPs, relieving α-syn pathology by targeting relevant miRNA/RBP interactions will provide a new avenue to PD therapy.

This project aims to explore possible starting points for PD treatment, focusing on the miRNAs controlling the expression of α-syn. I will focus on:

1. Identification and functional characterisation of miRNAs that are dysregulated in PD and control α-syn expression.
2. Development of an on-bead screening technique to identify small-molecule inhibitors of pri-miR-7/HuR interaction.
3. Functional study of pri-miR-7/HuR inhibitors attenuating α-syn expression.

Materials and methods

1. Chemical libraries

The focused library contains 8 compounds targeting RNA-binding activities of HuR or MSI2. Quercetin, luteolin, OA, DHTS, CMLD-2, CPC and gossypol were purchased from Sigma-Aldrich. Ro 08–2750 was purchased from R&D Systems. All reagents were dissolved in dimethyl sulfoxide (DMSO, Sigma-Aldrich) to prepare 20 mM stock solutions.

The in-house random compound library was a gift from Prof. Neil Carragher. It consists of 54 FDA-approved drugs and natural products of well-established anti-cancer mechanisms. The compound concentrations were varied from 0.1 to 10 mM according to their optimal effects in previous cell studies in the Carragher's laboratory.

2. Tissue culture techniques

2.1 Mammalian cell culture

HeLa, P19 mouse embryonic carcinoma, HEK293T, astrocytoma 1321N1 and SH-SY5Y neuroblastoma cells were maintained in DMEM (Dulbecco's Modified Eagle Medium, Gibco) containing 10% foetal bovine serum (Gibco).

2.2 Transient transfection of mammalian cell lines

For miRNA overexpression assays, HeLa cells were plated in 6-well plates with $3.6x10^5$ cells per well prior to transfection. 500 ng of pCG-pri-miRNA plasmids and 5 µl of Lipofectamine™ 2000 Transfection Reagent (Invitrogen) were suspended in 250 µl of Opti-MEM Reduced Serum Media (Gibco) in separate tubes. The tubes were left for 5 min before the Lipofectamine suspension were added into the DNA suspension drop by drop. The reaction was then incubated for 30 min at room temperature. In the meantime, HeLa cells were washed with Opti-MEM and supplemented with 1.5 ml of fresh 10% DMEM to each well. Finally, the reaction mix was added to the cells drop by drop. Cells were harvested 48 hrs after transfection.

To overexpress fluorescent recombinant proteins, cells were plated in T75 flasks and left for 24 hrs. 120 µg of plasmids and 20 µl of Lipofectamine 2000 were incubated in 1.5 ml of Opti-MEM respectively and then mixed. Cells were transfected and harvested after 24 hrs. The concentration of mCherry or GFP was determined using an mCherry quantification kit (BioVision) or a GFP quantification kit (abcam) in a PolarStar OPTIMA Multidetection Microplate Reader (BMG LABTECH). The information of plasmids and cell lines used will be described in the following sections.

2.3 P19 cell differentiation

10^7 of P19 cells were plated in 10 cm non-adhesive petri dishes and supplemented with 5% DMEM containing 1 µM of retinoic acid (Sigma-Aldrich). The embryonic bodies were transferred to treated dishes and maintained in 10% DMEM on Day 4. Cells were harvested on specified dates.

2.4 mDA neuron differentiation

Day 16 iPSC-derived midbrain DA (mDA) neurons were provided by Dr. Tilo Kunath. Prior to cell plating, a 48-well plate (Costar, #3548) was coated by 5 µg/ml Laminin-111 （Biolamina）diluted in dPBS with Ca^{2+} and Mg^{2+} (Gibco) at 4℃ overnight. Neural differentiation media (NDM) was prepared with Neurobasal™ media (Gibco) containing 1× B-27™ Supplement (Gibco) and 2 mM L-Glutamine (Gibco). The Day 16 mDA neurons were thawed and plated in the 48-well plate containing 1.6 ml replating media, which is NDM containing 10 µM Y-27632 dihydrochloride (TOCRIS), 20 ng/ml brain-derived neurotrophic factor (BDNF, PeproTech), 10 ng/ml glial cell-derived neurotrophic factor (GDNF, PeproTech), 0.5 mM dibutyryl cyclic-AMP sodium salt (dcAMP, Sigma-Aldrich), 0.2 mM ascorbic acid (Sigma-Aldrich) and 1 µM DAPT (TOCRIS). Then the cells were maintained and differentiated in 1.6 ml culture media, which is NDM containing 20 ng/ml BDNF, 10 ng/ml GDNF, 0.5 mM dcAMP, 0.2 mM ascorbic acid and 1 µM DAPT. Cells were harvested on specified dates.

3. Molecular biology techniques

3.1 Construction of expression vectors

The pJW99 plasmid was a gift from Dr. Julie Welburn. The vector encodes mCherry upstream of a multiple cloning site. HuR, Lin28a and Trim25 open reading frames were inserted into pJW99 between XhoI and EcoRI sites. The pEGFP-N1-Lin28a was constructed previously[277], where Lin28a was inserted at the N-terminus of EGFP.

DNA segments encoding pri-miRNAs or the 3'-UTR of human α-syn were cloned from human genomic DNA of HeLa cells using Phusion® High-Fidelity DNA Polymerase (NEB) and propagated using the CloneJET PCR Cloning Kit (Thermo). After sequence confirmation, the pri-miRNA genes were cloned into the pCG plasmid between the XbaI and BamHI cleavage sites, while α-syn-3'-UTR was inserted into the psiCHECK-2 plasmid (Promega) between the XhoI and NotI sites downstream of the Renilla luciferase (Rluc) gene. During cloning, plasmids were cut by corresponding restriction endonucleases (NEB) at 37℃ overnight and ligation was performed using T4 DNA Ligase (NEB) at 4℃ overnight.

3.2 Mutagenesis PCR

Mutants of psiCHECK-2-α-syn-3'-UTR were generated using mutagenesis PCR by Saul Rooney, an undergraduate student in our lab. A pair of mutagenesis primers flanking the mutagenesis site were designed where the nucleotide for replacement was included at the 5' of the forward primer. PCR reactions were run according to the manufacture's protocol of Phusion polymerase but only with 18 cycles. The template plasmids were digested by DpnI (NEB) treatment at 37℃ for 1.5 hr, followed by T4 Polynucleotide Kinase (NEB) treatment at 37℃ for 1 hr. Blunt-end ligation was performed using T4 DNA Ligase at 4℃ overnight. The ligation products were transformed and propagated in *Escherichia coli*.

3.3 Bacteria transformation

50 µl of *E. coli* DH5α competent cells were thawed on ice. 10 µl of ligation products or 1 µl of plasmids were added into the cells and incubated on ice for 30 min. After that, the cells were incubated in a heat block at 42℃ for 90 s and immediately placed on ice for 2 min. Subsequently, cells were suspended in 500 µl of LB media and

incubated at 37℃ for 1 hr with 220 rpm shaking. Finally, 200 µl of cell suspension was plated on a LB agar plate containing the selection antibiotics and incubated overnight at 37℃. The next day, a single colony was inoculated to 5 ml of LB media containing 0.1% antibiotics and left growing at 37℃ with overnight shaking. Cells were spun down the next morning and DNA plasmids were harvested following the instructions of the QIAprep Spin Miniprep Kit (QIAGEN). For large amount of plasmids, QIAprep Spin Midiprep Kit and QIAprep Spin Maxiprep Kit (QIAGEN) were applied. Sequence confirmation was conducted by Edinburgh Genomics and Genewiz.

4. Protein analysis

4.1 Production of cell extracts

Cultured cells were washed once with PBS, resuspended in Roeder D (200 mg/ml glycerol, 100 mM KCl, 0.2 mM EDTA, 100 mM Tris pH 8.0, 500 µM DTT and 200 µM PMSF) and collected into 1.5 ml Eppendorf tubes by cell scrapers. Cell disruption was carried out in a Bioruptor® Plus sonication device (Diagenode) at 4℃ for 10 min (low intensity settings, 30s on/off). Cell extracts were obtained from the supernatant after centrifugation (13,000 rpm, 10 min, 4℃). Concentrations of total protein were determined at A280 in a NanoDrop 2000 Spectrophotometer (Thermo).

4.2 Western blot analysis

60 µg of proteins in cell lysates were mixed with NuPAGE™ Sample Reducing Agent and LDS Sample Buffer (Invitrogen) and denatured at 70℃ for 10 min. The proteins were separated on a NuPAGE™ 4-12% Bis-Tris Protein Gel (Invitrogen) and transferred onto a nitrocellulose membrane in a GENIE® blotter (Idea Scientific) at 12V for 1 hr. The membrane was blocked with Western Blocking Reagent (Roche) diluted (1:10) in TBST (20 mM Tris pH 7.5, 137 mM NaCl and 0.1% (v/v) Tween 20) overnight at 4℃ or 1 hr at room temperature. Then the membrane was incubated with the primary antibody in TBST containing 1:20 Western Blocking Reagent for 1 hr at room temperature. These antibodies include anti-HuR, MSI2, Lin28a (Millipore), DHX9, GAPDH (Proteintech), α-tubulin (Sigma-Aldrich), α-synuclein (BD Biosciences), and Trim25 (Abcam). Following three washes, the membrane

was incubated in horseradish peroxidase (HRP) conjugated secondary anti-rabbit or anti-mouse IgG antibodies (1:2000, Cell Signalling Technology) for 1 h at room temperature. After developed in chemiluminescent substrate (Thermo #34580), the specific proteins were detected and quantified using a C-DiGit® Blot Scanner (LI-COR). Protein levels were normalised to α-tubulin. None of the protein bands were saturated.

5. RNA analysis

5.1 RNA isolation

Cells plated in each well of a 6-well plate was dissolved in 1 ml of TRI Reagent™ Solution (Invitrogen) in RNase-free tubes. 200 µl of chloroform was added and mixed vigorously, followed by centrifugation at 13,000 rpm, 4℃ for 15 min. The supernatants were carefully transferred to new tubes and mixed with 500 µl of isopropanol, centrifuged at 13,000 rpm, 4℃ for 10 min. RNA pellets were washed by 1 ml of 70% ethanol, dried, and resuspended by appropriate amount of RNase-free water at 55℃ for 10 min. RNA concentration was determined using NanoDrop.

5.2 RNA quantification

Total RNAs were subjected to DNase treatment before quantification, especially for pri and pre-miRNAs. 10 µg of total RNA was treated with 1 µl of TURBO^{TM} DNase (Invitrogen) and 5 µl of 10×DNase Buffer (Invitrogen) in a total volume of 50 µl at 37℃ for 20 min. An equal volume of UltraPure™ Phenol:Chloroform:Isoamyl Alcohol (Invitrogen) was mixed with the reaction and centrifuged at 13,000 rpm for 10 min at room temperature. The supernatant was mixed with 10% of 3 M NaAc and two volumes of 100% cold ethanol and left overnight at -20 ℃. RNA was precipitated after 20 min centrifugation at 13,000 rpm at 4 ℃. The RNA pellets were washed with 70% ethanol and resuspend in RNase-free water.

To quantify mature miRNA levels, reverse transcription, and quantitative real-time PCR (qRT-PCR) were performed with the miScript II RT Kit and SYBR Green PCR Kit respectively (QIAGEN) according to the manufacture's protocol. Using the HiSpec Buffer provided by the miScript II RT Kit, only mature miRNAs and certain snoRNAs can be reverse transcribed by oligo-dT primers after polyadenylation[357].

The oligo-dT primers bear a universal tag which can be targeted by a universal reverse primer provided by the miScript PCR kit. The obtained cDNA was PCR amplified using the universal reverse primer and a specific forward primer encoding the sequence of the target mature miRNA. Mature miRNA levels were normalised with miR-16 or miR-181d. To quantify pri-miRNAs or mRNAs, the SuperScript™ III Platinum™ SYBR™ Green One-Step qRT-PCR Kit (Invitrogen) or GoTaq® 1-Step RT-qPCR System (Promega) were used. The primers designed for pri-miRNA detection were upstream of the stem-loop range, so only pri-miRNAs would be detected. Pri-miRNA and mRNA levels were normalised with GAPDH mRNA level.

To detect pre-miRNAs, DNase-treated total RNA was fractionated using a 6% Urea-PAGE gel. RNAs between the bromophenol blue (26 nt) and xylene cyanol (106 nt) dye were purified to exclude pri- and mature miRNAs. The purified RNAs were reverse transcribed following the instructions of the miScript II RT Kit for pre-miR. Instead of the HiSpec Buffer, HiFlex Buffer was used to reverse transcribe all types of RNAs. Since pri and mature miRNAs had been excluded, only pre-miRNAs were reverse transcribed. Then pre-miRNAs were quantified following the instructions of the SYBR Green PCR Kit (QIAGEN) using mature miRNA primers and the universal reverse primer provided. Pre-miRNA levels were normalised to pre-miR-181d.

The same method has been previously applied in our lab to distinguish and quantify pri-, pre- and mature miRNAs[358]. The qRT-PCR reactions were performed in an Agilent Mx3000P QPCR System or a Roche LightCycler®96 System.

5.3 RNA pull-down assay

5.3.1 Covalent RNA coupling to agarose resin

1 nmol of RNA was treated with 100 mM NaAc and 5 mM m-sodium periodate in 200 µl of water and rotated for 1 hr at room temperature in dark. The RNA was precipitated by adding 600 µl of 100% ethanol and 15 µl of 3 M NaAc in dry ice for 20 min, followed by centrifugation at 13,000 rpm, 4 ℃ for 10 min. The RNA pellet was washed by 1 ml of 70% ethanol and resuspended in 500 µl of 100 mM NaAc pH 5. Adipic acid dihidrazide-agarose (Sigma) were washed 3 times with 100 mM NaAc.

The washed resin was resuspended in 100 mM NaAc to have a 50% slurry. 200 µl of the beads were added to the 500 µl of the periodate oxidised RNA and left rotating overnight at 4℃ in dark. To wash out the non-bound RNA, the mix was supplemented with 700 µl of 4 M KCL and stirred for 30 min at room temperature. The resin was pelleted after centrifugation (3,000 rpm, 3 min) and washed twice with 2 M KCL, 3 times with Buffer G (20 mM Tris-HCl pH 7.5, 137 mM NaCl, 1 mM EDTA, 1% TritonX-100, 10% glycerol, 1.5 mM $MgCl_2$, 1 mM DTT, and 200 µM PMSF) and once with Roeder D.

5.3.2 Protein pull-down by RNA-coupled agarose

Generally, the pelleted agarose resin was incubated with 650 µl of working solution containing 1 mg of cell lysates, 1.5 mM $MgCl_2$, 25 mM creatine-phosphate, 0.5 mM ATP, and 1 µl RiboLock RNase Inhibitor (Thermo). The mix was shaken at 37 ℃ at 700 rpm for 30 min. After that, the resin was pelleted by centrifugation (1,000 rpm, 3 min) and the supernatant was kept as the loading control. The resin was washed three times with Buffer G and mixed with 6 µl of NuPAGE™ Sample Reducing Agent, 15 µl of LDS Sample Buffer and 39 µl of water (39 µl of supernatant for the loading control). Proteins captured by RNA were denatured at 70 ℃ for 10 min with shaking. After a short spin, 30 µl of the supernatant was loaded on an SDS-PAGE gel and western blot was performed to detect the level of proteins. To test RNA/protein disruptors, cell lysates were pre-incubated with 100 µM of test compounds in working solution at 37 ℃, 700 rpm for 30 min.

5.4 RNA immunoprecipitation (RIP) assay

HuR-bound RNAs were immunoprecipitated and quantified following a method developed from a previously published protocol[359]. 1.4×10^6 HuR KO HeLa cells were plated in p100 dishes, treated with DMSO or 20 µM quercetin and transfected with 500 ng of pCDNA-HuR at the same time. After 48 hrs, cells were incubated with 1% formaldehyde at room temperature for 10 min with rocking, to crosslink RNA/protein interactions. Then the cells were incubated with 0.25 M glycine (pH 7.0) at room temperature for 5 min, to stop the crosslink reaction. Cell extracts in RIPA buffer (50 mM Tris–HCl, pH 7.5, 1% Nonidet P-40 (NP-40), 0.5% sodium deoxycholate, 0.05% SDS, 1 mM EDTA, 150 mM NaCl) were obtained as described

in 3.1. The protein levels were determined using the Pierce® BCA Protein Assay Kit (Thermo). 50 µl of Dynabeads™ Protein A for Immunoprecipitation (Invitrogen) were coupled with 3 µl of HuR antibody in BWB (0.02% Tween-20 in PBS) for 30 min at room temperature with rocking, then washed 3 times with RIPA buffer. The extracts containing 100 µg of protein were diluted with 500 µl of RIPA buffer, mixed with the antibody-coated beads at room temperature for 30 min. The beads were collected at 6,000 g and the supernatant was kept for RNA extraction as loading control. The beads were washed 5 times with high-stringency RIPA buffer (50 mM Tris-Cl, pH 7.5, 1% NP-40, 1% sodium deoxycholate, 0.1% SDS, 1 mM EDTA, 1 M NaCl, 4 M urea, and 0.2 mM PMSF). The beads containing the immunoprecipitated samples were collected and resuspended in 100 µl of 50 mM Tris-HCl, pH 7.0, 5 mM EDTA, 10 mM DTT and 1% SDS. The beads were then incubated at 70°C for 45 min to reverse the crosslinking. The immunoprecipitated RNA was extracted from these samples using TRI Reagent® LS. qRT-PCR was performed to detect pri-miR-7-1 and α-syn mRNA levels. The experiments were conducted by Dr. Nila Roy Choudhury.

5.5 mRNA stability assay

1.44×10^5 WT or HuR KO HeLa cells were plated in 12-well plates and treated with DMSO or 20 µM of quercetin, together with 10 µg/ml actinomycin D (Sigma-Aldrich). The cells were harvested at 0, 6, or 12 hrs after actinomycin D treatment. Total RNA was isolated using TRI Reagent™. α-syn mRNA and 18S levels were quantified using qRT-PCR.

6. Luciferase reporter assays

Luciferase reporter assays were performed with the help of the Dual-Luciferase® Reporter Assay System (Promega) by S. Rooney. 1.2 $x10^4$ HeLa cells were plated in each well of 96-well plates. For each well, 30 ng of psiCHECK2-α-syn-3'-UTR and 16.7 ng of pCG-pri-miRNA plasmids were co-transfected into HeLa cells. DNA and 0.2 µl of Lipofectamine was suspended in 5 µl of OPTI-MEM respectively. The mixture was added into 90 µl of 10% DMEM cell culture. Cells were lysed 48 hrs after transfection by 50 µl of Passive Lysis Buffer with 15 min shaking. The plates were spun at 4,000 rpm for 10 min and the supernatants were transferred to new

plates. 8 µl to 12 µl of the supernatants were diluted by water to a total volume of 40 µl in white 96-well plates (Costar). 10 µl of Luciferase Assay Reagent II was added into the supernatants and the luminescence of firefly luciferase was read immediately in a plate reader. Afterwards, 10 µl of Stop & Glo® Reagent was added to the reaction and the Renilla luciferase levels were read immediately. The luminescence measurements were taken at a gain of 3000, 37 ℃ and with 5 s of double orbital plate shaking before reading. The Renilla luciferase luminescence level was normalised to the firefly one for each measurement.

7. Gene knockout using CRISPR-Cas9

7.1 HuR knockout by CRISPR-Cas9

The Alt-R® CRISPR-Cas9 crRNAs and tracRNA were synthesised by IDT. The sequences of the crRNAs were 5'-cgaagucuguucagcagcauguuuuagagcuaugcu and 5'-cuugggucauguucugaggguuuuagagcuaugcu respectively. 100 µM of each crRNA was mixed with 100 µM of tracRNA in 100 µl duplex buffer (IDT) at 95℃ for 5 min, to form crRNA-tracRNA duplexes. HEK293T or HeLa cells were seeded in 24-well plates with different densities. The well containing cells with around 60% of confluency was selected. 1.5 µl of each duplex were co-transfected with 1 µl of GeneArt™ CRISPR Nuclease mRNA (Invitrogen) using 1 µl of Lipofectamine 2000 in 125 µl Opti-MEM. The cells were incubated for about 1 week before being diluted and aliquoted to 96-well plates to make 0.5 or 1 cell count per well. The cells were split into two 96-well plates when most of the wells were confluent. One plate of the cells were lysed by 30 µl of Passive Lysis Buffer with 15 min shaking. 2 µl of the cell extracts were loaded onto nitrocellulose membrane (GE, #10600018) and tested against HuR and DHX9 antibodies. Cells showing both HuR negative and DHX9 positive were transferred to 6-well plates and confirmed using western blot analysis.

Both wildtype and HuR KO HeLa and HEK293T cells were plated in a 6-well plate and harvested when the cells reached about 90% confluency. The genomic DNA was isolated using the GenElute™ Mammalian Genomic DNA Miniprep Kit (Sigma-Aldrich). The fragments covering the expected HuR knockout sites were PCR amplified using the forward primer (5'-gccctggacagtacactcgcc) and reverse primer (5'-ccacatggccgaagactgca). The PCR products were visualised on a 1.2% agarose gel.

The DNA bands with anticipated sizes were purified using the QIAquick Gel Extraction Kit (QIAGEN). After ligating into the cloning vector using the CloneJET PCR Cloning Kit (Thermo), the DNA fragments were sequenced and the mutations in the HuR gene were identified.

7.2 MiR-7 knockout by CRISPR-Cas9

A pair of guide RNAs (5'-acauucaauacuaaucuugc and 5'-accaaucauuuguccuguag) were designed flanking the stem loop sequence of human pri-miR-7-1 gene. Transfection of the CRISPR-Cas9 system was carried out in HeLa cells as described above. Crude DNA was extracted by dissolving cells in solution 1 (25 mM NaOH, 0.2 mM EDTA) at 98℃ for 1 hr and terminated by equal volume of solution 2 (40 mM Tris-HCL pH5.5). PCR was performed using 100 ng of crude DNA with primers flanking the targeted region (F: 5'-ctgcagaacaggtcagtttaagtt, R: 5'-tgcagaaca cctatgaagcaga). The PCR products were visualised on a 1% agarose gel and cells generating band shifts were selected. The miR-7 levels were tested by qRT-PCR. Sequences were determined using PCR products amplified from purified genomic DNAs of putative miR-7 knockouts.

8. RP-SMS

8.1 RNA pulldown from SILAC samples

RP-SMS was performed to identify proteins that bind the CTL of human pri-miR-153-2. The human pri-miR-153-2-CTL (guugcagcuaguaauaugagcccaguugcaua) was synthesised by IDT. Heavy HeLa (^{13}C Arg/^{13}C Lys) and light SH-SY5Y (^{12}C Arg/^{12}C Lys) cell extracts were previously prepared according to our method paper[272]. The RNA pull-down assay was performed using human pri-miR-153-2-CTL with heavy HeLa extracts or light SH-SY5Y extracts as described above. Heavy/light agarose beads were combined during the final wash after pull-down. On-bead proteins were denatured as described above. 30 µl of supernatant was loaded into an SDS-PAGE gel and run until the dye migrated 1 cm into the gel. The gel was stained with GelCode^{TM} Blue Safe protein stain (Thermo).

To identify pri-miR-7-1-CTL-bound proteins interrupted by quercetin, heavy HeLa extracts (^{13}C-Arg/^{2}D-Lys) were treated with 100 µM quercetin and light HeLa

extracts (no labelling) were treated with equal volume of DMSO. Both cell extracts were incubated with pri-miR-7-1-CTL-linked beads, respectively. Heavy/light agarose beads were combined during the final wash and processed as just described.

8.2 In-gel digestion

The gel piece containing proteins was cut into small pieces (1 mm×1 mm) and transferred to an Eppendorf tube. The gel pieces were treated with 50 mM ammonium bicarbonate (ABC, sigma) and equal volume of acetonitrile (thermo) at 37°C, 900 rpm for 30 min, and repeated once. Then the gel pieces were covered with 10 mM DTT (Sigma), incubated at 37°C, 900 rpm for 30 min and dried by acetonitrile. Subsequently, 55 mM iodoacetamide (Sigma) was added to cover the gel pieces and incubated at RT for 20 min in the dark, followed by dehydration with acetonitrile. To prepare Trypsin buffer, 20 μg of trypsin (Sigma) was dissolved by 20 μl 0.1% trifluoroacetic acid (TFA, Sigma) and diluted by 150 μl acetonitrile, 300 μl 50mM ABC and 1,030 μl of water. Finally, the gel pieces were incubated in Trypsin buffer at 37°C overnight. The next day, 100 ul of 0.1% TFA and 20 ul of 10% TFA was added to gel solution. Stage tips were prepared with three pieces of Empore Disk C18 (Sigma, 66883-U) and washed by methanol and 0.1% TFA by spinning. The gel sample solution was passed through the tip and washed with 0.1% TFA. Stage tips were stored at -20°C before loading onto a mass spectrometer.

8.3 Mass spectrometry analysis

LC-MS/MS was performed using an Orbitrap^{TM} mass spectrometer (Thermo) and analysed using a MaxQuant software[360] platform by Dr. Chirstos Spanos. This allows the ratio of the heavy/light-labelled peptides to be determined from raw MS data. To identify proteins specifically pulled down from light SH-SY5Y extracts, peptides with intensity larger than 1 million and normalised H/L ratio less than 0.5 were selected. Peptides presented with frequency larger than 10% in CRAPome[361], a database of common contaminant from affinity purification-MS experiments, were further excluded.

9. Non-labelled protein quantification

HeLa cells were treated by DMSO or 20 μM quercetin for 48 hrs. Cell extracts

containing 10 μg of protein were loaded on to an SDS-PAGE gel. The in-gel digestion was the same as described in 7.2. MS experiments and analysis were performed by Dr. C. Spanos. Three repeats of untreated or treated samples were prepared and injected at the same time. Proteins identified with significantly different expression after quercetin treatment were analysed in DAVID Bioinformatics Resources 6.8[362].

10. RNA pull-down-confocal nanoscanning (RP-CONA)

10.1 Preparation of streptavidin beads

Ni-NTA agarose beads (Qiagen, 30250) were sieved using 100 μm (Corning, 431752) and 120 μm (Millipore, NY2H04700) pore size filters with 20% ethanol. The sieved beads were washed 3 times with binding buffer (0.3 M NaCl, 20 mM HEPES pH 7.5, 0.01% Triton X-100) and resuspended to make a 10% slurry. For each well, 150 pmol (7.5 μM) of His-streptavidin (ProteoGenix) was mixed with 5 μl of sieved beads (10% slurry) in a total volume of 20 μl binding buffer. The tubes were shaken immediately at 1,000 rpm at 4°C for 20 min. The resin was then pelleted and washed three times using PBS (0.01% Triton X-100).

10.2 RNA coupling to the streptavidin beads

Biotinylated FITC-pri-miR-7-1-CTL (5'-FITC-uguuguuuuuagauaacuaaaucgacaacaaa-bio-3'); FITC-pri-miR-7-1/30a-TL (5'-FITC-uguuguucugugaagccacagaugggacaacaaa-bio-3'); Cy5-pre-let-7a-1-CTL (5'-cy5-uuagggucacacccaccacugggagau-bio-3'); FITC-TNFα-ARE (5'-FITC-auuauuuauuauuuauuuauuauuua-bio-3'); and FITC-α-syn-ARE (5'-FITC-cuaaauccucacuauuuuuuuguugcug-bio-3') were synthesised by IDT. For each well, 40 pmol (2 μM) of RNA was mixed with 5 μl of streptavidin-agarose (10% slurry) in a total volume of 20 μl PBS (0.01% Triton X-100) and placed on a shaker immediately. The coupling was performed at 4°C, 1,100 rpm for 20 min. The beads were pelleted by centrifugation (1,000 rpm, 3 min) and washed three times using PBS (0.01% Triton X-100). The beads were resuspended into 10% slurry.

10.3 RNA pull-down from cell extracts

HuR KO HEK293T cell extracts containing overexpressed mCherry-HuR were

prepared in 20 µl of no glycerol-Roeder D (100 mM KCL, 0.2 mM EDTA, 100 mM Tris pH 8.0, 0.5 mM DTT and 0.2 mM PMSF). mCherry-Lin28a and Lin28a-GFP were overexpressed in wildtype HEK293T cells. mCherry-Trim25 was overexpressed in the previously made Trim25 KO HEK293 cell line. 20 µl of cell lysate solution was mixed with 30 µl of pull-down mix (1.5 mM $MgCl_2$, 25 mM creatine-phosphate, 0.5 mM ATP, and 0.25 µl Ribolock) and loaded to a well of a black glass (BD) or plastic (PE, Greiner) bottom 384-well plate. 5 µl of RNA coupled beads resin was added into each well. The plates were shaken at room temperature at 1,500 rpm for 1 to 2 hrs.

10.4 Beads imaging and data analysis

Beads images were acquired in the Opera® High Content Screening System (PerkinElmer) or ImageXpress Micro Confocal High Content Screening System (Molecular Devices) at 30 µm above well bottom and 20× magnification with air lenses. In Opera, three channels were detected to investigate FITC-RNA/mCherry-protein interaction: brightfield (690 nm diode, 690/70 detection filter), FITC (488 nm laser, 520/35 detection filter) and mCherry (561 nm laser, 600/40 detection filter). In ImageXpress, two channels were detected: FITC (FITC: excitation 475/34, emission 536/40) and mCherry (TEXASRED: excitation 560/32, emission 624/40). The exposure time was adjusted so that both FITC and mCherry ring intensities were around 2,000 RFU. Images were stitched and the ring intensities were quantified in Image J with a custom plugin Ring Measure developed by Dr. David Kelly (DOI:10.5281/ZENODO.4302193). The basic principle is as follows: On a FITC image, the fluorescent rings were identified and selected. A line was plotted across one bead and the average peak values of the plot profile were recorded as the FITC ring intensity. The mCherry ring intensity was measured according to the plot profile at the same place of the corresponding mCherry image. Four measurements were taken for each bead. The relative mCherry/FITC intensities were calculated and averaged. Similarly, to measure Cy5-RNA/GFP-protein interaction, Cy5 (excitation 631/28, emission 692/40) and FITC filter sets were used in ImageXpress, and the analysis was the same. Coefficient of variation (CV)= SD/Mean×100%. *Z*' factor was calculated using the equation $Z' = 1 - 3(SD_{positive\ control} + SD_{negative\ control})/|Mean_{positive\ control} - Mean_{negative\ control}|$[363].

11. Primer lists

qRT-PCR primer list

Target	Species	Sequence 5'
miR-7-5p	human/mouse	TGGAAGACTAGTGATTTTGTTGTT
miR-153-3p	human/mouse	TTGCATAGTCACAAAAGTGATC
miR-133b-3p	human/mouse	TTTGGTCCCCTTCAACCAGCTA
miR-16-5p	human/mouse	TAGCAGCACGTAAATATTGGCG
miR-181d-5p	human	AACATTCATTGTTGTCGGTGGGT
pri-miR-7-1-F	human	GCCATGGTGTCTCAACCTTT
pri-miR-7-1-R	human	GTGGTTTTGGCAGCAGTTTT
pri-miR-153-2-F	human	GAGGGAGCGCATTTACACTTTA
pri-miR-153-2-R	human	TTACCGTGAGCAGCGTTAGTG
GAPDH-F	human	AATCCCATCACCATCTTCCA
GAPDH-R	human	TGGACTCCACGACGTACTCA
αsyn-F	human	GTTGTGGCTGCTGCTGAGAAA
αsyn-R	human	TCCCTCCTTGGTTTTGGAGCCTAC
18S-F	human	GTAACCCGTTGAACCCCATT
18S-R	human	CCATCCAATCGGTAGTAGCG
hRluc-F	Renilla	GGAATGGGTAAGTCCGGCAA
hRluc-R	Renilla	CCAAGCGGTGAGGTACTTGT
ffluc-F	firefly	GAACAGCTCTGGGTCTACCG
ffluc-R	firefly	GGGATGATCTGGTTGCCGAA

Sequencing primer list

Name	Plasmid	Sequence 5'
pJW99-mCherry-F	pJW99	TCACCTCCCACAACGAGGACTA
pJW99-mCherry-R	pJW99	AGTCGAGGCTGATCAGCGGGT
CMV-F	G10/psiCHECK2	CGCAAATGGGCGGTAGGCGTG
psi-check2-R	psiCHECK2	CTCATTTAGATCCTCACA

Cloning PCR primer list

Target	Sequence 5'
pri-miR-133b-F	ACAAGGCAAGCTCCTGGCATTTG
pri-miR-133b-R	CCAGGACTCCTCTTCTCTTCCTTCC
miR-133b-Xba1-F	gactagTCTAGAACAAGGCAAGCTCCTGGCATTTG
miR-133b-BamH1-R	gaacgcGGATCCCCAGGACTCCTCTTCTCTTCCTTCC
pri-miR-34b-F	AGCTACGCGTGTTGTGCGCT
pri-miR-34b-R	TTTCCTCGCACTTGCAGCGGG
miR-34b-Xba1-F	gactagTCTAGAAGCTACGCGTGTTGTGCGCT
miR-34b-BamH1-R	gaacgcGGATCCTTTCCTCGCACTTGCAGCGGG
pri-miR-34c-F	TTGAGCTCCAACTCAACCAAT
pri-miR-34c-R	TGATGCACAGGCAGCTCAT
miR-34c-Xba1-F	gactagTCTAGATTGAGCTCCAACTCAACCAAT
miR-34c-BamH1-R	gaacgcGGATCCTGATGCACAGGCAGCTCAT
pri-miR-153-F	TGTCTCCAGGCCCTGCACTG
pri-miR-153-R	CACCTGCTCCACTGAGCCCC
miR-153-Xba1-F	gactagTCTAGATGTCTCCAGGCCCTGCACTG
miR-153-BamH1-R	gaacgcGGATCCCACCTGCTCCACTGAGCCCC
pri-miR-214-F	TCTCCCTTTCCCCTTACTCTCCAAA
pri-miR-214-R	CCCCGAGCCCCTCATTTTGGTT
miR-214-Xba1-F	gactagTCTAGATCTCCCTTTCCCCTTACTCTCCAAA
miR-214-BamH1-R	gaacgcGGATCCCCCCGAGCCCCTCATTTTGGTT
miR-3120-Xba1-F	gactagTCTAGACCCCGAGCCCCTCATTTTGGTT
miR-3120-BamH1-R	gaacgcGGATCCTCTCCCTTTCCCCTTACTCTCCAAA
α-syn-3UTR-F	CTTTGCTCCCAGTTTCTTGAGATCT
α-syn-3UTR-R	GTCACAAATAGCTACATACTGGATAAGCC
Xho1-α-syn-3UTR-F	GATCCGctcgagCTTTGCTCCCAGTTTCTTGAGATCT
Not1-α-syn-3UTR-R	AAGGATCAAAgcggccgcGTCACAAATAGCTACATAC TGGATAAGCC
Trim25-HR-F	CGGAGGTGGAGGTACTAGTctcgagGCTGAACTGTGT CCTCTGGC
Trim25-HR-R	CGCGGTACCGTCGACTGCAgaattcCTATTTGGGGGA GCAGATGCTCA
Xho1-Lin28a-F	CCGctcgagGGCTCCGTGTCCAACCAGCA
Lin28a-EcoR1-R	CCGgaattcTCAATTCTGTGCCTCCGGGAGCA

NB: Letters in small case designed for endonuclease sites.
All primers targeting human genes.

Mutagenesis PCR primer list

Target	**Species**	**Sequence 5'**
miR-7 mut-1-F	human	aCCATCAGCAGTGATTGAAGT
miR-7 mut-1-R	human	AGACTTCGAGATACACTGTAAA
miR-7 mut-2-F	human	aTTAATGATACTGTCTAAGAATAATG
miR-7 mut-2-R	human	AGACACCTAAAAATCTTATAATATAT
miR-7 mut-3-F	human	aCCCTTAATATTTATCTGACGGTA
miR-7 mut-3-R	human	AGAAACACTTTAAAGGAGAATTTG
miR-153-3p mut-1-F	human	cCACCTATAAATACTAAATATGAAATT
miR-153-3p mut-1-R	human	ATAGTTTCATGCTCACATATTTTTAA
miR-153 mut-2-F	human	cCACTGGTTCCTTAAGTGGCTG
miR-153 mut-2-R	human	ATACCAAAACACACTTCTGGCA
miR-153 mut-3-F	human	cCACTAGTGTGAGATGCAAACA
miR-153 mut-3-R	human	AGAGATTCTGAAAAAGACCCCA
miR-133b mut-F	human	gAAACACTTAAACAAAAAGTTCTTTA
miR-133b mut-R	human	GTCCCAAATAAACTATTAAGATATAT
miR-3120 mut-1-F	human	aGTTGTTCAGAAGTTGTTAGT
miR-3120 mut-1-R	human	GCAACAAAAAAATAGTGAGG
miR-3120 mut-2-F	human	aGTACCTTTCTGACAATAAAT
miR-3120 mut-2-R	human	GCATTCACACCAATATCAGA
miR-214 mut-F	human	gTGACAGATGTTCCATCCTGT
miR-214 mut-R	human	CAGATCTCAAGAAACTGGGA
miR-34b mut-1-F	human	tTTGAAGTATCTGTACCTGCC
miR-34b mut-1-R	human	CACTGCTGATGGAAGACTTC
miR-34b mut-2-F	human	tTTTGCTATCATATATTATAAGATTTTTA
miR-34b mut-2-R	human	CACTAACAACTTCTGAACAA
miR-34b mut-3-F	human	tTTTTGACTACACCCTCCTTA
miR-34b mut-3-R	human	CATCTTCTACACTGCTTAGT
miR-34c mut-1-F	human	cTCTAAGAATAATGACGTATTGTGA
miR-34c mut-1-R	human	AGTATCATTAAAAGACACCT
miR-34c mut-2-F	human	cCAAAAATATTTTATTTTTATCCCATCTCAC
miR-34c mut-2-R	human	AATGAGATAACGTTTTATTTTAATTC
miR-34c mut-3-F	human	cCCAGAAGTGTGTTTTGGTAT
miR-34c mut-3-R	human	AGTGTTGCTTCAGGGAATTC

NB: Letters in small case indicating the mutated nucleotide.

Results

1. The study of PD-related miRNAs

1.1 MiR-7 is a major inhibitor of α-syn expression

To find miRNAs that affect α-syn we decided to study a range of miRNAs that are downregulated in specimens from PD patients[186, 190, 206, 222, 229], and have potentials to target the 3'-UTR of α-syn mRNA, including miR-7, miR-153, miR-133b, miR-34b/c and miR-214 (**Figure 7**). Although miR-3120 levels in PD patients have not been reported, the miRNA is included as its sequence is complementary to miR-214.

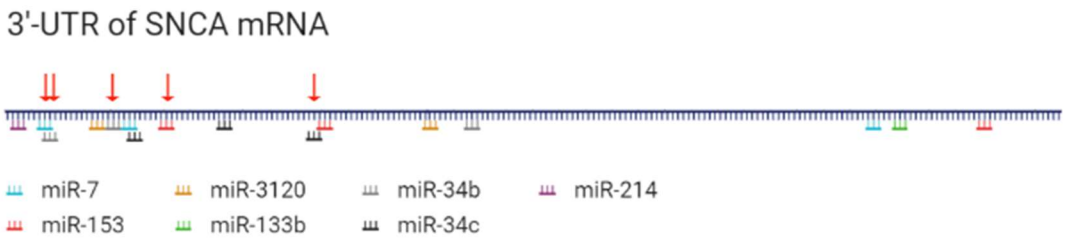

Figure 7 Predicted binding sites of miRNAs on the 3'-UTR of α-syn mRNA. The potential binding sites of different miRNAs are annotated at the approximate positions on the 3'-UTR of the α-syn mRNA (about 2,500 nt). These sites were predicted by TargetScan[234] or provided by miRTarBase[364]. Sites indicated by red arrows were previously reported. Figure was drawn in Biorender.

We constructed a luciferase reporter, carrying the gene of α-syn mRNA 3'-UTR downstream of the Renilla luciferase gene driven by a SV40 promoter. The reporter also coded the gene of firefly luciferase downstream of a HSV TK promoter. Therefore, firefly luciferase levels can be used as an internal control to eliminate the differences of transfection efficiency in individual assays. We then co-transfected the reporter with pCG plasmids encoding the above mentioned pri-miRNAs into HeLa cells, to test the effects of these miRNAs on the expression of Renilla luciferase. Only miR-7 exhibited significant suppression on Renilla luciferase levels, compared to other miRNAs (**Figure 8A**). The upregulation of each mature miRNA was confirmed by qRT-PCR (**Figure 8B**).

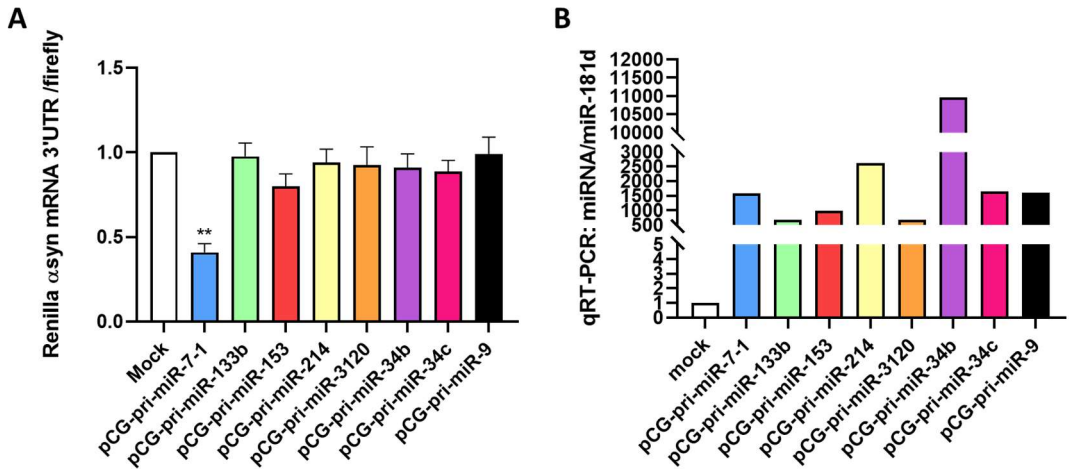

Figure 8 MiR-7 inhibits luciferase levels of a Renilla α-syn mRNA 3'-UTR reporter. Equal amounts of each pCG-pri-miR plasmid were co-transfected with the luciferase reporter carrying the α-syn 3'-UTR. pCG-pri-miR-9 was tested as a negative control. (A) Luciferase levels were recorded 48 hrs after transfection. Mean Renilla/firefly values and SEM from 6 independent repeats are shown. Statistically significant differences compared to mock were analysed using SPSS one-way ANOVA, **P<0.01. (B) Upregulation of miRNA levels were determined by qRT-PCR and normalised to mock (no DNA transfected).

To validate this, we performed single-nucleotide mutation at the 3rd position of the potential miRNA binding sites on the luciferase reporter individually and co-expressed the wildtype or mutated reporters with corresponding miRNAs. The mutation on the previous validated miR-7 targeting site[189] (miR-7_m1) desensitised the miR-7-mediated inhibitive effects, while the other two putative targeting sites seemed to not be involved (**Figure 9**). Interestingly, reporters bearing a mutated binding site of miR-133b (miR-133b_m1), miR-153 (miR-153_m1[209]) and miR-34c (miR-34c_m3[225]) generated significantly upregulated luciferase levels, although these three miRNAs didn't exert significant inhibition on the wildtype reporter, indicating that these three miRNAs also have α-syn inhibition potential.

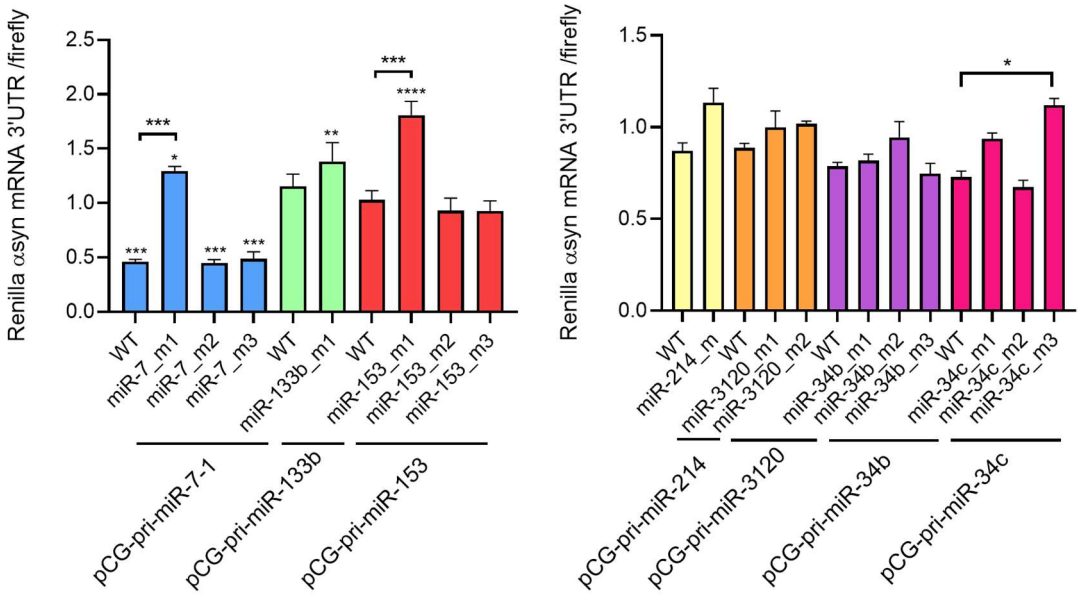

Figure 9. Single-nucleotide mutation of miR-7 binding site inactivates the inhibitive effects of miR-7. The nucleotide on the 3rd position of the miRNA-targeted seed regions on the α-syn mRNA 3'-UTR gene was mutated individually. The mutants were numbered according to the binding sites from 5' to 3' of the α-syn mRNA 3'-UTR. Luciferase levels were measured 48 hrs after co-transfection of the corresponding pCG-pri-miR plasmids with reporters bearing wildtype or mutated α-syn mRNA 3'-UTR gene. The luciferase levels are relative to co-transfection of pCG-pri-miR-9 with wildtype reporter. Mean Renilla/firefly values and SEM from three independent repeats are shown. Statistically significant differences compared to mock were analysed using SPSS one-way ANOVA, *P<0.05, **P<0.01, ***P<0.001, ****P<0.0001.

We subsequently transfected HeLa cells with an increasing amount of pCG-pri-miR-7-1, and tested α-syn expression with western blot. A significant dose-dependent inhibition on α-syn was identified (**Figure 10**). Overexpressed miR-153 and 133b showed less significant inhibitive effects compared to miR-7. Importantly, the upregulation of mature miR-7 was equal or less than the other two miRNAs, according to qRT-PCR (**Figure 11**).

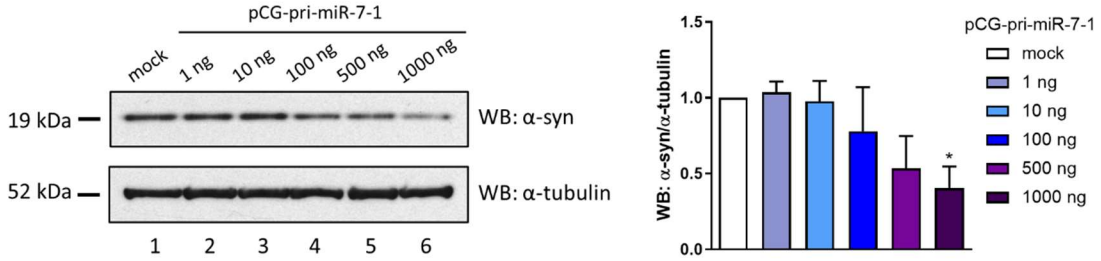

Figure 10 α-syn expression is inhibited by miR-7 in a dose-dependent manner. 1: Mock HeLa cells without DNA transfected. 2-6: An increasing amount of pCG-pri-miR-7-1 was transfected into HeLa cells. The expression of α-syn and α-tubulin were detected by western blot 48 hrs after transfection. Relative α-syn/α-tubulin levels were normalised to mock. Mean values and SEM from three independent repeats are shown. Statistically significant differences compared to mock were analysed using SPSS one-way ANOVA, *P<0.05.

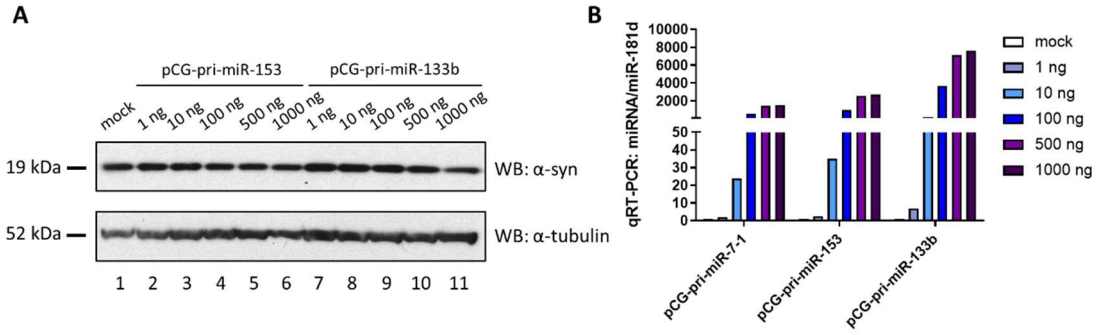

Figure 11 (A) MiR-153 and miR-133b exert mild inhibition of α-syn expression.1: Mock HeLa cells without DNA transfected. 2-6: Increasing amounts of pCG-pri-miR-153 was transfected into HeLa cells. 7-11: Increasing amounts of pCG-pri-miR-133b was transfected into HeLa cells. The expression of α-syn and α-tubulin were detected by western blot 48 hrs after transfection. **(B) Upregulation of miRNAs after overexpression.** Mature miR-7, miR-153 and miR-133b levels from HeLa cells transfected with increasing amounts of corresponding pCG plasmids were determined by qRT-PCR and normalised to mock (no DNA transfected).

To summarise, miR-7 is the most effective inhibitor of α-syn expression, compared to the other PD-related miRNAs. Moreover, the mechanism is highly dependent on a specific binding motif on the 3'-UTR of α-syn mRNA. MiR-153 and miR-133b are also involved in the regulation of α-syn expression, albeit to lesser extent and with more complex regulatory networks.

1.2 The biogenesis of miR-153 is post-transcriptionally inhibited

1.2.1 The terminal loop of human pri-miR-153-2 is conserved

According to our previous publications, conserved terminal loops (CTLs) of miRNA precursors may work as landing pads of trans-acting factors that affect miRNA maturation. Pri-miR-153-2 is annotated as one of the 74 pri-miRNAs that bear highly conserved terminal loops[273]. Here we aligned the stem-loop sequences of human pri-miR-153-2 and pri-miR-133b with their counterparts from 9 various vertebrate species. The terminal loop sequence of human pri-miR-153-2 is highly conserved among these 10 species, but less conserved in pri-miR-133b across the same species (**Figure 12**). Therefore, regulatory proteins may exist and act via the CTL of the miR-153 precursor.

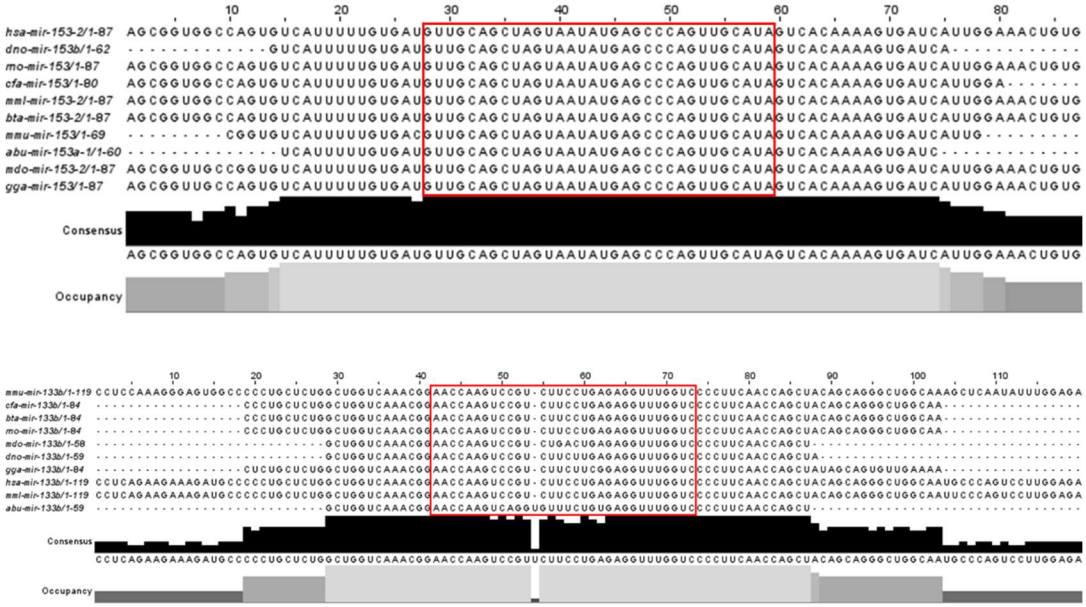

Figure 12 Conservation of PD-related miRNA precursors. Pri-miR-153-2 (top) and pri-miR-133b (bottom) stem-loop sequences from 10 species were fetched from miRBase, including human (hsa), monkey (mml), mouse (mmu), rat (rno), opposum (mdo), dog (cfa), cattle (bta), chicken (gga), armadillo (dno) and fish (abu). The sequences were aligned in CLUSTALW, and output in Jalview. The terminal loop regions were highlighted by red boxes.

1.2.2 The biogenesis of miR-153 is inhibited in neuroblastoma cells

To investigate if there is any post-transcriptional regulation during the biogenesis of miR-153, the levels of pri-miR-153-2 and its mature products were determined by

qRT-PCR in four human cell lines. Interestingly, pri-miR-153-2 is specifically enriched in SH-SY5Y neuroblastoma cells, reaching more than 1,000-fold than that in HeLa. In contrast, mature miR-153 levels are comparable across these cell lines (**Figure 13**). The discrepancy strongly implies the existence of inhibitory factors in neuroblastoma that prevent the processing of pri-miR-153 into its mature form.

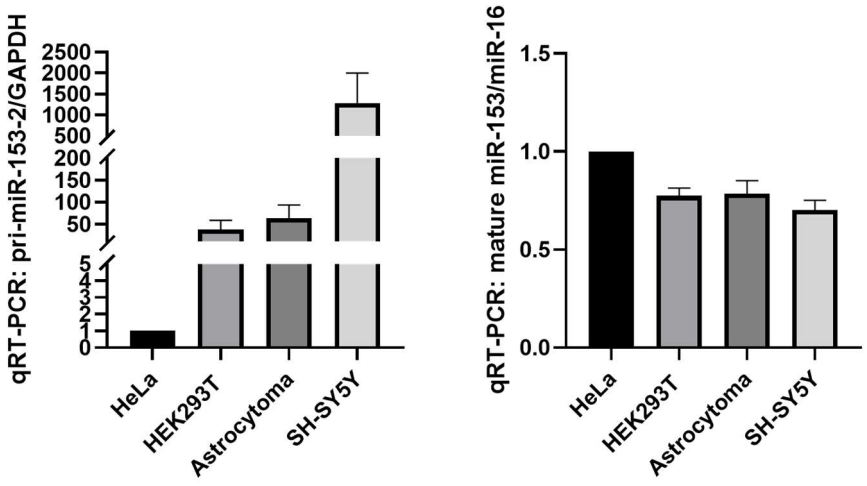

Figure 13 The biogenesis of miR-153 is inhibited in SH-SY5Y cells. qRT-PCR was performed using total RNA of HeLa, HEK293T, astrocytoma and neuroblastoma SH-SY5Y cells. The level of pri-miR-153-2 was normalised to GAPDH mRNA (left), and mature miR-153 was normalised to miR-16 (right). Mean relative RNA levels and SEM from three independent qRT-PCR repeats are shown.

1.2.3 Candidate proteins involved in the regulation of miR-153 biogenesis

To identify trans-acting factors that may regulate the biogenesis of miR-153, we performed RNA pull-down-SILAC mass spectrometry (RP-SMS)[272] to capture proteins from HeLa or SH-SY5Y extracts using the CTL of human pri-miR-153-2 (**Figure 14**). Proteins specifically pulled down from SH-SY5Y, but not HeLa cells are likely to be potential regulators. Among these proteins, retrotransposon-like protein 1 (RTL1), kinesin-like protein KIF21A (KIF21A) and dihydropyrimidinase-related protein 2 (DPYSL2) are brain or SH-SY5Y enriched proteins, according to The Human Protein Atlas[365]. These three proteins together with Ras-related protein Rab-7a (RAB7A) has not been reported to have RNA binding activities. Importantly, RNA-binding protein 14 (RBM14) and serine/arginine-rich splicing factor 10 (SRSF10) can interact with enzymes that are involved in the regulation of miRNA biogenesis[366]. Moreover, a few reports have suggested that RNA-binding protein 3

(RBM3) can alter miRNA abundance[367], and regulate a widespread or specific miRNA biogenesis[368, 369]. Crucially, Matrin-3 (MATR3) inhibits the processing of synaptic miR-138 through the CTL of pre-miR-138-2[273, 370]. To conclude, the aforementioned proteins are candidate regulatory factors that regulate the biogenesis of miR-153 by interacting with the CTL of its precursors. Further work will be focused on monitoring mature miR-153 levels upon knockdown of individual proteins. The identification of miR-153 regulators may serve as a drug target for PD treatment, through assisting the regulation of α-syn expression.

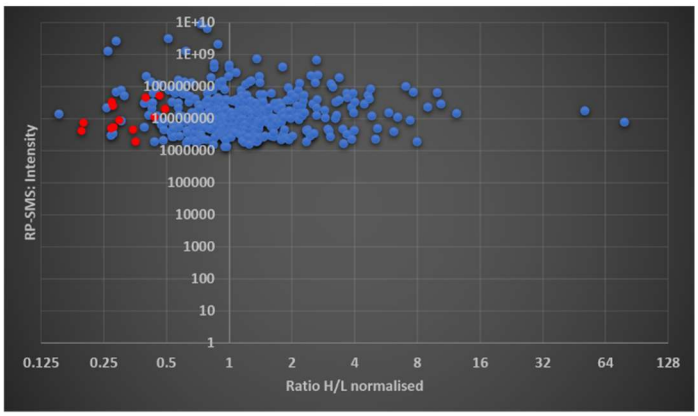

Protein	Highlights
RBMS3	
RTL1	SH-SY5Y enriched
TRPT1	
KIF21A	Brain/SH-SY5Y enriched
IDH2	
TIA1	
DPYSL2	Brain enriched
RAB7A	
RBM14	Interacts with TRBP
SRSF10	Interacts with TLS
TRA2B	
RBM3	Reduce miRNA abundance
MATR3	Inhibits miR-138 processing

Figure 14 Candidate proteins involved in the biogenesis of miR-153. RP-SMS was performed using the CTL of human pri-miR-153-2 to pull-down proteins from heavy HeLa (^{13}C Arg/^{13}C Lys) and light SH-SY5Y (^{12}C Arg/^{12}C Lys) cell extracts. Total intensity versus normalised heavy/light ratio of identified proteins are plotted. Selected proteins are highlighted in red and listed in the form. Selection criteria: intensity>1,000,000; H/L ratio<0.5; frequency of presence in CRAPome<10%. RBM3 and MATR3 are included because their indicated roles in miRNA biogenesis. The proteins highlighted in bold have not been reported to have RNA-binding activities previously.

1.3 Discussion

As described in the introduction, the α-syn inhibition effects of miR-7 has been wildly recognised. The targeting site on the 3'-UTR of α-syn mRNA was identified using a luciferase reporter assay, with the 3rd and 4th nucleotides of the seed both mutated (AA to UU)[189]. Here we validated this site with a single A to U mutation at the 3rd nucleotide, proving that miR-7 targeting is highly specific. We have also shown that the other two predicted sites may not be involved. Moreover, by comparing miR-7 with other α-syn targeted miRNAs according to luciferase levels and endogenous α-syn levels, we found miR-7 was the most effective inhibitor, while

miR-153 and miR-133b were milder inhibitors. It has been reported that miR-7 and miR-153 synergistically repress α-syn expression[209]. We also tried to co-express plasmids carrying pri-miR-7 or pri-miR-153. However, the upregulated levels of both mature miRNAs were largely reduced when the same quantity of plasmids were co-transfected compared to individual transfection. We suspect that the biogenesis of individual miRNAs is affected due to the limit of processing enzymes. MiR-133b has been implicated with both direct and indirect inhibition on α-syn, although the evidence seems to not be solid[219, 221]. We observed gentle dose-dependent inhibition on α-syn protein levels induced by miR-133b. But this inhibition was not seen on the luciferase bearing α-syn 3'-UTR. The point mutation on the predicted binding site elevated luciferase levels, but this site is not conserved in other mammalian species. Therefore, miR-133b mediated α-syn inhibition is more likely to be indirect. Additionally, the lengths of the 3'-UTR of α-syn mRNA vary from 290 to 2,520 nt, where the 560-nt and 2,520-nt isoforms are predominant. Here we chose the 2,520-nt 3'-UTR in our luciferase assays. We can see that most of the valid miRNA targeting sites are within the 560-nt range from 5'[227]. An extended 3,775-nt version was uncovered, which bears extra cis-elements downregulating α-syn translation, including 10 miRNA targeting sites such as miR-28-5p[371].

To the best of our knowledge, the post-transcriptional regulation of pri-miR-153-2 has not been reported. The terminal loop of pri-miR-153-2, but not pri-miR-153-1 is highly conserved, yet it's unknown which is the dominant source of mature miR-153. We spotted potential inhibitory factors of pri-miR-153-2 biogenesis in SH-SY5Y, and identified 13 candidate proteins, especially MATR3 and RBM3 with known miRNA inhibitive functions. In addition, nucleolysin TIA-1 isoform p40 (TIA1), transformer-2 protein homolog beta (TRA2B) and MATR3 are also predicted by RBPmap to bind pri-miR-153-2 through specific recognition motifs. MATR3 RRMs can recognise the MAUCUUR motif, therefore may bind AUGUUG at the 5' of pri-miR-153-2-CTL, with a P-value of 9.69×10^{-3} in RBPmap. Strikingly, MATR3 also interacts with the CTLs of pri-miR-138-2 and pri-miR-29b-2 through this motif[280]. Thereby, MATR3 may inhibit the biogenesis of pri-miR-138-2 via recognising a specific motif and this may be similar in terms of pri-miR-153-2 processing. In contrast, RBM3 seems to broadly regulate miRNA levels by associating with most

pre-miRNAs and modifying the accessibility of Dicer[368]. This cold-inducible protein also negatively regulates a range of temperature sensitive miRNAs, exemplified by miR-142 and miR-143[369]. However, miR-153 is not among the upregulated miRNAs upon RBM3 knockdown in either study[368, 369].

Importantly, four proteins, RTL1, KIF21A, DPYSL2 and Ras-related protein Rab-7a (RAB7A) have not been annotated with RNA binding activities before. Since the former three are brain or SH-SY5Y enriched, they may be indirectly pulled down by the pri-miR-153-2-CTL through protein-protein interactions. However, RAB7A can reduce α-syn aggregates through autophagic clearance and reduce the toxicity[372]. Thus, it would be interesting to see if this protein is an inhibitor of miR-153, which will paradoxically block α-syn degradation.

To validate these assumptions, first we need to confirm the presence of inhibitory factors by comparing miR-153 processing using cell extracts from SH-SY5Y and HeLa. Then use siRNAs to knockdown those candidate proteins and re-evaluate the levels of mature miR-153.

In summary, miR-7, miR-153 and miR-133b are α-syn inhibitors that may function against the development of PD pathogenesis, especially miR-7. The biogenesis of miR-153 may be post-transcriptionally regulated through the CTL of its precursor in neuroblastoma. MATR3 is one of the potential trans-acting factors. Understanding these is of great importance for future PD therapeutics that target α-syn expression.

2. The development of RP-CONA: an on-bead lysate-based technique for RNA/protein modulators

2.1 Introduction of RNA Pull-down Confocal Nanoscanning (RP-CONA)

Due to the supremacy of miR-7 in inhibiting α-syn expression, it will be crucial to identify small molecules as miR-7 enhancers targeting the miR-7/α-syn pathway for potential PD therapeutics. Previously in our lab, we have proved that the biogenesis of miR-7 is inhibited by a RBP, HuR, through interaction with the CTL of pri-miR-7-1, with the assistance of another RBP MSI2[268]. Notably, the pri-miR-7/HuR interaction can be disrupted by oleic acid, a known inhibitor of MSI2, which in turn facilitates the production of mature miR-7[325]. However, OA is not effective at micromolar concentrations, has poor bioavailability when tested in cells and is toxic in high concentrations[373]. We hypothesise that small molecules dissociating the pri-miR-7/HuR interaction will elevate miR-7 levels, therefore inhibiting miR-7 targets especially α-syn. Therefore, it will be important to develop a screening technique that identifies inhibitors of the pri-miR-7/HuR interaction, which may benefit the development of PD therapies in the future.

Here we combine the method of RNA pull-down from eukaryotic cell lysates[374], with an on-bead screening platform confocal nanoscanning, and name the new technique RP-CONA[350, 351, 375]. In RP-CONA (**Figure 15**), we link His_6-streptavidin onto Ni-NTA agarose beads and attach 5'-FITC and 3'-biotin tagged pri-miR-7-1-CTL to the streptavidin beads. To prepare cell extracts, we overexpress mCherry-HuR in HuR KO HEK293T (**Figure 16**). The knockout of endogenous HuR helps to eliminate the dilution of mCherry signals from untagged HuR. Then we incubate the RNA-coupled beads with mCherry-HuR overexpressed cell lysates, and specifically pull-down mCherry-HuR by the pri-miR-7-1-CTL. With a confocal nanoscanning image system, the bound RNA or HuR can be detected as fluorescent rings on the outer edge of the beads in the FITC or mCherry detection channel, respectively. Inhibitors of the RNA/protein interaction will attenuate the intensity of mCherry rings without affecting FITC levels. The ring intensities are proportional to the level of on-bead RNA or protein and can be quantified with a custom plugin in ImageJ.

The lysate-based RP-CONA has two major advantages compared to other

conventional screening techniques, such as FRET and FP, to identify inhibitors of RNA/protein interaction. First, cell lysates provide more physiological environment, therefore it may avoid false positive hits that are not effective *in vivo*. Second, RP-CONA removes the need of protein purification, sometimes a time-consuming and costly process. Thus, the technique will benefit the study of RNA/protein events, for those proteins with difficulties in purification.

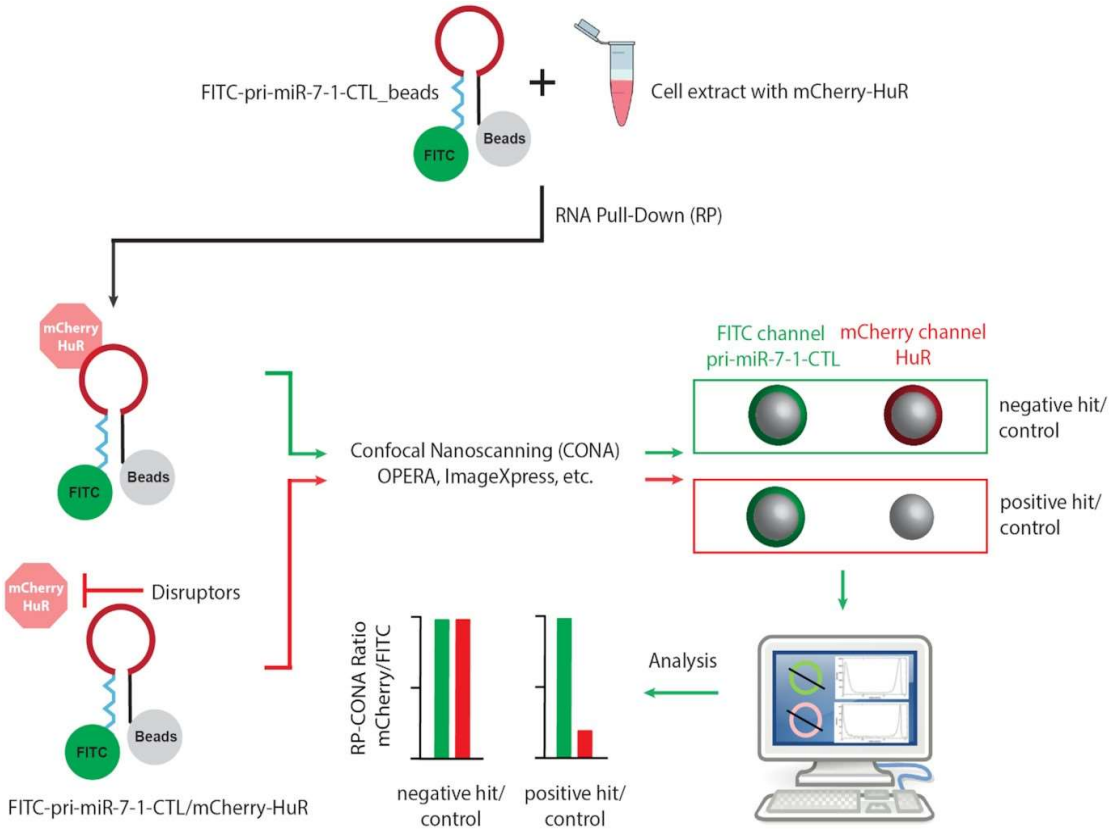

Figure 15 The working flow of RP-CONA. RNA Pull-down (RP): 5'-FITC-pri-miR-7-1-CTL-biotin-3' is coupled to streptavidin coated agarose beads. Cell lysates are extracted from HuR KO HEK293T cells overexpressing mCherry-HuR and treated with small molecules. The RNA-coupled beads are incubated with cell lysates to pull-down mCherry-HuR. Confocal Nanoscanning (CONA): Beads are imaged using a confocal image scanning platform. On-bead FITC-pri-miR-7-CTL and mCherry-HuR are detected with high sensitivity as fluorescent rings on the outer shell of bead in corresponding detection channels. Inhibitors can attenuate the mCherry fluorescence without affecting FITC signals. Analysis: The fluorescent rings are detected in imageJ. Four measurements are taken across each ring and generate the fluorescent intensity profiles to obtain intensity values.

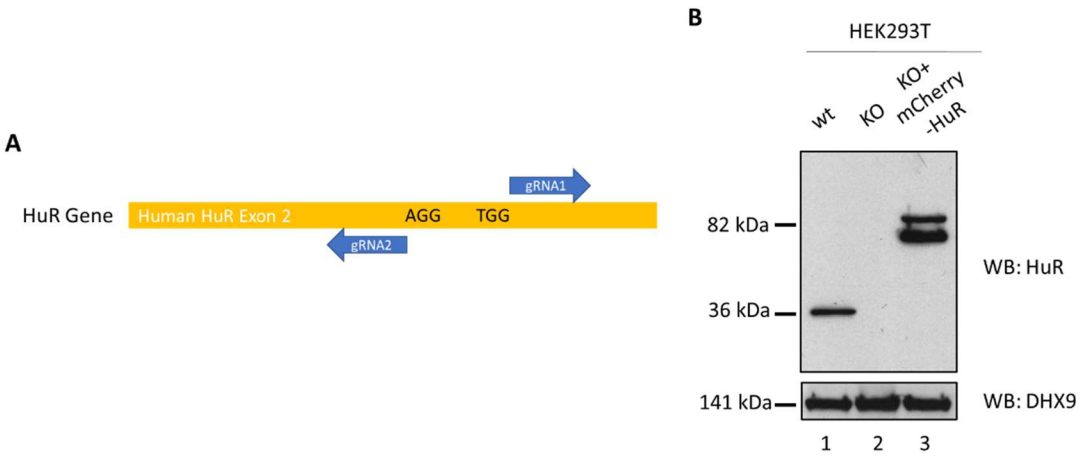

Figure 16 HuR knockout and overexpression. (A) Design of HuR knockout by CRISPR-Cas9. Human HuR exon2 is shown in orange. A pair of guide RNAs are shown in blue arrows. PAM sequences are presented. (B) Validation of HuR knockout and mCherry-HuR overexpression in HEK293T cells. The endogenous HuR and overexpressed mCherry-HuR levels were detected by HuR antibody using western blotting. DHX9 was used as a reference protein. 1: Wildtype HEK293T. 2: HuR KO HEK293T. 3: HuR KO HEK293T transfected with pJW99-HuR.

2.2 Homogenisation of RP-CONA signals

To begin with, we applied the methods of our classic RNA pull-down assay in RP-CONA. The adipic acid dihydrazide agarose beads were covalently conjugated with periodate oxidised FITC-pri-miR-7-1-CTL, incubated in cell lysates containing mCherry-HuR, and detected using an Opera HCS instrument (**Figure 17**). Blank beads did not generate any fluorescence in both detection channels. mCherry signals were not seen when blank beads were incubated with mCherry-HuR lysates, which means mCherry-HuR is not unspecifically associated with the beads. Fluorescent beads were detected in the FITC channel when the FITC-pri-miR-7-1-CTL was present on the beads and no overlapping signals were detected in the mCherry channel. Importantly, the on-bead mCherry were observed when mCherry-HuR was pulled-down by the FITC-pri-miR-7-1-CTL and the mCherry intensity seemed proportional to the FITC level. However, the fluorescence was not equally distributed among the beads. In many beads, the fluorescent components tended to penetrate into the beads, rather than concentrate on the outer edge to generate the quantifiable fluorescent rings. This can be attributed to the nature of covalent conjugation, which is slow and permanent. Therefore, a non-covalent coupling

chemistry with high affinity would be preferred in the RNA coupling strategy.

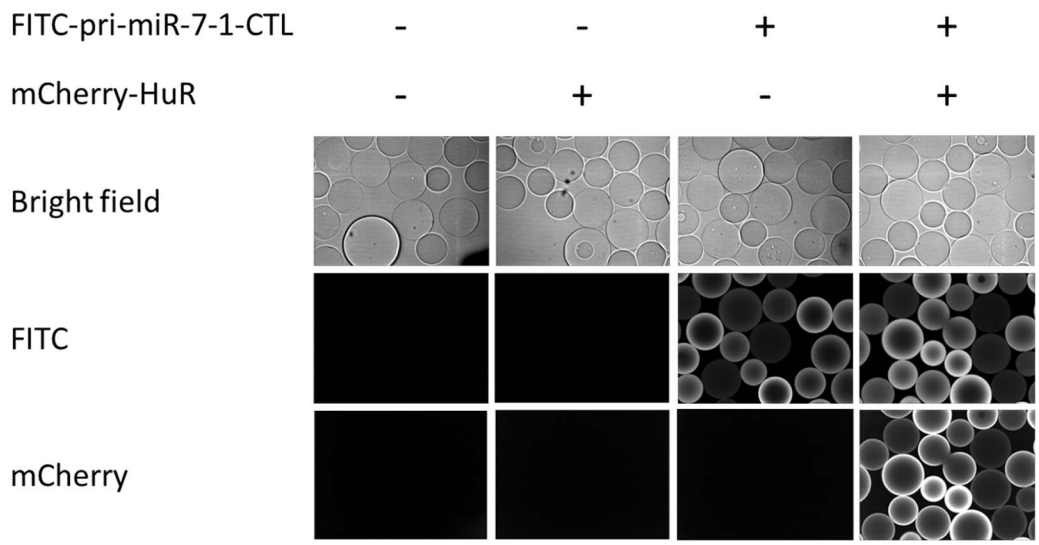

Figure 17 RP-CONA with covalently conjugated RNA beads. For each reaction, 250 pmol of FITC-pri-miR-7-1-CTL was periodate oxidised and covalently linked to 20 µl of adipic acid dihydrazide agarose beads. The beads were incubated with 500 µg of cell lysates containing mCherry-HuR. Images taken in an Opera HCS instrument at bright field, FITC, and mCherry channels. Images are shown with blank beads; blank beads incubated with cell lysates containing mCherry-HuR; FITC-pri-miR-7-1-CTL-beads incubated in lysates-free buffer; and FITC-pri-miR-7-1-CTL-beads after mCherry-HuR pull-down.

We subsequently applied the biotin-streptavidin interaction in RNA coupling, the known strongest non-covalent biological interaction with a remarkable dissociation constant (Kd) of 10^{-15} M[376]. 3' biotinylated FITC-pri-miR-7-1-CTL was coated onto commercial streptavidin agarose beads and pulled-down mCherry-HuR from cell extracts (**Figure 18**). With the new linking chemistry, both FITC-RNA and mCherry-HuR signals were homogenously distributed on the edge of a single bead and generated ring-like patterns. Moreover, the mCherry intensity became stronger with an increased concentration of mCherry-HuR. However, the ring intensities between different beads were variant and some beads were completely dark, which means streptavidin was not evenly coated onto the commercial beads.

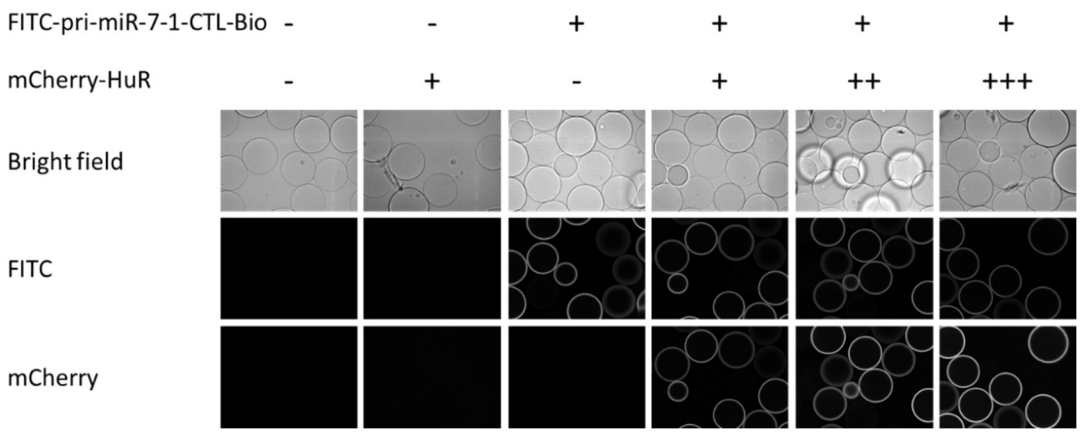

Figure 18 RP-CONA with biotinylated-RNA-streptavidin beads. Images taken in an Opera HCS instrument at bright field, FITC, and mCherry channels. For each reaction, 15 µl of 50% streptavidin beads were incubated with 62.5 pmol of FITC-pri-miR-7-1-CTL-biotin, and an increasing concentration of cell lysates containing mCherry-HuR. Images are shown with blank beads; blank beads incubated with cell lysates containing mCherry-HuR; FITC-pri-miR-7-1-CTL-beads incubated in lysates-free buffer; and FITC-pri-miR-7-1-CTL-beads after mCherry-HuR pull-down. Total protein levels of mCherry-HuR cell lysates: + 250 µg; ++ 500 µg; +++ 1 mg.

Due to the poor quality of the commercial streptavidin beads, we manufactured home-made beads by attaching His_6-streptavidin onto Ni-NTA agarose beads and imaged them by CONA (**Figure 19**). The combination of increased His_6-streptavidin monomer (10, 50 and 100 pmol) and FITC-pri-miR-7-1-CTL-biotin (50 and 100 pmol) were investigated. This time, homogenous fluorescent rings were obtained and the coefficient of variations (CVs) among the beads in each well were between 15-20%. Generally, FITC intensities increased proportionally along with the addition of streptavidin or FITC-RNA, unless the binding sites of streptavidin were saturated, or the RNA was depleted (**Figure 19A, B**). Crucially, the biotinylated FITC-RNA did not bind the beads when streptavidin was absent (**Figure 19C**).

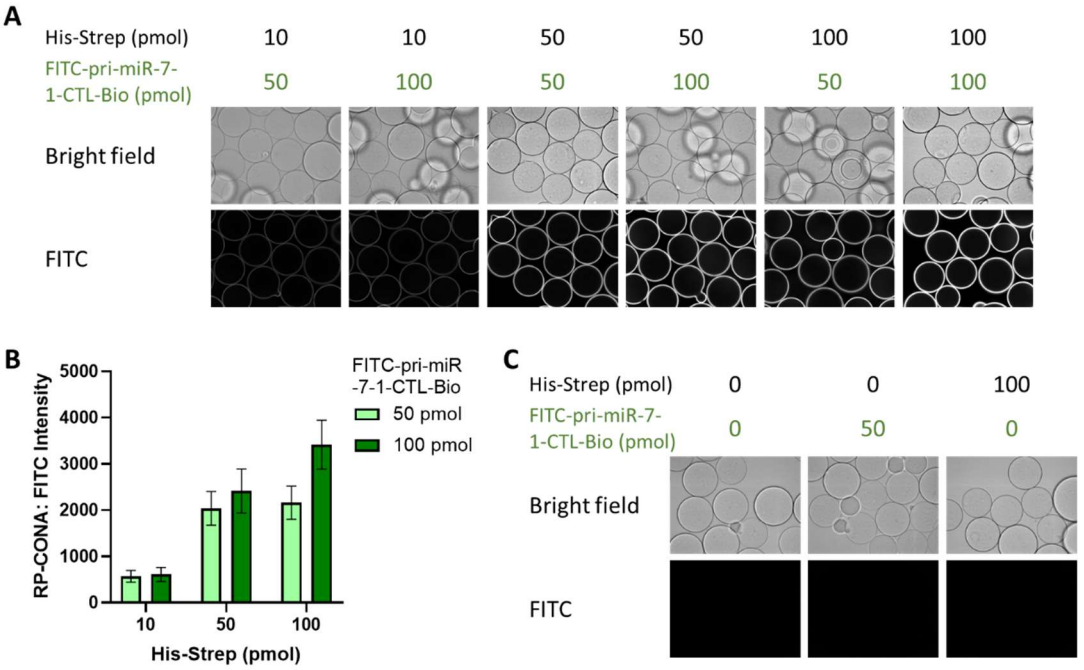

Figure 19 RNA coupling to streptavidin-Ni-NTA beads. (A, B) For each reaction, 1 µl of 50% Ni-NTA beads were treated with 10, 50, or 100 pmol of His_6-streptavidin, and then incubated with 50 or 100 pmol of FITC-pri-miR-7-1-CTL-biotin, respectively. The quantifications were obtained by BREAD from three technical repeats. Mean FITC ring intensities and maximum SD between the beads in each well are shown. (C) Control wells of blank Ni-NTA beads; blank beads incubated with 50 pmol of FITC-pri-miR-7-1-CTL-biotin; or blank beads incubated with 100 pmol His_6-streptavidin. All images were taken in an Opera HCS instrument at bright field and FITC channel.

Finally, we tested mCherry-HuR pull-down with these beads by RP-CONA (**Figure 20**). The on-bead pri-miR-7-1-CTL pulled-down mCherry-HuR and generated homogenous mCherry ring signals presenting similar quality as the FITC rings (CV< 20% between the beads in each well). There were weak background mCherry signals when mCherry-HuR was present in the system. We assume this is due to weak non-specific affinity between HuR and Ni-NTA beads. The analysis of FITC-pri-miR-7-1-CTL and mCherry-HuR rings of a single bead shows that the background signals of mCherry and FITC are similar. Therefore, the quantification of ring intensities, which are determined by the peak values of the plot profile, is not affected.

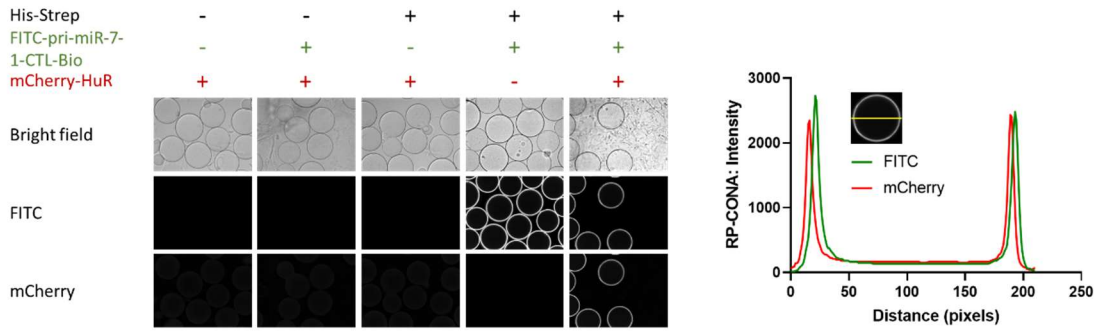

Figure 20 RP-CONA with RNA-coupled streptavidin-Ni-NTA beads. For each pull-down reaction, 1 µl of 50% Ni-NTA beads were treated with 50 pmol of His_6-streptavidin, incubated with 66.7 pmol of FITC-pri-miR-7-1-CTL-biotin and mixed with 166.7 µg of mCherry-HuR cell lysates (3 µg/µl). Images taken in an Opera HCS instrument at bright field, FITC, and mCherry channels. Images show: blank Ni-NTA beads incubated with mCherry-HuR cell lysates, blank Ni-NTA beads incubated with FITC-pri-miR-7-1-CTL-biotin and then lysates; His-streptavidin coated beads incubated with lysates; streptavidin beads coupled with FITC-RNA; FITC-RNA-streptavidin beads pulled-down mCherry-HuR from the lysates. A line was drawn across a single mCherry-HuR/FITC-RNA/streptavidin bead, and the plot profiles of FITC and mCherry intensities were generated in ImageJ. Peak values indicate the ring intensities, while the bottom values between the peaks are background signals.

To summarise, we developed the RP-CONA technique to monitor RNA/protein interactions and improved the fluorescent ring signals by modifying the RNA coupling strategy.

2.3 The sensitivity of RP-CONA

2.3.1 RP-CONA senses an untagged RNA competitor

To validate the sensitivity of RP-CONA, we investigated how RP-CONA would respond to the addition of a competitor. The mCherry-HuR cell lysates were treated with 32 or 64 µM of untagged pri-miR-7-1-CTL before pull-down (**Figure 21**). Both concentrations of the competitor reduced the mCherry ring signals without exerting obvious effects on FITC levels. The ratio of RP-CONA mCherry/FITC intensities was significantly inhibited by the competitor, compared to the untreated samples. This assay shows that in RP-CONA, the untagged pri-miR-7-1-CTL can associate with the free mCherry-HuR and prevent them from binding to the tagged RNA on the beads.

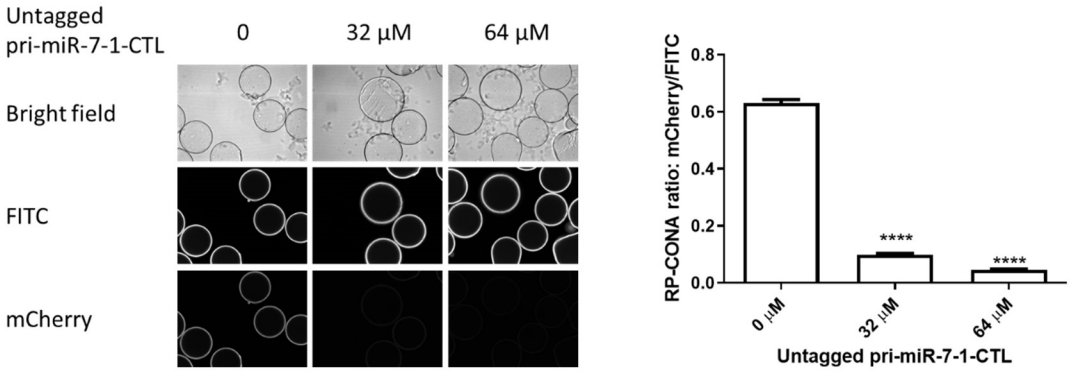

Figure 21 mCherry/FITC signals are reduced by untagged pri-miR-7-1-CTL. Cell lysates containing mCherry-HuR were treated with an increasing concentration of untagged pri-miR-7-1-CTL before pull-down. For each pull-down reaction, 1 μl of 50% Ni-NTA beads were treated with 50 pmol of His_6-streptavidin, incubated with 66.7 pmol of FITC-pri-miR-7-1-CTL-biotin, and mixed with 166.7 μg of mCherry-HuR cell lysates (3 μg/μl). Images taken in an Opera HCS instrument at bright field, FITC, and mCherry channels. The quantifications were obtained by BREAD from three technical repeats. Mean relative mCherry/FITC ring intensities and SD between triplicates are shown. Statistically significant differences compared to untreated samples were analysed using SPSS independent sample t-test, **** $P<0.0001$.

2.3.2 RP-CONA senses the small-molecule inhibitor of an RNA/protein interaction

Previously we have shown that OA can dissociate the pri-miR-7-1-CTL/HuR interaction at 500 μM[325]. Here we treated the mCherry-HuR cell lysates with an increasing concentration of OA before pull-down and tested by RP-CONA (**Figure 22**). A dose-dependent inhibition of mCherry ring intensities was observed. Importantly, the mCherry/FITC ratio was significantly reduced by 500 μM of OA, compared to the DMSO control, which is consistent with our previous findings. Moreover, the interaction of mCherry-HuR with FITC-pri-miR-7-1-CTL was almost entirely inhibited when OA reached 2 mM. Therefore, RP-CONA is effective when pri-miR-7/HuR interaction is inhibited by a small molecule.

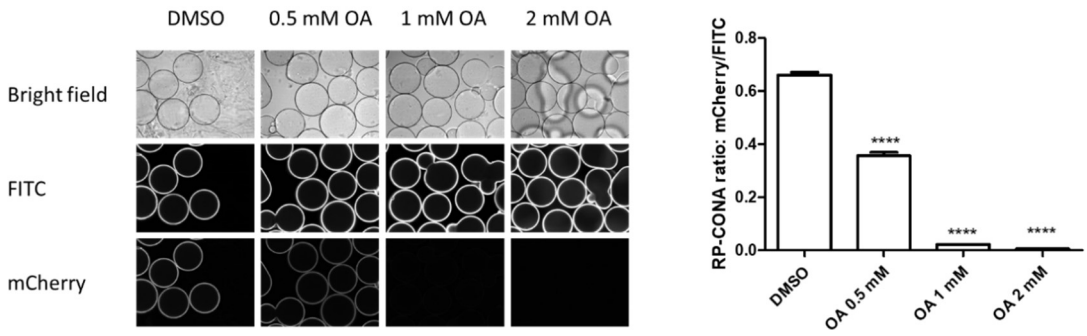

Figure 22 mCherry/FITC signals are reduced by a pri-miR-7/HuR inhibitor. Cell lysates containing mCherry-HuR were treated with DMSO, or an increasing concentration of OA before pull-down. For each pull-down reaction, 1 µl of 50% Ni-NTA beads were treated with 50 pmol of His_6-streptavidin, incubated with 66.7 pmol of FITC-pri-miR-7-1-CTL-biotin and mixed with 166.7 µg of mCherry-HuR cell lysates (3 µg/µl). Images taken in an Opera HCS instrument at bright field, FITC, and mCherry channels. The quantifications were obtained by BREAD from three technical repeats. Mean mCherry/FITC ring intensities and SD between triplicates are shown. Statistically significant differences compared to DMSO treated samples were analysed using SPSS independent sample t-test, **** $P<0.0001$.

2.3.3 RP-CONA senses the increase in RNA levels

To identify an optimal concentration of FITC-RNA for future screens, we tested the responses of RP-CONA upon an increase in RNA levels. The streptavidin-Ni-NTA beads were incubated with an increasing concentration of FITC-pri-miR-7-1-CTL-biotin (**Figure 23**). The FITC signal increased rapidly when RNA increased from 0 to 3.5 µM and started to saturate from 5 µM. 2 µM of FITC-RNA was selected for further RP-CONA assays, as the system is sensitive towards the RNA levels at this concentration. For each concentration, the beads were distributed into 5 wells after RNA-coupling. Although the variations between the beads in each well seemed large (**Figure 23B**), with CVs between 10-30%, the SDs between the 5 repeated wells were almost neglectable (**Figure 23C**), with CVs smaller than 5%. This means the FITC signals are very stable from well to well. Moreover, since we will calculate relative mCherry/FITC intensity for each measurement and the level of on-bead mCherry-HuR is presumably proportional to on-bead FITC-RNA, the massive variations between the beads may be complemented when we analyse the mCherry-HuR pull-down in RP-CONA.

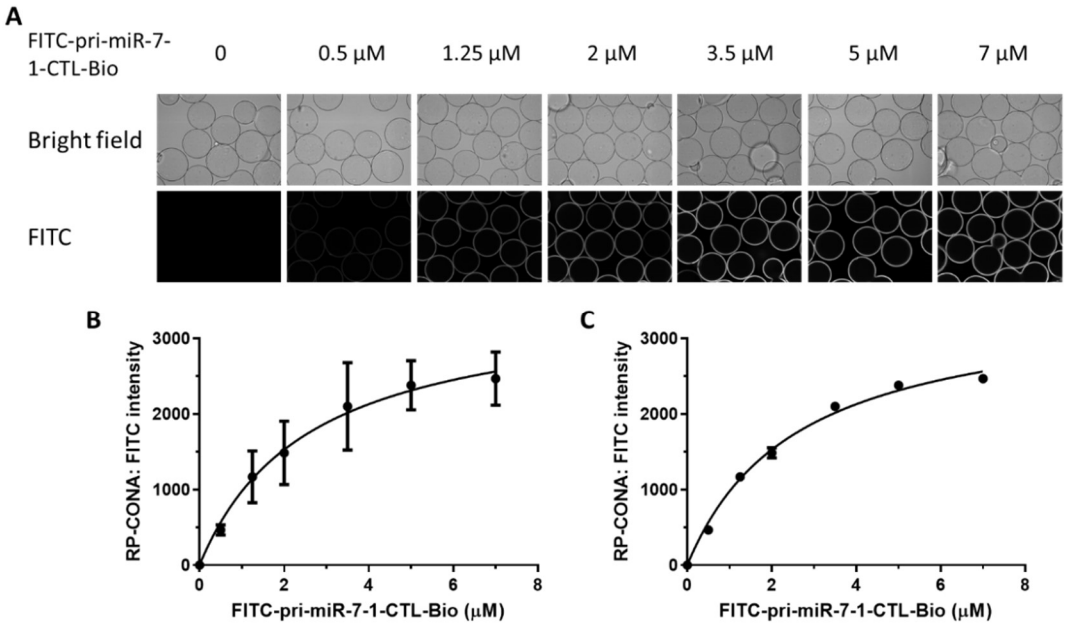

Figure 23 RP-CONA senses the increase in FITC-RNA levels. For each reaction, 1 µl of 50% Ni-NTA beads were treated with 150 pmol of His_6-streptavidin and then incubated with an increasing concentration of FITC-pri-miR-7-1-CTL-biotin. Images taken in an Opera HCS system at bright field and FITC channel. The quantifications were obtained by BREAD from 5 technical repeats. Mean FITC ring intensities and maximum SD between the beads in each well (B), and SD between 5 repeated wells (C) are shown. Data was curve fitted by non-linear regression (one site-specific binding) in Prism 8.

2.3.4 RP-CONA senses the increase in protein levels

Finally, we tested the sensitivity of RP-CONA as a response to mCherry-HuR levels. From here, we switched the image system to ImageXpress. Compared to Opera HCS, ImageXpress provides faster imaging settings while generating images of similar qualities. These would advance the application of ImageXpress in robust screens. In the previous assays the concentrations of cell lysates were determined by the total protein levels according to the absorbance at 280 nm. In this assay, the mCherry-HuR in the lysates was quantified by mCherry intensity with the help of an mCherry standard, which is more precise than the previous method. Here we aliquoted cell lysates containing an increasing concentration of mCherry-HuR and dispensed FITC-pri-miR-7-CTL-1-biotin coupled streptavidin-Ni-NTA beads into the lysates (**Figure 24**). There was a linear increase of mCherry/FITC signals along with the increased level of mCherry-HuR. Notably, the relative intensities were stable from bead to bead (**Figure 24B**) and well to well (**Figure 24C**), with both CVs less than 20%.

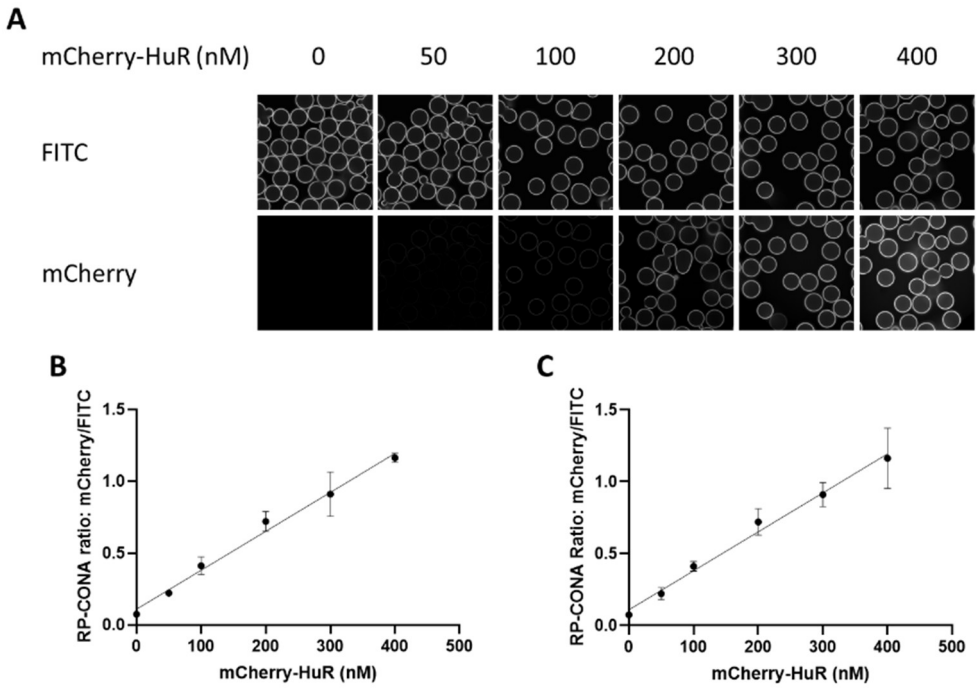

Figure 24 RP-CONA senses the increase in mCherry-HuR levels. For each reaction, 1 µl of 50% Ni-NTA beads were treated with 150 pmol of His_6-streptavidin and then incubated with 40 pmol (2 µM) of FITC-pri-miR-7-1-CTL-biotin. The RNA-coupled beads were mixed with cell lysates containing an increasing concentration of mCherry-HuR in a plate. Images taken in ImageXpress at FITC and mCherry channels. The quantifications were obtained in ImageJ with the Ring Measure plugin from three technical repeats. Mean mCherry/FITC ring intensities and maximum SD between the beads in each well (B), and SD between three repeated wells (C) are shown. The data was curve fitted by linear regression, R^2=0.9902.

The above assays prove that RP-CONA is a sensitive technique that monitors the interaction between pri-miR-7 and HuR. Moreover, the platform is highly flexible and can be applied in various confocal image scanning systems.

2.4 The specificity of RP-CONA

2.4.1 RP-CONA recognises specific RNA motifs

To confirm that the mCherry ring signals are representing specific binding events between pri-miR-7 and HuR, we swapped the CTL of pri-miR-7-1 with the non-conserved TL of pri-miR-30a that does not bind HuR (**Figure 25A**). In RP-CONA mCherry-HuR only bound FITC-pri-miR-7-1-CTL but not the chimeric FITC-pri-miR-7-1/30a TL (**Figure 25B**). Therefore, RP-CONA reveals the interaction between

an RBP and the specific RNA motif it recognises.

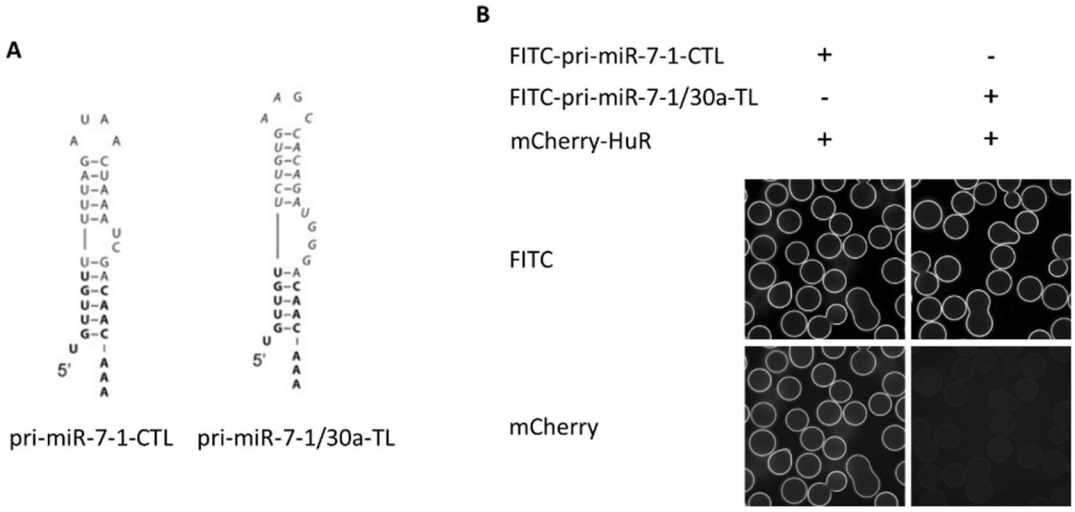

Figure 25 RP-CONA recognises specific RNA motifs. (A) A diagram illustrating the sequences of the pri-miR-7-1-CTL and the pri-miR-7-1/30a-TL. (B) For each RP-CONA reaction, 1 μl of 50% Ni-NTA beads were treated with 150 pmol of His_6-streptavidin and then incubated with 40 pmol (2 μM) of FITC-pri-miR-7-1-CTL-biotin or FITC-pri-miR-7-1/30a-TL-biotin. RNA-coupled beads were incubated in cell lysates containing 300 nM of mCherry-HuR. Beads images taken in ImageXpress at FITC and mCherry channels.

2.4.2 RP-CONA recognises specific RBPs

To test the specificity of RP-CONA towards RBPs, we incubated FITC-pri-miR-7-1-CTL beads in cell extracts with mCherry or mCherry-HuR. It was obvious that mCherry itself did not bind the RNA (**Figure 26A**), which means that it is HuR that mediates the binding activity in RP-CONA. Some RBPs that are not supposed to bind pri-miR-7-1-CTL were also investigated using RP-CONA. As previously mentioned, Lin28a recognises the GGAG motif through its zinc finger domain[264]. Only weak binding was detected between mCherry-Lin28a and FITC-pri-miR-7-1-CTL (**Figure 26B**). Since pri-miR-7-1-CTL does not possess a GGAG motif, the binding implies some weak affinity with the CSD of Lin28a. Trim25 was identified to have RNA binding activities in our previous research[377]. In RP-CONA, mCherry ring signals were not observed between mCherry-Trim25 and FITC-pri-miR-7-1-CTL (**Figure 26B**). We confirmed the overexpression of mCherry-Lin28a and mCherry-Trim25 (**Figure 27A, B**). We also verified that endogenous Trim25 was not pulled down by pri-miR-7-1-CTL, compared to the strong levels of HuR pull-down

(**Figure 27C**). As Lin28a is not expressed in wildtype HeLa, we did not test it using RNA pull-down assay here. To conclude, RP-CONA generates signals from fluorescent RBPs specifically bound to the RNA of interest.

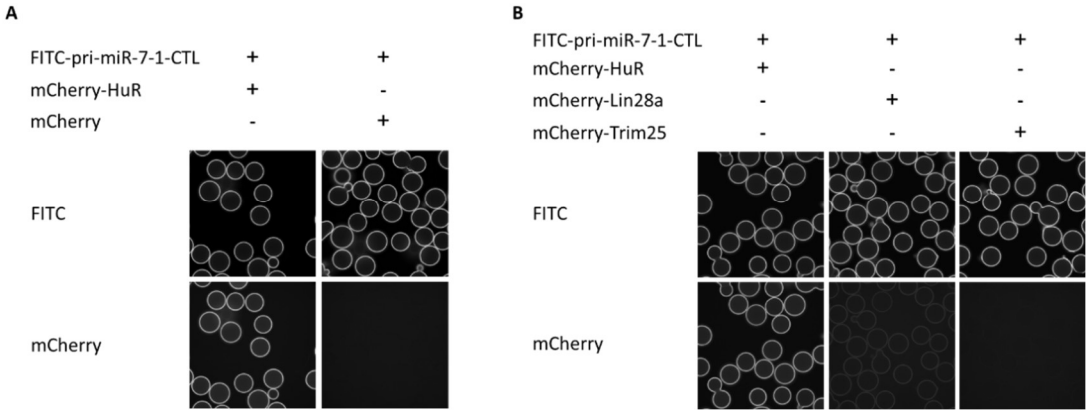

Figure 26 RP-CONA recognises specific RBPs. (A) Pri-miR-7-1-CTL binds mCherry-HuR but not mCherry. (B) Pri-miR-7-1-CTL binds mCherry-HuR but not other RBPs. For each RP-CONA reaction, 1 µl of 50% Ni-NTA beads were treated with 150 pmol of His_6-streptavidin, and then incubated with 40 pmol (2 µM) of FITC-pri-miR-7-1-CTL-biotin. RNA-coupled beads were incubated in cell lysates containing 300 nM of mCherry, mCherry-HuR, mCherry-Lin28a or mCherry-Trim25. Beads images taken in ImageXpress at FITC and mCherry channels.

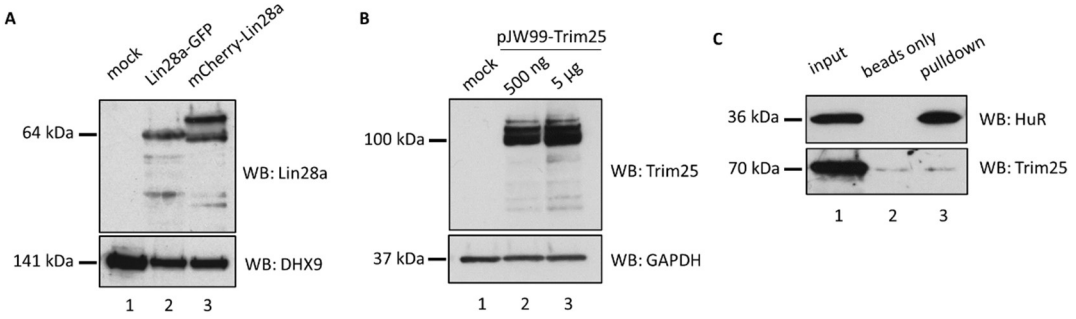

Figure 27 Characterisation of recombinant RBPs. (A) Expression of Lin28a-GFP and mCherry-Lin28a. Wildtype HEK293T were transfected with 1: mock (non-transfected), 2: pEGFP-N1-Lin28a, or 3: pJW99-Lin28a for 24 hrs. The overexpressed recombinant Lin28a levels were tested against anti-Lin28a antibody in western blot. DHX9 was tested as a reference protein. (B) Expression of mCherry-Trim25. Trim25 KO HEK293T were transfected with 1: mock (non-transfected), 2: 500 ng or 3: 5 µg of pJW99-Trim25 for 24 hrs. The overexpressed mCherry-Trim25 levels were tested against anti-Trim25 antibody in western blot. GAPDH was tested as a reference protein. (C) Trim25 pull-down by pri-miR-7-CTL-1. Periodate oxidised pri-miR-7-1-CTL was covalently linked to adipic acid dihydrazide agarose beads and incubated with wildtype HeLa extracts. HuR and Trim25 in the pull-down components were detected by western blot. 1: Input. Unbound proteins from the lysates after pull-down. 2: Proteins pulled down by blank beads without RNA. 3:

Proteins pulled down by pri-miR-7-1-CTL.

2.4.3 RP-CONA signals are reduced by antibodies targeting specific RBPs

Finally, we showed that the anti-HuR antibody can reduce mCherry ring intensities in a concentration-dependent manner. Furthermore, this reduction was not seen with the addition of anti-Lin28a antibody (**Figure 28**). To sum up, we prove that the RP-CONA signals are highly specific towards the target RNA/protein interaction.

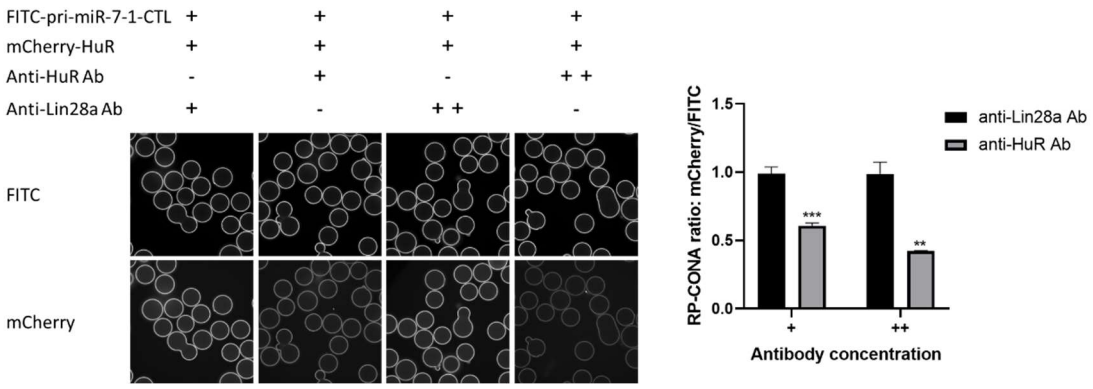

Figure 28 RP-CONA signals are reduced by specific antibodies. Cell extracts containing 300 nM mCherry-HuR were pre-incubated with 20 ng/µl (+) or 40 ng/µl (++) of anti-Lin28a antibody (control) or anti-HuR antibody prior pull-down by FITC-pri-miR-7-1-CTL-beads. Beads images taken in ImageXpress at FITC and mCherry channels. Mean mCherry/FITC ring intensities and SD between triplicates are shown. Statistically significant differences compared to anti-Lin28a antibody treated samples were analysed using SPSS independent sample t-test, ** $P<0.01$, *** $P<0.001$.

2.5 RP-CONA detects the let-7/Lin28a interaction

After successfully establishing RP-CONA in pri-miR-7/HuR interaction, we asked if this technique can be extended to other RNA/protein combinations. We tested the well-established pre-let-7a/Lin28a interaction with different fluorophores, where the Cy5 tagged pre-let-7a-1-CTL was incubated in HEK293T extracts overexpressing recombinant Lin28a-GFP. Wildtype HEK293T was chosen as it does not express Lin28a （**Figure 27A**） [365]. Similarly, GFP rings were only formed when Lin28a-GFP was pulled down by pre-let-7a (**Figure 29**).

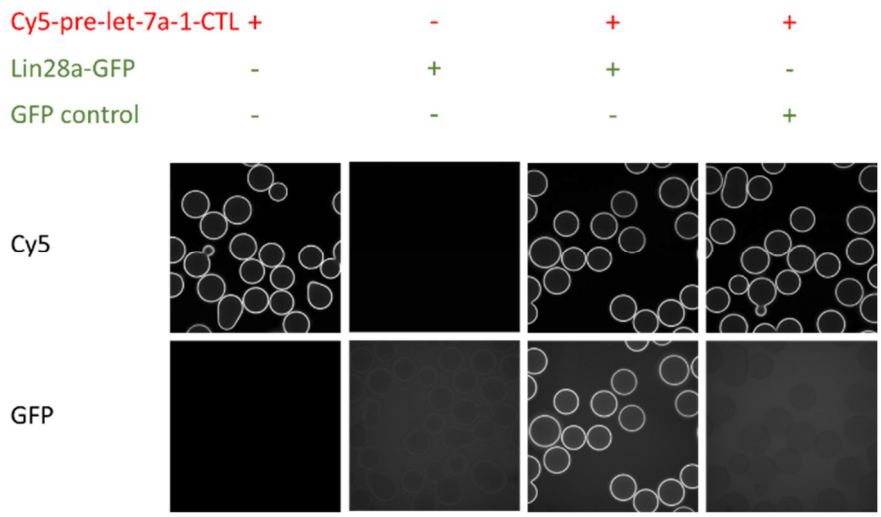

Figure 29 RP-CONA detects the let-7a/Lin28a interaction. For each RP-CONA reaction, 1 µl of 50% Ni-NTA beads were treated with 150 pmol of His_6-streptavidin and then incubated with 40 pmol (2 µM) of Cy5-pre-let-7a-1-CTL-biotin. RNA-coupled beads were incubated in cell lysates containing 300 nM of Lin28a-GFP. Beads images taken in ImageXpress at Cy5 and GFP channels, shown with Cy5-pre-let-7a-1-CTL-beads incubated in lysates-free buffer; blank beads incubated with cell lysates containing Lin28a-GFP; Cy5-pre-let-7a-1-CTL-beads incubated with cell lysates containing Lin28a-GFP; and Cy5-pre-let-7a-1-CTL-beads incubated with cell lysates containing 300 nM GFP.

To test if this RP-CONA assay can detect specific competitors, we subsequently introduced non-labelled pre-let-7a-1, or chimeric pre-let-7a-1/miR-16-1 into the let-7a/Lin28a RP-CONA reactions. In the chimera RNA, the CTL of pre-let-7a-1 was replaced by the TL of pre-miR-16-1 (**Figure 30A**), which is not a Lin28a binder according to our previous research[277]. As expected, the Lin28a-GFP signals were significantly reduced by pre-let-7a-1, compared to the chimeric pre-let-7a-1/miR-16-1, because of the competitive binding between non-labelled pre-let-7a-1-CTL and Lin28a (**Figure 30B**).

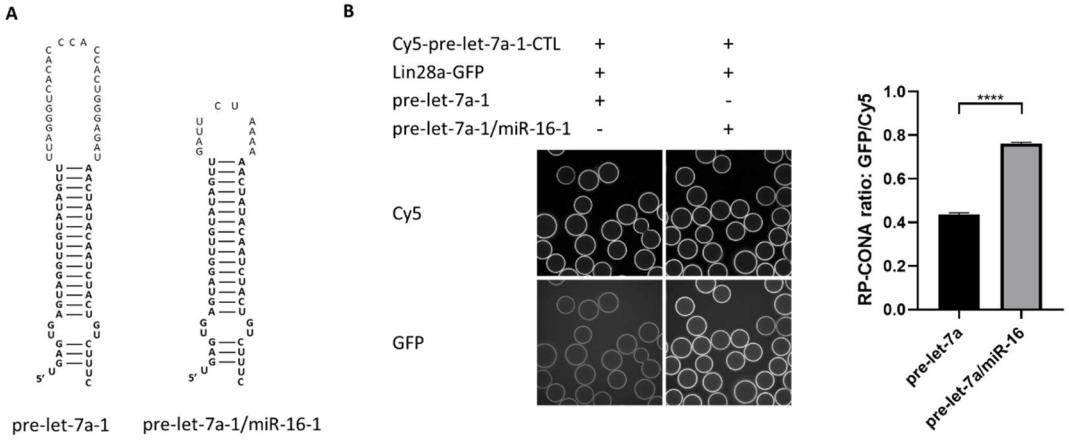

Figure 30 Let-7a/Lin28a interaction signals are reduced by unlabelled pre-let-7a in RP-CONA. (A) A diagram illustrating the sequences of pre-let-7a-1 and pre-let-7a-1/miR-16-1. (B) Cell extracts containing 300 nM of GFP-Lin28a were incubated with 80 pmol of pre-let-7a-1 or pre-let-7a-1/miR-16-TL (control), prior to pull-down with Cy5-pre-let-7a-1-CTL-beads. Beads images taken in ImageXpress at Cy5 and GFP channels. Mean GFP/Cy5 ring intensities and SD between triplicates are shown. Statistically significant differences compared to pre-let-7a-1/miR-16-1 treated samples were analysed using SPSS independent sample t-test, ****P<0.0001.

We also validated the specificity of this assay by introducing polyclonal anti-Lin28a antibody, which significantly reduced Lin28a-GFP signals compared to the reference anti-HuR antibody (**Figure 31**). This shows that RP-CONA can be applied to monitor different RNA/protein interactions, with high sensitivity, specificity, and flexibility.

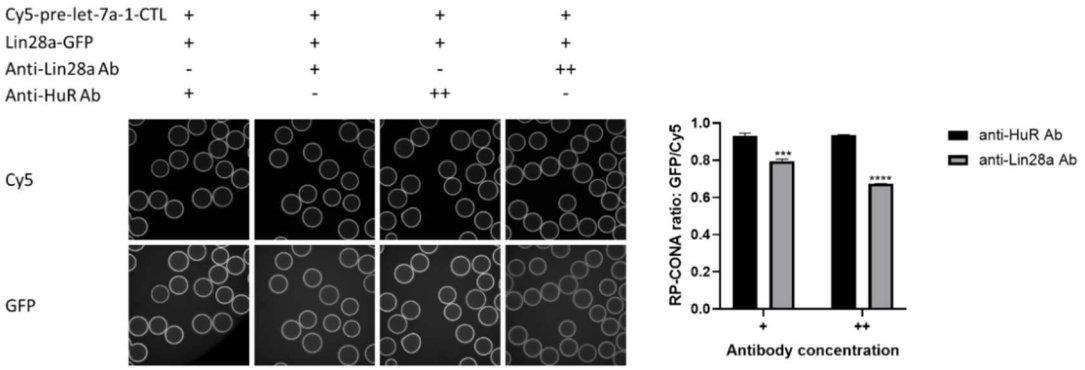

Figure 31 Let-7a/Lin28a interaction signals were reduced by anti-Lin28a antibody in RP-CONA. Cell extracts containing 300 nM Lin28a-GFP were pre-incubated with 20 ng/µl (+) or 40 ng/µl (++) of anti-HuR antibody (control) or anti-Lin28a antibody prior pull-down by Cy5-pre-let7a-1-CTL-beads. Beads images taken in ImageXpress at Cy5 and GFP channels. Mean GFP/Cy5 ring intensities and SD between triplicates are shown. Statistically significant differences compared to anti-HuR antibody treated samples were analysed using SPSS independent sample t-

test, *** P<0.001, ****P<0.0001.

2.6 Identification of pri-miR-7/HuR inhibitors by RP-CONA

2.6.1 Pilot RP-CONA screen from a focused library

A number of small-molecule inhibitors of HuR or Musashi proteins (MSI1 and MSI2) have previously been identified, which dissociate the interactions between the proteins and their target mRNAs[311]. We collected the commercially available compounds and incubated them in mCherry-HuR cell lysates at 100 μM before pull-down by FITC-pri-miR-7-CTL using the RP-CONA system (**Figure 32**). Most of the FITC signals remained unchanged after the treatment, except with Ro and DHTS which reduced FITC level by 34% and 18% respectively, compared to DMSO (**Figure 32B**). One possible reason is that these compounds convey extreme pH that dissociates the His-streptavidin or biotin-Ni interactions at high concentrations. Importantly, quercetin, luteolin and gossypol largely inhibited the mCherry signals without affecting FITC levels. OA did not show obvious inhibitive effects at 100 μM as previously reported[325]. The Z' factor of the screen was 0.93, and the CVs of the negative control (DMSO) and positive control (untagged pri-miR-7-CTL) equal to 1.75% and 0.96%, respectively (**Figure 32C**). Here we define quercetin, luteolin and gossypol as potential pri-miR-7/HuR inhibitors, reducing the mCherry/FITC level in RP-CONA by more than 50% (**Table 3**).

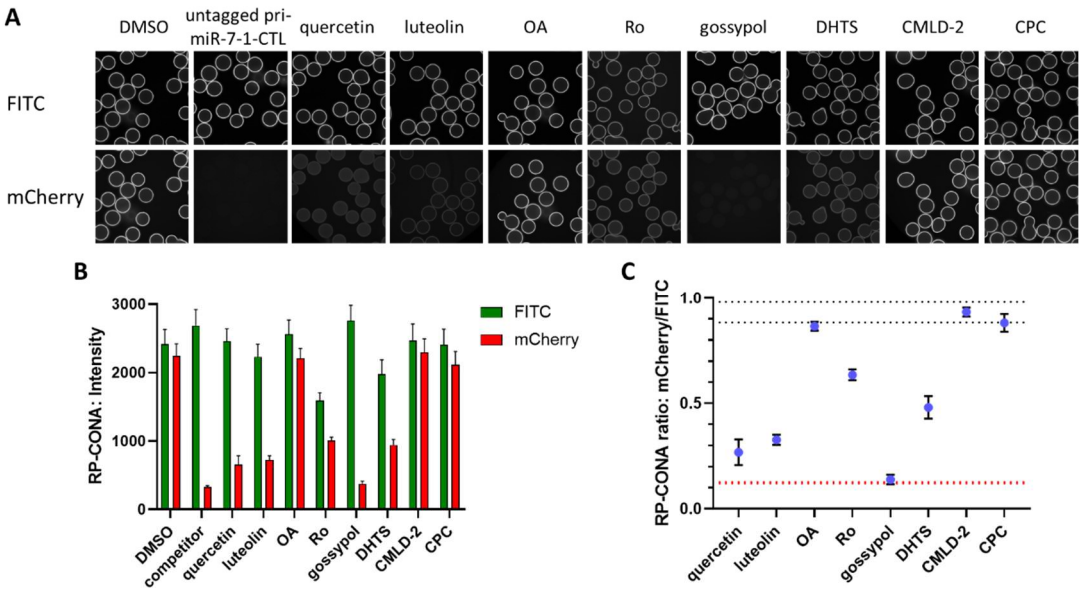

Figure 32 RP-CONA identifies pri-miR-7/HuR inhibitors from a focused library. For each reaction, 1 µl of 50% Ni-NTA beads were treated with 150 pmol of His_6-streptavidin and then incubated with 40 pmol (2 µM) of FITC-pri-miR-7-1-CTL-biotin. Cell lysates containing 300 nM of mCherry-HuR were treated with DMSO, 50 µM of untagged pri-miR-7-1-CTL or 100 µM of compounds before pull-down. (A) Beads images taken in ImageXpress at FITC and mCherry channels. (B) Average FITC or mCherry ring intensities and SD between the beads in each well after compound treatment are shown. (C) Relative mCherry/FITC ring intensity mean and SD between the beads in each well after compound treatment are shown. DMSO (RP-CONA ratio: 0.932±0.016, CV: 1.75%, n=5) served as a negative control while 50 µM of untagged pri-miR-7-1-CTL (RP-CONA ratio: 0.124±0.001, CV: 0.96%, n=5) served as a positive control. Z' = 0.93. Black lines: DMSO mean ± 3×SD between 5 repeated wells. Red lines: untagged pri-miR-7-1-CTL mean ± 3×SD between 5 repeated wells. At least 400 beads were included in each control analysis.

Table 3 Inhibition caused by the compounds from the focused library

Compound	Inhibition±SD† (%)
un.pri-miR-7-1-CTL	86.70±9.79
quercetin	71.22±16.54
luteolin	64.88±5.78
OA	7.08±0.39
Ro	31.85±2.04
gossypol	85.09±14.42
DHTS	48.44±5.87
CMLD-2	-0.10±0.01
CPC	5.41±0.38

† The inhibition caused by the compounds was calculated by mCherry/FITC level relative to the average mCherry/FITC of DMSO treated samples. The SD of relative inhibitions between the beads in each well after compound treatment are shown.

2.6.2 Small-scale RP-CONA screen from an enlarged library

To analyse RP-CONA's ability to scale up and to confirm the results of the pilot screen, we performed a small-scale screen using an in-house "random" library containing 54 FDA-approved drugs or natural products, together with 8 compounds from the previous focused library (**Figure 33**). Here, we applied quercetin as a positive control and DMSO as a negative control, which generated CVs of 2.18% and 6.70%, respectively. Most compounds did not show significant stabilisation or destabilisation of the pri-miR-7/HuR complex compared to DMSO. The primary hits, quercetin, luteolin and gossypol showed similar inhibition in these two RP-CONA screens. Additionally, we identified that genistein also inhibited the pri-miR-7/HuR interaction (48.96±2.33%), albeit less effectively than the previous hits.

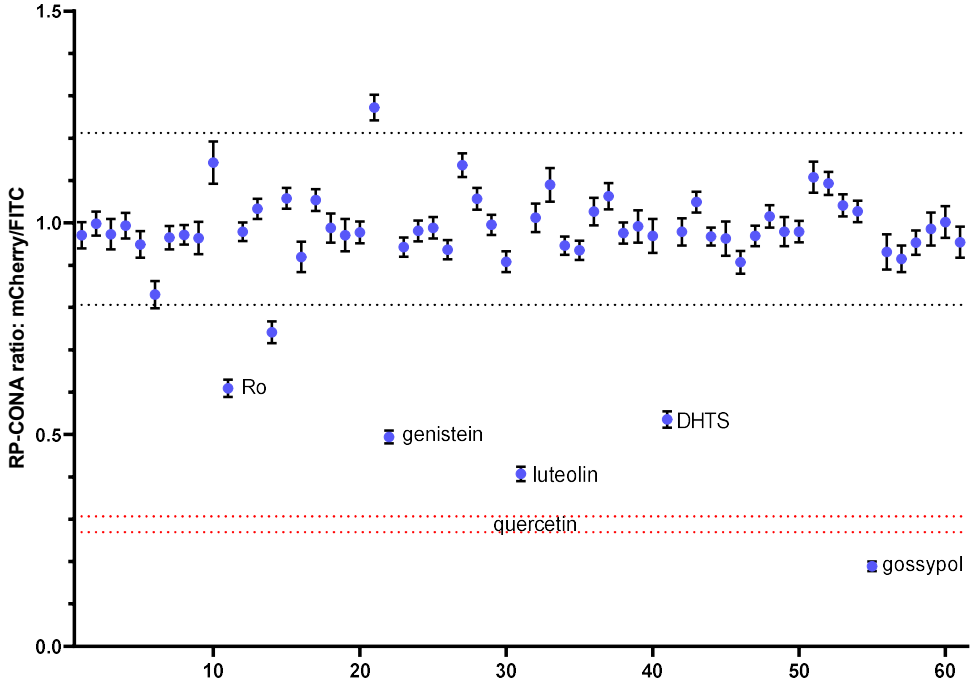

Figure 33 Identification of pri-miR-7/HuR inhibitors from an enlarged library. A small-scale RP-CONA screen testing the inhibitive effects of 62 compounds (54 from an in-house library varied from 1 to 100 μM and 8 from the previous identified HuR or MSI2 inhibitors at 100 μM) on pri-miR-7/HuR. Relative mCherry/FITC ring intensity mean and SD between the beads in each well after compound treatment are shown. DMSO (RP-CONA ratio: 1.009±0.067, CV: 6.70%, n=6) served as a negative control while 100 μM of quercetin (RP-CONA ratio: 0.288±0.006, CV: 2.18%, n=6) served as a positive control. Z' = 0.69. Black lines: DMSO mean ± 3×SD between 6 repeated wells. Red lines: quercetin mean ± 3×SD between 6 repeated wells. At least 500 beads were included in each control analysis.

Compounds generating larger than 40% (6 times CV of negative controls) inhibition are annotated.

2.6.3 Validation of RP-CONA hits

To validate the potential pri-miR-7/HuR inhibitors identified by RP-CONA, we tested them in a classic RNA pull-down assay, where the pri-miR-7-1-CTL was covalently conjugated to the beads and the protein levels after pull-down was investigated by western blot (**Figure 34**). The pull-down of endogenous HuR was largely reduced by quercetin and luteolin, compared to DMSO. Inhibitive effects of DHTS, Ro and genistein were also observed. However, gossypol interrupted the pull-down of the RNA helicase DHX9, which recognises double-stranded RNAs so universally binds miRNA precursors. Therefore, the inhibitive effect of gossypol is unspecific.

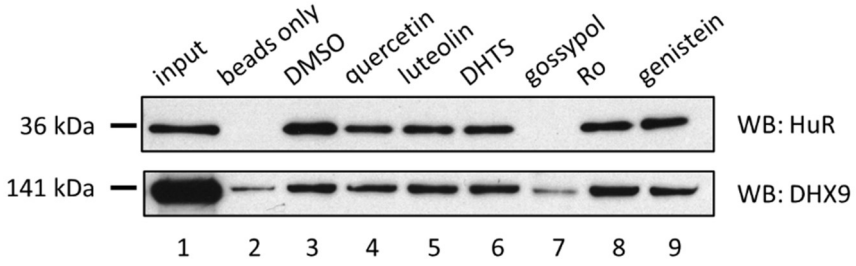

Figure 34 Inhibition of endogenous HuR pull-down by pri-miR-7-1-CTL. Periodate oxidised pri-miR-7-1-CTL was covalently linked to adipic acid dihydrazide agarose beads. HeLa extracts were treated with DMSO or 100 μM of each compound prior to pull-down. HuR and DHX9 in the pull-down components were detected by western blot. 1: Input. Unbound proteins from the lysates after pull-down. 2: Proteins pulled down by blank beads without RNA. 3-9: Proteins pulled down by pri-miR-7-1-CTL-beads after compound treatment.

We subsequently focused on the two most effective compounds, quercetin and luteolin, and tested their dose-response at a low range of concentrations in RP-CONA (**Figure 35**). Interestingly, quercetin and luteolin are close analogues (**Figure 35A**) and they showed similar dose-dependent inhibition on mCherry/FITC intensities with IC_{50}s of 2.15±0.16 μM and 2.03±0.25 μM, respectively. These observations validate the RP-CONA primary hits using a classic biochemical method and further confirm quercetin and luteolin as the most promising inhibitors of the pri-miR-7/HuR complex.

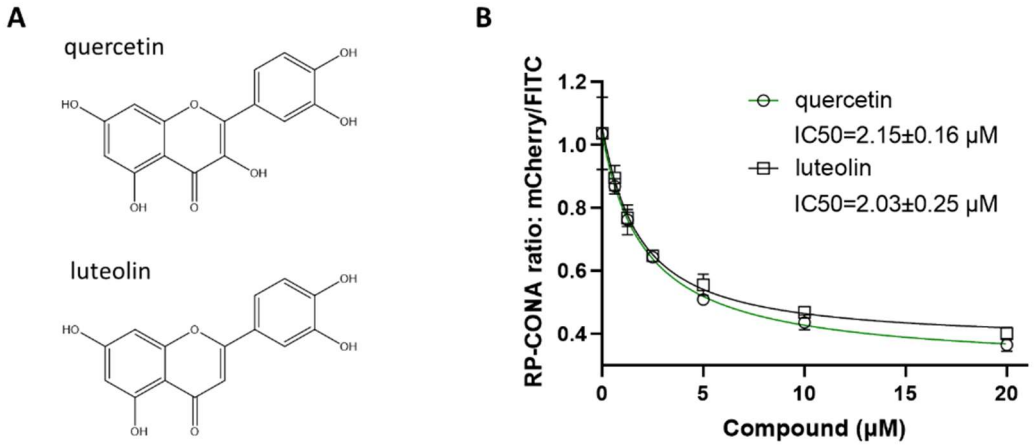

Figure 35 Dose-dependent inhibition of quercetin and luteolin in RP-CONA (A) Chemical structures of quercetin and luteolin. (B) Increasing concentrations of quercetin and luteolin were tested in RP-CONA. Relative mCherry/FITC ring intensity mean and SD between triplicated wells after compound treatment are shown. The RP-CONA signals were curve fitted by non-linear regression-four parameter [inhibitor] versus response, and IC_{50}s were determined with the 4-parameter equation in GraFit v7.0.3 (Erithacus Software Limited)[351]. The IC_{50}s of quercetin and luteolin were 2.15±0.16 μM and 2.03±0.25 μM, respectively.

2.7 Summary

In this chapter, we describe the development and optimisation of a novel fluorescent on-bead screening platform RP-CONA, with which we identified two pri-miR-7/HuR inhibitors from small-scale libraries, which are characterised further in the following chapter. We believe that RP-CONA will become a useful technique for monitoring RNA/protein interactions, as well as for the identification of RNA/protein regulators. Since Chapter 2&3 are closely related, the discussion of this chapter is combined with the next one, which can be found in session 3.8.

3. Functional study of pri-miR-7/HuR inhibitors on α-syn expression

3.1 Quercetin inhibits α-syn expression while upregulating miR-7

With the hypothesis that pri-miR-7/HuR inhibitors may inhibit α-syn expression by inducing mature miR-7 levels, we tested quercetin and luteolin in HeLa cells at 20 μM concentrations (**Figure 36**). Notably, quercetin induced a significant downregulation of α-syn protein (**Figure 36A, B**), while upregulating mature miR-7 by 1.5-fold (**Figure 36C**). However, luteolin had no significant effect on α-syn or miR-7 levels, suggesting different bioavailability, dynamics or cellular metabolism compared to quercetin.

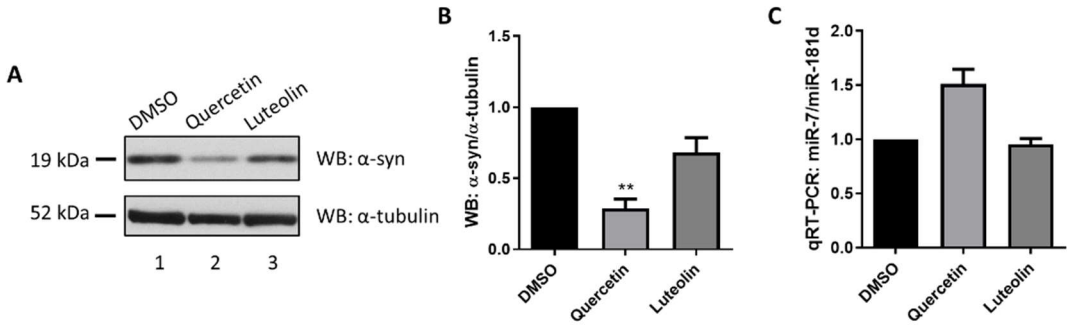

Figure 36 Quercetin inhibits α-syn and upregulates miR-7 in HeLa cells. (A, B) HeLa cells were treated with 1: DMSO, 2: 20 μM of quercetin or 3: 20 μM of luteolin and harvested 48 hrs after treatment. Levels of α-syn and α-tubulin were detected by western blot. Mean α-syn/α-tubulin and SEM from three independent repeats are shown. (C) HeLa cells were treated with DMSO, 20 μM of quercetin or luteolin and harvested 48 hrs after treatment. Mature miR-7 and miR-181d levels were determined by qRT-PCR. Mean miR-7/miR-181d and SEM from three independent repeats are shown. Statistically significant differences compared to DMSO were analysed using SPSS independent sample t-test, ** $P<0.01$.

We then tested the levels of pri-miR-7-1 and pre-miR-7-1 after quercetin treatment in HeLa cells. Pri-miR-7-1 levels were not changed, while pre-miR-7-1 was significantly upregulated (**Figure 37A, B**). Notably, HuR co-precipitated pri-miR-7-1 was significantly reduced after quercetin treatment (**Figure 37C**). Moreover, an RP-SMS analysis identified HuR and MSI2 among the proteins that were significantly reduced by quercetin after pri-miR-7-1-CTL pull-down (**Figure 38**). Collectively, quercetin inhibits pri-miR-7-1/HuR interaction in cells, therefore rescuing the inhibited pri-miR-7-1 processing mediated by HuR/MSI2.

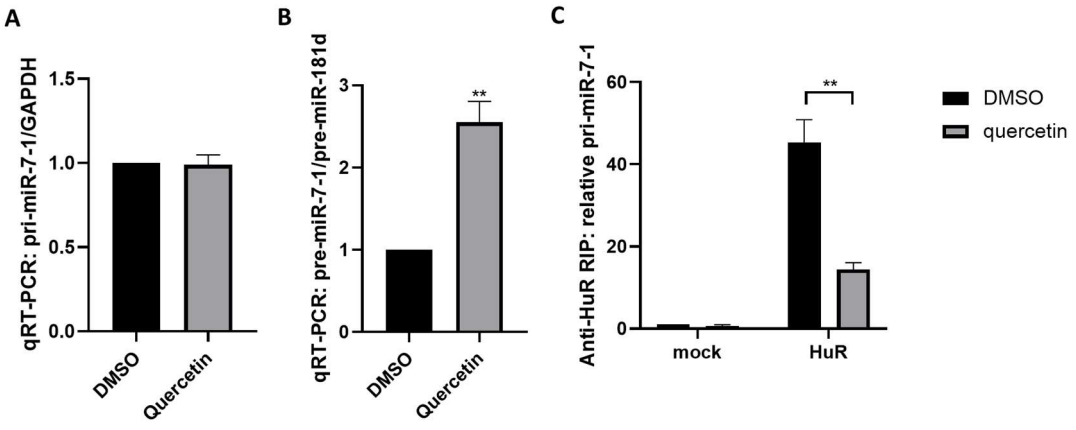

Figure 37 The effects of quercetin on miR-7 precursors. (A, B) Quercetin increased pre-miR-7-1 levels but not pri-miR-7-1. Wildtype HeLa cells were treated by 20 μM of quercetin for 48 hrs. The levels of (A) pri-miR-7-1 and (B) pre-miR-7-1 were quantified by qRT-PCR. Mean pri-miR-7-1/GAPDH, pre-miR-7-1/pre-miR-181d and SEM from three independent repeats are shown. (C) Quercetin dissociates the interaction of pri-miR-7-1 with HuR in cells. Mock or HuR-overexpressed HuR KO HeLa cells were treated with DMSO or 20 μM of quercetin and harvested 48 hrs after treatment. HuR bound RNAs from cell lysates were immunoprecipitated by anti-HuR antibody-coated beads and quantified by qRT-PCR. The levels of pri-miR-7-1 were normalised to DMSO treated mock samples. Mean relative pri-miR-7-1 levels and SEM from three independent repeats are shown. Statistical tests were analysed using SPSS independent sample t-test, ** $P<0.01$.

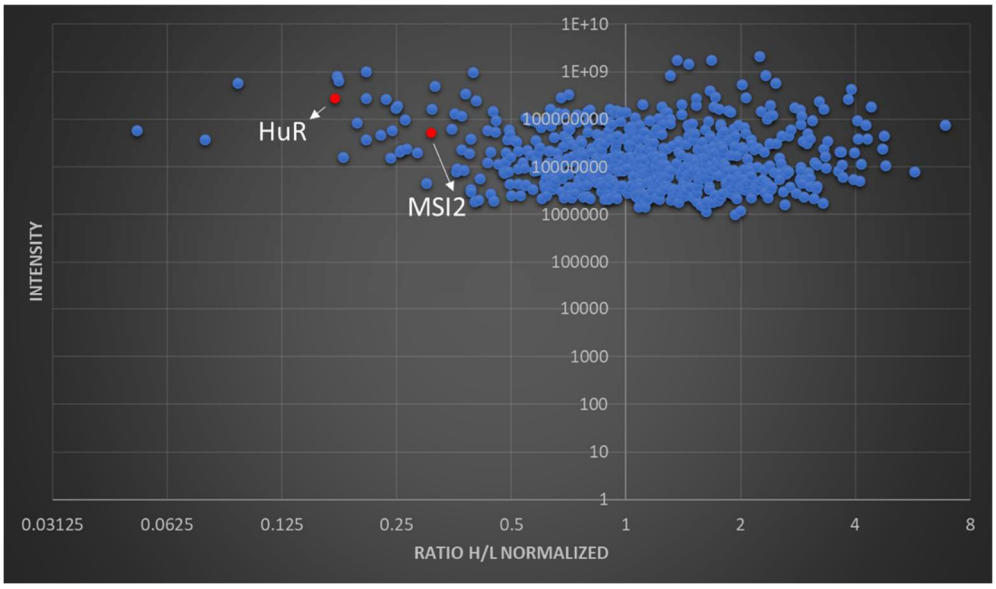

Figure 38 Quercetin inhibits HuR and MSI2 binding to pri-miR-7. RNA pull-down-SILAC mass spectrometry was performed using heavy HeLa extracts (^{13}C-arginine and ^{2}D-lysine) pre-treated with 100 μM quercetin while light HeLa extracts (no labelling) pre-treated with DMSO. The experiment was repeated twice. Identified peptides with intensities larger than 1×10^{6} are shown in blue dots. The corresponding normalised relative heavy/light intensity ratios are shown. Proteins with H/L ratios

less than 0.5 were considered as enriched in light pull-down components. HuR and MSI2 are highlighted with red dots.

We also observed that an increased concentration of quercetin gradually inhibited α-syn expression (**Figure 39A, B**). However, a dose-dependent upregulation of miR-7 was not seen (**Figure 39C**) and none of these concentrations can induce a statistically significant upregulation

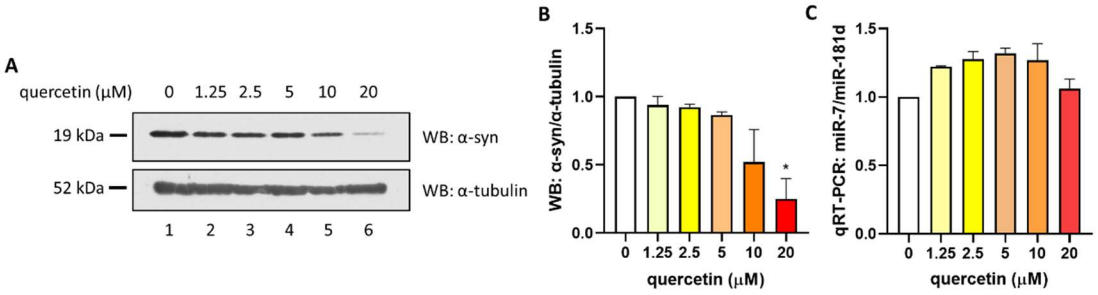

Figure 39 Quercetin inhibits α-syn expression in a dose dependent manner. HeLa cells were treated with 1: DMSO, or 2-6: an increasing concentration of quercetin and harvested 48 hrs after treatment. (A, B) Levels of α-syn and α-tubulin were detected by western blot. Mean α-syn/α-tubulin and SEM from three independent repeats are shown. Statistically significant differences compared to DMSO were analysed using SPSS independent sample t-test, * $P<0.05$. (C) MiR-7 levels were detected by qRT-PCR. Mean miR-7/miR-181d and SEM from three independent repeats are shown.

We started these tests with HeLa cells, because these cells have high basal levels of α-syn transcripts compared to most other cultured cells, according to The Human Protein Atlas[365].We then wondered if quercetin also inhibits α-syn expression in other types of cells, especially in neurons. We first tested HEK293T cells, but significant effects were not seen (**Figure 40A**). Subsequently, we treated human neuroblastoma SH-SY5Y and neuron-like mouse embryonic carcinoma P19 cell lines with quercetin and luteolin. Both compounds mediated α-syn inhibition in these neuronal cell lines. Nevertheless, the effects were not significant, and the miR-7 levels were not upregulated (**Figure 40B**).

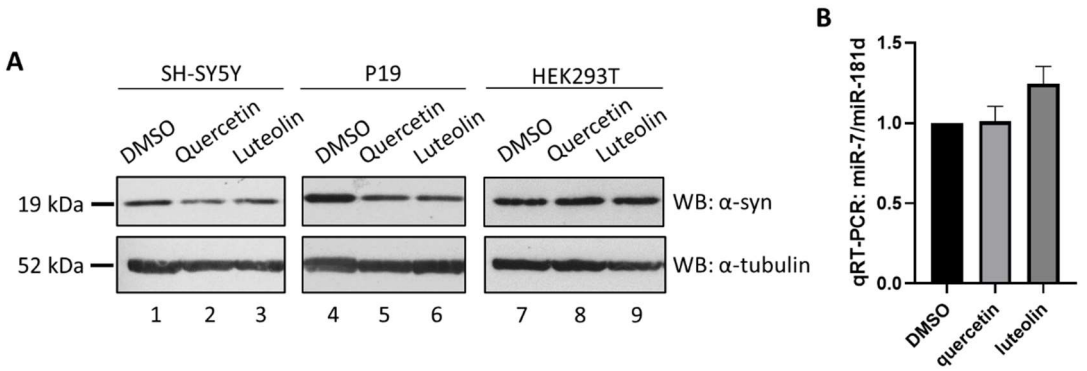

Figure 40 Quercetin and luteolin inhibit α-syn expression in neuronal cells. (A) SH-SY5Y cells were treated with 1: DMSO, 2: 20 μM of quercetin or 3: 20 μM of luteolin. P19 cells were treated with 4: DMSO, 5: 20 μM of quercetin or 6: 20 μM of luteolin on Day 7 after retinoic acid-induced differentiation. HEK293T cells were treated with 7: DMSO, 8: 20 μM of quercetin or 9: 20 μM of luteolin. Cells were harvested 48 hrs after treatment. Levels of α-syn and α-tubulin were detected by western blot. The experiments were repeated three times independently. (B) SH-SY5Y cells were treated with DMSO, 20 μM of quercetin or luteolin and harvested 48 hrs after treatment. Mature miR-7 and miR-181d levels were determined by qRT-PCR. Mean miR-7/miR-181d and SEM from three independent repeats are shown.

These results suggest that quercetin is an α-syn inhibitor. However, since an enhancement of miR-7 production is not consistently observed, it is uncertain whether quercetin acts through the miR-7/α-syn pathway.

3.2 Quercetin-induced α-syn inhibition is miR-7 independent

3.2.1 Generation of miR-7 KO cell lines

To understand if miR-7 is a key factor of quercetin inhibiting α-syn, we generated miR-7 KO cell lines by deleting the stem-loop sequence of pri-miR-7-1 in HeLa cells with CRISPR-Cas9 (**Figure 41**). MiR-7 has three loci but dominantly originated from pri-miR-7-1, which is regulated by HuR[268]. The potential miR-7 KO cells were initially selected by PCR, since KO cells would have smaller PCR products than the wildtype cells at the targeted region (**Figure 41B**). Afterwards, the miR-7 levels of these primary KO cells were quantified by qRT-PCR (**Figure 41C**). 6 of the cell lines (B4, A3, D3, E3, H3 and C5) did not generate detectable miR-7, so these could be double KOs. The miR-7 of C3 was depleted by half when compared to the wildtype cells, indicating C3 as a single KO. Finally, we chose three cell lines and confirmed their sequences (**Figure 41D**). C3 is a miR-$7^{+/-}$ as miR-7 was deleted in

one of its alleles while the other one is intact. B4 is a miR-7$^{-/-}$, since the miR-7 stem loop was removed from both alleles. H3 has miR-7 deleted in one allele. In the other allele, however, the fragment was cut off and re-assembled in the opposite orientation. Therefore, H3 is a miR-7$^{-/-}$. The genotyping results match well with the qRT-PCR data. In other words, we obtained two miR-7$^{-/-}$ cell lines that did not produce detectable miR-7 and one miR-7$^{+/-}$ cell line only expressing half of the original miR-7 level. The results also show that pri-miR-7-1 is the dominant source of mature miR-7, since the single KO had exact half of miR-7 level compared to wildtype cells, while double KO had almost undetectable levels (cycle number>34, 100-fold lower relative to wildtype cells).

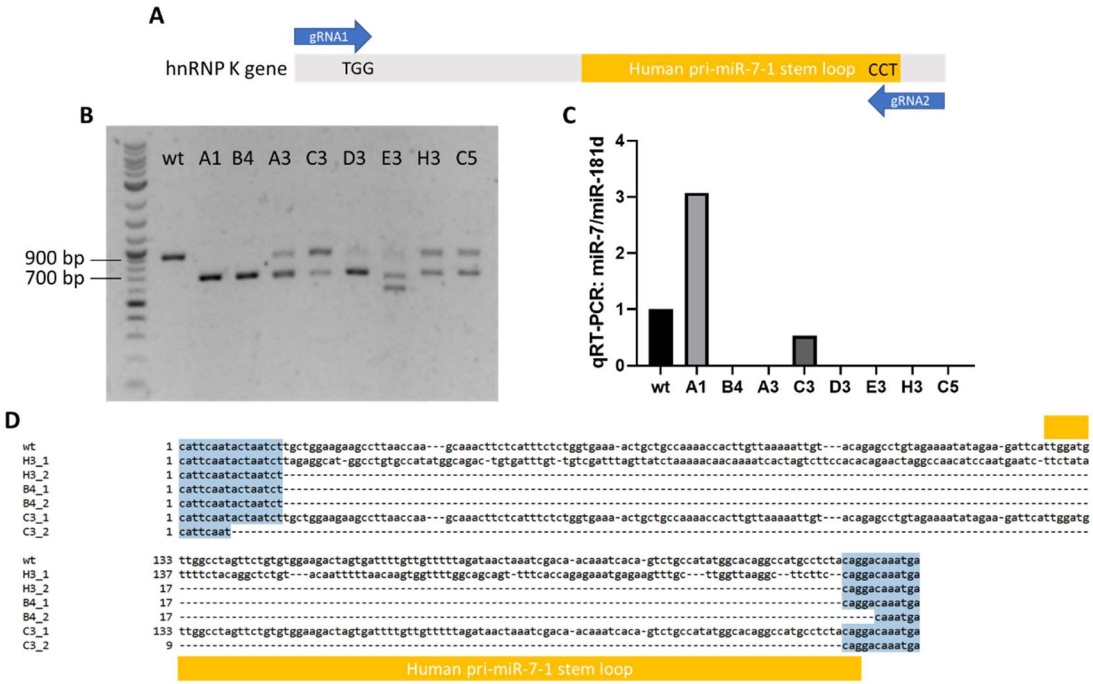

Figure 41 Generation of miR-7 KO cell lines. (A) Design of miR-7 knockout by CRISPR-Cas9. The human pri-miR-7-1 stem loop sequence is shown in orange. Other Regions are in grey. A pair of guide RNAs flanking the pri-miR-7-1 stem loop gene are shown as blue arrows. PAM sequences are presented. (B) Selection of miR-7 KO HeLa cell lines. Genomic DNA was PCR amplified using a pair of primers flanking the pri-miR-7-1 stem loop and analysed on an agarose gel. The deleted stem loop region was expected to be around 200 bp. Bands around 700 bp represent a potential KO. (C) MiR-7 level of miR-7 KO HeLa. Mature miR-7 and miR-181d levels of wildtype HeLa or miR-7 KOs were determined by qRT-PCR. (D) Sequence alignment of miR-7 KOs. Sequencing results of miR-7 KOs were aligned to the same region of the wildtype HeLa gene in Clone Manager 10. Regions originally encoding pri-miR-7-1 stem loop are indicated.

3.2.2 Quercetin inhibits α-syn expression in miR-7 KO cells

The effects of quercetin and luteolin were investigated in both miR-7$^{-/-}$ and miR-7$^{+/-}$ HeLa cell lines (**Figure 42**). Strikingly, α-syn levels showed similar patterns as in wildtype HeLa cells (**Figure 36A**) after treatment with the compounds, with quercetin inhibiting α-syn expression in all three cell lines. Thus, the quercetin-mediated α-syn repression is not dependent on the miR-7/α-syn pathway.

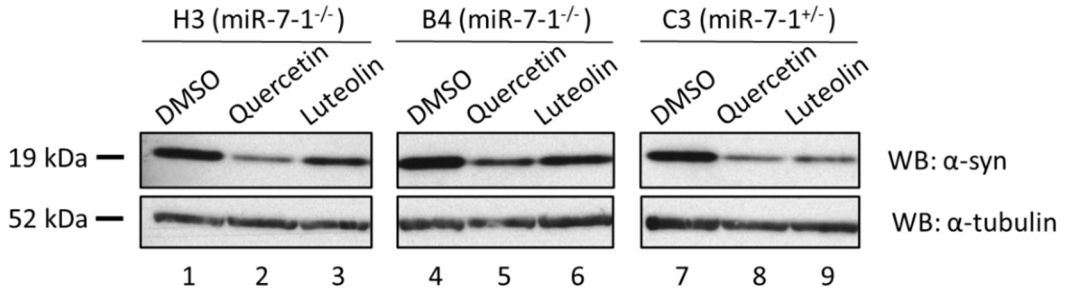

Figure 42 Quercetin inhibits α-syn expression in miR-7 KO cells. HeLa miR-7 KO H3 (miR-7-1$^{-/-}$), B4 (miR-7-1$^{-/-}$) and C3 (miR-7-1$^{+/-}$) were treated with 1, 4, 7: DMSO, 2, 5, 8: 20 μM of quercetin, or 3, 6, 9: 20 μM of luteolin for 48 hrs. Expression of α-syn and α-tubulin were detected by western blot.

3.3 Quercetin inhibits α-syn in an HuR-dependent pathway

3.3.1 Generation of HuR KO cells

Previously, we assumed that quercetin worked by disrupting the interaction between HuR and pri-miR-7, thereby activating the miR-7/α-syn axis. With the knowledge that miR-7 is not essential in the quercetin-induced α-syn repression, it is important to know if HuR participates in this pathway. We knocked out HuR in HeLa cells by CRISPR-Cas9 and validated the absence of this protein by western blot (**Figure 43**).

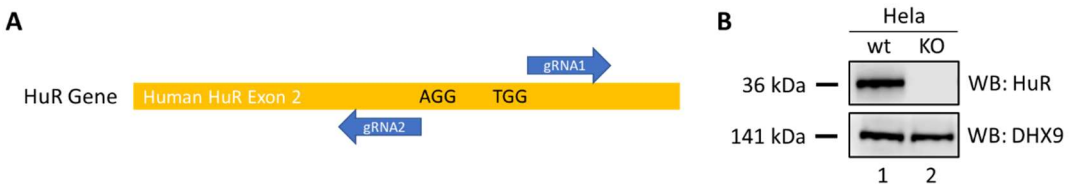

Figure 43 Generation of HuR KO cells. (A) Design of HuR KO by CRISPR-Cas9. Human HuR exon2 is shown in orange. A pair of guide RNAs are shown as blue arrows. PAM sequences are presented. (B) Validation of HuR knockout in HeLa cells. The HuR levels were tested by western blot. DHX9 was tested as a reference protein. 1: Wildtype HeLa. 2: HuR KO HeLa.

3.3.2 Quercetin does not inhibit α-syn in HeLa HuR KO cells

The HeLa HuR KO cells were treated with DMSO, quercetin or luteolin, and the levels of α-syn protein and miR-7 were analysed (**Figure 44**). Intriguingly, α-syn expression remained unchanged after compound treatment (**Figure 44A, B**). This strongly implies that HuR is an essential part in the pathway of quercetin-mediated α-syn inhibition. Nevertheless, quercetin and luteolin induced miR-7 levels in HuR KO cells by 2 and 3-fold, respectively (**Figure 44C**), suggesting a more complex machinery of miRNA regulation in the absence of HuR.

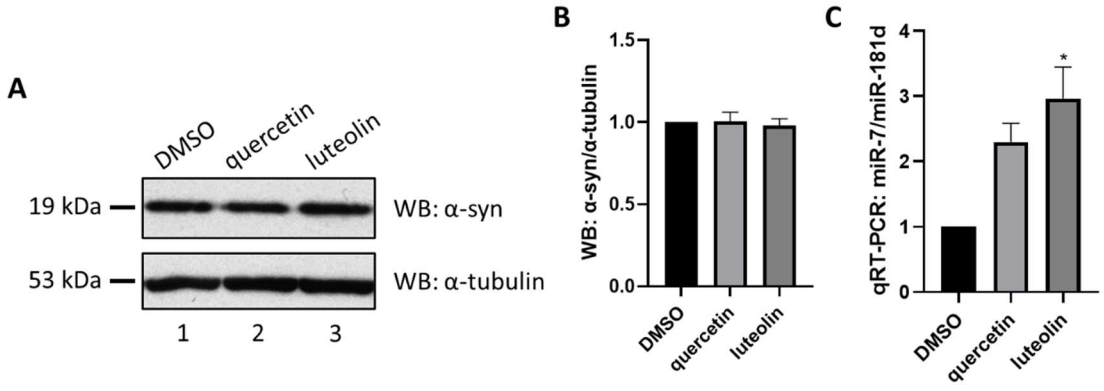

Figure 44 Quercetin does not inhibit α-syn in HeLa HuR KO cells. (A, B) HuR KO HeLa cells were treated with 1: DMSO, 2: 20 μM of quercetin or 3: 20 μM of luteolin and harvested 48 hrs after treatment. Levels of α-syn and α-tubulin were detected by western blot. Mean α-syn/α-tubulin and SEM from three independent repeats are shown. (C) HuR KO HeLa cells were treated with DMSO, 20 μM of quercetin or luteolin and harvested 48 hrs after treatment. Mature miR-7 and miR-181d levels were determined by qRT-PCR. Mean miR-7/miR-181d and SEM from three independent repeats are shown. Statistically significant differences compared to DMSO were analysed using SPSS independent sample t-test, * $P<0.05$.

3.3.3 Quercetin downregulates α-syn mRNA in an HuR-dependent pathway

Finally, we investigated the effects of quercetin on α-syn mRNA in wildtype, HuR KO, and miR-7 KO HeLa cells (**Figure 45**). Quercetin mediates a significant 50% downregulation in wildtype and all three miR-7 KO cell lines, compared to DMSO treated cells. While in HuR KO cells, the α-syn mRNA level was significantly higher than it was in other cell lines. This confirms that HuR plays an important role in quercetin-mediated α-syn inhibition, and this happens at mRNA level. Moreover, in HuR KO cells, quercetin exerted a slight but significant inhibition on α-syn mRNA

when compared to DMSO treated samples. This implies the existence of HuR-independent, alternative pathways that contribute to the α-syn inhibition.

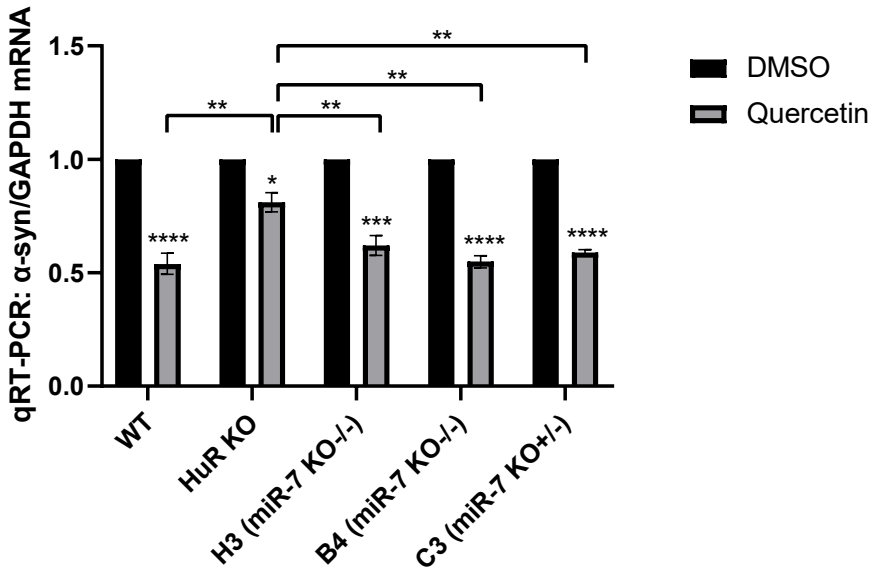

Figure 45 Quercetin downregulates α-syn mRNA in an HuR-dependent pathway. Wildtype, HuR KO and miR-7 KO (H3, B4 and C3) HeLa were treated with DMSO or 20 μM of quercetin and harvested 48 hrs after treatment. α-syn and GAPDH mRNA levels were determined by qRT-PCR. Mean α-syn/GAPDH and SEM from three independent repeats are shown. Statistically significant differences compared to DMSO, or between quercetin treated cells were analysed using SPSS independent sample t-test, * P<0.05, ** P<0.01, *** P<0.001, **** P<0.0001.

3.4 Quercetin inhibits HuR regulation of α-syn mRNA

3.4.1 Quercetin inhibits the interaction of HuR/α-syn mRNA

The 3'-UTR of α-syn mRNA bears AREs that are common binding targets of HuR[312]. Interestingly, the knockout of HuR resulted in a significant decrease of both α-syn protein and mRNA (**Figure 46**). Therefore, α-syn is positively regulated by HuR and this can be miR-7 dependent or independent.

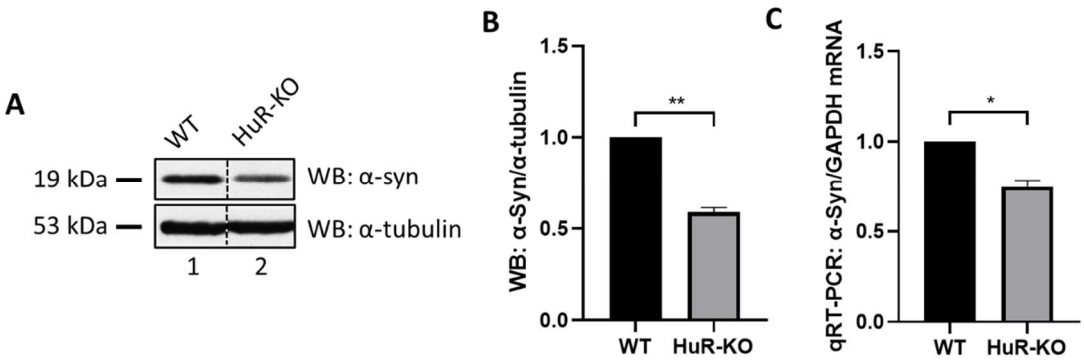

Figure 46 α-syn is positively regulated by HuR. (A, B) HuR KO leads to decreased levels of α-syn protein. Levels of α-syn and α-tubulin in 1: wildtype HeLa, or 2: HuR-KO HeLa were detected by western blot. Mean α-syn/α-tubulin and SEM from three independent repeats are shown. (C) HuR KO leads to a decreased level of α-syn mRNA. α-syn and GAPDH mRNA levels in wildtype or HuR-KO HeLa were determined by qRT-PCR. Mean α-syn/GAPDH and SEM from three independent repeats are shown. Statistically significant differences compared to wildtype cells were analysed using SPSS independent sample t-test, * P<0.05, ** P<0.01.

To validate the interaction between HuR and α-syn-ARE, we incubated FITC-α-syn-ARE beads with cell extracts containing overexpressed mCherry-HuR in RP-CONA. FITC-TNFα-ARE was also tested as a positive control. The ring signals clearly confirmed the strong affinity between HuR and α-syn-ARE *in vitro* (**Figure 47**). Furthermore, the binding activity showed a linear does-dependent manner, which is similar to the TNFα-ARE binding to HuR (**Figure 48**).

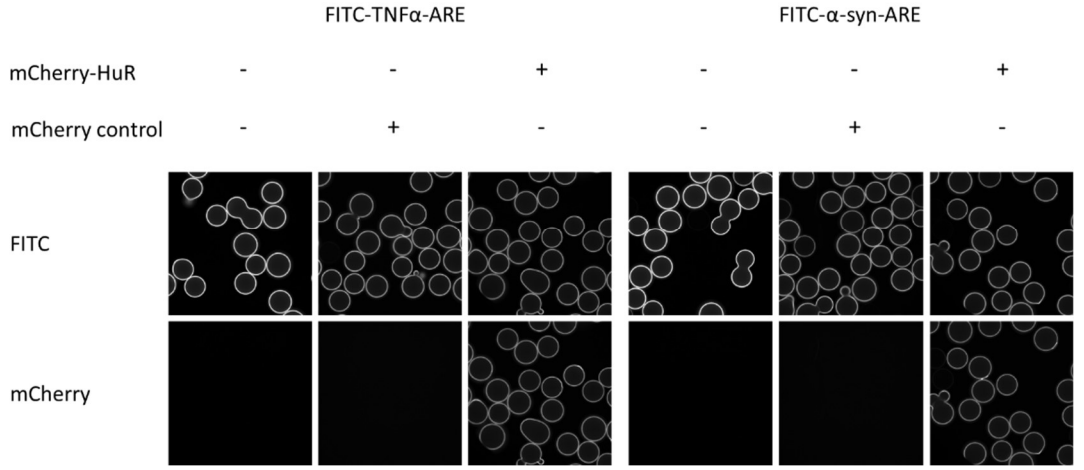

Figure 47 HuR interacts with α-syn-ARE. For each reaction, 1 μl of 50% Ni-NTA beads were treated with 150 pmol of His_6-streptavidin, and then incubated with 40 pmol (2 μM) of FITC-TNFα-ARE-biotin (A) or FITC-α-syn-ARE-biotin (B). RNA-coupled beads were incubated in lysate-free buffer, or cell lysates containing 300 nM

of mCherry or mCherry-HuR. Beads images taken in ImageXpress at FITC and mCherry channels. TNFα-ARE was used as a positive control.

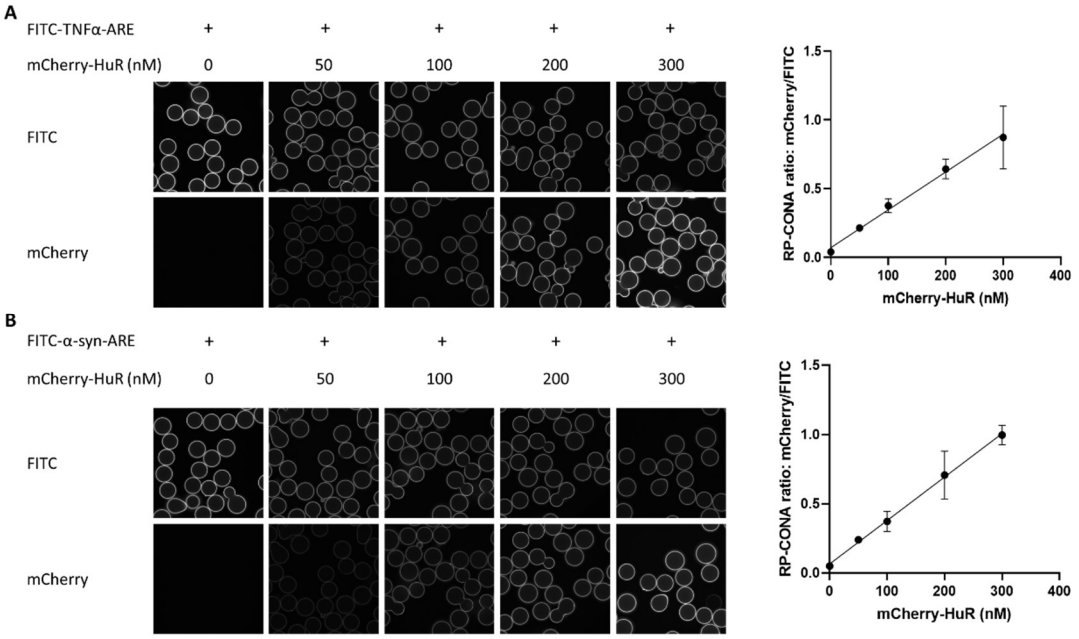

Figure 48 HuR binds α-syn-ARE in a dose-dependent manner. For each reaction, 1 µl of 50% Ni-NTA beads were treated with 150 pmol of His_6-streptavidin and then incubated with 40 pmol (2 µM) of FITC-TNFα-ARE-biotin (A) or FITC-α-syn-ARE-biotin (B). RNA-coupled beads were incubated in cell lysates containing an increasing concentration of mCherry-HuR. Beads images taken in ImageXpress at FITC and mCherry channels. TNFα-ARE was used as a positive control. Mean mCherry/FITC ring intensities and SD between triplicates are shown. The results were curve fitted by linear regression in Prism 8.

We subsequently tested the inhibitive effects of quercetin on TNFα or α-syn-ARE/HuR interaction in RP-CONA. Interestingly, quercetin only exhibited dose-dependent inhibition at high concentrations (**Figure 49**), implying stronger affinity between ARE/HuR, compared to pri-miR-7-1-CTL/HuR. Alternatively, quercetin may act through different mechanisms on these two types of interactions.

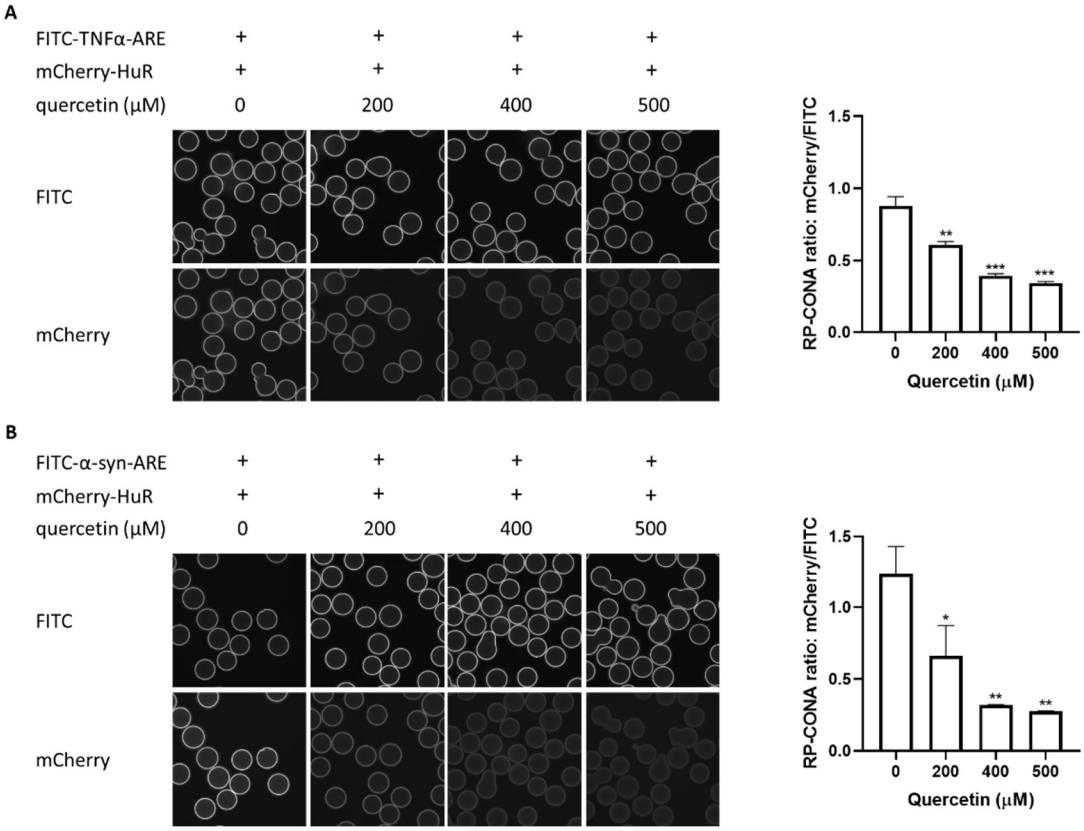

Figure 49 Quercetin inhibits α-syn-ARE/HuR interaction in RP-CONA. For each reaction, 1 μl of 50% Ni-NTA beads were treated with 150 pmol of His_6-streptavidin, and then incubated with 40 pmol (2 μM) of FITC-TNFα-ARE-biotin (A) or FITC-α-syn-ARE-biotin (B) Cell lysates containing 50 nM of mCherry-HuR were pre-incubated with an increased concentration of quercetin before pulldown. Beads images taken in ImageXpress at FITC and mCherry channels. TNFα-ARE was used as a positive control. Mean mCherry/FITC ring intensities and SD between triplicates are shown. Statistically significant differences compared to no quercetin were analysed using SPSS independent sample t-test, * P<0.05, ** P<0.01, *** P<0.001.

Importantly, the treatment of quercetin in HeLa cells resulted in a decreased binding of α-syn mRNA on HuR, according to a RIP assay (**Figure 50**). Thus, we prove that quercetin can directly interrupt the interaction of α-syn mRNA with HuR not only *in vitro*, but also in cells.

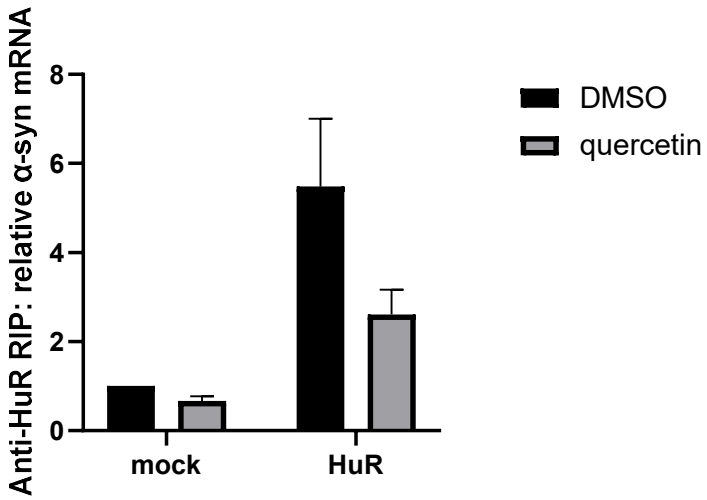

Figure 50 Quercetin dissociates the interaction of α-syn mRNA with HuR in cells. Mock or HuR-overexpressed HuR KO HeLa cells were treated with DMSO or 20 μM of quercetin and harvested 48 hrs after treatment. HuR bound RNAs from cell lysates were immunoprecipitated by anti-HuR antibody-coated beads and quantified by qRT-PCR. α-syn mRNA levels were normalised to DMSO treated mock samples. Mean relative α-syn mRNA level and SEM from three independent repeats are shown. Experiments conducted by Dr. N. Roy Choudhury.

3.4.2 Quercetin reverses the positive regulation of HuR on α-syn expression

Using our previous dual luciferase assay, we found that overexpression of HuR could significantly induce the levels of Renilla luciferase bearing the α-syn 3'-UTR (**Figure 51A**), however, without increasing its mRNA levels (**Figure 51B**). Quercetin treatment inhibited both luciferase and its mRNA levels in mock cells. Interestingly, when HuR was overexpressed, quercetin reversed the luciferase levels without posing significant alterations on its mRNA levels. From this, we conclude that HuR positively regulates α-syn expression via its 3'-UTR at translational levels and that this regulation can be reversed by quercetin treatment.

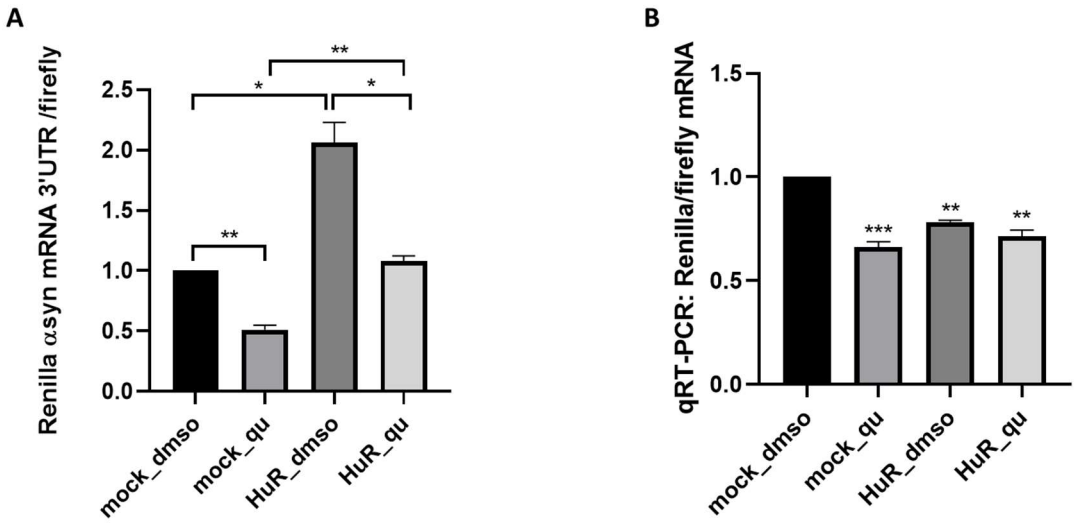

Figure 51 Quercetin inhibits the HuR-induced expression of luciferase bearing the 3'UTR of α-syn mRNA. Mock or HuR overexpressed HeLa cells were treated with DMSO or 20 μM of quercetin and transfected with the dual luciferase reporter carrying α-syn-3'UTR downstream of the Renilla luciferase gene. Mean luminescence levels (A) and mRNA levels (B) of Renilla/firefly luciferases, and SEM from 3 independent repeats are shown. Statistically significant differences between groups or compared to mock DMSO were analysed using SPSS independent sample t-test, * P<0.05, ** P<0.01, *** P<0.001.

Finally, we tested the effects of quercetin on α-syn mRNA stability. After actinomycin D treatment for 6 h, quercetin seemed to slightly destabilise α-syn mRNA in wildtype cells, but not HuR-KO cells (**Figure 52**). To sum up, quercetin inhibits α-syn mainly at translational level, with some contribution from regulating mRNA levels, including decreasing α-syn mRNA stability. Moreover, the subtle contribution from increased miR-7 levels should not be neglected.

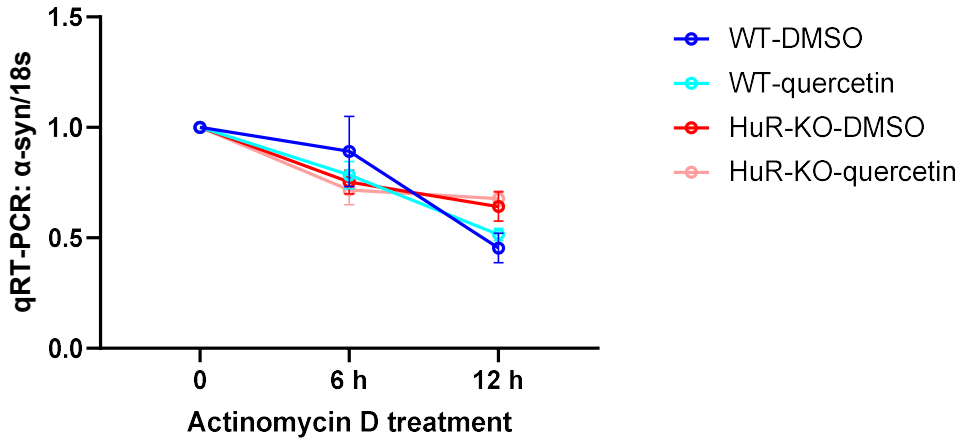

Figure 52 The effects of quercetin on α-syn mRNA decay. Wildtype and HuR KO HeLa cells were treated with DMSO or 20 μM of quercetin, supplemented with 10 μg/mL of actinomycin D for 0, 6 and 12 hrs respectively. α-syn mRNA and 18S levels were determined by qRT-PCR. Mean α-syn/18S and SEM from three independent repeats are shown.

3.5 The effects of quercetin in midbrain dopaminergic neurons

With firm evidence that quercetin downregulates α-syn in HeLa cells in an HuR-dependent pathway, it would be interesting to investigate its effects in midbrain DA (mDA) neurons, which could be a more relevant model to study PD pathologies. We treated the mDA neurons differentiated from human iPSCs with 20 μM of quercetin for 5 days. However, neither of the α-syn protein or mRNA levels showed significant changes (**Figure 53A, B**). One possibility is that mDA neurons don't have abundant HuR that allows quercetin to target. The other possibility is that mDA neurons have low α-syn levels to start with, therefore the downregulation is difficult to observe. With these assumptions, we compared the mRNA levels of HuR and α-syn between HeLa and mDA neurons. Interestingly, there is three times more HuR, but only half of α-syn in mDA neurons (**Figure 53C**). Since the materials of mDA neurons are limited, we were unable to compare the protein levels here. Moreover, the comparison of mRNA between different cell lines may not reflect the differences of true expression levels, if the mRNA and protein levels are not correlated[378]. Thus, the lack of effects of quercetin in mDA neurons could be a result of its low level of α-syn, but this needs further evidence. This doesn't mean quercetin is not applicable in PD treatment. mDA neurons derived from PD patients should be tested in the future, where α-syn is supposed to be abnormally overexpressed.

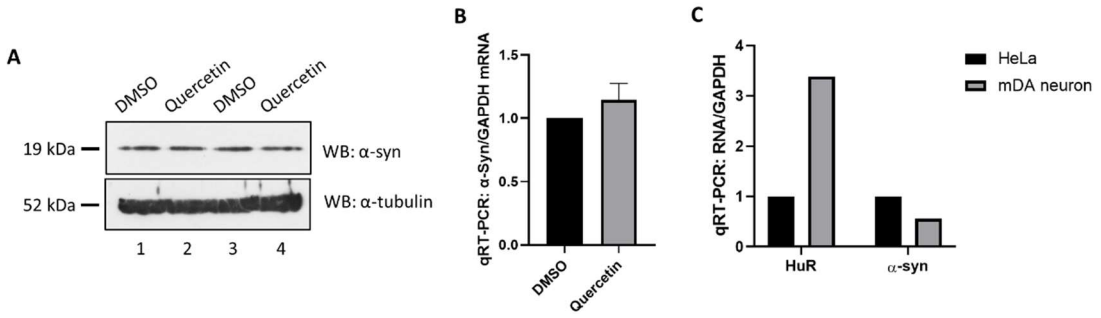

Figure 53 The effects of quercetin in mDA neurons. (A) Levels of α-syn and α-tubulin in mDA neurons detected by western blot after treatment of 1,3: DMSO, or 2,4: 20 μM of quercetin from Day 45 to 51. (B) α-syn and GAPDH mRNA levels in DMSO or quercetin treated mDA neurons were determined by qRT-PCR. Mean mRNA levels of α-syn/GAPDH and SEM from two independent repeats are shown. (C) HuR, α-syn and GAPDH mRNA levels in HeLa and mDA neurons were determined by qRT-PCR.

3.6 Quercetin specifically alters RBPs and HuR-binding proteins

Using a non-labelled protein quantification MS technique, we compared the proteomics with or without quercetin treatment in HeLa cells. Out of 3048 proteins/peptides identified, 96 were significantly altered by quercetin with 25 upregulated and 71 downregulated (**Figure 54**). Among these, a large percentage of proteins are RBPs, or HuR interactors. Interestingly, although α-syn was not identified in this assay, we found that two upregulated protein groups, namely serine/threonine-protein phosphatase 2B catalytic subunit α/β isoform (PP2B-Aα/β) and glycogen synthase kinase-3α (GSK-3α), are involved in the dopaminergic synapse pathway. Notably, HuR was identified among those unchanged proteins, meaning quercetin treatment does not alter HuR levels. These data clearly confirms that quercetin specifically targets HuR, affecting RNA binding activities and participating in the DA synaptic transmission.

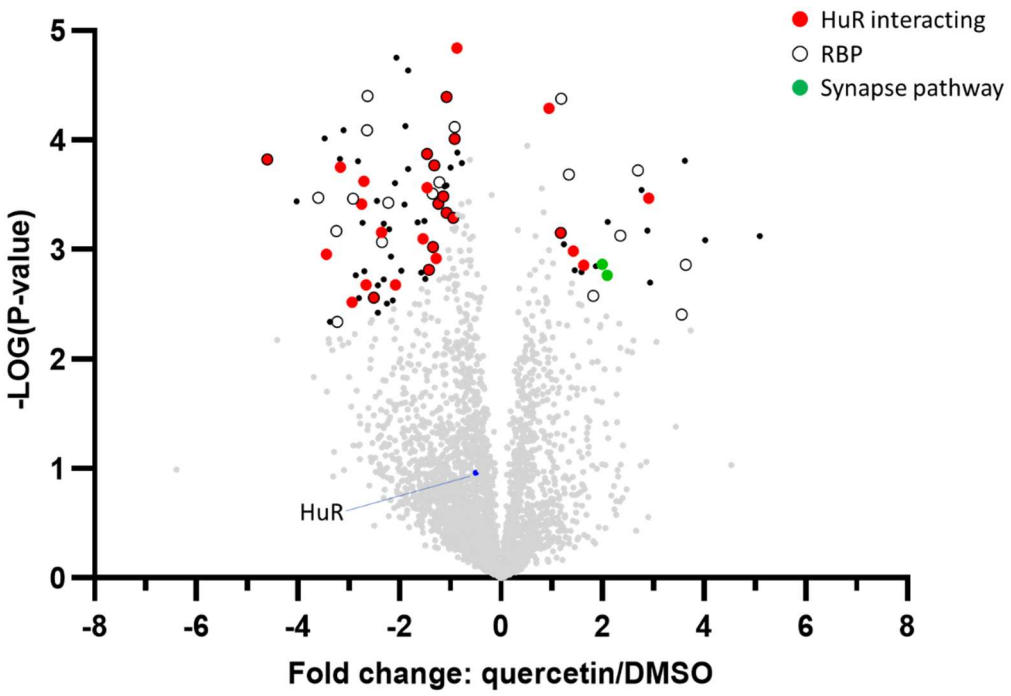

Figure 54 Quercetin specifically alters RBPs and HuR-binding proteins. Wildtype HeLa cells were treated with DMSO or 20 μM of quercetin for 48 hrs. The protein levels were quantified by MS. The volcano plots reveal the average fold changes of quercetin/DMSO versus -log(P-value) from three repeats. Dots representing protein/peptides with significant alterations are annotated with black, while others are grey. The significance was automatically determined by the MS software. Proteins/peptides with positive fold changes are upregulated by quercetin, while those with negative fold changes are downregulated. The significantly altered proteins/peptides were analysed by DAVID. RBPs are highlighted as black circles, HuR-interacting proteins as red dots and players in the DA synapse pathway as green dots. HuR is highlighted as a blue dot.

3.7 Summary

In this chapter, we showed a pri-miR-7/HuR inhibitor identified from RP-CONA, quercetin, as a miR-7 inducer and α-syn inhibitor. Unexpectedly, in addition to the HuR/miR-7/α-syn pathway, we identified an alternative miR-7 independent pathway that α-syn is directly regulated by HuR. The quercetin-mediated α-syn inhibition largely relies on HuR at both mRNA and protein levels. It will be interesting to plan follow-up research to fully elucidate the mechanism of this HuR-dependent regulation.

3.8 Discussion

3.8.1 Targeting RBPs and miRNAs

An increasing number of RNA-targeted therapies have drawn global attention in recent years. Through the regulation of RNA metabolism, people can find solutions for those "incurable" diseases. For instance, SMA is a severe progressive motor neuron disorder, caused by the lack of SMN proteins. The aforementioned drugs, nusinersen[379] and risdiplam[380] have shown lifesaving and long-lasting benefits for all types of SMA patients, by correcting the abnormal splicing of SMN2 mRNA. Current RNA-targeted therapies are mainly focused on the antagonism of RNAs, regulating the post-transcriptional events, including maturation, localisation, modification, and translation, all of which require cross talk with RBPs[311, 381]. Oligonucleotide drugs enable precise targeting and several RNA modification techniques provide improved binding affinity while reducing RNase resistance[382]. Shortly after the outbreak of the COVID-19 pandemic, mRNA vaccines encoding the spike protein of SARS-CoV-2 were approved and wildly administrated[383]. However, reports of the rare complication myocarditis after mRNA vaccination are raising concerns about the long-term safety of therapeutic nucleotide acids[384], yet it is uncertain whether this is specific to the mRNA platforms, or SARS-CoV-2 related[385]. On the other hand, small-molecule RNA regulators can largely improve patient accessibility compared to oligonucleotide drugs, as the small-molecule SMA drug risdiplam is administrated orally, while the ASO drug nusinersen requires intrathecal injection[311].

So far, more than 1,000 RBPs have been annotated in humans. Most RBPs are ubiquitously expressed, while only a small proportion have tissue-specific expression patterns[386]. There are a diversity of RNA binding domains, including RRM (or RBD), K-homology (KH) domain; zinc finger; double stranded RNA-binding domain (dsRBD); CSD; Piwi/Argonaute/Zwille (PAZ) domain and others, with more to be identified[381]. Sometimes RBPs contain multiple RNA binding domains and it is often difficult to get a full picture of RNA/protein interactions, such as the exact RNA motifs and the involvement of auxiliary domains. With the novel protein structure predicting algorithm Alphafold[387], the full-length structures of many RBPs may be

solved soon, which will be helpful to have a better understanding of RBP-mediated post-transcriptional regulation.

As to miRNA-targeted therapies, all the ongoing clinical trials are oligonucleotide drugs. Since none of them have entered Phase III (**Table 1**), it's hard to predict their safety and efficacy. Recently, a Phase III study of an ASO drug tominersen to treat HD was terminated for unknown reasons (NCT03761849). Although several siRNA and ASOs targeting mRNAs have been approved to treat sever diseases like SMA, Duchenne's muscular dystrophy (DMD) and transthyretin-mediated amyloidosis[311], these artificial oligos are designed to modify specific mRNA expression. Unlike that, endogenous miRNAs can target numerous mRNAs and participate in complicated biological networks[388], as such introducing or silencing miRNAs will be more challenging. As described before, miravirsen is an anti-miR-122 ASO against HCV infection[88]. However, the loss of miR-122 can reactivate embryo-expressed adult-silenced genes, which may ultimately result in hepatocellular carcinoma[389]. In human, miR-7-5p is predicted to target 558 transcripts with conserved sites[234]. In addition to PD, miR-7 is also downregulated in most types of cancer. It has shown anti-tumour potentials by targeting proteins involved in apoptosis or multidrug resistance, including breast cancer, glioblastoma, and NSCLC[390]. Regardless of this anti-cancer property, the risks of a miR-7 replacement therapy are not known. Therefore, we believe to enhance miR-7 levels by rescuing the HuR-blocked biogenesis, may advance the miR-7 supplement strategy, in terms of efficacy and safety.

3.8.2 RP-CONA: advantages and concerns

Here we developed the on-bead screening technique RP-CONA to identify RNA/protein modulators. Using whole cell extracts, the network of interactive proteins is largely maintained, therefore allowing the screens to take place in a physiologically relevant environment. The lysate-based technique also advances conventional screen methods, such as FRET and FP, which requires the purification of recombinant fluorescent proteins, usually a time-consuming step. Moreover, some proteins form inclusion bodies, making them extremely difficult to be purified. Therefore, RP-CONA provides a simple alternative for the study of these proteins.

However, there are a couple of problems that need to be further optimised if RP-

CONA is going to be used in a wide range of applications, as well as in large scale circumstances. Firstly, the distribution of beads should be improved. Currently, the beads are distributed manually. Even with vigorous shaking and a lot of practice, the variations of bead numbers across different wells are not avoidable. These variations result in variations of ring signals from pull-down proteins. For example, if the number of beads increases, more on-bead pri-miR-7-CTL will be presented in the solution that allows mCherry-HuR to bind. Considering a fixed concentration of mCherry-HuR distributed across the beads, a well with more beads will have less mCherry-HuR enriched on each bead, in another word, a false-positively decreased mCherry ring signal. To overcome this, techniques of beads dispensing, or beads sorting can be tested. Currently we are using beads with 100 μm diameters. Ideally nozzles need to be at least 10 times the size of each bead. We have tested a dispenser with a 200 μm nozzle, which was completely blocked by our beads. Therefore, we are now exploring the possibility of switching to smaller beads (20 to 50 μm) that can go through the nozzles as well as can be piped efficiently. Although a bead sorting technique can be more costly, it can guarantee the exact same number of beads in each well. With the help of novel techniques to achieve robust and precise beads distribution, it looks promising to scale up RP-CONA into an industrial level.

We have conducted a number of experiments to prove that RP-CONA only shows the specific interactions between the target RNA and protein. In addition to pri-miR-7/HuR, we also successfully applied this technique to identify the interaction of let-7/Lin28a, TNFα-ARE/HuR, as well as α-syn-ARE/HuR. Importantly, the selection of fluorophores is not restricted to FITC/mCherry. Cy5 labelled RNA and GFP tagged protein also generated bright ring signals while bound on beads, without the interference of bleed-through. Generally, to separate the fluorescent signals of RNA and protein, one of them should be labelled by a cyan/green fluorophore, while the other one should be chosen from the orange/red range. Furthermore, we observed some weak FRET effects between these fluorophore pairs. FRET occurs when two fluorophores are in close proximity sharing substantial overlap between the emission (donor) and absorption (acceptor) spectra, which results in a transfer of excitation energy from the donor to the acceptor fluorophore[391]. In RP-CONA, the increase of mCherry-HuR binding resulted in slight decrease of FITC-ARE signals (**Figure 47**).

On the contrary, an increasing concentration of quercetin led to the slight increase of FITC levels (**Figure 48**). Fortunately, these FRET effects were not seen in the pri-miR-7/HuR binding, otherwise the inhibition rates would be affected. This is probably because that the affinity between pri-miR-7/HuR is weaker than that of ARE/HuR. Indeed, most of ARE/HuR possess nanomolar Kd. TNFα-ARE even has an impressive picomolar affinity towards HuR[392]. Compared to FITC/mCherry, the emission spectra of GFP and the absorption spectra of Cy5 are overlapped to a much lesser extent. However, in terms of Cy5-let-7/Lin28-GFP, the situation is more complicated. If the green/red FRET exists, the interruption of RNA/protein binding may intensify GFP (donor), but quench Cy5 (acceptor). If this happens, the inhibitive effects from a let-7/Lin28a inhibitor determined by GFP/Cy5 ratio will be compensated. Therefore, to use a cyan/red fluorophore pair may prevent FRET effects to the largest extent. If FRET is unavoidable, it will be better to choose donor labelled RNA and acceptor tethered protein to identify RNA/protein inhibitors, such as FITC-RNA/mCherry-protein, which will amplify the inhibition effects instead of compensating them.

We chose transient transfection to prepare the mCherry-HuR overexpressed cell extracts, to obtain a robust enrichment of the fluorescent proteins. We tried to establish a stable cell line with the mCherry-HuR gene randomly integrated in the genome of HuR KO HEK293T cells, with the help of a *mariner* transposase MosI[393]. However, the stable cell line had much weaker mCherry fluorescence and HuR expression levels, compared to the products of transient transfection. To achieve stable overexpression levels across different batches of cell extracts, we combined all the batches, aliquoted and stored them at -80 ℃, which can be kept for at least one year. Our collaborator suggested us to use (-) glycerol Roeder D buffer to prepare cell extracts, in case the glycerol made the confocal images blurry. We compared the images with or without glycerol in the buffer but didn't observe any differences showing a decrease in quality. Although mCherry-HuR seemed happy in (-) glycerol buffer, some proteins such as Trim25 formed aggregations when glycerol was absent. Therefore, we would suggest including glycerol in the cell extracts buffer to protect the proteins during storage.

In this research, two of high-content imaging systems were applied. Although both

achieved optimal outcomes, their differences should be discussed. Firstly, Opera HCS uses two distinct lasers to excite different fluorophores, with an additional LED to acquire bright field images. Bright field images are very important at the set-up stage for RP-CONA, to check if all the beads are successfully labelled with fluorescent RNA. To image the fluorescent beads, the filter settings can be adjusted in Opera to acquire maximum fluorescence signals while minimise bleed-through. In ImageXpress, fluorescence is powered by a light engine with fixed band filters for fluorophores. Thus, it is better to choose fluorophores with little overlap. Secondly, we stuck to our collaborator's protocol of CONA during image acquisition in Opera, which requires 35 images to be taken in each well. In ImageXpress, we largely saved the time by acquiring 16 images per well. Finally, the Opera images can be automatically analysed using our collaborator's software BREAD, while the ImageXpress images require more manpower to get the quantification in ImageJ. We have confirmed the reliability of the output after switching the RP-CONA assays from Opera to ImageXpress, by comparing the ring intensities. To conclude, despite the slight differences, both imaging systems work well for our RP-CONA assays. We believe that alternative facilities will also be applicable after certain optimisation soon.

3.8.3 Quercetin: the potential as a future PD therapy

Using a focused library composed of compounds interrupting the RNA binding activities of HuR or MSI2, we identified quercetin, luteolin and gossypol as the most potent pri-miR-7/HuR inhibitors (**Figure 32**). However, the inhibitive effects of gossypol showed a lack of specificity according to the RNA pull-down assay (**Figure 34**). Quercetin and luteolin are natural flavonoids that ubiquitously exist in vegetables and fruits. The extra hydroxyl distinguishes them as flavanol and flavone, respectively. Here we identified that only quercetin showed strong inhibitive effects on α-syn expression while upregulating miR-7. This suggests quercetin and luteolin may present different bioavailability in living cells, despite their similar performance in cell extracts. Indeed, quercetin was readily incorporated into the nuclei of SH-SY5Y cells, while another close flavonoid analogue myrincetin had poor cellular uptake[394]. We have observed that mCherry-HuR is dominantly enriched in the nuclei, so it is possible that quercetin is effective due to its accessibility towards HuR.

Quercetin is marketed as a nutraceutical, with a recommended daily dose between 200 to 1,200 mg for dietary supplement[395]. In nature, this chemical exists as quercetin glycosides or aglycone (sugar-free), both of which can be absorbed by humans[396]. The antioxidant properties through multiple pathways of quercetin have been widely acknowledged[397]. Accumulating preclinical and clinical evidence is suggesting its protective benefits against diseases related to oxidative stress, including cancer and cardiovascular diseases[398, 399].

Importantly, quercetin has shown neuroprotective effects against neurodegenerative diseases, especially PD and AD[399, 400]. Quercetin was proved to be the most effective compound from coffee that protects SH-SY5Y cells from glial-mediated neuronal toxicity[401]. Quercetin treatment can inhibit MPP+ induced neuronal PC12 apoptosis[402]. A quercetin glycoside named hyperoside suppressed 6-OHDA induced oxidative stress in dopaminergic SH-SY5Y cells, by inducing Nrf2[403]. This is consistent with a previous report demonstrating that Nrf2 can be activated by miR-7[203].

The accumulation of quercetin metabolites was detected in the brain of quercetin-fed rats, exhibiting attenuated oxidative stress induced by chronic forced-swimming[404]. Oral delivery of nanoparticle encapsulated quercetin gained an enhanced bioavailability across BBB, as well as increased antioxidative effects in different animal models of neurological disorders, including AD[405]. The oral administration of quercetin alone, or in combination with peperine, a bioavailability enhancer, significantly ameliorated the MPTP and 6-OHDA induced motor deficits in PD rat models[406]. The protective effects of quercetin treatment against dopaminergic neurodegeneration were also seen in a MitoPark transgenic PD mouse model, which is believed to be achieved through an activation of the PKD1-Akt cell survival signalling pathway[407]. Intraperitoneal injection of quercetin completely reversed striatal DA loss in rotenone-infused PD rats, by rescuing mitochondrial dysfunction upon oxidative stress[408]. However, some have reported contradictory results that the systematic administration of quercetin did not exert significant neuronal protection against 6-OHDA toxicity *in vivo*[409]. This could be a lack of bioavailability caused by variations from quercetin solvents preparation, or the administration methods. Noteworthy, a delayed toxicity of quercetin was reported in 6-OHDA-induced SH-

SY5Y cells, beyond the early protection[410]. This has drawn the concern about the safety of prolonged quercetin treatment in patients.

Interestingly, a few reports have addressed the effects of quercetin on α-syn protein. Oxidised quercetin can prevent α-syn fibrillization *in vitro*[411]. 20 μM of quercetin treatment decreased α-syn expression that was induced by 6-OHDA in neuron-like PC12 cells, and this is dependent on the mitophagy markers PINK1 and Parkin[412]. Moreover, similar inhibition of midbrain α-syn was also observed in 6-OHDA-lesioned PD rats, together with relieved motor deficits, reduced neuronal death, and partially repaired mitochondrial damage[412]. On the contrary, an independent research found that in PC12 cells α-syn expression was induced by 50 to 500 μM of quercetin, albeit reduced when quercetin reached 1 mM[413]. We found that 20 μM quercetin significantly inhibited α-syn expression in HeLa cells (**Figure 36**), although this effect was less obvious in SH-SY5Y and P19 neuronal cells (**Figure 40**), yet not observed in mDA neurons (**Figure 53**). According to the Human Protein Atlas[365], HeLa cells have high basal levels of α-syn transcripts when compared with most other cultured cell lines, including SH-SY5Y. Therefore, we deduce that quercetin may be more effective when the level of α-syn is pathologically enriched. Further work should be focused on the treatment of quercetin in different PD modelled cells and animals, as well as cells derived from PD patients.

Moreover, our MS data displays that quercetin can induce the protein levels of PP2B (calcineurin) and GSK-3α, both of which are annotated as key players in the DA synapse pathway. The identified catalytic PP2B subunits (Aα and Aβ) are highly enriched in human brain[365]. This calcium-regulated protein phosphatase has shown pivotal roles in hippocampal-based learning and memory[414]. A Purkinje cell-specific knockout of PP2B in mice impaired potentiation and cerebellar motor learning[415]. PP2B also partially contributes to the dephosphorylation of tau protein, where abnormal hyperphosphorylation of tau is seen in AD[416]. Early evidence has shown decreased activity and protein level of PP2B in AD brains[417]. An accumulation of hyperphosphorylated tau, cytoskeletal changes, and learning and memory deficits were observed in PP2B-Aα KO mice[418]. However, PP2B-mediated dephosphorylation may stimulate a chain reaction to antagonise dopamine[419]. Therefore, the consequence of PP2B upregulation against neurodegeneration remains

uncertain. As to GSK-3, however, the quercetin-induced expression seems to pose negative effects on neurodegenerative diseases. α-syn accumulation induces GSK-3β activity, enhancing the phosphorylation of α-syn and tau[420]. GSK-3α facilitates the production of Aβ peptides[421]. Interestingly, although a few studies showed that GSK-3 inhibition relived pathogenesis in animal models of PD and AD, the treatments were found to decrease dopamine release, neither were effective in preventing DA neuron loss in PD animals[422]. Thus, quercetin-mediated α-syn accompanied by GSK-3 elevation may reveal an unknown mechanism underlying PD pathogenesis. Due to the limitation of the MS technique, or the relatively small size of α-syn (19 kDa), we failed to detect this protein in this assay, therefore losing an important positive control for these upregulated and downregulated proteins driven by quercetin. These protein alterations should be validated using other proteomics quantification methods, such as isobaric tags for relative and absolute quantitation (iTRAQ).

In sum, quercetin has shown a great potential in PD treatment, with its role as a ROS scavenger, as well as an effective α-syn inhibitor.

3.8.4 HuR plays a pivotal role in α-syn regulation

We hypothesised that quercetin inhibits α-syn via induced miR-7 levels. We did observe around 2-fold upregulation of pre-miR-7-1 and mature miR-7, which indicates a facilitated miR-7 biogenesis (**Figure 36, 37**). Unexpectedly, the inhibitive effect was still significant in miR-7 depleted cells (**Figure 42**), implying that the increased miR-7 is not the major contributor of α-syn suppression. Indeed, quercetin reduced α-syn protein levels by around 60% in wildtype HeLa cells, so it would require more than 1000-fold miR-7 upregulation to achieve a similar extent of α-syn inhibition in the same cell line (**Figure 10, 11**). In addition, sometimes miRNA abundance is not proportional to their mRNA repressing activities, since many AGO-bound miRNAs can exist in an inactive reservoir not associated with mRNAs[423]. Alternatively, the upregulated miR-7 may be sponged by ciRS-7, which can substantially reduce the potential of miR-7-mediated inhibition[191].

Subsequently, we investigated the effect of quercetin on HuR KO HeLa and found α-syn expression unchanged after treatment (**Figure 44**). This shows that HuR is an essential regulator for quercetin-mediated α-syn inhibition. Nevertheless, an induced

miR-7 level was still observed when HuR was absent. As reviewed in the introduction, the biogenesis of miR-7 is also regulated by some other protein complexes, including ZC3H7A/B SF2/ASF, NF45-NF90 and QKI[269, 280, 289, 290]. Therefore, the removal of HuR may allow alternative miR-7 regulation pathways to take over. This may explain why luteolin did not alter miR-7 levels in wildtype HeLa, but significantly induced it by 3-fold in HuR-KO HeLa cells.

A recent study indicates that HuR binds the 3'-UTR of α-syn mRNA HeLa cells and stabilises α-syn mRNA independently from miR-7, although the knockdown of HuR only showed mild inhibition on α-syn expression[424]. In our research, both mRNA and protein levels of α-syn were significantly lower in HuR-KO HeLa, compared to the wildtype cells (**Figure 46**). Furthermore, overexpressed HuR largely induced the level of a luciferase encoding the 3'-UTR of α-syn (**Figure 51**). We also validated the interaction between HuR protein and α-syn mRNA in cells (**Figure 50**) and in RP-CONA (**Figure 48**). Taken together, apart from the miR-7 pathway, HuR also directly regulates α-syn expression.

We found a less significant interruptive effect of quercetin on cellular α-syn mRNA/HuR, than pri-miR-7-1/HuR (**Figure 50, 37C**). The *in vitro* RP-CONA assays displayed consistent results. Quercetin was effective at 20 μM in inhibiting pri-miR-7-1-CTL/HuR, containing 300 nM of mCherry-HuR in the reactions (**Figure 35**), while it required 200 μM of quercetin to interrupt α-syn-ARE/HuR (as well as TNFα-ARE/HuR) with 50 nM mCherry-HuR (**Figure 49**). This suggests higher affinity between the α-syn-ARE/HuR than pri-miR-7-1-CTL/HuR, or different acting mechanisms of quercetin. Interestingly, the IC_{50} of quercetin inhibiting HuR interaction with TNF-α mRNA in a RNA electrophoretic mobility gel shift assay (EMSA) is only 1.4 μM[337]. Thereby, the RP-CONA results imply that the intervention of RNA/protein binding events are different when they take place in cell extracts.

HuR directly binds more than 2,000 transcripts, predominantly at 3'-UTRs (>60%) and with a large portion (30-35%) at introns[425]. Predicted by beRBP[426], HuR binds the α-syn mRNA at the 7-mer polyU motif at the 3'-UTR, a Class III ARE[427] found at ~180 nt downstream of the validated miR-7 targeted seed. This motif was

previously identified with high affinity to HuR[428]. Both HuR and miR-7 targeted sites are conserved across the variants of α-syn mRNAs. We confirmed this binding motif in RP-CONA, using a 28-nt RNA fragment flanking this ARE from α-syn 3'-UTR. To validate this, more experiments, such as luciferase assays on wildtype or ARE-deleted α-syn 3'-UTR, will be necessary in the follow-up research.

The biological function of full-length HuR is still poorly understood and the contribution of RRM3 to RNA-binding has long been neglected. Actually, HuR-RRM3 plays a crucial role in Class III ARE binding and RRM3-mediated dimerisation enhances binding affinity[317]. Around 250 nt downstream of our proposed α-syn-ARE, there is another potential HuR-binding motif (UUUAUUU). Dimerised HuR may interact with both AREs and bring them to a closer proximity, posing strong effects.

ARE initiates deadenylation and mediates rapid mRNA decay. HuR may sequester essential trans-acting factors from degrading mRNAs bearing AREs[429]. In addition to recognising specific AREs, the stabilisation is also influenced by RNA secondary structures beyond ARE regions, which determine the accessibility of HuR[392]. HuR undergoes post-translational modifications as well as nucleocytoplasmic shuttling through protein-protein interactions. The cytoplasmic localisation of HuR is also important to mRNA stabilisation[429].

In the present research, it remains unclear how HuR promotes α-syn expression. The mRNA stability assay showed that the knockout of endogenous HuR only slightly destabilised α-syn mRNA (**Figure 52**). However, the HuR knockout cells have a significantly less level of α-syn mRNA at the starting point (**Figure 46**). It is difficult to compare the rates of mRNA decay during actinomycin D treatment after the steady state levels have already been affected. We tend to believe HuR exerts its common stabilisation effects through α-syn-ARE, according to the previous report using transient siRNA-mediated HuR knockdown in the same stability assay[424]. Moreover, HuR seems to promote α-syn translation, since HuR significantly induced the luciferase level without increasing its mRNA level (**Figure 51**). This is consistent with the previously published research observing induced translational activities via HuR/ARE targeting[430].

It is not known how quercetin interacts with HuR and leads to reduced mRNA and protein levels of α-syn. A simple idea is that quercetin blocks HuR/ARE binding, inducing α-syn mRNA decay and inhibiting its translation. However, we cannot exclude the possibilities that quercetin may interfere with HuR dimerisation, or other protein/protein interactions that would affect HuR trafficking and other post-transcriptional/post-translational processes. For instance, HuR regulates mRNA abundancies through alternative splicing[431], as well as alternative polyadenylation[432]. Sometimes, HuR is involved in miRNA-mediated gene repression[433].

The proteomic quantifications identified 31 proteins with RNA-binding activities and 29 with HuR interactions that are significantly altered by quercetin treatment in HeLa cells (**Figure 54**). 13 proteins fall into both categories. Particularly, the downregulated SF3B2 (splicing factor 3B subunit 2) was found to be upregulated in PD patients[434]. Trim28 (transcription intermediary factor 1-beta) was downregulated by quercetin. As a key regulator of both α-syn and tau, aberrantly increased Trim28 was present in cases of synucleinopathy and tauopathy[435]. Notably, genetic suppression of Trim28 reduced the levels of α-syn and tau in mice[436]. Combining the fact that Trim28 is annotated to be interacting with HuR, there may exist an uncovered HuR/Trim28/α-syn signalling pathway.

Among the identified RBPs, we observed that quercetin upregulated the levels of NQO1 (NAD(P)H dehydrogenase [quinone] 1), which was also observed by other independent research groups in different cell lines[437]. NQO1 effectively prevented aminochrome-induced α-syn oligomerisation as well as the resultant neurotoxicity in DA neurons[438]. Phosphorylated NQO1 can be degraded by the E3 ubiquitin ligase Parkin, abolishing its antioxidative activities in PD, while the unphosphorylatable NQO1 can prevent MPTP-induced DA neuron loss and rescue motor dysfunctions. Notably, the blockage of NQO1 phosphorylation also reduced ROS and α-syn pathologies in SNCA transgenic mice[439]. Other NQO1 inducers, including a nutraceutical sulforaphane, a synthesised compound KMS04014, and a natural compound β-caryophyllene, have exhibited neuroprotection against different neurotoxins in PD models *in vitro* or *in vivo*[440].

As to the HuR-interacting proteins, the quercetin-induced PLK1 (serine/threonine-

protein kinase) plays a double-edged role in neurodegenerative diseases. This kinase is upregulated in AD brains and phosphorylates Ser129 of aggregated α-syn[441]. On the other hand, PLK1 is essential for corynoxine-induced neuronal autophagy, including the clearance of α-syn and Aβ[442].

Additionally, among the significantly altered proteins, 5 of them (U2SURP, TRIM33, SORT1, GLG1, and CHAMP1) are targeted by miR-7 according to TargetScan[234]. All these proteins are downregulated after quercetin treatment, which is very likely a result of the induced miR-7 production.

To conclude, with the help of quercetin, we confirm that HuR is a direct α-syn inducer, in addition to its indirect regulation through miR-7. In our current study in the context of HeLa cells, it seems that the direct HuR/α-syn pathway dominantly controls α-syn expression.

Concluding remarks

1. In this study, we identified miR-7 as the most effective miRNA inhibiting α-syn expression, a key protein for PD pathogenesis. Elevating miR-7 levels via exogenous or endogenous pathway may become promising PD therapeutic strategy. Meanwhile, miR-153 and miR-133b are also α-syn inhibitors. Our data strongly suggests that post-transcriptional regulation may exist through the CTL of pri-miR-153-2. Understanding the regulation of miR-153 biogenesis may provide novel therapeutic targets for PD treatment.

2. We developed an RNA/protein interaction detection technique RP-CONA, an on-bead, lysate-based method with high sensitivity, specificity as well as repeatability. This novel technique might benefit the discovery of drugs targeting RNA/protein interactions.

3. Using RP-CONA, we performed several small-scale screenings and identified a few potential small molecules inhibiting the interaction of pri-miR-7-1-CTL/HuR. Among them, quercetin and luteolin are the most potent inhibitors, with IC_{50}s around 2 μM in RP-CONA.

4. Quercetin treatment in HeLa cells can dissociate the pri-miR-7-1/HuR interaction, in turn facilitating mature miR-7 production. Quercetin also significantly inhibits both mRNA and protein levels of endogenous α-syn in an HuR-dependent manner. Combined with the fact that quercetin has shown strong neuroprotective effects in PD modelled cells and animals, quercetin treatment may benefit PD patients if applied in clinics.

5. The precise mechanism of quercetin mediated α-syn inhibition is yet to be understood. So far, we know that quercetin induces miR-7 by ~1.5-fold, but such level of upregulation has minor contribution to α-syn expression in HeLa cells. Alternatively, HuR can recognise and bind the ARE of α-syn mRNA 3'-UTR directly and mainly promote its translation, which can be interrupted and reversed by quercetin (**Figure 55**).

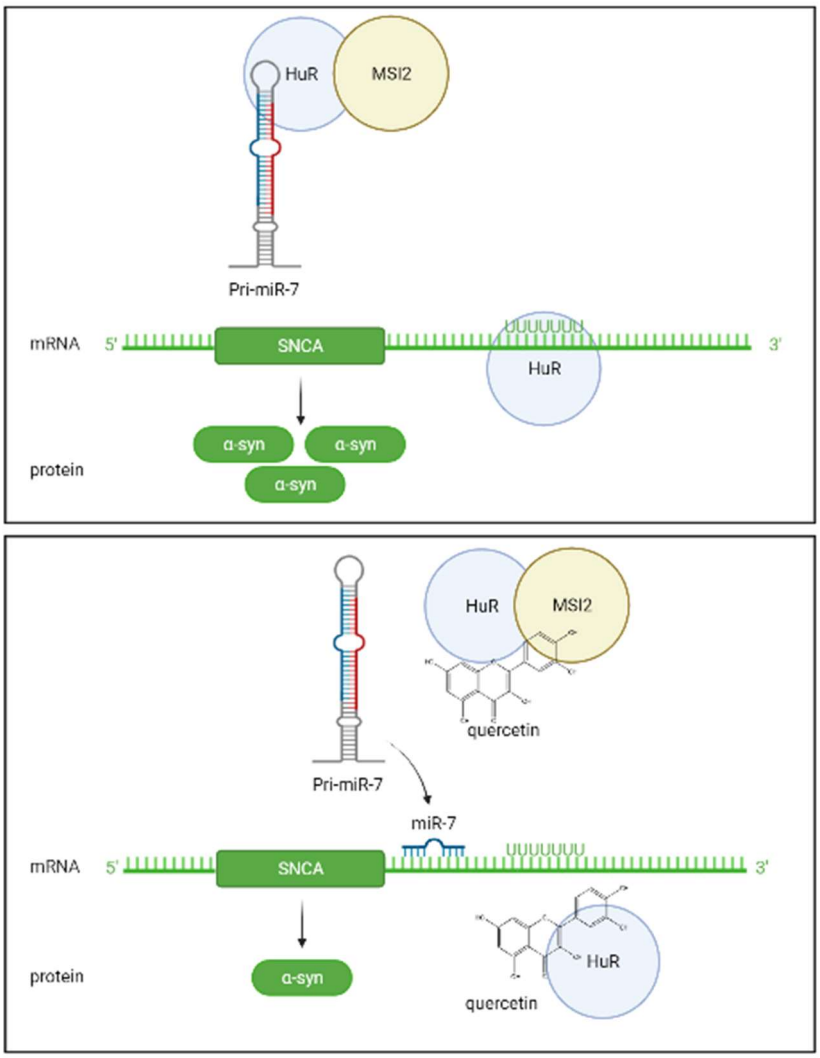

Figure 55 The putative mechanisms of quercetin mediated α-syn inhibition. Quercetin dissociates the interaction between pri-miR-7-CTL and the HuR/MSI2 complex, facilitating miR-7 biogenesis. The upregulated miR-7 can repress α-syn expression by targeting at a conserved binding site of the 3'-UTR. Alternatively, HuR directly interacts the ARE on the α-syn 3'-UTR and promote α-syn translation. Quercetin can disrupt this interaction and inhibits α-syn expression. Figure was drawn in Biorender.

Bibliography

(1) Lee, R. C.; Feinbaum, R. L.; Ambros, V. The C. elegans heterochronic gene lin-4 encodes small RNAs with antisense complementarity to lin-14. *Cell* **1993**, *75* (5), 843-854. Wightman, B.; Ha, I.; Ruvkun, G. Posttranscriptional regulation of the heterochronic gene lin-14 by lin-4 mediates temporal pattern formation in C. elegans. *Cell* **1993**, *75* (5), 855-862. DOI: 10.1016/0092-8674(93)90530-4.

(2) Reinhart, B. J.; Slack, F. J.; Basson, M.; Pasquinelli, A. E.; Bettinger, J. C.; Rougvie, A. E.; Horvitz, H. R.; Ruvkun, G. The 21-nucleotide let-7 RNA regulates developmental timing in Caenorhabditis elegans. *Nature* **2000**, *403* (6772), 901-906. DOI: 10.1038/35002607. Pasquinelli, A. E.; Reinhart, B. J.; Slack, F.; Martindale, M. Q.; Kuroda, M. I.; Maller, B.; Hayward, D. C.; Ball, E. E.; Degnan, B.; Müller, P.; et al. Conservation of the sequence and temporal expression of let-7 heterochronic regulatory RNA. *Nature* **2000**, *408* (6808), 86-89. DOI: 10.1038/35040556.

(3) Lagos-Quintana, M.; Rauhut, R.; Lendeckel, W.; Tuschl, T. Identification of novel genes coding for small expressed RNAs. *Science* **2001**, *294* (5543), 853-858. DOI: 10.1126/science.1064921. Lau, N. C.; Lim, L. P.; Weinstein, E. G.; Bartel, D. P. An abundant class of tiny RNAs with probable regulatory roles in Caenorhabditis elegans. *Science* **2001**, *294* (5543), 858-862. DOI: 10.1126/science.1065062. Lee, R. C.; Ambros, V. An extensive class of small RNAs in Caenorhabditis elegans. *Science* **2001**, *294* (5543), 862-864. DOI: 10.1126/science.1065329.

(4) Kozomara, A.; Griffiths-Jones, S. miRBase: annotating high confidence microRNAs using deep sequencing data. *Nucleic Acids Res* **2014**, *42* (Database issue), D68-73. DOI: 10.1093/nar/gkt1181.

(5) Alles, J.; Fehlmann, T.; Fischer, U.; Backes, C.; Galata, V.; Minet, M.; Hart, M.; Abu-Halima, M.; Grässer, F. A.; Lenhof, H. P.; et al. An estimate of the total number of true human miRNAs. *Nucleic Acids Res* **2019**, *47* (7), 3353-3364. DOI: 10.1093/nar/gkz097.

(6) Lee, Y.; Kim, M.; Han, J.; Yeom, K. H.; Lee, S.; Baek, S. H.; Kim, V. N. MicroRNA genes are transcribed by RNA polymerase II. *EMBO J* **2004**, *23* (20), 4051-4060. DOI: 10.1038/sj.emboj.7600385.

(7) Landthaler, M.; Yalcin, A.; Tuschl, T. The human DiGeorge syndrome critical region gene 8 and Its D. melanogaster homolog are required for miRNA biogenesis. *Curr Biol* **2004**, *14* (23), 2162-2167. DOI: 10.1016/j.cub.2004.11.001. Gregory, R. I.; Yan, K. P.; Amuthan, G.; Chendrimada, T.; Doratotaj, B.; Cooch, N.; Shiekhattar, R. The Microprocessor complex mediates the genesis of microRNAs. *Nature* **2004**, *432* (7014), 235-240. DOI: 10.1038/nature03120. Han, J.; Lee, Y.; Yeom, K. H.; Kim, Y. K.; Jin, H.; Kim, V. N. The Drosha-DGCR8 complex in primary microRNA processing. *Genes Dev* **2004**, *18* (24), 3016-3027. DOI: 10.1101/gad.1262504. Denli, A. M.; Tops, B. B.; Plasterk, R. H.; Ketting, R. F.; Hannon, G. J. Processing of primary microRNAs by the Microprocessor complex. *Nature* **2004**, *432* (7014), 231-235. DOI: 10.1038/nature03049.

(8) Nguyen, T. A.; Jo, M. H.; Choi, Y. G.; Park, J.; Kwon, S. C.; Hohng, S.; Kim, V. N.; Woo, J. S. Functional Anatomy of the Human Microprocessor. *Cell* **2015**, *161* (6), 1374-1387. DOI: 10.1016/j.cell.2015.05.010.

(9) Roth, B. M.; Ishimaru, D.; Hennig, M. The core microprocessor component DiGeorge syndrome critical region 8 (DGCR8) is a nonspecific RNA-binding protein. *J Biol Chem* **2013**, *288* (37), 26785-26799. DOI: 10.1074/jbc.M112.446880. Kwon, S. C.; Nguyen, T. A.; Choi, Y. G.; Jo, M. H.; Hohng, S.; Kim, V. N.; Woo, J. S. Structure of Human DROSHA. *Cell* **2016**, *164* (1-2), 81-90. DOI: 10.1016/j.cell.2015.12.019.

(10) Lee, Y.; Jeon, K.; Lee, J. T.; Kim, S.; Kim, V. N. MicroRNA maturation: stepwise processing and subcellular localization. *Embo j* **2002**, *21* (17), 4663-4670. From NLM.

(11) Yi, R.; Qin, Y.; Macara, I. G.; Cullen, B. R. Exportin-5 mediates the nuclear export of pre-microRNAs and short hairpin RNAs. *Genes Dev* **2003**, *17* (24), 3011-3016. DOI: 10.1101/gad.1158803. Bohnsack, M. T.; Czaplinski, K.; Gorlich, D. Exportin 5 is a

RanGTP-dependent dsRNA-binding protein that mediates nuclear export of pre-miRNAs. *RNA* **2004**, *10* (2), 185-191. DOI: 10.1261/rna.5167604. Lund, E.; Güttinger, S.; Calado, A.; Dahlberg, J. E.; Kutay, U. Nuclear export of microRNA precursors. *Science* **2004**, *303* (5654), 95-98. DOI: 10.1126/science.1090599.
(12) Hutvágner, G.; McLachlan, J.; Pasquinelli, A. E.; Bálint, E.; Tuschl, T.; Zamore, P. D. A cellular function for the RNA-interference enzyme Dicer in the maturation of the let-7 small temporal RNA. *Science* **2001**, *293* (5531), 834-838. DOI: 10.1126/science.1062961. Ketting, R. F.; Fischer, S. E.; Bernstein, E.; Sijen, T.; Hannon, G. J.; Plasterk, R. H. Dicer functions in RNA interference and in synthesis of small RNA involved in developmental timing in C. elegans. *Genes Dev* **2001**, *15* (20), 2654-2659. DOI: 10.1101/gad.927801.
(13) Chendrimada, T. P.; Gregory, R. I.; Kumaraswamy, E.; Norman, J.; Cooch, N.; Nishikura, K.; Shiekhattar, R. TRBP recruits the Dicer complex to Ago2 for microRNA processing and gene silencing. *Nature* **2005**, *436* (7051), 740-744. DOI: 10.1038/nature03868. Lee, Y.; Hur, I.; Park, S. Y.; Kim, Y. K.; Suh, M. R.; Kim, V. N. The role of PACT in the RNA silencing pathway. *EMBO J* **2006**, *25* (3), 522-532. DOI: 10.1038/sj.emboj.7600942.
(14) Ruby, J. G.; Jan, C. H.; Bartel, D. P. Intronic microRNA precursors that bypass Drosha processing. *Nature* **2007**, *448* (7149), 83-86. DOI: 10.1038/nature05983.
(15) Okamura, K.; Hagen, J. W.; Duan, H.; Tyler, D. M.; Lai, E. C. The mirtron pathway generates microRNA-class regulatory RNAs in Drosophila. *Cell* **2007**, *130* (1), 89-100. DOI: 10.1016/j.cell.2007.06.028.
(16) Babiarz, J. E.; Ruby, J. G.; Wang, Y.; Bartel, D. P.; Blelloch, R. Mouse ES cells express endogenous shRNAs, siRNAs, and other Microprocessor-independent, Dicer-dependent small RNAs. *Genes Dev* **2008**, *22* (20), 2773-2785. DOI: 10.1101/gad.1705308.
(17) Xie, M.; Li, M.; Vilborg, A.; Lee, N.; Shu, M. D.; Yartseva, V.; Šestan, N.; Steitz, J. A. Mammalian 5'-capped microRNA precursors that generate a single microRNA. *Cell* **2013**, *155* (7), 1568-1580. DOI: 10.1016/j.cell.2013.11.027.
(18) Abdelfattah, A. M.; Park, C.; Choi, M. Y. Update on non-canonical microRNAs. *Biomol Concepts* **2014**, *5* (4), 275-287. DOI: 10.1515/bmc-2014-0012.
(19) Bogerd, H. P.; Karnowski, H. W.; Cai, X.; Shin, J.; Pohlers, M.; Cullen, B. R. A mammalian herpesvirus uses noncanonical expression and processing mechanisms to generate viral MicroRNAs. *Mol Cell* **2010**, *37* (1), 135-142. DOI: 10.1016/j.molcel.2009.12.016.
(20) Ender, C.; Krek, A.; Friedländer, M. R.; Beitzinger, M.; Weinmann, L.; Chen, W.; Pfeffer, S.; Rajewsky, N.; Meister, G. A human snoRNA with microRNA-like functions. *Mol Cell* **2008**, *32* (4), 519-528. DOI: 10.1016/j.molcel.2008.10.017.
(21) Saraiya, A. A.; Wang, C. C. snoRNA, a novel precursor of microRNA in Giardia lamblia. *PLoS Pathog* **2008**, *4* (11), e1000224. DOI: 10.1371/journal.ppat.1000224.
(22) Cifuentes, D.; Xue, H.; Taylor, D. W.; Patnode, H.; Mishima, Y.; Cheloufi, S.; Ma, E.; Mane, S.; Hannon, G. J.; Lawson, N. D.; et al. A novel miRNA processing pathway independent of Dicer requires Argonaute2 catalytic activity. *Science* **2010**, *328* (5986), 1694-1698. DOI: 10.1126/science.1190809.
(23) Yoda, M.; Cifuentes, D.; Izumi, N.; Sakaguchi, Y.; Suzuki, T.; Giraldez, A. J.; Tomari, Y. Poly(A)-specific ribonuclease mediates 3'-end trimming of Argonaute2-cleaved precursor microRNAs. *Cell Rep* **2013**, *5* (3), 715-726. DOI: 10.1016/j.celrep.2013.09.029.
(24) Bhaskaran, M.; Mohan, M. MicroRNAs: history, biogenesis, and their evolving role in animal development and disease. *Vet Pathol* **2014**, *51* (4), 759-774. DOI: 10.1177/0300985813502820.
(25) Chipman, L. B.; Pasquinelli, A. E. miRNA Targeting: Growing beyond the Seed. *Trends Genet* **2019**, *35* (3), 215-222. DOI: 10.1016/j.tig.2018.12.005.
(26) Gebert, L. F. R.; MacRae, I. J. Regulation of microRNA function in animals. *Nat Rev Mol Cell Biol* **2019**, *20* (1), 21-37. DOI: 10.1038/s41580-018-0045-7.
(27) Ipsaro, J. J.; Joshua-Tor, L. From guide to target: molecular insights into eukaryotic

RNA-interference machinery. *Nat Struct Mol Biol* **2015**, *22* (1), 20-28. DOI: 10.1038/nsmb.2931.
(28) Jonas, S.; Izaurralde, E. Towards a molecular understanding of microRNA-mediated gene silencing. *Nat Rev Genet* **2015**, *16* (7), 421-433. DOI: 10.1038/nrg3965.
(29) Huntzinger, E.; Izaurralde, E. Gene silencing by microRNAs: contributions of translational repression and mRNA decay. *Nat Rev Genet* **2011**, *12* (2), 99-110. DOI: 10.1038/nrg2936.
(30) Huang, H. Y.; Lin, Y. C.; Li, J.; Huang, K. Y.; Shrestha, S.; Hong, H. C.; Tang, Y.; Chen, Y. G.; Jin, C. N.; Yu, Y.; et al. miRTarBase 2020: updates to the experimentally validated microRNA-target interaction database. *Nucleic Acids Res* **2020**, *48* (D1), D148-D154. DOI: 10.1093/nar/gkz896.
(31) Helwak, A.; Kudla, G.; Dudnakova, T.; Tollervey, D. Mapping the human miRNA interactome by CLASH reveals frequent noncanonical binding. *Cell* **2013**, *153* (3), 654-665. DOI: 10.1016/j.cell.2013.03.043 From NLM.
(32) Bustos-Sanmamed, P.; Bazin, J.; Hartmann, C.; Crespi, M.; Lelandais-Brière, C. Small RNA pathways and diversity in model legumes: lessons from genomics. *Front Plant Sci* **2013**, *4*, 236. DOI: 10.3389/fpls.2013.00236. Baltimore, D.; Boldin, M. P.; O'Connell, R. M.; Rao, D. S.; Taganov, K. D. MicroRNAs: new regulators of immune cell development and function. *Nat Immunol* **2008**, *9* (8), 839-845. DOI: 10.1038/ni.f.209. Fiore, R.; Siegel, G.; Schratt, G. MicroRNA function in neuronal development, plasticity and disease. *Biochim Biophys Acta* **2008**, *1779* (8), 471-478. DOI: 10.1016/j.bbagrm.2007.12.006. Hartig, S. M.; Hamilton, M. P.; Bader, D. A.; McGuire, S. E. The miRNA Interactome in Metabolic Homeostasis. *Trends Endocrinol Metab* **2015**, *26* (12), 733-745. DOI: 10.1016/j.tem.2015.09.006. Tsang, J.; Zhu, J.; van Oudenaarden, A. MicroRNA-mediated feedback and feedforward loops are recurrent network motifs in mammals. *Mol Cell* **2007**, *26* (5), 753-767. DOI: 10.1016/j.molcel.2007.05.018.
(33) Vidigal, J. A.; Ventura, A. The biological functions of miRNAs: lessons from in vivo studies. *Trends Cell Biol* **2015**, *25* (3), 137-147. DOI: 10.1016/j.tcb.2014.11.004.
(34) Rodriguez, A.; Vigorito, E.; Clare, S.; Warren, M. V.; Couttet, P.; Soond, D. R.; van Dongen, S.; Grocock, R. J.; Das, P. P.; Miska, E. A.; et al. Requirement of bic/microRNA-155 for normal immune function. *Science* **2007**, *316* (5824), 608-611. DOI: 10.1126/science.1139253.
(35) Tan, C. L.; Plotkin, J. L.; Venø, M. T.; von Schimmelmann, M.; Feinberg, P.; Mann, S.; Handler, A.; Kjems, J.; Surmeier, D. J.; O'Carroll, D.; et al. MicroRNA-128 governs neuronal excitability and motor behavior in mice. *Science* **2013**, *342* (6163), 1254-1258. DOI: 10.1126/science.1244193.
(36) van Rooij, E.; Sutherland, L. B.; Qi, X.; Richardson, J. A.; Hill, J.; Olson, E. N. Control of stress-dependent cardiac growth and gene expression by a microRNA. *Science* **2007**, *316* (5824), 575-579. DOI: 10.1126/science.1139089.
(37) Reddy, K. B. MicroRNA (miRNA) in cancer. *Cancer Cell Int* **2015**, *15*, 38. DOI: 10.1186/s12935-015-0185-1.
(38) Esteller, M. Non-coding RNAs in human disease. *Nat Rev Genet* **2011**, *12* (12), 861-874. DOI: 10.1038/nrg3074 From NLM.
(39) Rokavec, M.; Horst, D.; Hermeking, H. Cellular Model of Colon Cancer Progression Reveals Signatures of mRNAs, miRNA, lncRNAs, and Epigenetic Modifications Associated with Metastasis. *Cancer Res* **2017**, *77* (8), 1854-1867. DOI: 10.1158/0008-5472.CAN-16-3236. Yeh, C. H.; Moles, R.; Nicot, C. Clinical significance of microRNAs in chronic and acute human leukemia. *Mol Cancer* **2016**, *15* (1), 37. DOI: 10.1186/s12943-016-0518-2. Leichter, A. L.; Sullivan, M. J.; Eccles, M. R.; Chatterjee, A. MicroRNA expression patterns and signalling pathways in the development and progression of childhood solid tumours. *Mol Cancer* **2017**, *16* (1), 15. DOI: 10.1186/s12943-017-0584-0.
(40) Romero-Cordoba, S. L.; Salido-Guadarrama, I.; Rodriguez-Dorantes, M.; Hidalgo-Miranda, A. miRNA biogenesis: biological impact in the development of cancer. *Cancer*

Biol Ther **2014**, *15* (11), 1444-1455. DOI: 10.4161/15384047.2014.955442.
(41) Mittal, V. Epithelial Mesenchymal Transition in Tumor Metastasis. *Annu Rev Pathol* **2018**, *13*, 395-412. DOI: 10.1146/annurev-pathol-020117-043854.
(42) Davalos, V.; Moutinho, C.; Villanueva, A.; Boque, R.; Silva, P.; Carneiro, F.; Esteller, M. Dynamic epigenetic regulation of the microRNA-200 family mediates epithelial and mesenchymal transitions in human tumorigenesis. *Oncogene* **2012**, *31* (16), 2062-2074. DOI: 10.1038/onc.2011.383.
(43) Feng, X.; Wang, Z.; Fillmore, R.; Xi, Y. MiR-200, a new star miRNA in human cancer. *Cancer Lett* **2014**, *344* (2), 166-173. DOI: 10.1016/j.canlet.2013.11.004.
(44) O'Donnell, K. A.; Wentzel, E. A.; Zeller, K. I.; Dang, C. V.; Mendell, J. T. c-Myc-regulated microRNAs modulate E2F1 expression. *Nature* **2005**, *435* (7043), 839-843. DOI: 10.1038/nature03677.
(45) Jackstadt, R.; Hermeking, H. MicroRNAs as regulators and mediators of c-MYC function. *Biochim Biophys Acta* **2015**, *1849* (5), 544-553. DOI: 10.1016/j.bbagrm.2014.04.003.
(46) Chang, T. C.; Yu, D.; Lee, Y. S.; Wentzel, E. A.; Arking, D. E.; West, K. M.; Dang, C. V.; Thomas-Tikhonenko, A.; Mendell, J. T. Widespread microRNA repression by Myc contributes to tumorigenesis. *Nat Genet* **2008**, *40* (1), 43-50. DOI: 10.1038/ng.2007.30.
(47) Chang, T. C.; Zeitels, L. R.; Hwang, H. W.; Chivukula, R. R.; Wentzel, E. A.; Dews, M.; Jung, J.; Gao, P.; Dang, C. V.; Beer, M. A.; et al. Lin-28B transactivation is necessary for Myc-mediated let-7 repression and proliferation. *Proc Natl Acad Sci U S A* **2009**, *106* (9), 3384-3389. DOI: 10.1073/pnas.0808300106.
(48) Wu, J.; Bao, J.; Kim, M.; Yuan, S.; Tang, C.; Zheng, H.; Mastick, G. S.; Xu, C.; Yan, W. Two miRNA clusters, miR-34b/c and miR-449, are essential for normal brain development, motile ciliogenesis, and spermatogenesis. *Proc Natl Acad Sci U S A* **2014**, *111* (28), E2851-2857. DOI: 10.1073/pnas.1407777111. Radhakrishnan, B.; Alwin Prem Anand, A. Role of miRNA-9 in Brain Development. *J Exp Neurosci* **2016**, *10*, 101-120. DOI: 10.4137/JEN.S32843.
(49) Wen, M. M. Getting miRNA Therapeutics into the Target Cells for Neurodegenerative Diseases: A Mini-Review. *Front Mol Neurosci* **2016**, *9*, 129. DOI: 10.3389/fnmol.2016.00129.
(50) Hébert, S. S.; Horré, K.; Nicolaï, L.; Papadopoulou, A. S.; Mandemakers, W.; Silahtaroglu, A. N.; Kauppinen, S.; Delacourte, A.; De Strooper, B. Loss of microRNA cluster miR-29a/b-1 in sporadic Alzheimer's disease correlates with increased BACE1/beta-secretase expression. *Proc Natl Acad Sci U S A* **2008**, *105* (17), 6415-6420. DOI: 10.1073/pnas.0710263105.
(51) Hampel, H.; Vassar, R.; De Strooper, B.; Hardy, J.; Willem, M.; Singh, N.; Zhou, J.; Yan, R.; Vanmechelen, E.; De Vos, A.; et al. The β-Secretase BACE1 in Alzheimer's Disease. *Biol Psychiatry* **2020**. DOI: 10.1016/j.biopsych.2020.02.001.
(52) Roshan, R.; Shridhar, S.; Sarangdhar, M. A.; Banik, A.; Chawla, M.; Garg, M.; Singh, V. P.; Pillai, B. Brain-specific knockdown of miR-29 results in neuronal cell death and ataxia in mice. *RNA* **2014**, *20* (8), 1287-1297. DOI: 10.1261/rna.044008.113.
(53) Bazrgar, M.; Khodabakhsh, P.; Mohagheghi, F.; Prudencio, M.; Ahmadiani, A. Brain microRNAs dysregulation: Implication for missplicing and abnormal post-translational modifications of tau protein in Alzheimer's disease and related tauopathies. *Pharmacol Res* **2020**, *155*, 104729. DOI: 10.1016/j.phrs.2020.104729.
(54) Smith, P. Y.; Hernandez-Rapp, J.; Jolivette, F.; Lecours, C.; Bisht, K.; Goupil, C.; Dorval, V.; Parsi, S.; Morin, F.; Planel, E.; et al. miR-132/212 deficiency impairs tau metabolism and promotes pathological aggregation in vivo. *Hum Mol Genet* **2015**, *24* (23), 6721-6735. DOI: 10.1093/hmg/ddv377.
(55) Smith, P. Y.; Delay, C.; Girard, J.; Papon, M. A.; Planel, E.; Sergeant, N.; Buée, L.; Hébert, S. S. MicroRNA-132 loss is associated with tau exon 10 inclusion in progressive supranuclear palsy. *Hum Mol Genet* **2011**, *20* (20), 4016-4024. DOI: 10.1093/hmg/ddr330.

(56) El Fatimy, R.; Li, S.; Chen, Z.; Mushannen, T.; Gongala, S.; Wei, Z.; Balu, D. T.; Rabinovsky, R.; Cantlon, A.; Elkhal, A.; et al. MicroRNA-132 provides neuroprotection for tauopathies via multiple signaling pathways. *Acta Neuropathol* **2018**, *136* (4), 537-555. DOI: 10.1007/s00401-018-1880-5.
(57) Salta, E.; Sierksma, A.; Vanden Eynden, E.; De Strooper, B. miR-132 loss de-represses ITPKB and aggravates amyloid and TAU pathology in Alzheimer's brain. *EMBO Mol Med* **2016**, *8* (9), 1005-1018. DOI: 10.15252/emmm.201606520.
(58) Johnson, R.; Zuccato, C.; Belyaev, N. D.; Guest, D. J.; Cattaneo, E.; Buckley, N. J. A microRNA-based gene dysregulation pathway in Huntington's disease. *Neurobiol Dis* **2008**, *29* (3), 438-445. DOI: 10.1016/j.nbd.2007.11.001.
(59) Packer, A. N.; Xing, Y.; Harper, S. Q.; Jones, L.; Davidson, B. L. The bifunctional microRNA miR-9/miR-9* regulates REST and CoREST and is downregulated in Huntington's disease. *J Neurosci* **2008**, *28* (53), 14341-14346. DOI: 10.1523/JNEUROSCI.2390-08.2008.
(60) Montgomery, R. L.; Hullinger, T. G.; Semus, H. M.; Dickinson, B. A.; Seto, A. G.; Lynch, J. M.; Stack, C.; Latimer, P. A.; Olson, E. N.; van Rooij, E. Therapeutic inhibition of miR-208a improves cardiac function and survival during heart failure. *Circulation* **2011**, *124* (14), 1537-1547. DOI: 10.1161/CIRCULATIONAHA.111.030932.
(61) Thum, T.; Gross, C.; Fiedler, J.; Fischer, T.; Kissler, S.; Bussen, M.; Galuppo, P.; Just, S.; Rottbauer, W.; Frantz, S.; et al. MicroRNA-21 contributes to myocardial disease by stimulating MAP kinase signalling in fibroblasts. *Nature* **2008**, *456* (7224), 980-984. DOI: 10.1038/nature07511. Roy, S.; Khanna, S.; Hussain, S. R.; Biswas, S.; Azad, A.; Rink, C.; Gnyawali, S.; Shilo, S.; Nuovo, G. J.; Sen, C. K. MicroRNA expression in response to murine myocardial infarction: miR-21 regulates fibroblast metalloprotease-2 via phosphatase and tensin homologue. *Cardiovasc Res* **2009**, *82* (1), 21-29. DOI: 10.1093/cvr/cvp015.
(62) Patrick, D. M.; Montgomery, R. L.; Qi, X.; Obad, S.; Kauppinen, S.; Hill, J. A.; van Rooij, E.; Olson, E. N. Stress-dependent cardiac remodeling occurs in the absence of microRNA-21 in mice. *J Clin Invest* **2010**, *120* (11), 3912-3916. DOI: 10.1172/JCI43604.
(63) Carè, A.; Catalucci, D.; Felicetti, F.; Bonci, D.; Addario, A.; Gallo, P.; Bang, M. L.; Segnalini, P.; Gu, Y.; Dalton, N. D.; et al. MicroRNA-133 controls cardiac hypertrophy. *Nat Med* **2007**, *13* (5), 613-618. DOI: 10.1038/nm1582. Hua, Y.; Zhang, Y.; Ren, J. IGF-1 deficiency resists cardiac hypertrophy and myocardial contractile dysfunction: role of microRNA-1 and microRNA-133a. *J Cell Mol Med* **2012**, *16* (1), 83-95. DOI: 10.1111/j.1582-4934.2011.01307.x.
(64) Liu, N.; Bezprozvannaya, S.; Williams, A. H.; Qi, X.; Richardson, J. A.; Bassel-Duby, R.; Olson, E. N. microRNA-133a regulates cardiomyocyte proliferation and suppresses smooth muscle gene expression in the heart. *Genes Dev* **2008**, *22* (23), 3242-3254. DOI: 10.1101/gad.1738708.
(65) Yang, B.; Lin, H.; Xiao, J.; Lu, Y.; Luo, X.; Li, B.; Zhang, Y.; Xu, C.; Bai, Y.; Wang, H.; et al. The muscle-specific microRNA miR-1 regulates cardiac arrhythmogenic potential by targeting GJA1 and KCNJ2. *Nat Med* **2007**, *13* (4), 486-491. DOI: 10.1038/nm1569.
(66) Viereck, J.; Thum, T. Circulating Noncoding RNAs as Biomarkers of Cardiovascular Disease and Injury. *Circ Res* **2017**, *120* (2), 381-399. DOI: 10.1161/CIRCRESAHA.116.308434.
(67) Kondkar, A. A.; Abu-Amero, K. K. Utility of circulating microRNAs as clinical biomarkers for cardiovascular diseases. *Biomed Res Int* **2015**, *2015*, 821823. DOI: 10.1155/2015/821823.
(68) Willeit, P.; Skroblin, P.; Kiechl, S.; Fernández-Hernando, C.; Mayr, M. Liver microRNAs: potential mediators and biomarkers for metabolic and cardiovascular disease? *Eur Heart J* **2016**, *37* (43), 3260-3266. DOI: 10.1093/eurheartj/ehw146.
(69) Jopling, C. L.; Yi, M.; Lancaster, A. M.; Lemon, S. M.; Sarnow, P. Modulation of hepatitis C virus RNA abundance by a liver-specific MicroRNA. *Science* **2005**, *309* (5740), 1577-1581. DOI: 10.1126/science.1113329.

(70) Esau, C.; Davis, S.; Murray, S. F.; Yu, X. X.; Pandey, S. K.; Pear, M.; Watts, L.; Booten, S. L.; Graham, M.; McKay, R.; et al. miR-122 regulation of lipid metabolism revealed by in vivo antisense targeting. *Cell Metab* **2006**, *3* (2), 87-98. DOI: 10.1016/j.cmet.2006.01.005.
(71) Willeit, P.; Skroblin, P.; Moschen, A. R.; Yin, X.; Kaudewitz, D.; Zampetaki, A.; Barwari, T.; Whitehead, M.; Ramírez, C. M.; Goedeke, L.; et al. Circulating MicroRNA-122 Is Associated With the Risk of New-Onset Metabolic Syndrome and Type 2 Diabetes. *Diabetes* **2017**, *66* (2), 347-357. DOI: 10.2337/db16-0731.
(72) Esau, C.; Kang, X.; Peralta, E.; Hanson, E.; Marcusson, E. G.; Ravichandran, L. V.; Sun, Y.; Koo, S.; Perera, R. J.; Jain, R.; et al. MicroRNA-143 regulates adipocyte differentiation. *J Biol Chem* **2004**, *279* (50), 52361-52365. DOI: 10.1074/jbc.C400438200.
(73) Takanabe, R.; Ono, K.; Abe, Y.; Takaya, T.; Horie, T.; Wada, H.; Kita, T.; Satoh, N.; Shimatsu, A.; Hasegawa, K. Up-regulated expression of microRNA-143 in association with obesity in adipose tissue of mice fed high-fat diet. *Biochem Biophys Res Commun* **2008**, *376* (4), 728-732. DOI: 10.1016/j.bbrc.2008.09.050.
(74) Jordan, S. D.; Krüger, M.; Willmes, D. M.; Redemann, N.; Wunderlich, F. T.; Brönneke, H. S.; Merkwirth, C.; Kashkar, H.; Olkkonen, V. M.; Böttger, T.; et al. Obesity-induced overexpression of miRNA-143 inhibits insulin-stimulated AKT activation and impairs glucose metabolism. *Nat Cell Biol* **2011**, *13* (4), 434-446. DOI: 10.1038/ncb2211.
(75) Shi, Z.; Zhao, C.; Guo, X.; Ding, H.; Cui, Y.; Shen, R.; Liu, J. Differential expression of microRNAs in omental adipose tissue from gestational diabetes mellitus subjects reveals miR-222 as a regulator of ERα expression in estrogen-induced insulin resistance. *Endocrinology* **2014**, *155* (5), 1982-1990. DOI: 10.1210/en.2013-2046. Vickers, K. C.; Palmisano, B. T.; Shoucri, B. M.; Shamburek, R. D.; Remaley, A. T. MicroRNAs are transported in plasma and delivered to recipient cells by high-density lipoproteins. *Nat Cell Biol* **2011**, *13* (4), 423-433. DOI: 10.1038/ncb2210.
(76) Ortega, F. J.; Mercader, J. M.; Moreno-Navarrete, J. M.; Rovira, O.; Guerra, E.; Esteve, E.; Xifra, G.; Martínez, C.; Ricart, W.; Rieusset, J.; et al. Profiling of circulating microRNAs reveals common microRNAs linked to type 2 diabetes that change with insulin sensitization. *Diabetes Care* **2014**, *37* (5), 1375-1383. DOI: 10.2337/dc13-1847.
(77) Deiuliis, J. A. MicroRNAs as regulators of metabolic disease: pathophysiologic significance and emerging role as biomarkers and therapeutics. *Int J Obes (Lond)* **2016**, *40* (1), 88-101. DOI: 10.1038/ijo.2015.170.
(78) O'Connell, R. M.; Rao, D. S.; Chaudhuri, A. A.; Baltimore, D. Physiological and pathological roles for microRNAs in the immune system. *Nat Rev Immunol* **2010**, *10* (2), 111-122. DOI: 10.1038/nri2708.
(79) Hsin, J. P.; Lu, Y.; Loeb, G. B.; Leslie, C. S.; Rudensky, A. Y. The effect of cellular context on miR-155-mediated gene regulation in four major immune cell types. *Nat Immunol* **2018**, *19* (10), 1137-1145. DOI: 10.1038/s41590-018-0208-x.
(80) Lu, L. F.; Gasteiger, G.; Yu, I. S.; Chaudhry, A.; Hsin, J. P.; Lu, Y.; Bos, P. D.; Lin, L. L.; Zawislak, C. L.; Cho, S.; et al. A Single miRNA-mRNA Interaction Affects the Immune Response in a Context- and Cell-Type-Specific Manner. *Immunity* **2015**, *43* (1), 52-64. DOI: 10.1016/j.immuni.2015.04.022. Lu, L. F.; Thai, T. H.; Calado, D. P.; Chaudhry, A.; Kubo, M.; Tanaka, K.; Loeb, G. B.; Lee, H.; Yoshimura, A.; Rajewsky, K.; et al. Foxp3-dependent microRNA155 confers competitive fitness to regulatory T cells by targeting SOCS1 protein. *Immunity* **2009**, *30* (1), 80-91. DOI: 10.1016/j.immuni.2008.11.010.
(81) O'Connell, R. M.; Chaudhuri, A. A.; Rao, D. S.; Baltimore, D. Inositol phosphatase SHIP1 is a primary target of miR-155. *Proc Natl Acad Sci U S A* **2009**, *106* (17), 7113-7118. DOI: 10.1073/pnas.0902636106. Costinean, S.; Sandhu, S. K.; Pedersen, I. M.; Tili, E.; Trotta, R.; Perrotti, D.; Ciarlariello, D.; Neviani, P.; Harb, J.; Kauffman, L. R.; et al. Src homology 2 domain-containing inositol-5-phosphatase and CCAAT enhancer-binding protein beta are targeted by miR-155 in B cells of Emicro-MiR-155 transgenic mice. *Blood* **2009**, *114* (7), 1374-1382. DOI: 10.1182/blood-2009-05-220814.
(82) Vigorito, E.; Perks, K. L.; Abreu-Goodger, C.; Bunting, S.; Xiang, Z.; Kohlhaas, S.; Das,

P. P.; Miska, E. A.; Rodriguez, A.; Bradley, A.; et al. microRNA-155 regulates the generation of immunoglobulin class-switched plasma cells. *Immunity* **2007**, *27* (6), 847-859. DOI: 10.1016/j.immuni.2007.10.009. Dorsett, Y.; McBride, K. M.; Jankovic, M.; Gazumyan, A.; Thai, T. H.; Robbiani, D. F.; Di Virgilio, M.; Reina San-Martin, B.; Heidkamp, G.; Schwickert, T. A.; et al. MicroRNA-155 suppresses activation-induced cytidine deaminase-mediated Myc-Igh translocation. *Immunity* **2008**, *28* (5), 630-638. DOI: 10.1016/j.immuni.2008.04.002. Teng, G.; Hakimpour, P.; Landgraf, P.; Rice, A.; Tuschl, T.; Casellas, R.; Papavasiliou, F. N. MicroRNA-155 is a negative regulator of activation-induced cytidine deaminase. *Immunity* **2008**, *28* (5), 621-629. DOI: 10.1016/j.immuni.2008.03.015.
(83) Seddiki, N.; Brezar, V.; Ruffin, N.; Lévy, Y.; Swaminathan, S. Role of miR-155 in the regulation of lymphocyte immune function and disease. *Immunology* **2014**, *142* (1), 32-38. DOI: 10.1111/imm.12227.
(84) Tomankova, T.; Petrek, M.; Gallo, J.; Kriegova, E. MicroRNAs: Emerging Regulators of Immune-Mediated Diseases. *Scand J Immunol* **2012**, *75* (2), 129-141. DOI: 10.1111/j.1365-3083.2011.02650.x.
(85) Thai, T. H.; Calado, D. P.; Casola, S.; Ansel, K. M.; Xiao, C.; Xue, Y.; Murphy, A.; Frendewey, D.; Valenzuela, D.; Kutok, J. L.; et al. Regulation of the germinal center response by microRNA-155. *Science* **2007**, *316* (5824), 604-608. DOI: 10.1126/science.1141229. O'Connell, R. M.; Taganov, K. D.; Boldin, M. P.; Cheng, G.; Baltimore, D. MicroRNA-155 is induced during the macrophage inflammatory response. *Proc Natl Acad Sci U S A* **2007**, *104* (5), 1604-1609. DOI: 10.1073/pnas.0610731104.
(86) Najafi-Shoushtari, S. H.; Kristo, F.; Li, Y.; Shioda, T.; Cohen, D. E.; Gerszten, R. E.; Näär, A. M. MicroRNA-33 and the SREBP host genes cooperate to control cholesterol homeostasis. *Science* **2010**, *328* (5985), 1566-1569. DOI: 10.1126/science.1189123. Rayner, K. J.; Suárez, Y.; Dávalos, A.; Parathath, S.; Fitzgerald, M. L.; Tamehiro, N.; Fisher, E. A.; Moore, K. J.; Fernández-Hernando, C. MiR-33 contributes to the regulation of cholesterol homeostasis. *Science* **2010**, *328* (5985), 1570-1573. DOI: 10.1126/science.1189862.
(87) Rayner, K. J.; Sheedy, F. J.; Esau, C. C.; Hussain, F. N.; Temel, R. E.; Parathath, S.; van Gils, J. M.; Rayner, A. J.; Chang, A. N.; Suarez, Y.; et al. Antagonism of miR-33 in mice promotes reverse cholesterol transport and regression of atherosclerosis. *J Clin Invest* **2011**, *121* (7), 2921-2931. DOI: 10.1172/JCI57275. Rayner, K. J.; Esau, C. C.; Hussain, F. N.; McDaniel, A. L.; Marshall, S. M.; van Gils, J. M.; Ray, T. D.; Sheedy, F. J.; Goedeke, L.; Liu, X.; et al. Inhibition of miR-33a/b in non-human primates raises plasma HDL and lowers VLDL triglycerides. *Nature* **2011**, *478* (7369), 404-407. DOI: 10.1038/nature10486.
(88) Gebert, L. F.; Rebhan, M. A.; Crivelli, S. E.; Denzler, R.; Stoffel, M.; Hall, J. Miravirsen (SPC3649) can inhibit the biogenesis of miR-122. *Nucleic Acids Res* **2014**, *42* (1), 609-621. DOI: 10.1093/nar/gkt852.
(89) Machlin, E. S.; Sarnow, P.; Sagan, S. M. Masking the 5' terminal nucleotides of the hepatitis C virus genome by an unconventional microRNA-target RNA complex. *Proc Natl Acad Sci U S A* **2011**, *108* (8), 3193-3198. DOI: 10.1073/pnas.1012464108. Shimakami, T.; Yamane, D.; Jangra, R. K.; Kempf, B. J.; Spaniel, C.; Barton, D. J.; Lemon, S. M. Stabilization of hepatitis C virus RNA by an Ago2-miR-122 complex. *Proc Natl Acad Sci U S A* **2012**, *109* (3), 941-946. DOI: 10.1073/pnas.1112263109. Roberts, A. P.; Lewis, A. P.; Jopling, C. L. miR-122 activates hepatitis C virus translation by a specialized mechanism requiring particular RNA components. *Nucleic Acids Res* **2011**, *39* (17), 7716-7729. DOI: 10.1093/nar/gkr426. Li, Y.; Masaki, T.; Yamane, D.; McGivern, D. R.; Lemon, S. M. Competing and noncompeting activities of miR-122 and the 5' exonuclease Xrn1 in regulation of hepatitis C virus replication. *Proc Natl Acad Sci U S A* **2013**, *110* (5), 1881-1886. DOI: 10.1073/pnas.1213515110.
(90) Janssen, H. L.; Reesink, H. W.; Lawitz, E. J.; Zeuzem, S.; Rodriguez-Torres, M.; Patel, K.; van der Meer, A. J.; Patick, A. K.; Chen, A.; Zhou, Y.; et al. Treatment of HCV infection by targeting microRNA. *N Engl J Med* **2013**, *368* (18), 1685-1694. DOI:

10.1056/NEJMoa1209026.
(91) van der Ree, M. H.; de Vree, J. M.; Stelma, F.; Willemse, S.; van der Valk, M.; Rietdijk, S.; Molenkamp, R.; Schinkel, J.; van Nuenen, A. C.; Beuers, U.; et al. Safety, tolerability, and antiviral effect of RG-101 in patients with chronic hepatitis C: a phase 1B, double-blind, randomised controlled trial. *Lancet* **2017**, *389* (10070), 709-717. DOI: 10.1016/S0140-6736(16)31715-9. Zeisel, M. B.; Baumert, T. F. Clinical development of hepatitis C virus host-targeting agents. *Lancet* **2017**, *389* (10070), 674-675. DOI: 10.1016/S0140-6736(17)30043-0.
(92) **Regulus to discontinue clinical development of HCV candidate RG-101**. *Pharmaceutical business review*, 2017.
(93) Seto, A. G.; Beatty, X.; Lynch, J. M.; Hermreck, M.; Tetzlaff, M.; Duvic, M.; Jackson, A. L. Cobomarsen, an oligonucleotide inhibitor of miR-155, co-ordinately regulates multiple survival pathways to reduce cellular proliferation and survival in cutaneous T-cell lymphoma. *Br J Haematol* **2018**, *183* (3), 428-444. DOI: 10.1111/bjh.15547.
(94) Querfeld, C.; Foss, F. M.; Kim, Y. H.; Lauren; Pinter-Brown; William, B. M.; Porcu, P.; Pacheco, T.; M., B.; Haverkos; et al. Phase 1 Trial of Cobomarsen, an Inhibitor of Mir-155, in Cutaneous T Cell Lymphoma. *Blood* **2018**, *132* (Supplement 1), 2903-2903.
(95) Gomez, I. G.; MacKenna, D. A.; Johnson, B. G.; Kaimal, V.; Roach, A. M.; Ren, S.; Nakagawa, N.; Xin, C.; Newitt, R.; Pandya, S.; et al. Anti-microRNA-21 oligonucleotides prevent Alport nephropathy progression by stimulating metabolic pathways. *J Clin Invest* **2015**, *125* (1), 141-156. DOI: 10.1172/JCI75852.
(96) Täubel, J.; Hauke, W.; Rump, S.; Viereck, J.; Batkai, S.; Poetzsch, J.; Rode, L.; Weigt, H.; Genschel, C.; Lorch, U.; et al. Novel antisense therapy targeting microRNA-132 in patients with heart failure: results of a first-in-human Phase 1b randomized, double-blind, placebo-controlled study. *Eur Heart J* **2021**, *42* (2), 178-188. DOI: 10.1093/eurheartj/ehaa898.
(97) Beg, M. S.; Brenner, A. J.; Sachdev, J.; Borad, M.; Kang, Y. K.; Stoudemire, J.; Smith, S.; Bader, A. G.; Kim, S.; Hong, D. S. Phase I study of MRX34, a liposomal miR-34a mimic, administered twice weekly in patients with advanced solid tumors. *Invest New Drugs* **2017**, *35* (2), 180-188. DOI: 10.1007/s10637-016-0407-y.
(98) Reid, G.; Kao, S. C.; Pavlakis, N.; Brahmbhatt, H.; MacDiarmid, J.; Clarke, S.; Boyer, M.; van Zandwijk, N. Clinical development of TargomiRs, a miRNA mimic-based treatment for patients with recurrent thoracic cancer. *Epigenomics* **2016**, *8* (8), 1079-1085. DOI: 10.2217/epi-2016-0035.
(99) Kao, S. C.; Fulham, M.; Wong, K.; Cooper, W.; Brahmbhatt, H.; MacDiarmid, J.; Pattison, S.; Sagong, J. O.; Huynh, Y.; Leslie, F.; et al. A Significant Metabolic and Radiological Response after a Novel Targeted MicroRNA-based Treatment Approach in Malignant Pleural Mesothelioma. *Am J Respir Crit Care Med* **2015**, *191* (12), 1467-1469. DOI: 10.1164/rccm.201503-0461LE.
(100) Wu, Y.; Crawford, M.; Mao, Y.; Lee, R. J.; Davis, I. C.; Elton, T. S.; Lee, L. J.; Nana-Sinkam, S. P. Therapeutic Delivery of MicroRNA-29b by Cationic Lipoplexes for Lung Cancer. *Mol Ther Nucleic Acids* **2013**, *2*, e84. DOI: 10.1038/mtna.2013.14. Cortez, M. A.; Valdecanas, D.; Zhang, X.; Zhan, Y.; Bhardwaj, V.; Calin, G. A.; Komaki, R.; Giri, D. K.; Quini, C. C.; Wolfe, T.; et al. Therapeutic delivery of miR-200c enhances radiosensitivity in lung cancer. *Mol Ther* **2014**, *22* (8), 1494-1503. DOI: 10.1038/mt.2014.79. Kasinski, A. L.; Kelnar, K.; Stahlhut, C.; Orellana, E.; Zhao, J.; Shimer, E.; Dysart, S.; Chen, X.; Bader, A. G.; Slack, F. J. A combinatorial microRNA therapeutics approach to suppressing non-small cell lung cancer. *Oncogene* **2015**, *34* (27), 3547-3555. DOI: 10.1038/onc.2014.282.
(101) Gambari, R.; Brognara, E.; Spandidos, D. A.; Fabbri, E. Targeting oncomiRNAs and mimicking tumor suppressor miRNAs: New trends in the development of miRNA therapeutic strategies in oncology (Review). *Int J Oncol* **2016**, *49* (1), 5-32. DOI: 10.3892/ijo.2016.3503.
(102) Sveinbjornsdottir, S. The clinical symptoms of Parkinson's disease. *J Neurochem* **2016**,

139 Suppl 1, 318-324. DOI: 10.1111/jnc.13691.
(103) Reich, S. G.; Savitt, J. M. Parkinson's Disease. *Med Clin North Am* **2019**, *103* (2), 337-350. DOI: 10.1016/j.mcna.2018.10.014.
(104) Chaudhuri, K. R.; Schapira, A. H. Non-motor symptoms of Parkinson's disease: dopaminergic pathophysiology and treatment. *Lancet Neurol* **2009**, *8* (5), 464-474. DOI: 10.1016/S1474-4422(09)70068-7.
(105) Hirsch, L.; Jette, N.; Frolkis, A.; Steeves, T.; Pringsheim, T. The Incidence of Parkinson's Disease: A Systematic Review and Meta-Analysis. *Neuroepidemiology* **2016**, *46* (4), 292-300. DOI: 10.1159/000445751.
(106) Pringsheim, T.; Jette, N.; Frolkis, A.; Steeves, T. D. The prevalence of Parkinson's disease: a systematic review and meta-analysis. *Mov Disord* **2014**, *29* (13), 1583-1590. DOI: 10.1002/mds.25945.
(107) Dorsey, E. R.; Constantinescu, R.; Thompson, J. P.; Biglan, K. M.; Holloway, R. G.; Kieburtz, K.; Marshall, F. J.; Ravina, B. M.; Schifitto, G.; Siderowf, A.; et al. Projected number of people with Parkinson disease in the most populous nations, 2005 through 2030. *Neurology* **2007**, *68* (5), 384-386. DOI: 10.1212/01.wnl.0000247740.47667.03.
(108) Delamarre, A.; Meissner, W. G. Epidemiology, environmental risk factors and genetics of Parkinson's disease. *Presse Med* **2017**, *46* (2 Pt 1), 175-181. DOI: 10.1016/j.lpm.2017.01.001.
(109) Nalls, M. A.; Plagnol, V.; Hernandez, D. G.; Sharma, M.; Sheerin, U. M.; Saad, M.; Simón-Sánchez, J.; Schulte, C.; Lesage, S.; Sveinbjörnsdóttir, S.; et al. Imputation of sequence variants for identification of genetic risks for Parkinson's disease: a meta-analysis of genome-wide association studies. *Lancet* **2011**, *377* (9766), 641-649. DOI: 10.1016/S0140-6736(10)62345-8.
(110) Hernandez, D. G.; Reed, X.; Singleton, A. B. Genetics in Parkinson disease: Mendelian versus non-Mendelian inheritance. *J Neurochem* **2016**, *139 Suppl 1*, 59-74. DOI: 10.1111/jnc.13593.
(111) Kalia, L. V.; Lang, A. E. Parkinson's disease. *Lancet* **2015**, *386* (9996), 896-912. DOI: 10.1016/S0140-6736(14)61393-3.
(112) Poewe, W.; Seppi, K.; Tanner, C. M.; Halliday, G. M.; Brundin, P.; Volkmann, J.; Schrag, A. E.; Lang, A. E. Parkinson disease. *Nat Rev Dis Primers* **2017**, *3*, 17013. DOI: 10.1038/nrdp.2017.13.
(113) Spillantini, M. G.; Schmidt, M. L.; Lee, V. M.; Trojanowski, J. Q.; Jakes, R.; Goedert, M. Alpha-synuclein in Lewy bodies. *Nature* **1997**, *388* (6645), 839-840. DOI: 10.1038/42166.
(114) Davie, C. A. A review of Parkinson's disease. *Br Med Bull* **2008**, *86*, 109-127. DOI: 10.1093/bmb/ldn013.
(115) Polymeropoulos, M. H.; Lavedan, C.; Leroy, E.; Ide, S. E.; Dehejia, A.; Dutra, A.; Pike, B.; Root, H.; Rubenstein, J.; Boyer, R.; et al. Mutation in the alpha-synuclein gene identified in families with Parkinson's disease. *Science* **1997**, *276* (5321), 2045-2047.
(116) Singleton, A. B.; Farrer, M.; Johnson, J.; Singleton, A.; Hague, S.; Kachergus, J.; Hulihan, M.; Peuralinna, T.; Dutra, A.; Nussbaum, R.; et al. alpha-Synuclein locus triplication causes Parkinson's disease. *Science* **2003**, *302* (5646), 841. DOI: 10.1126/science.1090278.
(117) Chartier-Harlin, M. C.; Kachergus, J.; Roumier, C.; Mouroux, V.; Douay, X.; Lincoln, S.; Levecque, C.; Larvor, L.; Andrieux, J.; Hulihan, M.; et al. Alpha-synuclein locus duplication as a cause of familial Parkinson's disease. *Lancet* **2004**, *364* (9440), 1167-1169. DOI: 10.1016/S0140-6736(04)17103-1. Troiano, A. R.; Cazeneuve, C.; Le Ber, I.; Bonnet, A. M.; Lesage, S.; Brice, A. Re: Alpha-synuclein gene duplication is present in sporadic Parkinson disease. *Neurology* **2008**, *71* (16), 1295; author reply 1295. DOI: 10.1212/01.wnl.0000338435.78120.0f.
(118) Villar-Piqué, A.; Lopes da Fonseca, T.; Outeiro, T. F. Structure, function and toxicity of alpha-synuclein: the Bermuda triangle in synucleinopathies. *J Neurochem* **2016**, *139*

Suppl 1, 240-255. DOI: 10.1111/jnc.13249.
(119) Guerrero-Ferreira, R.; Taylor, N. M.; Mona, D.; Ringler, P.; Lauer, M. E.; Riek, R.; Britschgi, M.; Stahlberg, H. Cryo-EM structure of alpha-synuclein fibrils. *Elife* **2018**, *7*. DOI: 10.7554/eLife.36402.
(120) Burré, J.; Sharma, M.; Südhof, T. C. Definition of a molecular pathway mediating α-synuclein neurotoxicity. *J Neurosci* **2015**, *35* (13), 5221-5232. DOI: 10.1523/JNEUROSCI.4650-14.2015.
(121) Stefanis, L.; Emmanouilidou, E.; Pantazopoulou, M.; Kirik, D.; Vekrellis, K.; Tofaris, G. K. How is alpha-synuclein cleared from the cell? *J Neurochem* **2019**, *150* (5), 577-590. DOI: 10.1111/jnc.14704.
(122) Angot, E.; Steiner, J. A.; Hansen, C.; Li, J. Y.; Brundin, P. Are synucleinopathies prion-like disorders? *Lancet Neurol* **2010**, *9* (11), 1128-1138. DOI: 10.1016/S1474-4422(10)70213-1. Steiner, J. A.; Quansah, E.; Brundin, P. The concept of alpha-synuclein as a prion-like protein: ten years after. *Cell Tissue Res* **2018**, *373* (1), 161-173. DOI: 10.1007/s00441-018-2814-1.
(123) Rocha, E. M.; De Miranda, B.; Sanders, L. H. Alpha-synuclein: Pathology, mitochondrial dysfunction and neuroinflammation in Parkinson's disease. *Neurobiol Dis* **2018**, *109* (Pt B), 249-257. DOI: 10.1016/j.nbd.2017.04.004.
(124) Burré, J. The Synaptic Function of α-Synuclein. *J Parkinsons Dis* **2015**, *5* (4), 699-713. DOI: 10.3233/JPD-150642. Burré, J.; Sharma, M.; Südhof, T. C. Cell Biology and Pathophysiology of α-Synuclein. *Cold Spring Harb Perspect Med* **2018**, *8* (3). DOI: 10.1101/cshperspect.a024091.
(125) Kanaan, N. M.; Manfredsson, F. P. Loss of functional alpha-synuclein: a toxic event in Parkinson's disease? *J Parkinsons Dis* **2012**, *2* (4), 249-267. DOI: 10.3233/JPD-012138.
(126) Collier, T. J.; Redmond, D. E.; Steece-Collier, K.; Lipton, J. W.; Manfredsson, F. P. Is Alpha-Synuclein Loss-of-Function a Contributor to Parkinsonian Pathology? Evidence from Non-human Primates. *Front Neurosci* **2016**, *10*, 12. DOI: 10.3389/fnins.2016.00012.
(127) Melo, T. Q.; Copray, S. J. C. V.; Ferrari, M. F. R. Alpha-Synuclein Toxicity on Protein Quality Control, Mitochondria and Endoplasmic Reticulum. *Neurochem Res* **2018**, *43* (12), 2212-2223. DOI: 10.1007/s11064-018-2673-x.
(128) Bose, A.; Beal, M. F. Mitochondrial dysfunction in Parkinson's disease. *J Neurochem* **2016**, *139 Suppl 1*, 216-231. DOI: 10.1111/jnc.13731.
(129) Gao, F.; Yang, J.; Wang, D.; Li, C.; Fu, Y.; Wang, H.; He, W.; Zhang, J. Mitophagy in Parkinson's Disease: Pathogenic and Therapeutic Implications. *Front Neurol* **2017**, *8*, 527. DOI: 10.3389/fneur.2017.00527. McLelland, G. L.; Soubannier, V.; Chen, C. X.; McBride, H. M.; Fon, E. A. Parkin and PINK1 function in a vesicular trafficking pathway regulating mitochondrial quality control. *EMBO J* **2014**, *33* (4), 282-295. DOI: 10.1002/embj.201385902.
(130) Thomas, K. J.; McCoy, M. K.; Blackinton, J.; Beilina, A.; van der Brug, M.; Sandebring, A.; Miller, D.; Maric, D.; Cedazo-Minguez, A.; Cookson, M. R. DJ-1 acts in parallel to the PINK1/parkin pathway to control mitochondrial function and autophagy. *Hum Mol Genet* **2011**, *20* (1), 40-50. DOI: 10.1093/hmg/ddq430.
(131) Grünewald, A.; Kumar, K. R.; Sue, C. M. New insights into the complex role of mitochondria in Parkinson's disease. *Prog Neurobiol* **2019**, *177*, 73-93. DOI: 10.1016/j.pneurobio.2018.09.003.
(132) Pickrell, A. M.; Youle, R. J. The roles of PINK1, parkin, and mitochondrial fidelity in Parkinson's disease. *Neuron* **2015**, *85* (2), 257-273. DOI: 10.1016/j.neuron.2014.12.007. Bonifati, V.; Rizzu, P.; van Baren, M. J.; Schaap, O.; Breedveld, G. J.; Krieger, E.; Dekker, M. C.; Squitieri, F.; Ibanez, P.; Joosse, M.; et al. Mutations in the DJ-1 gene associated with autosomal recessive early-onset parkinsonism. *Science* **2003**, *299* (5604), 256-259. DOI: 10.1126/science.1077209.
(133) Tapias, V.; Hu, X.; Luk, K. C.; Sanders, L. H.; Lee, V. M.; Greenamyre, J. T. Synthetic alpha-synuclein fibrils cause mitochondrial impairment and selective dopamine

neurodegeneration in part via iNOS-mediated nitric oxide production. *Cell Mol Life Sci* **2017**, *74* (15), 2851-2874. DOI: 10.1007/s00018-017-2541-x. Maturana, M. G.; Pinheiro, A. S.; de Souza, T. L.; Follmer, C. Unveiling the role of the pesticides paraquat and rotenone on α-synuclein fibrillation in vitro. *Neurotoxicology* **2015**, *46*, 35-43. DOI: 10.1016/j.neuro.2014.11.006.
(134) De Virgilio, A.; Greco, A.; Fabbrini, G.; Inghilleri, M.; Rizzo, M. I.; Gallo, A.; Conte, M.; Rosato, C.; Ciniglio Appiani, M.; de Vincentiis, M. Parkinson's disease: Autoimmunity and neuroinflammation. *Autoimmun Rev* **2016**, *15* (10), 1005-1011. DOI: 10.1016/j.autrev.2016.07.022. Ransohoff, R. M. How neuroinflammation contributes to neurodegeneration. *Science* **2016**, *353* (6301), 777-783. DOI: 10.1126/science.aag2590.
(135) Hoenen, C.; Gustin, A.; Birck, C.; Kirchmeyer, M.; Beaume, N.; Felten, P.; Grandbarbe, L.; Heuschling, P.; Heurtaux, T. Alpha-Synuclein Proteins Promote Pro-Inflammatory Cascades in Microglia: Stronger Effects of the A53T Mutant. *PLoS One* **2016**, *11* (9), e0162717. DOI: 10.1371/journal.pone.0162717. Gao, H. M.; Kotzbauer, P. T.; Uryu, K.; Leight, S.; Trojanowski, J. Q.; Lee, V. M. Neuroinflammation and oxidation/nitration of alpha-synuclein linked to dopaminergic neurodegeneration. *J Neurosci* **2008**, *28* (30), 7687-7698. DOI: 10.1523/JNEUROSCI.0143-07.2008.
(136) Barker, R. A.; Drouin-Ouellet, J.; Parmar, M. Cell-based therapies for Parkinson disease—past insights and future potential. *Nat Rev Neurol* **2015**, *11* (9), 492-503. DOI: 10.1038/nrneurol.2015.123. Barker, R. A.; consortium, T. Designing stem-cell-based dopamine cell replacement trials for Parkinson's disease. *Nat Med* **2019**, *25* (7), 1045-1053. DOI: 10.1038/s41591-019-0507-2.
(137) Brundin, P.; Atkin, G.; Lamberts, J. T. Basic science breaks through: New therapeutic advances in Parkinson's disease. *Mov Disord* **2015**, *30* (11), 1521-1527. DOI: 10.1002/mds.26332.
(138) Brundin, P.; Dave, K. D.; Kordower, J. H. Therapeutic approaches to target alpha-synuclein pathology. *Exp Neurol* **2017**, *298* (Pt B), 225-235. DOI: 10.1016/j.expneurol.2017.10.003.
(139) Zharikov, A. D.; Cannon, J. R.; Tapias, V.; Bai, Q.; Horowitz, M. P.; Shah, V.; El Ayadi, A.; Hastings, T. G.; Greenamyre, J. T.; Burton, E. A. shRNA targeting α-synuclein prevents neurodegeneration in a Parkinson's disease model. *J Clin Invest* **2015**, *125* (7), 2721-2735. DOI: 10.1172/JCI64502.
(140) Gorbatyuk, O. S.; Li, S.; Nash, K.; Gorbatyuk, M.; Lewin, A. S.; Sullivan, L. F.; Mandel, R. J.; Chen, W.; Meyers, C.; Manfredsson, F. P.; et al. In vivo RNAi-mediated alpha-synuclein silencing induces nigrostriatal degeneration. *Mol Ther* **2010**, *18* (8), 1450-1457. DOI: 10.1038/mt.2010.115.
(141) McCormack, A. L.; Mak, S. K.; Henderson, J. M.; Bumcrot, D.; Farrer, M. J.; Di Monte, D. A. Alpha-synuclein suppression by targeted small interfering RNA in the primate substantia nigra. *PLoS One* **2010**, *5* (8), e12122. DOI: 10.1371/journal.pone.0012122.
(142) Han, Y.; Khodr, C. E.; Sapru, M. K.; Pedapati, J.; Bohn, M. C. A microRNA embedded AAV α-synuclein gene silencing vector for dopaminergic neurons. *Brain Res* **2011**, *1386*, 15-24. DOI: 10.1016/j.brainres.2011.02.041. Khodr, C. E.; Becerra, A.; Han, Y.; Bohn, M. C. Targeting alpha-synuclein with a microRNA-embedded silencing vector in the rat substantia nigra: positive and negative effects. *Brain Res* **2014**, *1550*, 47-60. DOI: 10.1016/j.brainres.2014.01.010.
(143) Teil, M.; Arotcarena, M. L.; Faggiani, E.; Laferriere, F.; Bezard, E.; Dehay, B. Targeting α-synuclein for PD Therapeutics: A Pursuit on All Fronts. *Biomolecules* **2020**, *10* (3). DOI: 10.3390/biom10030391.
(144) Hayashita-Kinoh, H.; Yamada, M.; Yokota, T.; Mizuno, Y.; Mochizuki, H. Down-regulation of alpha-synuclein expression can rescue dopaminergic cells from cell death in the substantia nigra of Parkinson's disease rat model. *Biochem Biophys Res Commun* **2006**, *341* (4), 1088-1095. DOI: 10.1016/j.bbrc.2006.01.057.
(145) Mittal, S.; Bjørnevik, K.; Im, D. S.; Flierl, A.; Dong, X.; Locascio, J. J.; Abo, K. M.;

Long, E.; Jin, M.; Xu, B.; et al. β2-Adrenoreceptor is a regulator of the α-synuclein gene driving risk of Parkinson's disease. *Science* **2017**, *357* (6354), 891-898. DOI: 10.1126/science.aaf3934.
(146) Zhang, P.; Park, H. J.; Zhang, J.; Junn, E.; Andrews, R. J.; Velagapudi, S. P.; Abegg, D.; Vishnu, K.; Costales, M. G.; Childs-Disney, J. L.; et al. Translation of the intrinsically disordered protein α-synuclein is inhibited by a small molecule targeting its structured mRNA. *Proc Natl Acad Sci U S A* **2020**, *117* (3), 1457-1467. DOI: 10.1073/pnas.1905057117.
(147) Price, D. L.; Koike, M. A.; Khan, A.; Wrasidlo, W.; Rockenstein, E.; Masliah, E.; Bonhaus, D. The small molecule alpha-synuclein misfolding inhibitor, NPT200-11, produces multiple benefits in an animal model of Parkinson's disease. *Sci Rep* **2018**, *8* (1), 16165. DOI: 10.1038/s41598-018-34490-9.
(148) Wrasidlo, W.; Tsigelny, I. F.; Price, D. L.; Dutta, G.; Rockenstein, E.; Schwarz, T. C.; Ledolter, K.; Bonhaus, D.; Paulino, A.; Eleuteri, S.; et al. A de novo compound targeting α-synuclein improves deficits in models of Parkinson's disease. *Brain* **2016**, *139* (Pt 12), 3217-3236. DOI: 10.1093/brain/aww238.
(149) Wagner, J.; Ryazanov, S.; Leonov, A.; Levin, J.; Shi, S.; Schmidt, F.; Prix, C.; Pan-Montojo, F.; Bertsch, U.; Mitteregger-Kretzschmar, G.; et al. Anle138b: a novel oligomer modulator for disease-modifying therapy of neurodegenerative diseases such as prion and Parkinson's disease. *Acta Neuropathol* **2013**, *125* (6), 795-813. DOI: 10.1007/s00401-013-1114-9. Levin, J.; Schmidt, F.; Boehm, C.; Prix, C.; Bötzel, K.; Ryazanov, S.; Leonov, A.; Griesinger, C.; Giese, A. The oligomer modulator anle138b inhibits disease progression in a Parkinson mouse model even with treatment started after disease onset. *Acta Neuropathol* **2014**, *127* (5), 779-780. DOI: 10.1007/s00401-014-1265-3.
(150) Bhatt, M. A.; Messer, A.; Kordower, J. H. Can intrabodies serve as neuroprotective therapies for Parkinson's disease? Beginning thoughts. *J Parkinsons Dis* **2013**, *3* (4), 581-591. DOI: 10.3233/JPD-130252.
(151) Guilliams, T.; El-Turk, F.; Buell, A. K.; O'Day, E. M.; Aprile, F. A.; Esbjörner, E. K.; Vendruscolo, M.; Cremades, N.; Pardon, E.; Wyns, L.; et al. Nanobodies raised against monomeric α-synuclein distinguish between fibrils at different maturation stages. *J Mol Biol* **2013**, *425* (14), 2397-2411. DOI: 10.1016/j.jmb.2013.01.040. Lynch, S. M.; Zhou, C.; Messer, A. An scFv intrabody against the nonamyloid component of alpha-synuclein reduces intracellular aggregation and toxicity. *J Mol Biol* **2008**, *377* (1), 136-147. DOI: 10.1016/j.jmb.2007.11.096.
(152) Joshi, S. N.; Butler, D. C.; Messer, A. Fusion to a highly charged proteasomal retargeting sequence increases soluble cytoplasmic expression and efficacy of diverse anti-synuclein intrabodies. *MAbs* **2012**, *4* (6), 686-693. DOI: 10.4161/mabs.21696. Butler, D. C.; Joshi, S. N.; Genst, E.; Baghel, A. S.; Dobson, C. M.; Messer, A. Bifunctional Anti-Non-Amyloid Component α-Synuclein Nanobodies Are Protective In Situ. *PLoS One* **2016**, *11* (11), e0165964. DOI: 10.1371/journal.pone.0165964.
(153) Chatterjee, D.; Bhatt, M.; Butler, D.; De Genst, E.; Dobson, C. M.; Messer, A.; Kordower, J. H. Proteasome-targeted nanobodies alleviate pathology and functional decline in an α-synuclein-based Parkinson's disease model. *NPJ Parkinsons Dis* **2018**, *4*, 25. DOI: 10.1038/s41531-018-0062-4.
(154) Migdalska-Richards, A.; Schapira, A. H. The relationship between glucocerebrosidase mutations and Parkinson disease. *J Neurochem* **2016**, *139 Suppl 1*, 77-90. DOI: 10.1111/jnc.13385.
(155) Rockenstein, E.; Clarke, J.; Viel, C.; Panarello, N.; Treleaven, C. M.; Kim, C.; Spencer, B.; Adame, A.; Park, H.; Dodge, J. C.; et al. Glucocerebrosidase modulates cognitive and motor activities in murine models of Parkinson's disease. *Hum Mol Genet* **2016**, *25* (13), 2645-2660. DOI: 10.1093/hmg/ddw124. Sardi, S. P.; Clarke, J.; Viel, C.; Chan, M.; Tamsett, T. J.; Treleaven, C. M.; Bu, J.; Sweet, L.; Passini, M. A.; Dodge, J. C.; et al. Augmenting CNS glucocerebrosidase activity as a therapeutic strategy for parkinsonism and other

Gaucher-related synucleinopathies. *Proc Natl Acad Sci U S A* **2013**, *110* (9), 3537-3542. DOI: 10.1073/pnas.1220464110. Rocha, E. M.; Smith, G. A.; Park, E.; Cao, H.; Brown, E.; Hayes, M. A.; Beagan, J.; McLean, J. R.; Izen, S. C.; Perez-Torres, E.; et al. Glucocerebrosidase gene therapy prevents α-synucleinopathy of midbrain dopamine neurons. *Neurobiol Dis* **2015**, *82*, 495-503. DOI: 10.1016/j.nbd.2015.09.009.
(156) Sardi, S. P.; Viel, C.; Clarke, J.; Treleaven, C. M.; Richards, A. M.; Park, H.; Olszewski, M. A.; Dodge, J. C.; Marshall, J.; Makino, E.; et al. Glucosylceramide synthase inhibition alleviates aberrations in synucleinopathy models. *Proc Natl Acad Sci U S A* **2017**, *114* (10), 2699-2704. DOI: 10.1073/pnas.1616152114.
(157) Migdalska-Richards, A.; Daly, L.; Bezard, E.; Schapira, A. H. Ambroxol effects in glucocerebrosidase and α-synuclein transgenic mice. *Ann Neurol* **2016**, *80* (5), 766-775. DOI: 10.1002/ana.24790. Mishra, A.; Chandravanshi, L. P.; Trigun, S. K.; Krishnamurthy, S. Ambroxol modulates 6-Hydroxydopamine-induced temporal reduction in Glucocerebrosidase (GCase) enzymatic activity and Parkinson's disease symptoms. *Biochem Pharmacol* **2018**, *155*, 479-493. DOI: 10.1016/j.bcp.2018.07.028. Mishra, A.; Krishnamurthy, S. Neurorestorative effects of sub-chronic administration of ambroxol in rodent model of Parkinson's disease. *Naunyn Schmiedebergs Arch Pharmacol* **2020**, *393* (3), 429-444. DOI: 10.1007/s00210-019-01737-9.
(158) Migdalska-Richards, A.; Ko, W. K. D.; Li, Q.; Bezard, E.; Schapira, A. H. V. Oral ambroxol increases brain glucocerebrosidase activity in a nonhuman primate. *Synapse* **2017**, *71* (7). DOI: 10.1002/syn.21967.
(159) Mullin, S.; Smith, L.; Lee, K.; D'Souza, G.; Woodgate, P.; Elflein, J.; Hällqvist, J.; Toffoli, M.; Streeter, A.; Hosking, J.; et al. Ambroxol for the Treatment of Patients With Parkinson Disease With and Without Glucocerebrosidase Gene Mutations: A Nonrandomized, Noncontrolled Trial. *JAMA Neurol* **2020**, *77* (4), 427-434. DOI: 10.1001/jamaneurol.2019.4611. Schneider, S. A.; Alcalay, R. N. Precision Medicine for Parkinson's Disease: Ambroxol for Glucocerebrosidase-Associated Parkinson's Disease, First Trial Completed. *Mov Disord* **2020**. DOI: 10.1002/mds.28072.
(160) Silveira, C. R. A.; MacKinley, J.; Coleman, K.; Li, Z.; Finger, E.; Bartha, R.; Morrow, S. A.; Wells, J.; Borrie, M.; Tirona, R. G.; et al. Ambroxol as a novel disease-modifying treatment for Parkinson's disease dementia: protocol for a single-centre, randomized, double-blind, placebo-controlled trial. *BMC Neurol* **2019**, *19* (1), 20. DOI: 10.1186/s12883-019-1252-3.
(161) Richter, F.; Fleming, S. M.; Watson, M.; Lemesre, V.; Pellegrino, L.; Ranes, B.; Zhu, C.; Mortazavi, F.; Mulligan, C. K.; Sioshansi, P. C.; et al. A GCase chaperone improves motor function in a mouse model of synucleinopathy. *Neurotherapeutics* **2014**, *11* (4), 840-856. DOI: 10.1007/s13311-014-0294-x.
(162) Moors, T. E.; Hoozemans, J. J.; Ingrassia, A.; Beccari, T.; Parnetti, L.; Chartier-Harlin, M. C.; van de Berg, W. D. Therapeutic potential of autophagy-enhancing agents in Parkinson's disease. *Mol Neurodegener* **2017**, *12* (1), 11. DOI: 10.1186/s13024-017-0154-3.
(163) Hebron, M. L.; Lonskaya, I.; Moussa, C. E. Nilotinib reverses loss of dopamine neurons and improves motor behavior via autophagic degradation of α-synuclein in Parkinson's disease models. *Hum Mol Genet* **2013**, *22* (16), 3315-3328. DOI: 10.1093/hmg/ddt192.
(164) Karuppagounder, S. S.; Brahmachari, S.; Lee, Y.; Dawson, V. L.; Dawson, T. M.; Ko, H. S. The c-Abl inhibitor, nilotinib, protects dopaminergic neurons in a preclinical animal model of Parkinson's disease. *Sci Rep* **2014**, *4*, 4874. DOI: 10.1038/srep04874.
(165) Pagan, F.; Hebron, M.; Valadez, E. H.; Torres-Yaghi, Y.; Huang, X.; Mills, R. R.; Wilmarth, B. M.; Howard, H.; Dunn, C.; Carlson, A.; et al. Nilotinib Effects in Parkinson's disease and Dementia with Lewy bodies. *J Parkinsons Dis* **2016**, *6* (3), 503-517. DOI: 10.3233/JPD-160867. Pagan, F. L.; Hebron, M. L.; Wilmarth, B.; Torres-Yaghi, Y.; Lawler, A.; Mundel, E. E.; Yusuf, N.; Starr, N. J.; Arellano, J.; Howard, H. H.; et al. Pharmacokinetics and pharmacodynamics of a single dose Nilotinib in individuals with

Parkinson's disease. *Pharmacol Res Perspect* **2019**, *7* (2), e00470. DOI: 10.1002/prp2.470. Pagan, F. L.; Hebron, M. L.; Wilmarth, B.; Torres-Yaghi, Y.; Lawler, A.; Mundel, E. E.; Yusuf, N.; Starr, N. J.; Anjum, M.; Arellano, J.; et al. Nilotinib Effects on Safety, Tolerability, and Potential Biomarkers in Parkinson Disease: A Phase 2 Randomized Clinical Trial. *JAMA Neurol* **2019**. DOI: 10.1001/jamaneurol.2019.4200.
(166) Masliah, E.; Rockenstein, E.; Adame, A.; Alford, M.; Crews, L.; Hashimoto, M.; Seubert, P.; Lee, M.; Goldstein, J.; Chilcote, T.; et al. Effects of alpha-synuclein immunization in a mouse model of Parkinson's disease. *Neuron* **2005**, *46* (6), 857-868. DOI: 10.1016/j.neuron.2005.05.010. Chen, Z.; Yang, Y.; Yang, X.; Zhou, C.; Li, F.; Lei, P.; Zhong, L.; Jin, X.; Peng, G. Immune effects of optimized DNA vaccine and protective effects in a MPTP model of Parkinson's disease. *Neurol Sci* **2013**, *34* (9), 1559-1570. DOI: 10.1007/s10072-012-1284-6. Ugen, K. E.; Lin, X.; Bai, G.; Liang, Z.; Cai, J.; Li, K.; Song, S.; Cao, C.; Sanchez-Ramos, J. Evaluation of an α synuclein sensitized dendritic cell based vaccine in a transgenic mouse model of Parkinson disease. *Hum Vaccin Immunother* **2015**, *11* (4), 922-930. DOI: 10.1080/21645515.2015.1012033. Schneeberger, A.; Tierney, L.; Mandler, M. Active immunization therapies for Parkinson's disease and multiple system atrophy. *Mov Disord* **2016**, *31* (2), 214-224. DOI: 10.1002/mds.26377.
(167) Mandler, M.; Valera, E.; Rockenstein, E.; Weninger, H.; Patrick, C.; Adame, A.; Santic, R.; Meindl, S.; Vigl, B.; Smrzka, O.; et al. Next-generation active immunization approach for synucleinopathies: implications for Parkinson's disease clinical trials. *Acta Neuropathol* **2014**, *127* (6), 861-879. DOI: 10.1007/s00401-014-1256-4. Mandler, M.; Valera, E.; Rockenstein, E.; Mante, M.; Weninger, H.; Patrick, C.; Adame, A.; Schmidhuber, S.; Santic, R.; Schneeberger, A.; et al. Active immunization against alpha-synuclein ameliorates the degenerative pathology and prevents demyelination in a model of multiple system atrophy. *Mol Neurodegener* **2015**, *10*, 10. DOI: 10.1186/s13024-015-0008-9.
(168) *Affitope PD01A*. Parkinsons News Today, 2020. (accessed *2020*. *Affitope PD03A*. Parkinsons News Today, (accessed.
(169) Schofield, D. J.; Irving, L.; Calo, L.; Bogstedt, A.; Rees, G.; Nuccitelli, A.; Narwal, R.; Petrone, M.; Roberts, J.; Brown, L.; et al. Preclinical development of a high affinity α-synuclein antibody, MEDI1341, that can enter the brain, sequester extracellular α-synuclein and attenuate α-synuclein spreading in vivo. *Neurobiol Dis* **2019**, *132*, 104582. DOI: 10.1016/j.nbd.2019.104582.
(170) Masliah, E.; Rockenstein, E.; Mante, M.; Crews, L.; Spencer, B.; Adame, A.; Patrick, C.; Trejo, M.; Ubhi, K.; Rohn, T. T.; et al. Passive immunization reduces behavioral and neuropathological deficits in an alpha-synuclein transgenic model of Lewy body disease. *PLoS One* **2011**, *6* (4), e19338. DOI: 10.1371/journal.pone.0019338.
(171) Games, D.; Valera, E.; Spencer, B.; Rockenstein, E.; Mante, M.; Adame, A.; Patrick, C.; Ubhi, K.; Nuber, S.; Sacayon, P.; et al. Reducing C-terminal-truncated alpha-synuclein by immunotherapy attenuates neurodegeneration and propagation in Parkinson's disease-like models. *J Neurosci* **2014**, *34* (28), 9441-9454. DOI: 10.1523/JNEUROSCI.5314-13.2014.
(172) Schenk, D. B.; Koller, M.; Ness, D. K.; Griffith, S. G.; Grundman, M.; Zago, W.; Soto, J.; Atiee, G.; Ostrowitzki, S.; Kinney, G. G. First-in-human assessment of PRX002, an anti-α-synuclein monoclonal antibody, in healthy volunteers. *Mov Disord* **2017**, *32* (2), 211-218. DOI: 10.1002/mds.26878. Jankovic, J.; Goodman, I.; Safirstein, B.; Marmon, T. K.; Schenk, D. B.; Koller, M.; Zago, W.; Ness, D. K.; Griffith, S. G.; Grundman, M.; et al. Safety and Tolerability of Multiple Ascending Doses of PRX002/RG7935, an Anti-α-Synuclein Monoclonal Antibody, in Patients With Parkinson Disease: A Randomized Clinical Trial. *JAMA Neurol* **2018**, *75* (10), 1206-1214. DOI: 10.1001/jamaneurol.2018.1487.
(173) Weihofen, A.; Liu, Y.; Arndt, J. W.; Huy, C.; Quan, C.; Smith, B. A.; Baeriswyl, J. L.; Cavegn, N.; Senn, L.; Su, L.; et al. Development of an aggregate-selective, human-derived α-synuclein antibody BIIB054 that ameliorates disease phenotypes in Parkinson's disease models. *Neurobiol Dis* **2019**, *124*, 276-288. DOI: 10.1016/j.nbd.2018.10.016.
(174) Brys, M.; Fanning, L.; Hung, S.; Ellenbogen, A.; Penner, N.; Yang, M.; Welch, M.;

Koenig, E.; David, E.; Fox, T.; et al. Randomized phase I clinical trial of anti-α-synuclein antibody BIIB054. *Mov Disord* **2019**, *34* (8), 1154-1163. DOI: 10.1002/mds.27738.
(175) Mao, X.; Ou, M. T.; Karuppagounder, S. S.; Kam, T. I.; Yin, X.; Xiong, Y.; Ge, P.; Umanah, G. E.; Brahmachari, S.; Shin, J. H.; et al. Pathological α-synuclein transmission initiated by binding lymphocyte-activation gene 3. *Science* **2016**, *353* (6307). DOI: 10.1126/science.aah3374.
(176) Andrews, L. P.; Marciscano, A. E.; Drake, C. G.; Vignali, D. A. LAG3 (CD223) as a cancer immunotherapy target. *Immunol Rev* **2017**, *276* (1), 80-96. DOI: 10.1111/imr.12519.
(177) Holmes, B. B.; DeVos, S. L.; Kfoury, N.; Li, M.; Jacks, R.; Yanamandra, K.; Ouidja, M. O.; Brodsky, F. M.; Marasa, J.; Bagchi, D. P.; et al. Heparan sulfate proteoglycans mediate internalization and propagation of specific proteopathic seeds. *Proc Natl Acad Sci U S A* **2013**, *110* (33), E3138-3147. DOI: 10.1073/pnas.1301440110.
(178) Zhou, W.; Bercury, K.; Cummiskey, J.; Luong, N.; Lebin, J.; Freed, C. R. Phenylbutyrate up-regulates the DJ-1 protein and protects neurons in cell culture and in animal models of Parkinson disease. *J Biol Chem* **2011**, *286* (17), 14941-14951. DOI: 10.1074/jbc.M110.211029.
(179) Orgaz, L.; Bueno Gil, G. Modulating mitochondrial pyruvate carrier: A promising therapeutic target in Parkinson's disease. *Mov Disord* **2017**, *32* (5), 719. DOI: 10.1002/mds.26962.
(180) Colca, J. R.; VanderLugt, J. T.; Adams, W. J.; Shashlo, A.; McDonald, W. G.; Liang, J.; Zhou, R.; Orloff, D. G. Clinical proof-of-concept study with MSDC-0160, a prototype mTOT-modulating insulin sensitizer. *Clin Pharmacol Ther* **2013**, *93* (4), 352-359. DOI: 10.1038/clpt.2013.10. Shah, R. C.; Matthews, D. C.; Andrews, R. D.; Capuano, A. W.; Fleischman, D. A.; VanderLugt, J. T.; Colca, J. R. An evaluation of MSDC-0160, a prototype mTOT modulating insulin sensitizer, in patients with mild Alzheimer's disease. *Curr Alzheimer Res* **2014**, *11* (6), 564-573. DOI: 10.2174/1567205011666140616113406.
(181) Piguet, F.; Alves, S.; Cartier, N. Clinical Gene Therapy for Neurodegenerative Diseases: Past, Present, and Future. *Hum Gene Ther* **2017**, *28* (11), 988-1003. DOI: 10.1089/hum.2017.160. Warren Olanow, C.; Bartus, R. T.; Baumann, T. L.; Factor, S.; Boulis, N.; Stacy, M.; Turner, D. A.; Marks, W.; Larson, P.; Starr, P. A.; et al. Gene delivery of neurturin to putamen and substantia nigra in Parkinson disease: A double-blind, randomized, controlled trial. *Ann Neurol* **2015**, *78* (2), 248-257. DOI: 10.1002/ana.24436. LeWitt, P. A.; Rezai, A. R.; Leehey, M. A.; Ojemann, S. G.; Flaherty, A. W.; Eskandar, E. N.; Kostyk, S. K.; Thomas, K.; Sarkar, A.; Siddiqui, M. S.; et al. AAV2-GAD gene therapy for advanced Parkinson's disease: a double-blind, sham-surgery controlled, randomised trial. *Lancet Neurol* **2011**, *10* (4), 309-319. DOI: 10.1016/S1474-4422(11)70039-4. Salvatore, M. F.; Ai, Y.; Fischer, B.; Zhang, A. M.; Grondin, R. C.; Zhang, Z.; Gerhardt, G. A.; Gash, D. M. Point source concentration of GDNF may explain failure of phase II clinical trial. *Exp Neurol* **2006**, *202* (2), 497-505. DOI: 10.1016/j.expneurol.2006.07.015. Sudhakar, V.; Richardson, R. M. Gene Therapy for Neurodegenerative Diseases. *Neurotherapeutics* **2019**, *16* (1), 166-175. DOI: 10.1007/s13311-018-00694-0.
(182) Christine, C. W.; Bankiewicz, K. S.; Van Laar, A. D.; Richardson, R. M.; Ravina, B.; Kells, A. P.; Boot, B.; Martin, A. J.; Nutt, J.; Thompson, M. E.; et al. Magnetic resonance imaging-guided phase 1 trial of putaminal AADC gene therapy for Parkinson's disease. *Ann Neurol* **2019**, *85* (5), 704-714. DOI: 10.1002/ana.25450. Nutt, J. G.; Curtze, C.; Hiller, A.; Anderson, S.; Larson, P. S.; Van Laar, A. D.; Richardson, R. M.; Thompson, M. E.; Sedkov, A.; Leinonen, M.; et al. Aromatic L-Amino Acid Decarboxylase Gene Therapy Enhances Levodopa Response in Parkinson's Disease. *Mov Disord* **2020**, *35* (5), 851-858. DOI: 10.1002/mds.27993. Palfi, S.; Gurruchaga, J. M.; Ralph, G. S.; Lepetit, H.; Lavisse, S.; Buttery, P. C.; Watts, C.; Miskin, J.; Kelleher, M.; Deeley, S.; et al. Long-term safety and tolerability of ProSavin, a lentiviral vector-based gene therapy for Parkinson's disease: a dose escalation, open-label, phase 1/2 trial. *Lancet* **2014**, *383* (9923), 1138-1146. DOI: 10.1016/S0140-6736(13)61939-X. Palfi, S.; Gurruchaga, J. M.; Lepetit, H.; Howard, K.;

Ralph, G. S.; Mason, S.; Gouello, G.; Domenech, P.; Buttery, P. C.; Hantraye, P.; et al. Long-Term Follow-Up of a Phase I/II Study of ProSavin, a Lentiviral Vector Gene Therapy for Parkinson's Disease. *Hum Gene Ther Clin Dev* **2018**, *29* (3), 148-155. DOI: 10.1089/humc.2018.081.
(183) Athauda, D.; Foltynie, T. Protective effects of the GLP-1 mimetic exendin-4 in Parkinson's disease. *Neuropharmacology* **2018**, *136* (Pt B), 260-270. DOI: 10.1016/j.neuropharm.2017.09.023.
(184) Boot, E.; Bassett, A. S.; Marras, C. 22q11.2 Deletion Syndrome-Associated Parkinson's Disease. *Mov Disord Clin Pract* **2019**, *6* (1), 11-16. DOI: 10.1002/mdc3.12687.
(185) Sumitomo, A.; Horike, K.; Hirai, K.; Butcher, N.; Boot, E.; Sakurai, T.; Nucifora, F. C.; Bassett, A. S.; Sawa, A.; Tomoda, T. A mouse model of 22q11.2 deletions: Molecular and behavioral signatures of Parkinson's disease and schizophrenia. *Sci Adv* **2018**, *4* (8), eaar6637. DOI: 10.1126/sciadv.aar6637.
(186) Kim, J.; Inoue, K.; Ishii, J.; Vanti, W. B.; Voronov, S. V.; Murchison, E.; Hannon, G.; Abeliovich, A. A MicroRNA feedback circuit in midbrain dopamine neurons. *Science* **2007**, *317* (5842), 1220-1224. DOI: 10.1126/science.1140481.
(187) Chmielarz, P.; Konovalova, J.; Najam, S. S.; Alter, H.; Piepponen, T. P.; Erfle, H.; Sonntag, K. C.; Schütz, G.; Vinnikov, I. A.; Domanskyi, A. Dicer and microRNAs protect adult dopamine neurons. *Cell Death Dis* **2017**, *8* (5), e2813. DOI: 10.1038/cddis.2017.214.
(188) Schulz, J.; Takousis, P.; Wohlers, I.; Itua, I. O. G.; Dobricic, V.; Rücker, G.; Binder, H.; Middleton, L.; Ioannidis, J. P. A.; Perneczky, R.; et al. Meta-analyses identify differentially expressed micrornas in Parkinson's disease. *Ann Neurol* **2019**, *85* (6), 835-851. DOI: 10.1002/ana.25490.
(189) Junn, E.; Lee, K. W.; Jeong, B. S.; Chan, T. W.; Im, J. Y.; Mouradian, M. M. Repression of alpha-synuclein expression and toxicity by microRNA-7. *Proc Natl Acad Sci U S A* **2009**, *106* (31), 13052-13057. DOI: 10.1073/pnas.0906277106.
(190) McMillan, K. J.; Murray, T. K.; Bengoa-Vergniory, N.; Cordero-Llana, O.; Cooper, J.; Buckley, A.; Wade-Martins, R.; Uney, J. B.; O'Neill, M. J.; Wong, L. F.; et al. Loss of MicroRNA-7 Regulation Leads to α-Synuclein Accumulation and Dopaminergic Neuronal Loss In Vivo. *Mol Ther* **2017**, *25* (10), 2404-2414. DOI: 10.1016/j.ymthe.2017.08.017.
(191) Hansen, T. B.; Jensen, T. I.; Clausen, B. H.; Bramsen, J. B.; Finsen, B.; Damgaard, C. K.; Kjems, J. Natural RNA circles function as efficient microRNA sponges. *Nature* **2013**, *495* (7441), 384-388. DOI: 10.1038/nature11993.
(192) Sang, Q.; Liu, X.; Wang, L.; Qi, L.; Sun, W.; Wang, W.; Sun, Y.; Zhang, H. CircSNCA downregulation by pramipexole treatment mediates cell apoptosis and autophagy in Parkinson's disease by targeting miR-7. *Aging (Albany NY)* **2018**, *10* (6), 1281-1293. DOI: 10.18632/aging.101466.
(193) Shen, D. F.; Qi, H. P.; Ma, C.; Chang, M. X.; Zhang, W. N.; Song, R. R. Astaxanthin suppresses endoplasmic reticulum stress and protects against neuron damage in Parkinson's disease by regulating miR-7/SNCA axis. *Neurosci Res* **2020**. DOI: 10.1016/j.neures.2020.04.003.
(194) Filipov, N. M.; Stewart, M. A.; Carr, R. L.; Sistrunk, S. C. Dopaminergic toxicity of the herbicide atrazine in rat striatal slices. *Toxicology* **2007**, *232* (1-2), 68-78. DOI: 10.1016/j.tox.2006.12.007.
(195) Li, B.; Jiang, Y.; Xu, Y.; Li, Y. Identification of miRNA-7 as a regulator of brain-derived neurotrophic factor/α-synuclein axis in atrazine-induced Parkinson's disease by peripheral blood and brain microRNA profiling. *Chemosphere* **2019**, *233*, 542-548. DOI: 10.1016/j.chemosphere.2019.05.064.
(196) Covy, J. P.; Giasson, B. I. α-Synuclein, leucine-rich repeat kinase-2, and manganese in the pathogenesis of Parkinson disease. *Neurotoxicology* **2011**, *32* (5), 622-629. DOI: 10.1016/j.neuro.2011.01.003.
(197) Tarale, P.; Daiwile, A. P.; Sivanesan, S.; Stöger, R.; Bafana, A.; Naoghare, P. K.; Parmar, D.; Chakrabarti, T.; Krishnamurthi, K. Manganese exposure: Linking down-

regulation of miRNA-7 and miRNA-433 with α-synuclein overexpression and risk of idiopathic Parkinson's disease. *Toxicol In Vitro* **2018**, *46*, 94-101. DOI: 10.1016/j.tiv.2017.10.003.
(198) Zhou, Y.; Lu, M.; Du, R. H.; Qiao, C.; Jiang, C. Y.; Zhang, K. Z.; Ding, J. H.; Hu, G. MicroRNA-7 targets Nod-like receptor protein 3 inflammasome to modulate neuroinflammation in the pathogenesis of Parkinson's disease. *Mol Neurodegener* **2016**, *11*, 28. DOI: 10.1186/s13024-016-0094-3.
(199) Kim, T.; Mehta, S. L.; Morris-Blanco, K. C.; Chokkalla, A. K.; Chelluboina, B.; Lopez, M.; Sullivan, R.; Kim, H. T.; Cook, T. D.; Kim, J. Y.; et al. The microRNA miR-7a-5p ameliorates ischemic brain damage by repressing α-synuclein. *Sci Signal* **2018**, *11* (560). DOI: 10.1126/scisignal.aat4285.
(200) Choi, D. C.; Yoo, M.; Kabaria, S.; Junn, E. MicroRNA-7 facilitates the degradation of alpha-synuclein and its aggregates by promoting autophagy. *Neurosci Lett* **2018**, *678*, 118-123. DOI: 10.1016/j.neulet.2018.05.009.
(201) Choi, D. C.; Chae, Y. J.; Kabaria, S.; Chaudhuri, A. D.; Jain, M. R.; Li, H.; Mouradian, M. M.; Junn, E. MicroRNA-7 protects against 1-methyl-4-phenylpyridinium-induced cell death by targeting RelA. *J Neurosci* **2014**, *34* (38), 12725-12737. DOI: 10.1523/JNEUROSCI.0985-14.2014.
(202) Chaudhuri, A. D.; Choi, D. C.; Kabaria, S.; Tran, A.; Junn, E. MicroRNA-7 Regulates the Function of Mitochondrial Permeability Transition Pore by Targeting VDAC1 Expression. *J Biol Chem* **2016**, *291* (12), 6483-6493. DOI: 10.1074/jbc.M115.691352.
(203) Kabaria, S.; Choi, D. C.; Chaudhuri, A. D.; Jain, M. R.; Li, H.; Junn, E. MicroRNA-7 activates Nrf2 pathway by targeting Keap1 expression. *Free Radic Biol Med* **2015**, *89*, 548-556. DOI: 10.1016/j.freeradbiomed.2015.09.010.
(204) Li, S.; Lv, X.; Zhai, K.; Xu, R.; Zhang, Y.; Zhao, S.; Qin, X.; Yin, L.; Lou, J. MicroRNA-7 inhibits neuronal apoptosis in a cellular Parkinson's disease model by targeting Bax and Sirt2. *Am J Transl Res* **2016**, *8* (2), 993-1004.
(205) Cao, B.; Wang, T.; Qu, Q.; Kang, T.; Yang, Q. Long Noncoding RNA SNHG1 Promotes Neuroinflammation in Parkinson's Disease via Regulating miR-7/NLRP3 Pathway. *Neuroscience* **2018**, *388*, 118-127. DOI: 10.1016/j.neuroscience.2018.07.019.
(206) Cressatti, M.; Juwara, L.; Galindez, J. M.; Velly, A. M.; Nkurunziza, E. S.; Marier, S.; Canie, O.; Gornistky, M.; Schipper, H. M. Salivary microR-153 and microR-223 Levels as Potential Diagnostic Biomarkers of Idiopathic Parkinson's Disease. *Mov Disord* **2020**, *35* (3), 468-477. DOI: 10.1002/mds.27935.
(207) Gui, Y.; Liu, H.; Zhang, L.; Lv, W.; Hu, X. Altered microRNA profiles in cerebrospinal fluid exosome in Parkinson disease and Alzheimer disease. *Oncotarget* **2015**, *6* (35), 37043-37053. DOI: 10.18632/oncotarget.6158.
(208) Zhang, X.; Yang, R.; Hu, B. L.; Lu, P.; Zhou, L. L.; He, Z. Y.; Wu, H. M.; Zhu, J. H. Reduced Circulating Levels of miR-433 and miR-133b Are Potential Biomarkers for Parkinson's Disease. *Front Cell Neurosci* **2017**, *11*, 170. DOI: 10.3389/fncel.2017.00170.
(209) Doxakis, E. Post-transcriptional regulation of alpha-synuclein expression by mir-7 and mir-153. *J Biol Chem* **2010**, *285* (17), 12726-12734. DOI: 10.1074/jbc.M109.086827.
(210) Cressatti, M.; Song, W.; Turk, A. Z.; Garabed, L. R.; Benchaya, J. A.; Galindez, C.; Liberman, A.; Schipper, H. M. Glial HMOX1 expression promotes central and peripheral α-synuclein dysregulation and pathogenicity in parkinsonian mice. *Glia* **2019**, *67* (9), 1730-1744. DOI: 10.1002/glia.23645.
(211) Fragkouli, A.; Doxakis, E. miR-7 and miR-153 protect neurons against MPP(+)-induced cell death via upregulation of mTOR pathway. *Front Cell Neurosci* **2014**, *8*, 182. DOI: 10.3389/fncel.2014.00182.
(212) Je, G.; Kim, Y. S. Mitochondrial ROS-mediated post-transcriptional regulation of α-synuclein through miR-7 and miR-153. *Neurosci Lett* **2017**, *661*, 132-136. DOI: 10.1016/j.neulet.2017.09.065.
(213) Kim, H. J.; Park, G.; Jeon, B. S.; Park, W. Y.; Kim, Y. E. A mir-153 binding site

variation in SNCA in a patient with Parkinson's disease. *Mov Disord* **2013**, *28* (12), 1755-1756. DOI: 10.1002/mds.25505.
(214) Zhu, J.; Wang, S.; Qi, W.; Xu, X.; Liang, Y. Overexpression of miR-153 promotes oxidative stress in MPP. *Int J Clin Exp Pathol* **2018**, *11* (8), 4179-4187.
(215) Zhang, X. S.; Ha, S.; Wang, X. L.; Shi, Y. L.; Duan, S. S.; Li, Z. A. Tanshinone IIA protects dopaminergic neurons against 6-hydroxydopamine-induced neurotoxicity through miR-153/NF-E2-related factor 2/antioxidant response element signaling pathway. *Neuroscience* **2015**, *303*, 489-502. DOI: 10.1016/j.neuroscience.2015.06.030.
(216) Schlaudraff, F.; Gründemann, J.; Fauler, M.; Dragicevic, E.; Hardy, J.; Liss, B. Orchestrated increase of dopamine and PARK mRNAs but not miR-133b in dopamine neurons in Parkinson's disease. *Neurobiol Aging* **2014**, *35* (10), 2302-2315. DOI: 10.1016/j.neurobiolaging.2014.03.016.
(217) Heyer, M. P.; Pani, A. K.; Smeyne, R. J.; Kenny, P. J.; Feng, G. Normal midbrain dopaminergic neuron development and function in miR-133b mutant mice. *J Neurosci* **2012**, *32* (32), 10887-10894. DOI: 10.1523/JNEUROSCI.1732-12.2012.
(218) Zhao, N.; Jin, L.; Fei, G.; Zheng, Z.; Zhong, C. Serum microRNA-133b is associated with low ceruloplasmin levels in Parkinson's disease. *Parkinsonism Relat Disord* **2014**, *20* (11), 1177-1180. DOI: 10.1016/j.parkreldis.2014.08.016.
(219) Niu, M.; Xu, R.; Wang, J.; Hou, B.; Xie, A. MiR-133b ameliorates axon degeneration induced by MPP(+) via targeting RhoA. *Neuroscience* **2016**, *325*, 39-49. DOI: 10.1016/j.neuroscience.2016.03.042.
(220) Zhou, Z.; Kim, J.; Insolera, R.; Peng, X.; Fink, D. J.; Mata, M. Rho GTPase regulation of α-synuclein and VMAT2: implications for pathogenesis of Parkinson's disease. *Mol Cell Neurosci* **2011**, *48* (1), 29-37. DOI: 10.1016/j.mcn.2011.06.002.
(221) Zhang, L. M.; Wang, M. H.; Yang, H. C.; Tian, T.; Sun, G. F.; Ji, Y. F.; Hu, W. T.; Liu, X.; Wang, J. P.; Lu, H. Dopaminergic neuron injury in Parkinson's disease is mitigated by interfering lncRNA SNHG14 expression to regulate the miR-133b/ α-synuclein pathway. *Aging (Albany NY)* **2019**, *11* (21), 9264-9279. DOI: 10.18632/aging.102330.
(222) Miñones-Moyano, E.; Porta, S.; Escaramís, G.; Rabionet, R.; Iraola, S.; Kagerbauer, B.; Espinosa-Parrilla, Y.; Ferrer, I.; Estivill, X.; Martí, E. MicroRNA profiling of Parkinson's disease brains identifies early downregulation of miR-34b/c which modulate mitochondrial function. *Hum Mol Genet* **2011**, *20* (15), 3067-3078. DOI: 10.1093/hmg/ddr210.
(223) Villar-Menéndez, I.; Porta, S.; Buira, S. P.; Pereira-Veiga, T.; Díaz-Sánchez, S.; Albasanz, J. L.; Ferrer, I.; Martín, M.; Barrachina, M. Increased striatal adenosine A2A receptor levels is an early event in Parkinson's disease-related pathology and it is potentially regulated by miR-34b. *Neurobiol Dis* **2014**, *69*, 206-214. DOI: 10.1016/j.nbd.2014.05.030.
(224) Fanciulli, A.; Wenning, G. K. Multiple-system atrophy. *N Engl J Med* **2015**, *372* (3), 249-263. DOI: 10.1056/NEJMra1311488. Marques, T. M.; Kuiperij, H. B.; Bruinsma, I. B.; van Rumund, A.; Aerts, M. B.; Esselink, R. A. J.; Bloem, B. R.; Verbeek, M. M. MicroRNAs in Cerebrospinal Fluid as Potential Biomarkers for Parkinson's Disease and Multiple System Atrophy. *Mol Neurobiol* **2017**, *54* (10), 7736-7745. DOI: 10.1007/s12035-016-0253-0.
(225) Kabaria, S.; Choi, D. C.; Chaudhuri, A. D.; Mouradian, M. M.; Junn, E. Inhibition of miR-34b and miR-34c enhances α-synuclein expression in Parkinson's disease. *FEBS Lett* **2015**, *589* (3), 319-325. DOI: 10.1016/j.febslet.2014.12.014.
(226) Consales, C.; Cirotti, C.; Filomeni, G.; Panatta, M.; Butera, A.; Merla, C.; Lopresto, V.; Pinto, R.; Marino, C.; Benassi, B. Fifty-Hertz Magnetic Field Affects the Epigenetic Modulation of the miR-34b/c in Neuronal Cells. *Mol Neurobiol* **2018**, *55* (7), 5698-5714. DOI: 10.1007/s12035-017-0791-0.
(227) Rhinn, H.; Qiang, L.; Yamashita, T.; Rhee, D.; Zolin, A.; Vanti, W.; Abeliovich, A. Alternative α-synuclein transcript usage as a convergent mechanism in Parkinson's disease pathology. *Nat Commun* **2012**, *3*, 1084. DOI: 10.1038/ncomms2032.
(228) Chen, H.; Shalom-Feuerstein, R.; Riley, J.; Zhang, S. D.; Tucci, P.; Agostini, M.;

Aberdam, D.; Knight, R. A.; Genchi, G.; Nicotera, P.; et al. miR-7 and miR-214 are specifically expressed during neuroblastoma differentiation, cortical development and embryonic stem cells differentiation, and control neurite outgrowth in vitro. *Biochem Biophys Res Commun* **2010**, *394* (4), 921-927. DOI: 10.1016/j.bbrc.2010.03.076.
(229) Dong, H.; Wang, C.; Lu, S.; Yu, C.; Huang, L.; Feng, W.; Xu, H.; Chen, X.; Zen, K.; Yan, Q.; et al. A panel of four decreased serum microRNAs as a novel biomarker for early Parkinson's disease. *Biomarkers* **2016**, *21* (2), 129-137. DOI: 10.3109/1354750X.2015.1118544.
(230) Wang, Z. H.; Zhang, J. L.; Duan, Y. L.; Zhang, Q. S.; Li, G. F.; Zheng, D. L. MicroRNA-214 participates in the neuroprotective effect of Resveratrol via inhibiting α-synuclein expression in MPTP-induced Parkinson's disease mouse. *Biomed Pharmacother* **2015**, *74*, 252-256. DOI: 10.1016/j.biopha.2015.08.025.
(231) Lee, Y. B.; Bantounas, I.; Lee, D. Y.; Phylactou, L.; Caldwell, M. A.; Uney, J. B. Twist-1 regulates the miR-199a/214 cluster during development. *Nucleic Acids Res* **2009**, *37* (1), 123-128. DOI: 10.1093/nar/gkn920.
(232) Martins, M.; Rosa, A.; Guedes, L. C.; Fonseca, B. V.; Gotovac, K.; Violante, S.; Mestre, T.; Coelho, M.; Rosa, M. M.; Martin, E. R.; et al. Convergence of miRNA expression profiling, α-synuclein interacton and GWAS in Parkinson's disease. *PLoS One* **2011**, *6* (10), e25443. DOI: 10.1371/journal.pone.0025443. Tolosa, E.; Botta-Orfila, T.; Morató, X.; Calatayud, C.; Ferrer-Lorente, R.; Martí, M. J.; Fernández, M.; Gaig, C.; Raya, Á.; Consiglio, A.; et al. MicroRNA alterations in iPSC-derived dopaminergic neurons from Parkinson disease patients. *Neurobiol Aging* **2018**, *69*, 283-291. DOI: 10.1016/j.neurobiolaging.2018.05.032.
(233) Scott, H.; Howarth, J.; Lee, Y. B.; Wong, L. F.; Bantounas, I.; Phylactou, L.; Verkade, P.; Uney, J. B. MiR-3120 is a mirror microRNA that targets heat shock cognate protein 70 and auxilin messenger RNAs and regulates clathrin vesicle uncoating. *J Biol Chem* **2012**, *287* (18), 14726-14733. DOI: 10.1074/jbc.M111.326041.
(234) Agarwal, V.; Bell, G. W.; Nam, J. W.; Bartel, D. P. Predicting effective microRNA target sites in mammalian mRNAs. *Elife* **2015**, *4*. DOI: 10.7554/eLife.05005.
(235) Burgos, K.; Malenica, I.; Metpally, R.; Courtright, A.; Rakela, B.; Beach, T.; Shill, H.; Adler, C.; Sabbagh, M.; Villa, S.; et al. Profiles of extracellular miRNA in cerebrospinal fluid and serum from patients with Alzheimer's and Parkinson's diseases correlate with disease status and features of pathology. *PLoS One* **2014**, *9* (5), e94839. DOI: 10.1371/journal.pone.0094839.
(236) Wang, G.; van der Walt, J. M.; Mayhew, G.; Li, Y. J.; Züchner, S.; Scott, W. K.; Martin, E. R.; Vance, J. M. Variation in the miRNA-433 binding site of FGF20 confers risk for Parkinson disease by overexpression of alpha-synuclein. *Am J Hum Genet* **2008**, *82* (2), 283-289. DOI: 10.1016/j.ajhg.2007.09.021.
(237) de Mena, L.; Cardo, L. F.; Coto, E.; Miar, A.; Díaz, M.; Corao, A. I.; Alonso, B.; Ribacoba, R.; Salvador, C.; Menéndez, M.; et al. FGF20 rs12720208 SNP and microRNA-433 variation: no association with Parkinson's disease in Spanish patients. *Neurosci Lett* **2010**, *479* (1), 22-25. DOI: 10.1016/j.neulet.2010.05.019.
(238) Gillardon, F.; Mack, M.; Rist, W.; Schnack, C.; Lenter, M.; Hildebrandt, T.; Hengerer, B. MicroRNA and proteome expression profiling in early-symptomatic α-synuclein(A30P)-transgenic mice. *Proteomics Clin Appl* **2008**, *2* (5), 697-705. DOI: 10.1002/prca.200780025.
(239) Boudreau, R. L.; Jiang, P.; Gilmore, B. L.; Spengler, R. M.; Tirabassi, R.; Nelson, J. A.; Ross, C. A.; Xing, Y.; Davidson, B. L. Transcriptome-wide discovery of microRNA binding sites in human brain. *Neuron* **2014**, *81* (2), 294-305. DOI: 10.1016/j.neuron.2013.10.062.
(240) Alvarez-Erviti, L.; Seow, Y.; Schapira, A. H.; Rodriguez-Oroz, M. C.; Obeso, J. A.; Cooper, J. M. Influence of microRNA deregulation on chaperone-mediated autophagy and α-synuclein pathology in Parkinson's disease. *Cell Death Dis* **2013**, *4*, e545. DOI: 10.1038/cddis.2013.73.

(241) Su, C.; Yang, X.; Lou, J. Geniposide reduces α-synuclein by blocking microRNA-21/lysosome-associated membrane protein 2A interaction in Parkinson disease models. *Brain Res* **2016**, *1644*, 98-106. DOI: 10.1016/j.brainres.2016.05.011.
(242) Mao, H.; Ding, L. Downregulation of miR-21 suppresses 1-methyl-4-phenylpyridinium-induced neuronal damage in MES23.5 cells. *Exp Ther Med* **2019**, *18* (4), 2467-2474. DOI: 10.3892/etm.2019.7853.
(243) Chen, Y.; Gao, C.; Sun, Q.; Pan, H.; Huang, P.; Ding, J.; Chen, S. MicroRNA-4639 Is a Regulator of DJ-1 Expression and a Potential Early Diagnostic Marker for Parkinson's Disease. *Front Aging Neurosci* **2017**, *9*, 232. DOI: 10.3389/fnagi.2017.00232.
(244) Kim, J.; Fiesel, F. C.; Belmonte, K. C.; Hudec, R.; Wang, W. X.; Kim, C.; Nelson, P. T.; Springer, W. miR-27a and miR-27b regulate autophagic clearance of damaged mitochondria by targeting PTEN-induced putative kinase 1 (PINK1). *Mol Neurodegener* **2016**, *11* (1), 55. DOI: 10.1186/s13024-016-0121-4.
(245) Prajapati, P.; Sripada, L.; Singh, K.; Roy, M.; Bhatelia, K.; Dalwadi, P.; Singh, R. Systemic Analysis of miRNAs in PD Stress Condition: miR-5701 Modulates Mitochondrial-Lysosomal Cross Talk to Regulate Neuronal Death. *Mol Neurobiol* **2018**, *55* (6), 4689-4701. DOI: 10.1007/s12035-017-0664-6.
(246) Gehrke, S.; Imai, Y.; Sokol, N.; Lu, B. Pathogenic LRRK2 negatively regulates microRNA-mediated translational repression. *Nature* **2010**, *466* (7306), 637-641. DOI: 10.1038/nature09191.
(247) Cho, H. J.; Liu, G.; Jin, S. M.; Parisiadou, L.; Xie, C.; Yu, J.; Sun, L.; Ma, B.; Ding, J.; Vancraenenbroeck, R.; et al. MicroRNA-205 regulates the expression of Parkinson's disease-related leucine-rich repeat kinase 2 protein. *Hum Mol Genet* **2013**, *22* (3), 608-620. DOI: 10.1093/hmg/dds470.
(248) Chen, Q.; Huang, X.; Li, R. lncRNA MALAT1/miR-205-5p axis regulates MPP. *Am J Transl Res* **2018**, *10* (2), 563-572.
(249) Zhang, Q. S.; Wang, Z. H.; Zhang, J. L.; Duan, Y. L.; Li, G. F.; Zheng, D. L. Beta-asarone protects against MPTP-induced Parkinson's disease via regulating long non-coding RNA MALAT1 and inhibiting α-synuclein protein expression. *Biomed Pharmacother* **2016**, *83*, 153-159. DOI: 10.1016/j.biopha.2016.06.017.
(250) Li, N.; Pan, X.; Zhang, J.; Ma, A.; Yang, S.; Ma, J.; Xie, A. Plasma levels of miR-137 and miR-124 are associated with Parkinson's disease but not with Parkinson's disease with depression. *Neurol Sci* **2017**, *38* (5), 761-767. DOI: 10.1007/s10072-017-2841-9.
(251) Kanagaraj, N.; Beiping, H.; Dheen, S. T.; Tay, S. S. Downregulation of miR-124 in MPTP-treated mouse model of Parkinson's disease and MPP iodide-treated MN9D cells modulates the expression of the calpain/cdk5 pathway proteins. *Neuroscience* **2014**, *272*, 167-179. DOI: 10.1016/j.neuroscience.2014.04.039.
(252) Geng, L.; Liu, W.; Chen, Y. miR-124-3p Attenuates MPP^{+}-induced Neuronal Injury by Targeting STAT3 in SH-SY5Y Cells. *Exp Biol Med (Maywood)* **2017**, *242* (18), 1757-1764. DOI: 10.1177/1535370217734492. Gong, X.; Wang, H.; Ye, Y.; Shu, Y.; Deng, Y.; He, X.; Lu, G.; Zhang, S. miR-124 regulates cell apoptosis and autophagy in dopaminergic neurons and protects them by regulating AMPK/mTOR pathway in Parkinson's disease. *Am J Transl Res* **2016**, *8* (5), 2127-2137. Yao, L.; Ye, Y.; Mao, H.; Lu, F.; He, X.; Lu, G.; Zhang, S. MicroRNA-124 regulates the expression of MEKK3 in the inflammatory pathogenesis of Parkinson's disease. *J Neuroinflammation* **2018**, *15* (1), 13. DOI: 10.1186/s12974-018-1053-4. Wang, H.; Ye, Y.; Zhu, Z.; Mo, L.; Lin, C.; Wang, Q.; Gong, X.; He, X.; Lu, G.; Lu, F.; et al. MiR-124 Regulates Apoptosis and Autophagy Process in MPTP Model of Parkinson's Disease by Targeting to Bim. *Brain Pathol* **2016**, *26* (2), 167-176. DOI: 10.1111/bpa.12267. Dong, R. F.; Zhang, B.; Tai, L. W.; Liu, H. M.; Shi, F. K.; Liu, N. N. The Neuroprotective Role of MiR-124-3p in a 6-Hydroxydopamine-Induced Cell Model of Parkinson's Disease via the Regulation of ANAX5. *J Cell Biochem* **2018**, *119* (1), 269-277. DOI: 10.1002/jcb.26170.
(253) Liu, W.; Zhang, Q.; Zhang, J.; Pan, W.; Zhao, J.; Xu, Y. Long non-coding RNA

MALAT1 contributes to cell apoptosis by sponging miR-124 in Parkinson disease. *Cell Biosci* **2017**, *7*, 19. DOI: 10.1186/s13578-017-0147-5.
(254) Saraiva, C.; Paiva, J.; Santos, T.; Ferreira, L.; Bernardino, L. MicroRNA-124 loaded nanoparticles enhance brain repair in Parkinson's disease. *J Control Release* **2016**, *235*, 291-305. DOI: 10.1016/j.jconrel.2016.06.005. Saraiva, C.; Ferreira, L.; Bernardino, L. Traceable microRNA-124 loaded nanoparticles as a new promising therapeutic tool for Parkinson's disease. *Neurogenesis (Austin)* **2016**, *3* (1), e1256855. DOI: 10.1080/23262133.2016.1256855.
(255) Krol, J.; Loedige, I.; Filipowicz, W. The widespread regulation of microRNA biogenesis, function and decay. *Nat Rev Genet* **2010**, *11* (9), 597-610. DOI: 10.1038/nrg2843.
(256) Michlewski, G.; Caceres, J. F. Post-transcriptional control of miRNA biogenesis. *Rna* **2018**. DOI: 10.1261/rna.068692.118 From NLM.
(257) He, L.; He, X.; Lim, L. P.; de Stanchina, E.; Xuan, Z.; Liang, Y.; Xue, W.; Zender, L.; Magnus, J.; Ridzon, D.; et al. A microRNA component of the p53 tumour suppressor network. *Nature* **2007**, *447* (7148), 1130-1134. DOI: 10.1038/nature05939. Conaco, C.; Otto, S.; Han, J. J.; Mandel, G. Reciprocal actions of REST and a microRNA promote neuronal identity. *Proc Natl Acad Sci U S A* **2006**, *103* (7), 2422-2427. DOI: 10.1073/pnas.0511041103.
(258) Choudhury, N. R.; Michlewski, G. Terminal loop-mediated control of microRNA biogenesis. *Biochem Soc Trans* **2012**, *40* (4), 789-793. DOI: 10.1042/BST20120053.
(259) Lee, H.; Han, S.; Kwon, C. S.; Lee, D. Biogenesis and regulation of the let-7 miRNAs and their functional implications. *Protein Cell* **2016**, *7* (2), 100-113. DOI: 10.1007/s13238-015-0212-y.
(260) Heo, I.; Joo, C.; Cho, J.; Ha, M.; Han, J.; Kim, V. N. Lin28 mediates the terminal uridylation of let-7 precursor MicroRNA. *Mol Cell* **2008**, *32* (2), 276-284. DOI: 10.1016/j.molcel.2008.09.014. Newman, M. A.; Thomson, J. M.; Hammond, S. M. Lin-28 interaction with the Let-7 precursor loop mediates regulated microRNA processing. *RNA* **2008**, *14* (8), 1539-1549. DOI: 10.1261/rna.1155108. Viswanathan, S. R.; Daley, G. Q.; Gregory, R. I. Selective blockade of microRNA processing by Lin28. *Science* **2008**, *320* (5872), 97-100. DOI: 10.1126/science.1154040.
(261) Rybak, A.; Fuchs, H.; Smirnova, L.; Brandt, C.; Pohl, E. E.; Nitsch, R.; Wulczyn, F. G. A feedback loop comprising lin-28 and let-7 controls pre-let-7 maturation during neural stem-cell commitment. *Nat Cell Biol* **2008**, *10* (8), 987-993. DOI: 10.1038/ncb1759.
(262) Triboulet, R.; Pirouz, M.; Gregory, R. I. A Single Let-7 MicroRNA Bypasses LIN28-Mediated Repression. *Cell Rep* **2015**, *13* (2), 260-266. DOI: 10.1016/j.celrep.2015.08.086.
(263) Büssing, I.; Slack, F. J.; Grosshans, H. let-7 microRNAs in development, stem cells and cancer. *Trends Mol Med* **2008**, *14* (9), 400-409. DOI: 10.1016/j.molmed.2008.07.001.
(264) Nam, Y.; Chen, C.; Gregory, R. I.; Chou, J. J.; Sliz, P. Molecular basis for interaction of let-7 microRNAs with Lin28. *Cell* **2011**, *147* (5), 1080-1091. DOI: 10.1016/j.cell.2011.10.020.
(265) Heo, I.; Joo, C.; Kim, Y. K.; Ha, M.; Yoon, M. J.; Cho, J.; Yeom, K. H.; Han, J.; Kim, V. N. TUT4 in concert with Lin28 suppresses microRNA biogenesis through pre-microRNA uridylation. *Cell* **2009**, *138* (4), 696-708. DOI: 10.1016/j.cell.2009.08.002. Choudhury, N. R.; Nowak, J. S.; Zuo, J.; Rappsilber, J.; Spoel, S. H.; Michlewski, G. Trim25 Is an RNA-Specific Activator of Lin28a/TuT4-Mediated Uridylation. *Cell Rep* **2014**, *9* (4), 1265-1272. DOI: 10.1016/j.celrep.2014.10.017.
(266) Ustianenko, D.; Hrossova, D.; Potesil, D.; Chalupnikova, K.; Hrazdilova, K.; Pachernik, J.; Cetkovska, K.; Uldrijan, S.; Zdrahal, Z.; Vanacova, S. Mammalian DIS3L2 exoribonuclease targets the uridylated precursors of let-7 miRNAs. *RNA* **2013**, *19* (12), 1632-1638. DOI: 10.1261/rna.040055.113. Chang, H. M.; Triboulet, R.; Thornton, J. E.; Gregory, R. I. A role for the Perlman syndrome exonuclease Dis3l2 in the Lin28-let-7 pathway. *Nature* **2013**, *497* (7448), 244-248. DOI: 10.1038/nature12119.
(267) Piskounova, E.; Polytarchou, C.; Thornton, J. E.; LaPierre, R. J.; Pothoulakis, C.;

Hagan, J. P.; Iliopoulos, D.; Gregory, R. I. Lin28A and Lin28B inhibit let-7 microRNA biogenesis by distinct mechanisms. *Cell* **2011**, *147* (5), 1066-1079. DOI: 10.1016/j.cell.2011.10.039.
(268) Choudhury, N. R.; de Lima Alves, F.; de Andres-Aguayo, L.; Graf, T.; Caceres, J. F.; Rappsilber, J.; Michlewski, G. Tissue-specific control of brain-enriched miR-7 biogenesis. *Genes Dev* **2013**, *27* (1), 24-38. DOI: 10.1101/gad.199190.112 From NLM.
(269) Wang, Y.; Vogel, G.; Yu, Z.; Richard, S. The QKI-5 and QKI-6 RNA binding proteins regulate the expression of microRNA 7 in glial cells. *Mol Cell Biol* **2013**, *33* (6), 1233-1243. DOI: 10.1128/MCB.01604-12.
(270) Horsham, J. L.; Ganda, C.; Kalinowski, F. C.; Brown, R. A.; Epis, M. R.; Leedman, P. J. MicroRNA-7: A miRNA with expanding roles in development and disease. *Int J Biochem Cell Biol* **2015**, *69*, 215-224. DOI: 10.1016/j.biocel.2015.11.001.
(271) Webster, R. J.; Giles, K. M.; Price, K. J.; Zhang, P. M.; Mattick, J. S.; Leedman, P. J. Regulation of epidermal growth factor receptor signaling in human cancer cells by microRNA-7. *J Biol Chem* **2009**, *284* (9), 5731-5741. DOI: 10.1074/jbc.M804280200.
(272) Choudhury, N. R.; Michlewski, G. Quantitative identification of proteins that influence miRNA biogenesis by RNA pull-down-SILAC mass spectrometry (RP-SMS). *Methods* **2018**. DOI: 10.1016/j.ymeth.2018.06.006 From NLM.
(273) Michlewski, G.; Guil, S.; Semple, C. A.; Cáceres, J. F. Posttranscriptional regulation of miRNAs harboring conserved terminal loops. *Mol Cell* **2008**, *32* (3), 383-393. DOI: 10.1016/j.molcel.2008.10.013.
(274) Guil, S.; Cáceres, J. F. The multifunctional RNA-binding protein hnRNP A1 is required for processing of miR-18a. *Nat Struct Mol Biol* **2007**, *14* (7), 591-596. DOI: 10.1038/nsmb1250. Kooshapur, H.; Choudhury, N. R.; Simon, B.; Mühlbauer, M.; Jussupow, A.; Fernandez, N.; Jones, A. N.; Dallmann, A.; Gabel, F.; Camilloni, C.; et al. Structural basis for terminal loop recognition and stimulation of pri-miRNA-18a processing by hnRNP A1. *Nat Commun* **2018**, *9* (1), 2479. DOI: 10.1038/s41467-018-04871-9.
(275) Michlewski, G.; Cáceres, J. F. Antagonistic role of hnRNP A1 and KSRP in the regulation of let-7a biogenesis. *Nat Struct Mol Biol* **2010**, *17* (8), 1011-1018. DOI: 10.1038/nsmb.1874.
(276) Trabucchi, M.; Briata, P.; Garcia-Mayoral, M.; Haase, A. D.; Filipowicz, W.; Ramos, A.; Gherzi, R.; Rosenfeld, M. G. The RNA-binding protein KSRP promotes the biogenesis of a subset of microRNAs. *Nature* **2009**, *459* (7249), 1010-1014. DOI: 10.1038/nature08025. Trabucchi, M.; Briata, P.; Filipowicz, W.; Ramos, A.; Gherzi, R.; Rosenfeld, M. G. KSRP promotes the maturation of a group of miRNA precursors. *Adv Exp Med Biol* **2010**, *700*, 36-42.
(277) Nowak, J. S.; Choudhury, N. R.; de Lima Alves, F.; Rappsilber, J.; Michlewski, G. Lin28a regulates neuronal differentiation and controls miR-9 production. *Nat Commun* **2014**, *5*, 3687. DOI: 10.1038/ncomms4687.
(278) Rau, F.; Freyermuth, F.; Fugier, C.; Villemin, J. P.; Fischer, M. C.; Jost, B.; Dembele, D.; Gourdon, G.; Nicole, A.; Duboc, D.; et al. Misregulation of miR-1 processing is associated with heart defects in myotonic dystrophy. *Nat Struct Mol Biol* **2011**, *18* (7), 840-845. DOI: 10.1038/nsmb.2067.
(279) Suzuki, H. I.; Arase, M.; Matsuyama, H.; Choi, Y. L.; Ueno, T.; Mano, H.; Sugimoto, K.; Miyazono, K. MCPIP1 ribonuclease antagonizes dicer and terminates microRNA biogenesis through precursor microRNA degradation. *Mol Cell* **2011**, *44* (3), 424-436. DOI: 10.1016/j.molcel.2011.09.012.
(280) Treiber, T.; Treiber, N.; Plessmann, U.; Harlander, S.; Daiß, J. L.; Eichner, N.; Lehmann, G.; Schall, K.; Urlaub, H.; Meister, G. A Compendium of RNA-Binding Proteins that Regulate MicroRNA Biogenesis. *Mol Cell* **2017**, *66* (2), 270-284.e213. DOI: 10.1016/j.molcel.2017.03.014.
(281) Wu, S. L.; Fu, X.; Huang, J.; Jia, T. T.; Zong, F. Y.; Mu, S. R.; Zhu, H.; Yan, Y.; Qiu, S.; Wu, Q.; et al. Genome-wide analysis of YB-1-RNA interactions reveals a novel role of

YB-1 in miRNA processing in glioblastoma multiforme. *Nucleic Acids Res* **2015**, *43* (17), 8516-8528. DOI: 10.1093/nar/gkv779.
(282) Kim, K. K.; Yang, Y.; Zhu, J.; Adelstein, R. S.; Kawamoto, S. Rbfox3 controls the biogenesis of a subset of microRNAs. *Nat Struct Mol Biol* **2014**, *21* (10), 901-910. DOI: 10.1038/nsmb.2892.
(283) Chen, Y.; Zubovic, L.; Yang, F.; Godin, K.; Pavelitz, T.; Castellanos, J.; Macchi, P.; Varani, G. Rbfox proteins regulate microRNA biogenesis by sequence-specific binding to their precursors and target downstream Dicer. *Nucleic Acids Res* **2016**, *44* (9), 4381-4395. DOI: 10.1093/nar/gkw177.
(284) Kawahara, Y.; Mieda-Sato, A. TDP-43 promotes microRNA biogenesis as a component of the Drosha and Dicer complexes. *Proc Natl Acad Sci U S A* **2012**, *109* (9), 3347-3352. DOI: 10.1073/pnas.1112427109.
(285) Michlewski, G.; Cáceres, J. F. Post-transcriptional control of miRNA biogenesis. *RNA* **2019**, *25* (1), 1-16. DOI: 10.1261/rna.068692.118. Ha, M.; Kim, V. N. Regulation of microRNA biogenesis. *Nat Rev Mol Cell Biol* **2014**, *15* (8), 509-524. DOI: 10.1038/nrm3838.
(286) Morlando, M.; Dini Modigliani, S.; Torrelli, G.; Rosa, A.; Di Carlo, V.; Caffarelli, E.; Bozzoni, I. FUS stimulates microRNA biogenesis by facilitating co-transcriptional Drosha recruitment. *EMBO J* **2012**, *31* (24), 4502-4510. DOI: 10.1038/emboj.2012.319.
(287) Ouyang, H.; Zhang, K.; Fox-Walsh, K.; Yang, Y.; Zhang, C.; Huang, J.; Li, H.; Zhou, Y.; Fu, X. D. The RNA binding protein EWS is broadly involved in the regulation of pri-miRNA processing in mammalian cells. *Nucleic Acids Res* **2017**, *45* (21), 12481-12495. DOI: 10.1093/nar/gkx912.
(288) Kim, K. Y.; Hwang, Y. J.; Jung, M. K.; Choe, J.; Kim, Y.; Kim, S.; Lee, C. J.; Ahn, H.; Lee, J.; Kowall, N. W.; et al. A multifunctional protein EWS regulates the expression of Drosha and microRNAs. *Cell Death Differ* **2014**, *21* (1), 136-145. DOI: 10.1038/cdd.2013.144.
(289) Wu, H.; Sun, S.; Tu, K.; Gao, Y.; Xie, B.; Krainer, A. R.; Zhu, J. A splicing-independent function of SF2/ASF in microRNA processing. *Mol Cell* **2010**, *38* (1), 67-77. DOI: 10.1016/j.molcel.2010.02.021.
(290) Higuchi, T.; Todaka, H.; Sugiyama, Y.; Ono, M.; Tamaki, N.; Hatano, E.; Takezaki, Y.; Hanazaki, K.; Miwa, T.; Lai, S.; et al. Suppression of MicroRNA-7 (miR-7) Biogenesis by Nuclear Factor 90-Nuclear Factor 45 Complex (NF90-NF45) Controls Cell Proliferation in Hepatocellular Carcinoma. *J Biol Chem* **2016**, *291* (40), 21074-21084. DOI: 10.1074/jbc.M116.748210.
(291) Auyeung, V. C.; Ulitsky, I.; McGeary, S. E.; Bartel, D. P. Beyond secondary structure: primary-sequence determinants license pri-miRNA hairpins for processing. *Cell* **2013**, *152* (4), 844-858. DOI: 10.1016/j.cell.2013.01.031.
(292) Fernandez, N.; Cordiner, R. A.; Young, R. S.; Hug, N.; Macias, S.; Cáceres, J. F. Genetic variation and RNA structure regulate microRNA biogenesis. *Nat Commun* **2017**, *8*, 15114. DOI: 10.1038/ncomms15114.
(293) Kim, K.; Baek, S. C.; Lee, Y. Y.; Bastiaanssen, C.; Kim, J.; Kim, H.; Kim, V. N. A quantitative map of human primary microRNA processing sites. *Mol Cell* **2021**. DOI: 10.1016/j.molcel.2021.07.002.
(294) Davis, B. N.; Hilyard, A. C.; Lagna, G.; Hata, A. SMAD proteins control DROSHA-mediated microRNA maturation. *Nature* **2008**, *454* (7200), 56-61. DOI: 10.1038/nature07086. Davis, B. N.; Hilyard, A. C.; Nguyen, P. H.; Lagna, G.; Hata, A. Smad proteins bind a conserved RNA sequence to promote microRNA maturation by Drosha. *Mol Cell* **2010**, *39* (3), 373-384. DOI: 10.1016/j.molcel.2010.07.011.
(295) Suzuki, H. I.; Yamagata, K.; Sugimoto, K.; Iwamoto, T.; Kato, S.; Miyazono, K. Modulation of microRNA processing by p53. *Nature* **2009**, *460* (7254), 529-533. DOI: 10.1038/nature08199.
(296) Kawai, S.; Amano, A. BRCA1 regulates microRNA biogenesis via the DROSHA microprocessor complex. *J Cell Biol* **2012**, *197* (2), 201-208. DOI: 10.1083/jcb.201110008.

(297) Xhemalce, B.; Robson, S. C.; Kouzarides, T. Human RNA methyltransferase BCDIN3D regulates microRNA processing. *Cell* **2012**, *151* (2), 278-288. DOI: 10.1016/j.cell.2012.08.041.
(298) Yang, W.; Chendrimada, T. P.; Wang, Q.; Higuchi, M.; Seeburg, P. H.; Shiekhattar, R.; Nishikura, K. Modulation of microRNA processing and expression through RNA editing by ADAR deaminases. *Nat Struct Mol Biol* **2006**, *13* (1), 13-21. DOI: 10.1038/nsmb1041.
(299) Kawahara, Y.; Zinshteyn, B.; Chendrimada, T. P.; Shiekhattar, R.; Nishikura, K. RNA editing of the microRNA-151 precursor blocks cleavage by the Dicer-TRBP complex. *EMBO Rep* **2007**, *8* (8), 763-769. DOI: 10.1038/sj.embor.7401011.
(300) Tomaselli, S.; Galeano, F.; Alon, S.; Raho, S.; Galardi, S.; Polito, V. A.; Presutti, C.; Vincenti, S.; Eisenberg, E.; Locatelli, F.; et al. Modulation of microRNA editing, expression and processing by ADAR2 deaminase in glioblastoma. *Genome Biol* **2015**, *16*, 5. DOI: 10.1186/s13059-014-0575-z.
(301) Heale, B. S.; Keegan, L. P.; McGurk, L.; Michlewski, G.; Brindle, J.; Stanton, C. M.; Caceres, J. F.; O'Connell, M. A. Editing independent effects of ADARs on the miRNA/siRNA pathways. *EMBO J* **2009**, *28* (20), 3145-3156. DOI: 10.1038/emboj.2009.244.
(302) Upton, J. P.; Wang, L.; Han, D.; Wang, E. S.; Huskey, N. E.; Lim, L.; Truitt, M.; McManus, M. T.; Ruggero, D.; Goga, A.; et al. IRE1α cleaves select microRNAs during ER stress to derepress translation of proapoptotic Caspase-2. *Science* **2012**, *338* (6108), 818-822. DOI: 10.1126/science.1226191.
(303) Das, S. K.; Sokhi, U. K.; Bhutia, S. K.; Azab, B.; Su, Z. Z.; Sarkar, D.; Fisher, P. B. Human polynucleotide phosphorylase selectively and preferentially degrades microRNA-221 in human melanoma cells. *Proc Natl Acad Sci U S A* **2010**, *107* (26), 11948-11953. DOI: 10.1073/pnas.0914143107.
(304) Kleaveland, B.; Shi, C. Y.; Stefano, J.; Bartel, D. P. A Network of Noncoding Regulatory RNAs Acts in the Mammalian Brain. *Cell* **2018**, *174* (2), 350-362.e317. DOI: 10.1016/j.cell.2018.05.022.
(305) Cazalla, D.; Yario, T.; Steitz, J. A.; Steitz, J. Down-regulation of a host microRNA by a Herpesvirus saimiri noncoding RNA. *Science* **2010**, *328* (5985), 1563-1566. DOI: 10.1126/science.1187197.
(306) Lee, S.; Song, J.; Kim, S.; Kim, J.; Hong, Y.; Kim, Y.; Kim, D.; Baek, D.; Ahn, K. Selective degradation of host MicroRNAs by an intergenic HCMV noncoding RNA accelerates virus production. *Cell Host Microbe* **2013**, *13* (6), 678-690. DOI: 10.1016/j.chom.2013.05.007.
(307) Manier, S.; Powers, J. T.; Sacco, A.; Glavey, S. V.; Huynh, D.; Reagan, M. R.; Salem, K. Z.; Moschetta, M.; Shi, J.; Mishima, Y.; et al. The LIN28B/let-7 axis is a novel therapeutic pathway in multiple myeloma. *Leukemia* **2017**, *31* (4), 853-860. DOI: 10.1038/leu.2016.296.
(308) Mizuguchi, Y.; Takizawa, T.; Yoshida, H.; Uchida, E. Dysregulated miRNA in progression of hepatocellular carcinoma: A systematic review. *Hepatol Res* **2016**, *46* (5), 391-406. DOI: 10.1111/hepr.12606. Chirshev, E.; Oberg, K. C.; Ioffe, Y. J.; Unternaehrer, J. J. Let-7 as biomarker, prognostic indicator, and therapy for precision medicine in cancer. *Clin Transl Med* **2019**, *8* (1), 24. DOI: 10.1186/s40169-019-0240-y.
(309) Albino, D.; Civenni, G.; Dallavalle, C.; Roos, M.; Jahns, H.; Curti, L.; Rossi, S.; Pinton, S.; D'Ambrosio, G.; Sessa, F.; et al. Activation of the Lin28/let-7 Axis by Loss of ESE3/EHF Promotes a Tumorigenic and Stem-like Phenotype in Prostate Cancer. *Cancer Res* **2016**, *76* (12), 3629-3643. DOI: 10.1158/0008-5472.CAN-15-2665. Carmel-Gross, I.; Bollag, N.; Armon, L.; Urbach, A. LIN28: A Stem Cell Factor with a Key Role in Pediatric Tumor Formation. *Stem Cells Dev* **2016**, *25* (5), 367-377. DOI: 10.1089/scd.2015.0322. Mizuno, R.; Kawada, K.; Sakai, Y. The Molecular Basis and Therapeutic Potential of. *Can J Gastroenterol Hepatol* **2018**, *2018*, 5769591. DOI: 10.1155/2018/5769591.
(310) Balzeau, J.; Menezes, M. R.; Cao, S.; Hagan, J. P. The LIN28/let-7 Pathway in Cancer.

Front Genet **2017**, *8*, 31. DOI: 10.3389/fgene.2017.00031. Wang, T.; Wang, G.; Hao, D.; Liu, X.; Wang, D.; Ning, N.; Li, X. Aberrant regulation of the LIN28A/LIN28B and let-7 loop in human malignant tumors and its effects on the hallmarks of cancer. *Mol Cancer* **2015**, *14*, 125. DOI: 10.1186/s12943-015-0402-5.
(311) Zhu, S.; Rooney, S.; Michlewski, G. RNA-Targeted Therapies and High-Throughput Screening Methods. *Int J Mol Sci* **2020**, *21* (8). DOI: 10.3390/ijms21082996.
(312) Schultz, C. W.; Preet, R.; Dhir, T.; Dixon, D. A.; Brody, J. R. Understanding and targeting the disease-related RNA binding protein human antigen R (HuR). *Wiley Interdiscip Rev RNA* **2020**, e1581. DOI: 10.1002/wrna.1581.
(313) Zarei, M.; Lal, S.; Parker, S. J.; Nevler, A.; Vaziri-Gohar, A.; Dukleska, K.; Mambelli-Lisboa, N. C.; Moffat, C.; Blanco, F. F.; Chand, S. N.; et al. Posttranscriptional Upregulation of IDH1 by HuR Establishes a Powerful Survival Phenotype in Pancreatic Cancer Cells. *Cancer Res* **2017**, *77* (16), 4460-4471. DOI: 10.1158/0008-5472.CAN-17-0015.
(314) Blanco, F. F.; Jimbo, M.; Wulfkuhle, J.; Gallagher, I.; Deng, J.; Enyenihi, L.; Meisner-Kober, N.; Londin, E.; Rigoutsos, I.; Sawicki, J. A.; et al. The mRNA-binding protein HuR promotes hypoxia-induced chemoresistance through posttranscriptional regulation of the proto-oncogene PIM1 in pancreatic cancer cells. *Oncogene* **2016**, *35* (19), 2529-2541. DOI: 10.1038/onc.2015.325.
(315) Meisner, N. C.; Hintersteiner, M.; Seifert, J. M.; Bauer, R.; Benoit, R. M.; Widmer, A.; Schindler, T.; Uhl, V.; Lang, M.; Gstach, H.; et al. Terminal adenosyl transferase activity of posttranscriptional regulator HuR revealed by confocal on-bead screening. *J Mol Biol* **2009**, *386* (2), 435-450. DOI: 10.1016/j.jmb.2008.12.020 From NLM.
(316) Ripin, N.; Boudet, J.; Duszczyk, M. M.; Hinniger, A.; Faller, M.; Krepl, M.; Gadi, A.; Schneider, R. J.; Šponer, J.; Meisner-Kober, N. C.; et al. Molecular basis for AU-rich element recognition and dimerization by the HuR C-terminal RRM. *Proc Natl Acad Sci U S A* **2019**, *116* (8), 2935-2944. DOI: 10.1073/pnas.1808696116.
(317) Pabis, M.; Popowicz, G. M.; Stehle, R.; Fernández-Ramos, D.; Asami, S.; Warner, L.; García-Mauriño, S. M.; Schlundt, A.; Martínez-Chantar, M. L.; Díaz-Moreno, I.; et al. HuR biological function involves RRM3-mediated dimerization and RNA binding by all three RRMs. *Nucleic Acids Res* **2019**, *47* (2), 1011-1029. DOI: 10.1093/nar/gky1138.
(318) Imai, T.; Tokunaga, A.; Yoshida, T.; Hashimoto, M.; Mikoshiba, K.; Weinmaster, G.; Nakafuku, M.; Okano, H. The neural RNA-binding protein Musashi1 translationally regulates mammalian numb gene expression by interacting with its mRNA. *Mol Cell Biol* **2001**, *21* (12), 3888-3900. DOI: 10.1128/MCB.21.12.3888-3900.2001. Zearfoss, N. R.; Deveau, L. M.; Clingman, C. C.; Schmidt, E.; Johnson, E. S.; Massi, F.; Ryder, S. P. A conserved three-nucleotide core motif defines Musashi RNA binding specificity. *J Biol Chem* **2014**, *289* (51), 35530-35541. DOI: 10.1074/jbc.M114.597112.
(319) Wang, S.; Li, N.; Yousefi, M.; Nakauka-Ddamba, A.; Li, F.; Parada, K.; Rao, S.; Minuesa, G.; Katz, Y.; Gregory, B. D.; et al. Transformation of the intestinal epithelium by the MSI2 RNA-binding protein. *Nat Commun* **2015**, *6*, 6517. DOI: 10.1038/ncomms7517.
(320) Kawahara, H.; Imai, T.; Imataka, H.; Tsujimoto, M.; Matsumoto, K.; Okano, H. Neural RNA-binding protein Musashi1 inhibits translation initiation by competing with eIF4G for PABP. *J Cell Biol* **2008**, *181* (4), 639-653. DOI: 10.1083/jcb.200708004.
(321) Kudinov, A. E.; Karanicolas, J.; Golemis, E. A.; Boumber, Y. Musashi RNA-Binding Proteins as Cancer Drivers and Novel Therapeutic Targets. *Clin Cancer Res* **2017**, *23* (9), 2143-2153. DOI: 10.1158/1078-0432.CCR-16-2728.
(322) Lin, J. C.; Tsai, J. T.; Chao, T. Y.; Ma, H. I.; Chien, C. S.; Liu, W. H. MSI1 associates glioblastoma radioresistance via homologous recombination repair, tumor invasion and cancer stem-like cell properties. *Radiother Oncol* **2018**, *129* (2), 352-363. DOI: 10.1016/j.radonc.2018.09.014. Kharas, M. G.; Lengner, C. J. Stem Cells, Cancer, and MUSASHI in Blood and Guts. *Trends Cancer* **2017**, *3* (5), 347-356. DOI: 10.1016/j.trecan.2017.03.007.
(323) Vo, D. T.; Abdelmohsen, K.; Martindale, J. L.; Qiao, M.; Tominaga, K.; Burton, T. L.;

Gelfond, J. A.; Brenner, A. J.; Patel, V.; Trageser, D.; et al. The oncogenic RNA-binding protein Musashi1 is regulated by HuR via mRNA translation and stability in glioblastoma cells. *Mol Cancer Res* **2012**, *10* (1), 143-155. DOI: 10.1158/1541-7786.MCR-11-0208.
(324) Clingman, C. C.; Deveau, L. M.; Hay, S. A.; Genga, R. M.; Shandilya, S. M.; Massi, F.; Ryder, S. P. Allosteric inhibition of a stem cell RNA-binding protein by an intermediary metabolite. *Elife* **2014**, *3*. DOI: 10.7554/eLife.02848 From NLM.
(325) Kumar, S.; Downie Ruiz Velasco, A.; Michlewski, G. Oleic Acid Induces MiR-7 Processing through Remodeling of Pri-MiR-7/Protein Complex. *J Mol Biol* **2017**, *429* (11), 1638-1649. DOI: 10.1016/j.jmb.2017.05.001 From NLM.
(326) Meisner, N. C.; Hintersteiner, M.; Mueller, K.; Bauer, R.; Seifert, J. M.; Naegeli, H. U.; Ottl, J.; Oberer, L.; Guenat, C.; Moss, S.; et al. Identification and mechanistic characterization of low-molecular-weight inhibitors for HuR. *Nat Chem Biol* **2007**, *3* (8), 508-515. DOI: 10.1038/nchembio.2007.14 From NLM.
(327) Lu, L.; Zheng, L.; Si, Y.; Luo, W.; Dujardin, G.; Kwan, T.; Potochick, N. R.; Thompson, S. R.; Schneider, D. A.; King, P. H. Hu antigen R (HuR) is a positive regulator of the RNA-binding proteins TDP-43 and FUS/TLS: implications for amyotrophic lateral sclerosis. *J Biol Chem* **2014**, *289* (46), 31792-31804. DOI: 10.1074/jbc.M114.573246. Matsye, P.; Zheng, L.; Si, Y.; Kim, S.; Luo, W.; Crossman, D. K.; Bratcher, P. E.; King, P. H. HuR promotes the molecular signature and phenotype of activated microglia: Implications for amyotrophic lateral sclerosis and other neurodegenerative diseases. *Glia* **2017**, *65* (6), 945-963. DOI: 10.1002/glia.23137. Herdy, B.; Karonitsch, T.; Vladimer, G. I.; Tan, C. S.; Stukalov, A.; Trefzer, C.; Bigenzahn, J. W.; Theil, T.; Holinka, J.; Kiener, H. P.; et al. The RNA-binding protein HuR/ELAVL1 regulates IFN-β mRNA abundance and the type I IFN response. *Eur J Immunol* **2015**, *45* (5), 1500-1511. DOI: 10.1002/eji.201444979.
(328) Romeo, C.; Weber, M. C.; Zarei, M.; DeCicco, D.; Chand, S. N.; Lobo, A. D.; Winter, J. M.; Sawicki, J. A.; Sachs, J. N.; Meisner-Kober, N.; et al. HuR Contributes to TRAIL Resistance by Restricting Death Receptor 4 Expression in Pancreatic Cancer Cells. *Mol Cancer Res* **2016**, *14* (7), 599-611. DOI: 10.1158/1541-7786.MCR-15-0448.
(329) Blanco, F. F.; Preet, R.; Aguado, A.; Vishwakarma, V.; Stevens, L. E.; Vyas, A.; Padhye, S.; Xu, L.; Weir, S. J.; Anant, S.; et al. Impact of HuR inhibition by the small molecule MS-444 on colorectal cancer cell tumorigenesis. *Oncotarget* **2016**, *7* (45), 74043-74058. DOI: 10.18632/oncotarget.12189. Lang, M.; Berry, D.; Passecker, K.; Mesteri, I.; Bhuju, S.; Ebner, F.; Sedlyarov, V.; Evstatiev, R.; Dammann, K.; Loy, A.; et al. HuR Small-Molecule Inhibitor Elicits Differential Effects in Adenomatosis Polyposis and Colorectal Carcinogenesis. *Cancer Res* **2017**, *77* (9), 2424-2438. DOI: 10.1158/0008-5472.CAN-15-1726.
(330) Moradi, F.; Berglund, P.; Linnskog, R.; Leandersson, K.; Andersson, T.; Prasad, C. P. Dual mechanisms of action of the RNA-binding protein human antigen R explains its regulatory effect on melanoma cell migration. *Transl Res* **2016**, *172*, 45-60. DOI: 10.1016/j.trsl.2016.02.007.
(331) Wang, J.; Hjelmeland, A. B.; Nabors, L. B.; King, P. H. Anti-cancer effects of the HuR inhibitor, MS-444, in malignant glioma cells. *Cancer Biol Ther* **2019**, *20* (7), 979-988. DOI: 10.1080/15384047.2019.1591673.
(332) D'Agostino, V. G.; Lal, P.; Mantelli, B.; Tiedje, C.; Zucal, C.; Thongon, N.; Gaestel, M.; Latorre, E.; Marinelli, L.; Seneci, P.; et al. Dihydrotanshinone-I interferes with the RNA-binding activity of HuR affecting its post-transcriptional function. *Sci Rep* **2015**, *5*, 16478. DOI: 10.1038/srep16478. Lal, P.; Cerofolini, L.; D'Agostino, V. G.; Zucal, C.; Fuccio, C.; Bonomo, I.; Dassi, E.; Giuntini, S.; Di Maio, D.; Vishwakarma, V.; et al. Regulation of HuR structure and function by dihydrotanshinone-I. *Nucleic Acids Res* **2017**, *45* (16), 9514-9527. DOI: 10.1093/nar/gkx623.
(333) Filippova, N.; Yang, X.; Ananthan, S.; Sorochinsky, A.; Hackney, J. R.; Gentry, Z.; Bae, S.; King, P.; Nabors, L. B. Hu antigen R (HuR) multimerization contributes to glioma disease progression. *J Biol Chem* **2017**, *292* (41), 16999-17010. DOI:

10.1074/jbc.M117.797878. Manzoni, L.; Zucal, C.; Maio, D. D.; D'Agostino, V. G.; Thongon, N.; Bonomo, I.; Lal, P.; Miceli, M.; Baj, V.; Brambilla, M.; et al. Interfering with HuR-RNA Interaction: Design, Synthesis and Biological Characterization of Tanshinone Mimics as Novel, Effective HuR Inhibitors. *J Med Chem* **2018**, *61* (4), 1483-1498. DOI: 10.1021/acs.jmedchem.7b01176.
(334) Minuesa, G.; Antczak, C.; Shum, D.; Radu, C.; Bhinder, B.; Li, Y.; Djaballah, H.; Kharas, M. G. A 1536-well fluorescence polarization assay to screen for modulators of the MUSASHI family of RNA-binding proteins. *Comb Chem High Throughput Screen* **2014**, *17* (7), 596-609. DOI: 10.2174/1386207317666140609122714.
(335) Minuesa, G.; Albanese, S. K.; Xie, W.; Kazansky, Y.; Worroll, D.; Chow, A.; Schurer, A.; Park, S. M.; Rotsides, C. Z.; Taggart, J.; et al. Small-molecule targeting of MUSASHI RNA-binding activity in acute myeloid leukemia. *Nat Commun* **2019**, *10* (1), 2691. DOI: 10.1038/s41467-019-10523-3.
(336) Lan, L.; Appelman, C.; Smith, A. R.; Yu, J.; Larsen, S.; Marquez, R. T.; Liu, H.; Wu, X.; Gao, P.; Roy, A.; et al. Natural product (-)-gossypol inhibits colon cancer cell growth by targeting RNA-binding protein Musashi-1. *Mol Oncol* **2015**, *9* (7), 1406-1420. DOI: 10.1016/j.molonc.2015.03.014. Lan, L.; Liu, H.; Smith, A. R.; Appelman, C.; Yu, J.; Larsen, S.; Marquez, R. T.; Wu, X.; Liu, F. Y.; Gao, P.; et al. Natural product derivative Gossypolone inhibits Musashi family of RNA-binding proteins. *BMC Cancer* **2018**, *18* (1), 809. DOI: 10.1186/s12885-018-4704-z.
(337) Chae, M. J.; Sung, H. Y.; Kim, E. H.; Lee, M.; Kwak, H.; Chae, C. H.; Kim, S.; Park, W. Y. Chemical inhibitors destabilize HuR binding to the AU-rich element of TNF-alpha mRNA. *Exp Mol Med* **2009**, *41* (11), 824-831. DOI: 10.3858/emm.2009.41.11.088.
(338) Yi, C.; Li, G.; Ivanov, D. N.; Wang, Z.; Velasco, M. X.; Hernández, G.; Kaundal, S.; Villarreal, J.; Gupta, Y. K.; Qiao, M.; et al. Luteolin inhibits Musashi1 binding to RNA and disrupts cancer phenotypes in glioblastoma cells. *RNA Biol* **2018**, *15* (11), 1420-1432. DOI: 10.1080/15476286.2018.1539607.
(339) Iwaoka, R.; Nagata, T.; Tsuda, K.; Imai, T.; Okano, H.; Kobayashi, N.; Katahira, M. Structural Insight into the Recognition of r(UAG) by Musashi-1 RBD2, and Construction of a Model of Musashi-1 RBD1-2 Bound to the Minimum Target RNA. *Molecules* **2017**, *22* (7). DOI: 10.3390/molecules22071207.
(340) Di Giorgio, A.; Tran, T. P.; Duca, M. Small-molecule approaches toward the targeting of oncogenic miRNAs: roadmap for the discovery of RNA modulators. *Future Med Chem* **2016**, *8* (7), 803-816. DOI: 10.4155/fmc-2016-0018.
(341) Bose, D.; Jayaraj, G.; Suryawanshi, H.; Agarwala, P.; Pore, S. K.; Banerjee, R.; Maiti, S. The tuberculosis drug streptomycin as a potential cancer therapeutic: inhibition of miR-21 function by directly targeting its precursor. *Angew Chem Int Ed Engl* **2012**, *51* (4), 1019-1023. DOI: 10.1002/anie.201106455.
(342) Shi, Z.; Zhang, J.; Qian, X.; Han, L.; Zhang, K.; Chen, L.; Liu, J.; Ren, Y.; Yang, M.; Zhang, A.; et al. AC1MMYR2, an inhibitor of dicer-mediated biogenesis of Oncomir miR-21, reverses epithelial-mesenchymal transition and suppresses tumor growth and progression. *Cancer Res* **2013**, *73* (17), 5519-5531. DOI: 10.1158/0008-5472.CAN-13-0280. Bose, D.; Nahar, S.; Rai, M. K.; Ray, A.; Chakraborty, K.; Maiti, S. Selective inhibition of miR-21 by phage display screened peptide. *Nucleic Acids Res* **2015**, *43* (8), 4342-4352. DOI: 10.1093/nar/gkv185. Shortridge, M. D.; Walker, M. J.; Pavelitz, T.; Chen, Y.; Yang, W.; Varani, G. A Macrocyclic Peptide Ligand Binds the Oncogenic MicroRNA-21 Precursor and Suppresses Dicer Processing. *ACS Chem Biol* **2017**, *12* (6), 1611-1620. DOI: 10.1021/acschembio.7b00180.
(343) Disney, M. D.; Labuda, L. P.; Paul, D. J.; Poplawski, S. G.; Pushechnikov, A.; Tran, T.; Velagapudi, S. P.; Wu, M.; Childs-Disney, J. L. Two-dimensional combinatorial screening identifies specific aminoglycoside-RNA internal loop partners. *J Am Chem Soc* **2008**, *130* (33), 11185-11194. DOI: 10.1021/ja803234t. Childs-Disney, J. L.; Wu, M.; Pushechnikov, A.; Aminova, O.; Disney, M. D. A small molecule microarray platform to select RNA

internal loop-ligand interactions. *ACS Chem Biol* **2007**, *2* (11), 745-754. DOI: 10.1021/cb700174r.
(344) Velagapudi, S. P.; Disney, M. D. Two-dimensional combinatorial screening enables the bottom-up design of a microRNA-10b inhibitor. *Chem Commun (Camb)* **2014**, *50* (23), 3027-3029. DOI: 10.1039/c3cc00173c.
(345) Velagapudi, S. P.; Gallo, S. M.; Disney, M. D. Sequence-based design of bioactive small molecules that target precursor microRNAs. *Nat Chem Biol* **2014**, *10* (4), 291-297. DOI: 10.1038/nchembio.1452.
(346) Haga, C. L.; Velagapudi, S. P.; Strivelli, J. R.; Yang, W. Y.; Disney, M. D.; Phinney, D. G. Small Molecule Inhibition of miR-544 Biogenesis Disrupts Adaptive Responses to Hypoxia by Modulating ATM-mTOR Signaling. *ACS Chem Biol* **2015**, *10* (10), 2267-2276. DOI: 10.1021/acschembio.5b00265.
(347) Costales, M. G.; Haga, C. L.; Velagapudi, S. P.; Childs-Disney, J. L.; Phinney, D. G.; Disney, M. D. Small Molecule Inhibition of microRNA-210 Reprograms an Oncogenic Hypoxic Circuit. *J Am Chem Soc* **2017**, *139* (9), 3446-3455. DOI: 10.1021/jacs.6b11273.
(348) Liu, X.; Haniff, H. S.; Childs-Disney, J. L.; Shuster, A.; Aikawa, H.; Adibekian, A.; Disney, M. D. Targeted Degradation of the Oncogenic MicroRNA 17-92 Cluster by Structure-Targeting Ligands. *J Am Chem Soc* **2020**, *142* (15), 6970-6982. DOI: 10.1021/jacs.9b13159.
(349) Lorenz, D. A.; Kaur, T.; Kerk, S. A.; Gallagher, E. E.; Sandoval, J.; Garner, A. L. Expansion of cat-ELCCA for the Discovery of Small Molecule Inhibitors of the Pre-let-7-Lin28 RNA-Protein Interaction. *ACS Med Chem Lett* **2018**, *9* (6), 517-521. DOI: 10.1021/acsmedchemlett.8b00126.
(350) Koszela, J.; Pham, N. T.; Evans, D.; Mann, S.; Perez-Pi, I.; Shave, S.; Ceccarelli, D. F. J.; Sicheri, F.; Tyers, M.; Auer, M. Real-time tracking of complex ubiquitination cascades using a fluorescent confocal on-bead assay. *BMC Biol* **2018**, *16* (1), 88. DOI: 10.1186/s12915-018-0554-z.
(351) Pérez-Pi, I.; Evans, D. A.; Horrocks, M. H.; Pham, N. T.; Dolt, K. S.; Koszela, J.; Kunath, T.; Auer, M. ASYN-CONA, a novel bead-based assay for detecting early stage α-synuclein aggregation. *Anal Chem* **2019**. DOI: 10.1021/acs.analchem.8b03842.
(352) Hua, Y.; Vickers, T. A.; Okunola, H. L.; Bennett, C. F.; Krainer, A. R. Antisense masking of an hnRNP A1/A2 intronic splicing silencer corrects SMN2 splicing in transgenic mice. *Am J Hum Genet* **2008**, *82* (4), 834-848. DOI: 10.1016/j.ajhg.2008.01.014.
(353) Naryshkin, N. A.; Weetall, M.; Dakka, A.; Narasimhan, J.; Zhao, X.; Feng, Z.; Ling, K. K.; Karp, G. M.; Qi, H.; Woll, M. G.; et al. Motor neuron disease. SMN2 splicing modifiers improve motor function and longevity in mice with spinal muscular atrophy. *Science* **2014**, *345* (6197), 688-693. DOI: 10.1126/science.1250127.
(354) Palacino, J.; Swalley, S. E.; Song, C.; Cheung, A. K.; Shu, L.; Zhang, X.; Van Hoosear, M.; Shin, Y.; Chin, D. N.; Keller, C. G.; et al. SMN2 splice modulators enhance U1-pre-mRNA association and rescue SMA mice. *Nat Chem Biol* **2015**, *11* (7), 511-517. DOI: 10.1038/nchembio.1837.
(355) Campagne, S.; Boigner, S.; Rüdisser, S.; Moursy, A.; Gillioz, L.; Knörlein, A.; Hall, J.; Ratni, H.; Cléry, A.; Allain, F. H. Structural basis of a small molecule targeting RNA for a specific splicing correction. *Nat Chem Biol* **2019**, *15* (12), 1191-1198. DOI: 10.1038/s41589-019-0384-5.
(356) Gumireddy, K.; Young, D. D.; Xiong, X.; Hogenesch, J. B.; Huang, Q.; Deiters, A. Small-molecule inhibitors of microrna miR-21 function. *Angew Chem Int Ed Engl* **2008**, *47* (39), 7482-7484. DOI: 10.1002/anie.200801555.
(357) Fu, H. J.; Zhu, J.; Yang, M.; Zhang, Z. Y.; Tie, Y.; Jiang, H.; Sun, Z. X.; Zheng, X. F. A novel method to monitor the expression of microRNAs. *Mol Biotechnol* **2006**, *32* (3), 197-204. DOI: 10.1385/MB:32:3:197.
(358) Downie Ruiz Velasco, A.; Welten, S. M. J.; Goossens, E. A. C.; Quax, P. H. A.; Rappsilber, J.; Michlewski, G.; Nossent, A. Y. Posttranscriptional Regulation of 14q32

MicroRNAs by the CIRBP and HADHB during Vascular Regeneration after Ischemia. *Mol Ther Nucleic Acids* **2019**, *14*, 329-338. DOI: 10.1016/j.omtn.2018.11.017.
(359) Niranjanakumari, S.; Lasda, E.; Brazas, R.; Garcia-Blanco, M. A. Reversible cross-linking combined with immunoprecipitation to study RNA-protein interactions in vivo. *Methods* **2002**, *26* (2), 182-190. DOI: 10.1016/S1046-2023(02)00021-X.
(360) Cox, J.; Mann, M. MaxQuant enables high peptide identification rates, individualized p.p.b.-range mass accuracies and proteome-wide protein quantification. *Nat Biotechnol* **2008**, *26* (12), 1367-1372. DOI: 10.1038/nbt.1511.
(361) Mellacheruvu, D.; Wright, Z.; Couzens, A. L.; Lambert, J. P.; St-Denis, N. A.; Li, T.; Miteva, Y. V.; Hauri, S.; Sardiu, M. E.; Low, T. Y.; et al. The CRAPome: a contaminant repository for affinity purification-mass spectrometry data. *Nat Methods* **2013**, *10* (8), 730-736. DOI: 10.1038/nmeth.2557.
(362) Huang, d. W.; Sherman, B. T.; Lempicki, R. A. Systematic and integrative analysis of large gene lists using DAVID bioinformatics resources. *Nat Protoc* **2009**, *4* (1), 44-57. DOI: 10.1038/nprot.2008.211. Huang, d. W.; Sherman, B. T.; Lempicki, R. A. Bioinformatics enrichment tools: paths toward the comprehensive functional analysis of large gene lists. *Nucleic Acids Res* **2009**, *37* (1), 1-13. DOI: 10.1093/nar/gkn923.
(363) Zhang, J. H.; Chung, T. D.; Oldenburg, K. R. A Simple Statistical Parameter for Use in Evaluation and Validation of High Throughput Screening Assays. *J Biomol Screen* **1999**, *4* (2), 67-73. DOI: 10.1177/108705719900400206.
(364) Chou, C. H.; Shrestha, S.; Yang, C. D.; Chang, N. W.; Lin, Y. L.; Liao, K. W.; Huang, W. C.; Sun, T. H.; Tu, S. J.; Lee, W. H.; et al. miRTarBase update 2018: a resource for experimentally validated microRNA-target interactions. *Nucleic Acids Res* **2018**, *46* (D1), D296-D302. DOI: 10.1093/nar/gkx1067.
(365) Uhlen, M.; Zhang, C.; Lee, S.; Sjöstedt, E.; Fagerberg, L.; Bidkhori, G.; Benfeitas, R.; Arif, M.; Liu, Z.; Edfors, F.; et al. A pathology atlas of the human cancer transcriptome. *Science* **2017**, *357* (6352). DOI: 10.1126/science.aan2507.
(366) Iwasaki, T.; Chin, W. W.; Ko, L. Identification and characterization of RRM-containing coactivator activator (CoAA) as TRBP-interacting protein, and its splice variant as a coactivator modulator (CoAM). *J Biol Chem* **2001**, *276* (36), 33375-33383. DOI: 10.1074/jbc.M101517200. Yang, L.; Embree, L. J.; Tsai, S.; Hickstein, D. D. Oncoprotein TLS interacts with serine-arginine proteins involved in RNA splicing. *J Biol Chem* **1998**, *273* (43), 27761-27764. DOI: 10.1074/jbc.273.43.27761.
(367) Dresios, J.; Aschrafi, A.; Owens, G. C.; Vanderklish, P. W.; Edelman, G. M.; Mauro, V. P. Cold stress-induced protein Rbm3 binds 60S ribosomal subunits, alters microRNA levels, and enhances global protein synthesis. *Proc Natl Acad Sci U S A* **2005**, *102* (6), 1865-1870. DOI: 10.1073/pnas.0409764102.
(368) Pilotte, J.; Dupont-Versteegden, E. E.; Vanderklish, P. W. Widespread regulation of miRNA biogenesis at the Dicer step by the cold-inducible RNA-binding protein, RBM3. *PLoS One* **2011**, *6* (12), e28446. DOI: 10.1371/journal.pone.0028446.
(369) Wong, J. J.; Au, A. Y.; Gao, D.; Pinello, N.; Kwok, C. T.; Thoeng, A.; Lau, K. A.; Gordon, J. E.; Schmitz, U.; Feng, Y.; et al. RBM3 regulates temperature sensitive miR-142-5p and miR-143 (thermomiRs), which target immune genes and control fever. *Nucleic Acids Res* **2016**, *44* (6), 2888-2897. DOI: 10.1093/nar/gkw041.
(370) Weiss, K.; Treiber, T.; Meister, G.; Schratt, G. The nuclear matrix protein Matr3 regulates processing of the synaptic microRNA-138-5p. *Neurobiol Learn Mem* **2019**, *159*, 36-45. DOI: 10.1016/j.nlm.2019.02.008.
(371) Je, G.; Guhathakurta, S.; Yun, S. P.; Ko, H. S.; Kim, Y. S. A novel extended form of alpha-synuclein 3'UTR in the human brain. *Mol Brain* **2018**, *11* (1), 29. DOI: 10.1186/s13041-018-0371-x.
(372) Dinter, E.; Saridaki, T.; Nippold, M.; Plum, S.; Diederichs, L.; Komnig, D.; Fensky, L.; May, C.; Marcus, K.; Voigt, A.; et al. Rab7 induces clearance of α-synuclein aggregates. *J Neurochem* **2016**, *138* (5), 758-774. DOI: 10.1111/jnc.13712.

(373) Cury-Boaventura, M. F.; Pompeia, C.; Curi, R. Comparative toxicity of oleic acid and linoleic acid on Jurkat cells. *Clin Nutr* **2004**, *23* (4), 721-732. DOI: 10.1016/j.clnu.2003.12.004.
(374) Choudhury, N. R.; Michlewski, G. Quantitative identification of proteins that influence miRNA biogenesis by RNA pull-down-SILAC mass spectrometry (RP-SMS). *Methods* **2019**, *152*, 12-17. DOI: 10.1016/j.ymeth.2018.06.006.
(375) Hintersteiner, M.; Ambrus, G.; Bednenko, J.; Schmied, M.; Knox, A. J.; Meisner, N. C.; Gstach, H.; Seifert, J. M.; Singer, E. L.; Gerace, L.; et al. Identification of a small molecule inhibitor of importin beta mediated nuclear import by confocal on-bead screening of tagged one-bead one-compound libraries. *ACS Chem Biol* **2010**, *5* (10), 967-979. DOI: 10.1021/cb100094k.
(376) Green, N. M. Avidin. *Adv Protein Chem* **1975**, *29*, 85-133. DOI: 10.1016/s0065-3233(08)60411-8.
(377) Choudhury, N. R.; Heikel, G.; Trubitsyna, M.; Kubik, P.; Nowak, J. S.; Webb, S.; Granneman, S.; Spanos, C.; Rappsilber, J.; Castello, A.; et al. RNA-binding activity of TRIM25 is mediated by its PRY/SPRY domain and is required for ubiquitination. *BMC Biol* **2017**, *15* (1), 105. DOI: 10.1186/s12915-017-0444-9.
(378) Gry, M.; Rimini, R.; Strömberg, S.; Asplund, A.; Pontén, F.; Uhlén, M.; Nilsson, P. Correlations between RNA and protein expression profiles in 23 human cell lines. *BMC Genomics* **2009**, *10*, 365. DOI: 10.1186/1471-2164-10-365.
(379) Acsadi, G.; Crawford, T. O.; Müller-Felber, W.; Shieh, P. B.; Richardson, R.; Natarajan, N.; Castro, D.; Ramirez-Schrempp, D.; Gambino, G.; Sun, P.; et al. Safety and efficacy of nusinersen in spinal muscular atrophy: The EMBRACE study. *Muscle Nerve* **2021**, *63* (5), 668-677. DOI: 10.1002/mus.27187. Pane, M.; Coratti, G.; Sansone, V. A.; Messina, S.; Catteruccia, M.; Bruno, C.; Sframeli, M.; Albamonte, E.; Pedemonte, M.; D'Amico, A.; et al. Type I SMA "new natural history": long-term data in nusinersen-treated patients. *Ann Clin Transl Neurol* **2021**, *8* (3), 548-557. DOI: 10.1002/acn3.51276.
(380) Dangouloff, T.; Servais, L. Clinical Evidence Supporting Early Treatment Of Patients With Spinal Muscular Atrophy: Current Perspectives. *Ther Clin Risk Manag* **2019**, *15*, 1153-1161. DOI: 10.2147/TCRM.S172291.
(381) Glisovic, T.; Bachorik, J. L.; Yong, J.; Dreyfuss, G. RNA-binding proteins and post-transcriptional gene regulation. *FEBS Lett* **2008**, *582* (14), 1977-1986. DOI: 10.1016/j.febslet.2008.03.004.
(382) Juliano, R. L. The delivery of therapeutic oligonucleotides. *Nucleic Acids Res* **2016**, *44* (14), 6518-6548. DOI: 10.1093/nar/gkw236. Khvorova, A.; Watts, J. K. The chemical evolution of oligonucleotide therapies of clinical utility. *Nat Biotechnol* **2017**, *35* (3), 238-248. DOI: 10.1038/nbt.3765.
(383) Lamb, Y. N. BNT162b2 mRNA COVID-19 Vaccine: First Approval. *Drugs* **2021**, *81* (4), 495-501. DOI: 10.1007/s40265-021-01480-7. FDA authorizes Moderna COVID-19 vaccine. *Med Lett Drugs Ther* **2021**, *63* (1616), 9-10.
(384) Abu Mouch, S.; Roguin, A.; Hellou, E.; Ishai, A.; Shoshan, U.; Mahamid, L.; Zoabi, M.; Aisman, M.; Goldschmid, N.; Berar Yanay, N. Myocarditis following COVID-19 mRNA vaccination. *Vaccine* **2021**, *39* (29), 3790-3793. DOI: 10.1016/j.vaccine.2021.05.087. Larson, K. F.; Ammirati, E.; Adler, E. D.; Cooper, L. T.; Hong, K. N.; Saponara, G.; Couri, D.; Cereda, A.; Procopio, A.; Cavalotti, C.; et al. Myocarditis after BNT162b2 and mRNA-1273 Vaccination. *Circulation* **2021**. DOI: 10.1161/CIRCULATIONAHA.121.055913. Bozkurt, B.; Kamat, I.; Hotez, P. J. Myocarditis With COVID-19 mRNA Vaccines. *Circulation* **2021**, *144* (6), 471-484. DOI: 10.1161/CIRCULATIONAHA.121.056135.
(385) Haaf, P.; Kuster, G. M.; Mueller, C.; Berger, C. T.; Monney, P.; Burger, P.; Stämpfli, S. F.; Attenhofer Jost, C. H.; Zellweger, M. J.; Osswald, S.; et al. The very low risk of myocarditis and pericarditis after mRNA COVID-19 vaccination should not discourage vaccination. *Swiss Med Wkly* **2021**, *151*, w30087. DOI: 10.4414/smw.2021.w30087.
(386) Gerstberger, S.; Hafner, M.; Ascano, M.; Tuschl, T. Evolutionary conservation and

expression of human RNA-binding proteins and their role in human genetic disease. *Adv Exp Med Biol* **2014**, *825*, 1-55. DOI: 10.1007/978-1-4939-1221-6_1.
(387) Jumper, J.; Evans, R.; Pritzel, A.; Green, T.; Figurnov, M.; Ronneberger, O.; Tunyasuvunakool, K.; Bates, R.; Žídek, A.; Potapenko, A.; et al. Highly accurate protein structure prediction with AlphaFold. *Nature* **2021**. DOI: 10.1038/s41586-021-03819-2. Tunyasuvunakool, K.; Adler, J.; Wu, Z.; Green, T.; Zielinski, M.; Žídek, A.; Bridgland, A.; Cowie, A.; Meyer, C.; Laydon, A.; et al. Highly accurate protein structure prediction for the human proteome. *Nature* **2021**. DOI: 10.1038/s41586-021-03828-1.
(388) Zhang, S.; Cheng, Z.; Wang, Y.; Han, T. The Risks of miRNA Therapeutics: In a Drug Target Perspective. *Drug Des Devel Ther* **2021**, *15*, 721-733. DOI: 10.2147/DDDT.S288859.
(389) Valdmanis, P. N.; Kim, H. K.; Chu, K.; Zhang, F.; Xu, J.; Munding, E. M.; Shen, J.; Kay, M. A. miR-122 removal in the liver activates imprinted microRNAs and enables more effective microRNA-mediated gene repression. *Nat Commun* **2018**, *9* (1), 5321. DOI: 10.1038/s41467-018-07786-7.
(390) Kefas, B.; Godlewski, J.; Comeau, L.; Li, Y.; Abounader, R.; Hawkinson, M.; Lee, J.; Fine, H.; Chiocca, E. A.; Lawler, S.; et al. microRNA-7 inhibits the epidermal growth factor receptor and the Akt pathway and is down-regulated in glioblastoma. *Cancer Res* **2008**, *68* (10), 3566-3572. DOI: 10.1158/0008-5472.can-07-6639 From NLM. Gajda, E.; Grzanka, M.; Godlewska, M.; Gawel, D. The Role of miRNA-7 in the Biology of Cancer and Modulation of Drug Resistance. *Pharmaceuticals (Basel)* **2021**, *14* (2). DOI: 10.3390/ph14020149.
(391) Bajar, B. T.; Wang, E. S.; Zhang, S.; Lin, M. Z.; Chu, J. A Guide to Fluorescent Protein FRET Pairs. *Sensors (Basel)* **2016**, *16* (9). DOI: 10.3390/s16091488.
(392) Meisner, N. C.; Hackermüller, J.; Uhl, V.; Aszódi, A.; Jaritz, M.; Auer, M. mRNA openers and closers: modulating AU-rich element-controlled mRNA stability by a molecular switch in mRNA secondary structure. *Chembiochem* **2004**, *5* (10), 1432-1447. DOI: 10.1002/cbic.200400219.
(393) Trubitsyna, M.; Michlewski, G.; Finnegan, D. J.; Elfick, A.; Rosser, S. J.; Richardson, J. M.; French, C. E. Use of mariner transposases for one-step delivery and integration of DNA in prokaryotes and eukaryotes by transfection. *Nucleic Acids Res* **2017**, *45* (10), e89. DOI: 10.1093/nar/gkx113.
(394) Drummond, N. J.; Davies, N. O.; Lovett, J. E.; Miller, M. R.; Cook, G.; Becker, T.; Becker, C. G.; McPhail, D. B.; Kunath, T. A synthetic cell permeable antioxidant protects neurons against acute oxidative stress. *Sci Rep* **2017**, *7* (1), 11857. DOI: 10.1038/s41598-017-12072-5.
(395) Harwood, M.; Danielewska-Nikiel, B.; Borzelleca, J. F.; Flamm, G. W.; Williams, G. M.; Lines, T. C. A critical review of the data related to the safety of quercetin and lack of evidence of in vivo toxicity, including lack of genotoxic/carcinogenic properties. *Food Chem Toxicol* **2007**, *45* (11), 2179-2205. DOI: 10.1016/j.fct.2007.05.015.
(396) Boots, A. W.; Haenen, G. R.; Bast, A. Health effects of quercetin: from antioxidant to nutraceutical. *Eur J Pharmacol* **2008**, *585* (2-3), 325-337. DOI: 10.1016/j.ejphar.2008.03.008.
(397) Xu, D.; Hu, M. J.; Wang, Y. Q.; Cui, Y. L. Antioxidant Activities of Quercetin and Its Complexes for Medicinal Application. *Molecules* **2019**, *24* (6). DOI: 10.3390/molecules24061123.
(398) Maurya, A. K.; Vinayak, M. Modulation of PKC signaling and induction of apoptosis through suppression of reactive oxygen species and tumor necrosis factor receptor 1 (TNFR1): key role of quercetin in cancer prevention. *Tumour Biol* **2015**, *36* (11), 8913-8924. DOI: 10.1007/s13277-015-3634-5. Jing, Z.; Wang, Z.; Li, X.; Cao, T.; Bi, Y.; Zhou, J.; Chen, X.; Yu, D.; Zhu, L.; Li, S. Protective Effect of Quercetin on Posttraumatic Cardiac Injury. *Sci Rep* **2016**, *6*, 30812. DOI: 10.1038/srep30812. Zahedi, M.; Ghiasvand, R.; Feizi, A.; Asgari, G.; Darvish, L. Does Quercetin Improve Cardiovascular Risk factors and Inflammatory Biomarkers in Women with Type 2 Diabetes: A Double-blind Randomized

Controlled Clinical Trial. *Int J Prev Med* **2013**, *4* (7), 777-785.
(399) Ulusoy, H. G.; Sanlier, N. A minireview of quercetin: from its metabolism to possible mechanisms of its biological activities. *Crit Rev Food Sci Nutr* **2020**, *60* (19), 3290-3303. DOI: 10.1080/10408398.2019.1683810.
(400) Zaplatic, E.; Bule, M.; Shah, S. Z. A.; Uddin, M. S.; Niaz, K. Molecular mechanisms underlying protective role of quercetin in attenuating Alzheimer's disease. *Life Sci* **2019**, *224*, 109-119. DOI: 10.1016/j.lfs.2019.03.055.
(401) Lee, M.; McGeer, E. G.; McGeer, P. L. Quercetin, not caffeine, is a major neuroprotective component in coffee. *Neurobiol Aging* **2016**, *46*, 113-123. DOI: 10.1016/j.neurobiolaging.2016.06.015.
(402) Bournival, J.; Quessy, P.; Martinoli, M. G. Protective effects of resveratrol and quercetin against MPP+ -induced oxidative stress act by modulating markers of apoptotic death in dopaminergic neurons. *Cell Mol Neurobiol* **2009**, *29* (8), 1169-1180. DOI: 10.1007/s10571-009-9411-5.
(403) Kwon, S. H.; Lee, S. R.; Park, Y. J.; Ra, M.; Lee, Y.; Pang, C.; Kim, K. H. Suppression of 6-Hydroxydopamine-Induced Oxidative Stress by Hyperoside Via Activation of Nrf2/HO-1 Signaling in Dopaminergic Neurons. *Int J Mol Sci* **2019**, *20* (23). DOI: 10.3390/ijms20235832.
(404) Ishisaka, A.; Ichikawa, S.; Sakakibara, H.; Piskula, M. K.; Nakamura, T.; Kato, Y.; Ito, M.; Miyamoto, K.; Tsuji, A.; Kawai, Y.; et al. Accumulation of orally administered quercetin in brain tissue and its antioxidative effects in rats. *Free Radic Biol Med* **2011**, *51* (7), 1329-1336. DOI: 10.1016/j.freeradbiomed.2011.06.017.
(405) Ganesan, P.; Ko, H. M.; Kim, I. S.; Choi, D. K. Recent trends in the development of nanophytobioactive compounds and delivery systems for their possible role in reducing oxidative stress in Parkinson's disease models. *Int J Nanomedicine* **2015**, *10*, 6757-6772. DOI: 10.2147/IJN.S93918.
(406) Singh, S.; Jamwal, S.; Kumar, P. Neuroprotective potential of Quercetin in combination with piperine against 1-methyl-4-phenyl-1,2,3,6-tetrahydropyridine-induced neurotoxicity. *Neural Regen Res* **2017**, *12* (7), 1137-1144. DOI: 10.4103/1673-5374.211194.
Singh, S.; Kumar, P. Piperine in combination with quercetin halt 6-OHDA induced neurodegeneration in experimental rats: Biochemical and neurochemical evidences. *Neurosci Res* **2018**, *133*, 38-47. DOI: 10.1016/j.neures.2017.10.006.
(407) Ay, M.; Luo, J.; Langley, M.; Jin, H.; Anantharam, V.; Kanthasamy, A.; Kanthasamy, A. G. Molecular mechanisms underlying protective effects of quercetin against mitochondrial dysfunction and progressive dopaminergic neurodegeneration in cell culture and MitoPark transgenic mouse models of Parkinson's Disease. *J Neurochem* **2017**, *141* (5), 766-782. DOI: 10.1111/jnc.14033.
(408) Karuppagounder, S. S.; Madathil, S. K.; Pandey, M.; Haobam, R.; Rajamma, U.; Mohanakumar, K. P. Quercetin up-regulates mitochondrial complex-I activity to protect against programmed cell death in rotenone model of Parkinson's disease in rats. *Neuroscience* **2013**, *236*, 136-148. DOI: 10.1016/j.neuroscience.2013.01.032.
(409) Zbarsky, V.; Datla, K. P.; Parkar, S.; Rai, D. K.; Aruoma, O. I.; Dexter, D. T. Neuroprotective properties of the natural phenolic antioxidants curcumin and naringenin but not quercetin and fisetin in a 6-OHDA model of Parkinson's disease. *Free Radic Res* **2005**, *39* (10), 1119-1125. DOI: 10.1080/10715760500233113. Kääriäinen, T. M.; Piltonen, M.; Ossola, B.; Kekki, H.; Lehtonen, S.; Nenonen, T.; Lecklin, A.; Raasmaja, A.; Männistö, P. T. Lack of robust protective effect of quercetin in two types of 6-hydroxydopamine-induced parkinsonian models in rats and dopaminergic cell cultures. *Brain Res* **2008**, *1203*, 149-159. DOI: 10.1016/j.brainres.2008.01.089.
(410) Ossola, B.; Kääriäinen, T. M.; Raasmaja, A.; Männistö, P. T. Time-dependent protective and harmful effects of quercetin on 6-OHDA-induced toxicity in neuronal SH-SY5Y cells. *Toxicology* **2008**, *250* (1), 1-8. DOI: 10.1016/j.tox.2008.04.001.
(411) Zhu, M.; Han, S.; Fink, A. L. Oxidized quercetin inhibits α-synuclein fibrillization.

Biochim Biophys Acta **2013**, *1830* (4), 2872-2881. DOI: 10.1016/j.bbagen.2012.12.027.
(412) Wang, W. W.; Han, R.; He, H. J.; Li, J.; Chen, S. Y.; Gu, Y.; Xie, C. Administration of quercetin improves mitochondria quality control and protects the neurons in 6-OHDA-lesioned Parkinson's disease models. *Aging (Albany NY)* **2021**, *13* (8), 11738-11751. DOI: 10.18632/aging.202868.
(413) Ahn, T. B.; Jeon, B. S. The role of quercetin on the survival of neuron-like PC12 cells and the expression of α-synuclein. *Neural Regen Res* **2015**, *10* (7), 1113-1119. DOI: 10.4103/1673-5374.160106.
(414) Winder, D. G.; Sweatt, J. D. Roles of serine/threonine phosphatases in hippocampal synaptic plasticity. *Nat Rev Neurosci* **2001**, *2* (7), 461-474. DOI: 10.1038/35081514.
(415) Schonewille, M.; Belmeguenai, A.; Koekkoek, S. K.; Houtman, S. H.; Boele, H. J.; van Beugen, B. J.; Gao, Z.; Badura, A.; Ohtsuki, G.; Amerika, W. E.; et al. Purkinje cell-specific knockout of the protein phosphatase PP2B impairs potentiation and cerebellar motor learning. *Neuron* **2010**, *67* (4), 618-628. DOI: 10.1016/j.neuron.2010.07.009.
(416) Liu, F.; Grundke-Iqbal, I.; Iqbal, K.; Gong, C. X. Contributions of protein phosphatases PP1, PP2A, PP2B and PP5 to the regulation of tau phosphorylation. *Eur J Neurosci* **2005**, *22* (8), 1942-1950. DOI: 10.1111/j.1460-9568.2005.04391.x.
(417) Lian, Q.; Ladner, C. J.; Magnuson, D.; Lee, J. M. Selective changes of calcineurin (protein phosphatase 2B) activity in Alzheimer's disease cerebral cortex. *Exp Neurol* **2001**, *167* (1), 158-165. DOI: 10.1006/exnr.2000.7534. Gong, C. X.; Shaikh, S.; Wang, J. Z.; Zaidi, T.; Grundke-Iqbal, I.; Iqbal, K. Phosphatase activity toward abnormally phosphorylated tau: decrease in Alzheimer disease brain. *J Neurochem* **1995**, *65* (2), 732-738. DOI: 10.1046/j.1471-4159.1995.65020732.x.
(418) Kayyali, U. S.; Zhang, W.; Yee, A. G.; Seidman, J. G.; Potter, H. Cytoskeletal changes in the brains of mice lacking calcineurin A alpha. *J Neurochem* **1997**, *68* (4), 1668-1678. DOI: 10.1046/j.1471-4159.1997.68041668.x.
(419) Walaas, S. I.; Hemmings, H. C.; Greengard, P.; Nairn, A. C. Beyond the dopamine receptor: regulation and roles of serine/threonine protein phosphatases. *Front Neuroanat* **2011**, *5*, 50. DOI: 10.3389/fnana.2011.00050.
(420) Khandelwal, P. J.; Dumanis, S. B.; Feng, L. R.; Maguire-Zeiss, K.; Rebeck, G.; Lashuel, H. A.; Moussa, C. E. Parkinson-related parkin reduces α-Synuclein phosphorylation in a gene transfer model. *Mol Neurodegener* **2010**, *5*, 47. DOI: 10.1186/1750-1326-5-47.
(421) Phiel, C. J.; Wilson, C. A.; Lee, V. M.; Klein, P. S. GSK-3alpha regulates production of Alzheimer's disease amyloid-beta peptides. *Nature* **2003**, *423* (6938), 435-439. DOI: 10.1038/nature01640.
(422) Lei, P.; Ayton, S.; Bush, A. I.; Adlard, P. A. GSK-3 in Neurodegenerative Diseases. *Int J Alzheimers Dis* **2011**, *2011*, 189246. DOI: 10.4061/2011/189246.
(423) La Rocca, G.; Olejniczak, S. H.; González, A. J.; Briskin, D.; Vidigal, J. A.; Spraggon, L.; DeMatteo, R. G.; Radler, M. R.; Lindsten, T.; Ventura, A.; et al. In vivo, Argonaute-bound microRNAs exist predominantly in a reservoir of low molecular weight complexes not associated with mRNA. *Proc Natl Acad Sci U S A* **2015**, *112* (3), 767-772. DOI: 10.1073/pnas.1424217112.
(424) Marchese, D.; Botta-Orfila, T.; Cirillo, D.; Rodriguez, J. A.; Livi, C. M.; Fernández-Santiago, R.; Ezquerra, M.; Martí, M. J.; Bechara, E.; Tartaglia, G. G.; et al. Discovering the 3' UTR-mediated regulation of alpha-synuclein. *Nucleic Acids Res* **2017**, *45* (22), 12888-12903. DOI: 10.1093/nar/gkx1048.
(425) Lebedeva, S.; Jens, M.; Theil, K.; Schwanhäusser, B.; Selbach, M.; Landthaler, M.; Rajewsky, N. Transcriptome-wide analysis of regulatory interactions of the RNA-binding protein HuR. *Mol Cell* **2011**, *43* (3), 340-352. DOI: 10.1016/j.molcel.2011.06.008.
(426) Yu, H.; Wang, J.; Sheng, Q.; Liu, Q.; Shyr, Y. beRBP: binding estimation for human RNA-binding proteins. *Nucleic Acids Res* **2019**, *47* (5), e26. DOI: 10.1093/nar/gky1294.
(427) Chen, C. Y.; Shyu, A. B. AU-rich elements: characterization and importance in mRNA degradation. *Trends Biochem Sci* **1995**, *20* (11), 465-470. DOI: 10.1016/s0968-

0004(00)89102-1.
(428) Ray, D.; Kazan, H.; Chan, E. T.; Peña Castillo, L.; Chaudhry, S.; Talukder, S.; Blencowe, B. J.; Morris, Q.; Hughes, T. R. Rapid and systematic analysis of the RNA recognition specificities of RNA-binding proteins. *Nat Biotechnol* **2009**, *27* (7), 667-670. DOI: 10.1038/nbt.1550.
(429) Brennan, C. M.; Steitz, J. A. HuR and mRNA stability. *Cell Mol Life Sci* **2001**, *58* (2), 266-277. DOI: 10.1007/PL00000854.
(430) Mazan-Mamczarz, K.; Hagner, P. R.; Corl, S.; Srikantan, S.; Wood, W. H.; Becker, K. G.; Gorospe, M.; Keene, J. D.; Levenson, A. S.; Gartenhaus, R. B. Post-transcriptional gene regulation by HuR promotes a more tumorigenic phenotype. *Oncogene* **2008**, *27* (47), 6151-6163. DOI: 10.1038/onc.2008.215. Mazan-Mamczarz, K.; Galbán, S.; López de Silanes, I.; Martindale, J. L.; Atasoy, U.; Keene, J. D.; Gorospe, M. RNA-binding protein HuR enhances p53 translation in response to ultraviolet light irradiation. *Proc Natl Acad Sci U S A* **2003**, *100* (14), 8354-8359. DOI: 10.1073/pnas.1432104100. Lal, A.; Kawai, T.; Yang, X.; Mazan-Mamczarz, K.; Gorospe, M. Antiapoptotic function of RNA-binding protein HuR effected through prothymosin alpha. *EMBO J* **2005**, *24* (10), 1852-1862. DOI: 10.1038/sj.emboj.7600661.
(431) Lee, S.; Wei, L.; Zhang, B.; Goering, R.; Majumdar, S.; Wen, J.; Taliaferro, J. M.; Lai, E. C. ELAV/Hu RNA binding proteins determine multiple programs of neural alternative splicing. *PLoS Genet* **2021**, *17* (4), e1009439. DOI: 10.1371/journal.pgen.1009439.
(432) Pereira-Castro, I.; Moreira, A. On the function and relevance of alternative 3'-UTRs in gene expression regulation. *Wiley Interdiscip Rev RNA* **2021**, e1653. DOI: 10.1002/wrna.1653.
(433) Kim, H. H.; Kuwano, Y.; Srikantan, S.; Lee, E. K.; Martindale, J. L.; Gorospe, M. HuR recruits let-7/RISC to repress c-Myc expression. *Genes Dev* **2009**, *23* (15), 1743-1748. DOI: 10.1101/gad.1812509.
(434) Diao, H.; Li, X.; Hu, S. The identification of dysfunctional crosstalk of pathways in Parkinson disease. *Gene* **2013**, *515* (1), 159-162. DOI: 10.1016/j.gene.2012.11.003.
(435) Rousseaux, M. W.; de Haro, M.; Lasagna-Reeves, C. A.; De Maio, A.; Park, J.; Jafar-Nejad, P.; Al-Ramahi, I.; Sharma, A.; See, L.; Lu, N.; et al. TRIM28 regulates the nuclear accumulation and toxicity of both alpha-synuclein and tau. *Elife* **2016**, *5*. DOI: 10.7554/eLife.19809.
(436) Rousseaux, M. W.; Revelli, J. P.; Vázquez-Vélez, G. E.; Kim, J. Y.; Craigen, E.; Gonzales, K.; Beckinghausen, J.; Zoghbi, H. Y. Depleting Trim28 in adult mice is well tolerated and reduces levels of α-synuclein and tau. *Elife* **2018**, *7*. DOI: 10.7554/eLife.36768.
(437) Thangasamy, T.; Sittadjody, S.; Lanza-Jacoby, S.; Wachsberger, P. R.; Limesand, K. H.; Burd, R. Quercetin selectively inhibits bioreduction and enhances apoptosis in melanoma cells that overexpress tyrosinase. *Nutr Cancer* **2007**, *59* (2), 258-268. DOI: 10.1080/01635580701499545. Tanigawa, S.; Fujii, M.; Hou, D. X. Action of Nrf2 and Keap1 in ARE-mediated NQO1 expression by quercetin. *Free Radic Biol Med* **2007**, *42* (11), 1690-1703. DOI: 10.1016/j.freeradbiomed.2007.02.017. Valerio, L. G.; Kepa, J. K.; Pickwell, G. V.; Quattrochi, L. C. Induction of human NAD(P)H:quinone oxidoreductase (NQO1) gene expression by the flavonol quercetin. *Toxicol Lett* **2001**, *119* (1), 49-57. DOI: 10.1016/s0378-4274(00)00302-7.
(438) Muñoz, P.; Cardenas, S.; Huenchuguala, S.; Briceño, A.; Couve, E.; Paris, I.; Segura-Aguilar, J. DT-Diaphorase Prevents Aminochrome-Induced Alpha-Synuclein Oligomer Formation and Neurotoxicity. *Toxicol Sci* **2015**, *145* (1), 37-47. DOI: 10.1093/toxsci/kfv016.
(439) Luo, S.; Kang, S. S.; Wang, Z. H.; Liu, X.; Day, J. X.; Wu, Z.; Peng, J.; Xiang, D.; Springer, W.; Ye, K. Akt Phosphorylates NQO1 and Triggers its Degradation, Abolishing Its Antioxidative Activities in Parkinson's Disease. *J Neurosci* **2019**, *39* (37), 7291-7305. DOI: 10.1523/JNEUROSCI.0625-19.2019.
(440) Son, H. J.; Choi, J. H.; Lee, J. A.; Kim, D. J.; Shin, K. J.; Hwang, O. Induction of NQO1 and Neuroprotection by a Novel Compound KMS04014 in Parkinson's Disease

Models. *J Mol Neurosci* **2015**, *56* (2), 263-272. DOI: 10.1007/s12031-015-0516-7. Flores-Soto, M. E.; Corona-Angeles, J. A.; Tejeda-Martinez, A. R.; Flores-Guzman, P. A.; Luna-Mujica, I.; Chaparro-Huerta, V.; Viveros-Paredes, J. M. β-Caryophyllene exerts protective antioxidant effects through the activation of NQO1 in the MPTP model of Parkinson's disease. *Neurosci Lett* **2021**, *742*, 135534. DOI: 10.1016/j.neulet.2020.135534. Han, J. M.; Lee, Y. J.; Lee, S. Y.; Kim, E. M.; Moon, Y.; Kim, H. W.; Hwang, O. Protective effect of sulforaphane against dopaminergic cell death. *J Pharmacol Exp Ther* **2007**, *321* (1), 249-256. DOI: 10.1124/jpet.106.110866.
(441) Mbefo, M. K.; Paleologou, K. E.; Boucharaba, A.; Oueslati, A.; Schell, H.; Fournier, M.; Olschewski, D.; Yin, G.; Zweckstetter, M.; Masliah, E.; et al. Phosphorylation of synucleins by members of the Polo-like kinase family. *J Biol Chem* **2010**, *285* (4), 2807-2822. DOI: 10.1074/jbc.M109.081950. Waxman, E. A.; Giasson, B. I. Characterization of kinases involved in the phosphorylation of aggregated α-synuclein. *J Neurosci Res* **2011**, *89* (2), 231-247. DOI: 10.1002/jnr.22537. Song, B.; Davis, K.; Liu, X. S.; Lee, H. G.; Smith, M.; Liu, X. Inhibition of Polo-like kinase 1 reduces beta-amyloid-induced neuronal cell death in Alzheimer's disease. *Aging (Albany NY)* **2011**, *3* (9), 846-851. DOI: 10.18632/aging.100382.
(442) Chen, L. L.; Wang, Y. B.; Song, J. X.; Deng, W. K.; Lu, J. H.; Ma, L. L.; Yang, C. B.; Li, M.; Xue, Y. Phosphoproteome-based kinase activity profiling reveals the critical role of MAP2K2 and PLK1 in neuronal autophagy. *Autophagy* **2017**, *13* (11), 1969-1980. DOI: 10.1080/15548627.2017.1371393.